



HAL
open science

Dopamine and non-canonical signaling

Elia Marilia da Fonte Mota

► **To cite this version:**

Elia Marilia da Fonte Mota. Dopamine and non-canonical signaling. Neurons and Cognition [q-bio.NC]. Sorbonne Université, 2019. English. NNT : 2019SORUS600 . tel-03346728

HAL Id: tel-03346728

<https://theses.hal.science/tel-03346728v1>

Submitted on 16 Sep 2021

HAL is a multi-disciplinary open access archive for the deposit and dissemination of scientific research documents, whether they are published or not. The documents may come from teaching and research institutions in France or abroad, or from public or private research centers.

L'archive ouverte pluridisciplinaire **HAL**, est destinée au dépôt et à la diffusion de documents scientifiques de niveau recherche, publiés ou non, émanant des établissements d'enseignement et de recherche français ou étrangers, des laboratoires publics ou privés.

SORBONNE UNIVERSITÉ

Ecole doctorale 158 Cerveau-Cognition-Comportement - ED3C

Institut de Biologie Paris-Seine

CNRS UMR 8256 Biological Adaptation and Ageing

Team: Dynamics of Intracellular Signaling and Therapeutic Targets

DOPAMINE AND NON-CANONICAL SIGNALING

ÉLIA MARÍLIA DA FONTE MOTA

PHD THESIS IN NEUROSCIENCES

Funded by Labex BioPsy

Supervised by **PIERRE VINCENT**

Presented and defended in public on 23 October 2019

JURY:

VANHOUTTE Peter , Directeur de Recherche, Sorbonne Université	Président
RIQUET Franck , Professeur Universitaire, Ghent University	Rapporteur
VALJENT Emmanuel , Directeur de Recherche, Université Montpellier	Rapporteur
BEURRIER Corinne , Chargé de Recherche, Aix-Marseille Université	Examinatrice
MIKA Delphine , Chargé de Recherche, Université Paris-SUD	Examinatrice
VINCENT Pierre , Directeur de Recherche, Sorbonne Université	Directeur de thèse

“Magic is just science that we don't understand yet.”

Arthur C. Clarke

To my greatest love,

My father

Acknowledgements

My thesis work can be resumed in 3 beautiful years of adventure in the world of neurosciences, the writing of this manuscript and the defense on wednesday, 23 october 2019. This would not have been possible without the valuable contribution of all beings who have stimulated in me the desire to work in the field of science; the desire to learn and to explore. To all of you, THANK YOU for everything!

First and foremost, I would like to thank my supervisor **Pierre Vincent**, not only for the continuous guidance of this work, but also for the trust placed on me. Thank you for your critical sense, your rigor and your scientific integrity during the guidance of this work. I really appreciated all the dedication and availability throughout these 4 years; even if dealing with my character is not always easy... Your motivation and your investment in this project was decisive. You are highly responsible for the scientist I am today; without your support, fighting spirit, advices, objectivity and supervision, I will not be where I am. You were a source of inspiration and admiration. Thank you for all that I learned with you. A huge thank you for this adventure.

I am deeply grateful to my guide and dear friend, Professor **Liliana Castro**, for her scientific expertise, as well as the constructive criticisms, countless suggestions, lights, encouragement, availability, guidance, support and friendship that were crucial for the success of this work. Between a pause and a laugh in a french-portuguese language, she was conspicuous by her unspeakable patience and willingness that contributed for this work to move forward. I really appreciate the enthusiastic way how she share her knowledge, always being willing to fruitful discussions. Nearly four years by her side, during which I was able to learn and train myself, I took advantage of her availability and confidence. It has been a huge privilege for me to work and learn with you. Thank you for your trust and kindness. Thank you for sharing the portuguese mafia office with me.

I would like to thank Professor **Peter Vanhoutte** and Professor **Philippe Marin** for fruitful discussions during the first and second «Comité de Suivi Individuel de Thèse».

I would like to thank all the members of the jury for giving me the honor accepting to participate in my PhD defense. A special thanks to the “rapporteurs”, **Franck Riquet** and **Emmanuel Valjent** for their kindness and helpful comments regarding the content and organization of this thesis manuscript and the resulting papers and to the restant jury, **Peter Vanhoutte**, **Corinne Beurrier** and **Delphine Mika** for their patience and encouragements.

A big thank you to my team, “Dynamics of Intracellular Signaling and Therapeutic Targets” (DISTT) team, or the ancient “Intégration Cellulaire des Signaux Neuromodulateurs” (ICSN) team: **Pierre Vincent** and **Isabelle Limon**, as team leaders; **Liliana Castro**, **Régis Blaise**, **Martine Glorian** and **Bernard Brugg**, as staff scientists; **Julie Stoufflet**, **Ségolène Bompierre** and **Yohan Legueux-Cajgfinger**, as PhD students (Courage for your final straight!); **Célia Moulin** and **Eric Bun**, as scientific support staff; and the most recent acquisition **Samar Fathallah**, as M2. Without forgetting those who have already left the team: **Dahdjim Betolngar**, **Bryon Silva**, **Benjamin Vallin**, **Anissa Belhadef**, **Manon Dobrigna**, **Ilyes Nedjar**, **Mégane Babiak**, **Emilie Wong Chong** and **Yelyzaveta Byelyayeva**

(better known by Lise); and the collaborators who were temporarily on the team: **Anu Nair**, **Juan Llopis** and **Jussepe Salgado**. Thank you for the great atmosphere in the lab, for your help and for all friendliness. Thank you for the good times spent in our monday morning meetings. Thank you for your scientific expertise, as well as the constructive criticisms, suggestions made and invaluable help in preparing the thesis defense.

A special thanks to **Yohan Legueux-Cajgfinger** (Yoyo), **Célia Moulin** (élia avec C) and **Eric Bun** (le psychopathe) for all the good times we shared, for their spirit, their joy and their smiles. Thank you for the nice summer lunch time on the grass, every sunny day; it was like summer holidays for one hour a day ;) Thank you for fridays on the “quai de la Seine”; it really helped me to survive to this thesis. It has really been a great time!

To **Dahdjim Betolngar** and **Cédric Yapo** for the nice welcoming and all the support when I arrived to the lab, their presence during lunch time and experiments even on saturday, cinema suggestions between a panini, a crepe or galette, a sandwich, a pasta or a bagel. Thank you for your patience trying to understand my first baby steps speaking french; thank you for all the corrections and explanations.

I would like to thank **Dahdjim Betolngar**, for teaching me how to prepare Sindbis virus for biosensor expression. I had the privilege to learn with the best!

To **Julie Stoufflet**, for all the help with *Fmr1*-KO mice management, as well the company and nice talks during meetings and sharing rooms.

To **Dahdjim Betolngar**, **Julie Stoufflet**, **Yohan Legueux-Cajgfinger**, **Professor Régis Blaise**, **Benjamin Vallin** and **François Sipieter**, I would like to express my sincere gratitude for their contribution and availability to help with the molecular biology.

To **Anissa Belhadef**, **Manon Dobrigna** and **Ilyes Nedjar** as M1 students that I had the pleasure to transmit my knowledge of preparing slices and biosensor imaging, for the projects “Isoproterenol on the striatum” and “PDE2A activity during NO responses in the striatum”.

Moreover, I would also like to express my gratitude to the staff outside the team who have always contributed to its good functioning, especially to the Biological adaptation and ageing (B2A) unit (UMR8256) and his director **Bertrand Friguet**, and also all the “gestionnaires” **Florence Ladouce**, **Philippe Leballeur**, **Johanne De Marchi**, **Aurélie Prats** and **Sabrina Mamert**, for the nice way and patience how they always received and helped me.

Moreover, I would also like to express my gratitude to all the people that I met on ED 158 Cerveau-Cognition-Comportement (ED3C): his director **Alain Trembleau**, **Christelle Arruebo** and **Aude Cortot**.

I would also like to acknowledge the opportunity to develop this study on **Institut de Biologie Paris-Seine (IBPS)**, **Faculté des Sciences, Sorbonne Université, Campus Pierre et Marie Curie**, and express my gratitude to **Lundbeck company** (Denmark) by kindly providing us the PDE1 inhibitor for the development of part of this work; and to **Labex BioPsy** for funding my PhD work. A big thanks again to **Pierre Vincent** and **Liliana Castro**

for their help that was decisive to obtain this funding. I also would like to thank my previous supervisors, Professor **Fani Sousa** and Professor **Candida Tomaz** for their support and recommendation to obtain this funding.

To all the Lundbeck team **Jacob Nielsen**, **Claus Christoffersen** and **Jan Kehler**, for the collaboration that allowed the publication of the paper which I had the pleasure to work with **Dahdjim Betolngar**, **Pierre Vincent** and **Liliana Castro**; “Phosphodiesterase 1 bridges glutamate inputs with NO- and dopamine-induced cyclic nucleotide signals in the striatum”, in Cerebral Cortex.

Thanks to **Thomas Maurin** and **Barbara Bardoni** for the collaboration in the project with the publication of the paper “Involvement of phosphodiesterase 2A activity in the pathophysiology of fragile X syndrome”, in Cerebral Cortex.

Thanks to **Nicolas Gervasi** for providing us with the EKAREV biosensor; and to **Franck Riquet** for developing and providing us with the EKAR-EV GW4.0 biosensor for the project “imaging the ERK signaling cascade”.

Thanks to **Victor Gorgievski** for the collaboration on the DA-KO project.

To the B6 floor, since **Ivan** whom passes daily very soon in the morning, to **Marise** and all the people that I said “Saluuut” everyday during almost four years: **Maxime Chaulet**, **Oriane Pourchet**, **Marie-Pierre Morel**, **Isabelle Caillé**, **Caroline Dubacq**, **Oriane Trouillard**, **Natayme Tartaglia** (with whom I can speak portuguese from Brasil), **Francesca Farina**, **Julia Dancourt**, **Morgane Fontaine**, A2L2 space managers (**Isabelle Dusart**, **Coralie Fouquet**, **Vincent Kappes**, **Sandrine Picaud**), Animalerie B8 (**Marine Robouam** and others that I don't remember the name, so sorry!).

A big thanks to the amazing VMVDC team for the good time sharing our love for science with young people. You are the best ones! I will never forget you: **Claire Nguyen**, **Leonor Keating** and **Maxime Chaulet**; and the responsible **Isabelle Tratner**; and also to **Yohan Legueux-Cajgfinger**, **Yoann Kovacs**, **Natalia Belén**, the next team for the season 3.0 (Good luck!).

A big thanks to the IDPC club that I integrated to help organizing several nice activities very important for connecting all the people in the IBPS. It was a pleasure to be part of this multicultural family: **Claire Nguyen**, **Estefani Saint-Jour**, **Josquin Courte**, **Julie Stoufflet**, **Maxime Chaulet**, **Arturo Torres Herraéz**, **Anaïs Vitrac**, **Soumee Bhattacharya**, **Abraham Andreu**, **Jennifer Durant**, **Penélope Darnat**, **Sophie Fayad**, **Pauline Monnot**, **Séréna Prigent**, **Laura Goea**... Thanks to all the people that I had the pleasure to meet on IBPS corridors, IBPS events and IDPC activities: **Sarah Mondoloni**, **Elise Bousseynol**, **Benjamin Le Gac**, **Steve Didienne**, **Romain Durand-de Cuttoli**, **Jean Vincent**, **Enejda Subashi**, **Inês Palha**, **Mafalda Loreti**, **Tom Lemonier**, **Camille de Almeida**, **Fiona Henderson**, **Benjamin Lassus**, **Mehdi Fallahnezhad**, **Robin Justo**, **Dorian Battivelli**, **Jean Mariani**, **Régine Hepp**, **Ludovic Tricoire**, **Agnès Bonnot**, **Eric Duplus**, **Mohamed Doulazmi**, **Andry Andrianarivelo**, ... I will always keep the good memories in IBPS.

Thank to all the people that I had the pleasure to meet on the “recherche translationelle” course, namely **Celine Petitgas**, **Elise Liu**, all other colleagues and the

Professors (**Jesus Benavides, Michael Schumacher, Marc Dhenain** and **Alain Trembleau**).

Thanks to all the people that I had the pleasure to meet in the French course, especially to my good italian friend **Alexander Nasole** for the nice talks between a good pizza and a wine in a bar during winter or near to La Seine during summer.

I am also grateful to my friends for all the support even far they were always present: **Ana Luisa Arquilino, Silvia Baptista, Telma Reis, Rita Ferreira, Daniela Baptista, Filipa Pires, Filipa Ramilo Gomes, Joana Valente, Lucia Amorim, Catarina Inês Gonçalves, Adriana Afonso, Francisco Marques, Gonçalo Silva, Guilherme Espírito Santo, João Figueiredo, Luís Miguel, Agustina Bessa, Carolina Costa, Diana Santos, Ana Sofia Silva, Lara Torres, Rita Castel-Branco**... Even considering my absence and silence during months, when we speak is like if we were in contact everyday. Our friendship never changed with the distance. I know that you are always there, my friends!

Thanks to the portuguese friends that I made in Paris during the portuguese activities (Cap Magellan, AGRAFr, ...): **Fernando Vilela, Ana Isabel Freitas, Filipa França, Luciana Gouveia, Raquel Andrade**...

To all my tourist visitors in Paris for the company and support! By order of arrivals: **Gonçalo Silva, Filipe Frias, Joana Valente, Catarina Inês Gonçalves, Cláudia Frias, Bruna Costa, Rita Gonçalves, Beatriz Reis, Eunice Soares, Ana Luisa Arquilino, Luis Perdigo, Margarida Arquilino, Adriana Afonso, Silvia Baptista, Joana Pascoal, Sara Lourenço, Nádia Lourenço** and **Rita Ferreira**, and of course my lovely family, my **father, Ilda, Naida** and **Soraia** (it was like camping in my 30 m² studio in Asnières-sur-Seine).

I am deeply grateful to my lovely family in Paris: “prima Mila” (**Emilia Ribeiro**), “prima” **Lurdes** and “primo” **Beto**. They received and helped me a lot. They always give me a lot of support. With them, it was much more easy to come to Paris and concretise these achievements. I will be eternally grateful!

I am also grateful to all the family in Paris region: “prima” **Marília**, “Dona” **Adelaide**, “primo” **Rui Daniel, Vitoria** and **Matilda**, “primo” **Rui Pedro**, “primo” **Renato, Ricardina, Riana** and **Rubio**.

Finally and most importantly, to all my family in Portugal, especially to my sisters **Naida** and **Soraia**, for all their love. I will be eternally grateful to my **father** and **Ilda** for all their sacrifices, patience and support. I love you both. I am deeply thankful to you father, for your presence during the difficult moments, for your advices and encouragement to believe that it is possible to overcome all the challenges.

Dopamine and non-canonical signaling

Abstract

Striatal medium-sized spiny neurons (MSNs) integrate dopamine signals mainly through the cAMP signaling pathway. Dopamine D₁ or D₂ receptors trigger an increase or a decrease in cAMP levels, respectively. My thesis focuses on how phosphodiesterases (PDEs), which degrade cAMP, are involved in the integration of dopamine signals in the striatum. I used genetically-encoded FRET biosensors to monitor cAMP level in real time in individual living neurons in striatal brain slice preparations. I used selective inhibitors to determine the function of each PDE.

PDE1B, which is activated by calcium-calmodulin, appears as a detector of the coincidence of dopamine and glutamate signals, which is critical in the regulation of synaptic plasticity involved in reward-based learning. PDE10A shows the most prominent activity, efficiently degrading both high and low cAMP levels. PDE10A activity is required to allow for PKA de-activation, and therefore needed to transduce a dopamine signal through D₂ receptors into a decrease in PKA-dependent phosphorylation. PDE2A and PDE4 appeared to degrade only high levels of cAMP, preventing large increases in cAMP. PDE2A, which activity can be increased by cGMP, also appears as a detector of dopamine and NO coincidence.

Understanding PDE functions can highlight their potential as therapeutic targets in CNS pathologies. As an example, we showed an increased PDE2A function in the hippocampus of a mouse model of Fragile X syndrome.

Besides the cAMP/PKA pathway, dopamine D₂ receptors is reported to activate non-canonical pathways. Attempts to use biosensors for Akt and ERK pathways did not provide conclusive data.

Keywords

Dopamine, striatum, cAMP/PKA signaling pathway, phosphodiesterases, genetically-encoded FRET biosensor imaging, cyclic GMP.

Dopamine et signalisation non canonique

Résumé

Les neurones épineux striataux de taille moyenne (MSN) intègrent les signaux médiés par la dopamine principalement par la voie de signalisation de l'AMPC. Les récepteurs dopaminergiques D₁ ou D₂ déclenchent respectivement une augmentation ou une diminution du taux d'AMPC. Ma thèse porte sur la manière dont les phosphodiesterases (PDE), qui dégradent l'AMPC, sont impliquées dans l'intégration des signaux de dopamine dans le striatum. J'ai utilisé des biosenseurs FRET génétiquement codés pour surveiller le niveau d'AMPC en temps réel dans des neurones individuels vivants dans des préparations de tranches de cerveau striatal. J'ai utilisé des inhibiteurs sélectifs pour déterminer la fonction de chaque PDE.

La PDE1B, qui est activée par la calcium-calmoduline, apparaît comme un détecteur de la coïncidence des signaux de dopamine et de glutamate, ce qui est essentiel dans la régulation de la plasticité synaptique impliquée dans l'apprentissage par récompense. La PDE10A montre l'activité la plus importante, dégradant efficacement les taux d'AMPC élevés et faibles. L'activité PDE10A est nécessaire pour permettre la désactivation de la PKA, et donc nécessaire pour transduire un signal de dopamine à travers les récepteurs D₂ en une diminution de la phosphorylation dépendante de la PKA. PDE2A et PDE4 ont semblé ne dégrader que des niveaux élevés d'AMPC, empêchant de fortes augmentations d'AMPC. La PDE2A, dont l'activité peut être augmentée par le GMPc, apparaît également comme un détecteur de coïncidence dopamine et NO.

Comprendre les fonctions des PDE peut mettre en évidence leur potentiel en tant que cibles thérapeutiques dans les pathologies du SNC. A titre d'exemple, nous avons montré une fonction accrue de PDE2A dans un modèle de souris du syndrome du X fragile.

En plus de la voie AMPC/PKA, les récepteurs de la dopamine D₂ pourraient également activer des voies non canoniques. Les tentatives d'utilisation de biosenseurs pour les voies Akt et ERK n'ont pas fourni de données concluantes.

Mots clés

Dopamine, striatum, voie de signalisation AMPC/PKA, phosphodiesterases, imagerie par biosenseur FRET génétiquement codée, GMP cyclique.

Publications during the PhD

(1) Maurin T, Melancia F, Jarjat M, Castro L, Costa L, Delhayé S, Khayachi A, Castagnola S, **Mota E**, Di Giorgio A, Servadio M, Drozd M, Poupon G, Schiavi S, Sardone L, Azoulay S, Ciranna L, Martin S, Vincent P, Trezza V & Bardoni B (2018). Involvement of phosphodiesterase 2A activity in the pathophysiology of fragile X syndrome. *Cerebral Cortex* **29**, 3241–3252. DOI: 10.1093/cercor/bhy192.

(2) Betolngar DB, **Mota É**, Fabritius A, Nielsen J, Hougaard C, Christoffersen CT, Yang J, Kehler J, Griesbeck O, Castro LRV & Vincent P (2019). Phosphodiesterase 1 bridges glutamate inputs with NO- and dopamine-induced cyclic nucleotide signals in the striatum. *Cerebral Cortex* **29**, 5022–5036. DOI: 10.1093/cercor/bhz041.

(3) **Mota É**, Castro LRV & Vincent P. *in preparation*. “PDE10A is required for dopamine action in D2-expressing striatal medium spiny neurons”.

(4) **Mota É**, Stoufflet J, Legueux-Cajgfinger Y, Dobrigna M, Nedjar I, Castro LRV & Vincent P. *in preparation*. “Reduced striatal PDE10A activity in a mouse model of Fragile X syndrome”.

Table of contents

Acknowledgements	7
Abstract	11
Keywords	11
Résumé	13
Mots clés	13
Publications during the PhD	15
Table of contents.....	17
List of Figures	21
List of Tables	23
Abbreviations	25
I - Introduction.....	29
1. Dopamine and cyclic nucleotide signaling pathways	29
1.1. Signals integration through cAMP/PKA signaling pathway	29
1.2. Overview of the cGMP signaling pathway	31
1.3. Cyclic nucleotide degradation by phosphodiesterases	31
General features of phosphodiesterases	32
The regulatory domain and the compartmentation of PDEs	33
The catalytic domain of PDEs and the design of PDE inhibitors	33
Phosphodiesterases inhibition as therapeutic strategies	34
Alternative therapeutic strategies targeting PDEs	35
Phosphodiesterases as disease biomarkers	36
Striatal phosphodiesterases	37
PDE1	39
Molecular features	39
Expression in the brain	39
Activity and regulation	39
Pharmacology	39
PDE2	42
Molecular features	42
Expression in the brain	42
Activity and regulation	42
Pharmacology	43
PDE4	44
Molecular features	44
Expression in the brain	44
Activity and regulation	44
Pharmacology	44
PDE10	45
Molecular features	45
Expression in the brain	46
Activity and regulation	46

Pharmacology	47
2. Dopamine and noncanonical GPCR signaling pathways	49
3. Genetically encoded biosensors to monitor dopamine signals	52
3.1. A sensor domain to detect a biological signal of interest	52
3.2. Single-fluorophore biosensors	53
Calcium-sensitive sensors GCaMPs	53
3.3. Dual-fluorophore biosensors	54
Förster resonance energy transfer (FRET) to detect a conformational change	54
Measuring FRET changes	55
Ratiometric approach to measure FRET	55
Fluorescence life-time imaging microscopy (FLIM) to measure FRET	56
3.4. Biosensors for the cAMP/PKA signaling pathway	57
FRET-based biosensors to detect cAMP	57
FRET-based sensors to detect PKA-dependent phosphorylation	59
3.5. Biosensors for other kinase activities	59
FRET-based sensors to detect Akt-dependent phosphorylation	59
FRET-based sensors to detect ERK-dependent phosphorylation	60
3.6. Quantification and pitfalls	60
Calibration of a ratiometric biosensor	60
Buffering effect	60
4. Striatum as a target of dopamine inputs	61
4.1. Anatomy of the striatum	61
4.2. Striatal neurons	62
Medium-sized spiny neurons (MSNs)	62
Common features of MSNs	62
Anatomy	62
Biochemistry	62
Electrophysiology	63
D1 MSNs: striatonigral MSNs in direct pathway	66
Anatomy	66
Biochemistry	66
Dopamine modulation	66
Motor control	66
D2 MSNs: striatopallidal MSNs in indirect pathway	66
Anatomy	66
Biochemistry	67
Dopamine modulation	67
Motor control	67
Co-expression of D1 and D2 receptors in MSNs	67
Interneurons	68
4.3. Neuromodulatory inputs to MSNs	70
Dopamine	70
Other inputs	71

5. Striatal function and disorders	71
5.1. Reward-based learning	72
5.2. Direct- and indirect-pathways and action selection	73
Other models	74
5.3. Basal ganglia disorders	76
Schizophrenia	76
Autism-spectrum disorders	77
6. Objective	80
7. Protocol to monitor D1 and D2 dopamine responses in MSNs	81
II - Materials and Methods	83
1. Cloning biosensor sequences in a pSinRep5 vector for virus preparation	83
2. Biosensor construct and validation	83
3. Viral infection	83
4. Brain slice preparation	84
5. Optical recordings on brain slices	84
6. Fast drug release	85
7. Data analysis and statistics	85
8. Pharmacological stimulation of receptors	86
III - Results	89
Article 1: PDE1 - dopamine and glutamate coincidence	89
Article 2: PDE - dopamine	107
Article 3: PDE2A - Fragile X syndrome - hippocampus	141
Article 4: PDE10A - Fragile X syndrome - striatum	155
Unpublished data: non-canonical signaling	165
Imaging the Akt/GSK3 β signaling cascade	165
Imaging the ERK signaling cascade	166
Side project: β -adrenergic receptors in the striatum	169
IV - Discussion	171
1. PDE10A is a critical regulator of cAMP in D1 and D2 MSNs	171
2. PDE1B, PDE2A and PDE4 degrade high levels of cAMP	172
3. Phosphodiesterases as coincidence detectors	172
4. PDE2A is critical for normal hippocampal neurons maturation	173
5. Is striatal PDE10A activity decreased in a genetic model of mental retardation ?	174
6. Advantages and limitations of biosensor imaging	175
V - Conclusions and perspectives	177
VI - Bibliography	179
Abstract	207
Keywords	207
Résumé	208
Mots clés	208

List of Figures

Figure 1 - Cyclic nucleotide signaling pathways.

Figure 2 - Structure and domain organization of 11 mammalian PDE families.

Figure 3 - PDE isoform expression patterns in mouse brain.

Figure 4 - PDE expression in the mouse brain is most robust in the striatum.

Figure 5 - Mechanism that activate PDE1 catalytic activity.

Figure 6 - Mechanism that activate PDE2 catalytic activity.

Figure 7 - Mechanism that activate PDE4 catalytic activity.

Figure 8 - Schematic representation of PDE10A.

Figure 9 - Non-canonical G protein-coupled receptor (GPCR) signaling.

Figure 10 - Single-fluorophore biosensor.

Figure 11 - Intramolecular genetically encoded FRET biosensors with two fluorophores.

Figure 12 - Fluorescence and energy transfer through resonance.

Figure 13 - The Epac-S^{H150} sensor report cAMP signals in D1 and D2 MSNs.

Figure 14 - Mouse basal ganglia circuit organisation.

Figure 15 - Basal ganglia microcircuits.

Figure 16 - Cell types and functional organization of the rodent striatum.

Figure 17 - Schema of the canonical reward prediction error signals.

Figure 18 - Potential scenarios of how activity in direct and indirect pathway MSNs in the striatum is related to movement.

Figure 19 - *Fragile X mental retardation 1 (FMR1)* gene and its various allelic forms.

Figure 20 - The cAMP/PKA signaling cascade of the two types of MSNs in the Striatum.

Figure 21 - Akt ratio levels showed no change in MSNs during transient dopamine receptors activation.

Figure 22 - A_{2A} and D₁ receptors activation (with dopamine 10 μM and CGS21680 1 μM, respectively) increases ERK levels.

Figure 23 - Positive response to SKF81297, similar to what was obtained with EKAR-EV GW4.0.

List of Tables

Table 1 - Potential therapeutic applications of PDE inhibition, side effects and impact of knockout in mice.

Table 2 - Clinical trials to test the efficacy of the PDE10A inhibitors in CNS diseases.

Table 3 - Main characteristics of striatal GABAergic interneurons.

Table 4 - Drugs used in biosensor imaging recordings.

Table 5 - ERK responses in the striatum.

Abbreviations

A_{2A}	adenosine A _{2A} receptor
AC	adenylyl cyclase
AKAP	A kinase anchoring protein
AKAR	A kinase activity reporter
Akt	protein kinase B (PKB)
AktAR	Akt activity reporter
AMPA	α -amino-3-hydroxyl-5-methyl-4-isoxazole-propionate
Arr	arrestins
ASD	autism-spectrum disorders
BAC	bacterial artificial chromosome
BHK	baby hamster kidney cells
Ca²⁺	calcium
CaM	calmodulin
CaMKII	calcium/calmodulin-dependent protein kinase II
cAMP	cyclic adenosine monophosphate
CFP	cyan fluorescent protein
cGMP	cyclic guanosine monophosphate
CNG	cyclic nucleotide-gated ion channels
CNS	central nervous system
CREB	cAMP-responsive element binding protein
DIR	dopamine D ₁ receptor
D1 MSN	dopamine D ₁ MSN; also known by dMSN (direct pathway MSN)
D2R	dopamine D ₂ receptor
D2 MSN	dopamine D ₂ MSN; also known by iMSN (indirect pathway MSN)
DA	dopamine
DARPP-32	dopamine and cAMP-regulated phosphoprotein of 32 kDa
DEANO	2-(N,N-diethylamino)-diazeneolate 2-oxide sodium salt hydrate
DISC1	disrupted in schizophrenia 1
DLS	dorsolateral striatum
DMS	dorsomedial striatum
DMSO	dimethyl sulfoxide
DNA	deoxyribonucleic acid
dsDNA	double-stranded DNA
eCFP	enhanced CFP
eGFP	enhanced GFP
EKAR-EV	ERK activity reporter with enhanced visualization linker
EPAC	exchange protein directly activated by cAMP
Epac-S^{H150}	Epac-based cAMP biosensor number 150
ERK	extracellular signal-regulated kinase
FDA	food and drug administration
FLIM	fluorescence life-time imaging microscopy
FMRI	<i>fragile X mental retardation 1</i> gene
FMRP	fragile X mental retardation protein

FRET	Förster (fluorescence) resonance energy transfer
FS	fast spiking
FXS	fragile X syndrome
GABA	gamma-aminobutyric acid
GAF	cGMP-specific and stimulated PDE, <i>Anabaena</i> adenylyl cyclases and <i>Escherichia coli</i> FhlA
GC	guanylyl cyclase
GECI	genetically encoded calcium indicators
GFP	green fluorescent protein
G_{i/o}	inhibitory G protein alpha-subunit
GPCR	G-protein coupled receptor
GPI	internal segment of the globus pallidus; or MGP
GPe	external segment of the globus pallidus; or LGP
GRKs	G protein-coupled receptor kinases
G_{s/olf}	stimulatory G protein alpha-subunit
GSK3	glycogen synthase kinase 3
HD	Huntington's disease
HEK	human embryonic kidney 293 cells
IBMX	broad spectrum PDE inhibitor; 3-isobutyl-1-methylxanthine
iPDE	PDE inhibitor
K⁺	potassium
KO	knockout
L-DOPA	L-3,4-dihydroxyphenylalanine
LGP	lateral globus pallidus
LTD	long-term depression
LTP	long-term potentiation
LTS	low-threshold spiking
MAPK	mitogen-activated protein kinase
MEK	mitogen-extracellular activated protein kinase kinase
MGP	medial globus pallidus
MNI-NMDA	4-methoxy-7-nitroindoliny-1-caged NMDA
mRNA	messenger ribonucleic acid
MRP	multi-drug resistant proteins
MSNs	medium-sized spiny neurons
NAc	nucleus accumbens
NMDA	N-methyl-D-aspartic acid
NO	nitric oxide
NOS	nitric oxide synthase
NPEC-DA	NPEC-caged dopamine
PAABD	phosphoamino acid binding domain
PCR	polymerase chain reaction
PD	Parkinson's disease
PDE	phosphodiesterase
PDK	phosphatidylinositol-dependent kinase
PET	positron emission tomography
PFC	prefrontal cortex

pGC	particulate guanylyl cyclase
PI3K	phosphatidylinositol 3-kinase
PIP2	phosphatidylinositol-2-phosphate
PIP3	phosphatidylinositol-3-phosphate
PKA	cAMP-dependent protein kinase or protein kinase A
PKC	protein kinase C
PKG	cGMP-dependent protein kinase or protein kinase G
PLC	phospholipase C
PP1	phosphatase protein 1
PP2A	phosphatase protein 2A
PP2B	phosphatase protein 2B, calcineurin
qPCR	quantitative PCR
RNA	ribonucleic acid
ROI	region of interest
RT-PCR	reverse transcription-PCR
RTK	receptor tyrosine kinases
sAC	soluble adenylyl cyclase
sGC	soluble guanylyl cyclase
SNe	substantia nigra pars compacta
SNr	substantia nigra pars reticulata
STN	subthalamic nucleus
tAC	transmembrane adenylyl cyclase
TAN	tonically active neuron
TTX	tetrodotoxin
UCR	upstream conserved region
UV	ultraviolet
VTA	ventral tegmental area
YFP	yellow fluorescent protein

I - Introduction

1. Dopamine and cyclic nucleotide signaling pathways

In the central nervous system (CNS), dopamine is a neuromodulator of critical importance in the striatum. It is produced mainly by neurons located in substantia nigra pars compacta (SNc) and ventral tegmental area (VTA) in the midbrain. SNc dopaminergic neurons project primarily to the dorsal and lateral (sensorimotor and cognitive) portions of the striatum, while VTA dopaminergic neurons project primarily to the medial and ventral (cognitive, affective and limbic) portions of the striatum (Nicola, 2007; Simpson *et al.*, 2010). SNc dopamine neurons innervating the striatum are autonomous pacemakers, providing a tonic release of dopamine in the striatum. In the theory presented by Schultz, rewarding events transiently increase the activity of SNc dopamine neurons, leading to phasic release, whereas aversive events transiently decrease it (Brown *et al.*, 2009; Hikosaka *et al.*, 2008; Schultz, 1998; Schultz, 2007). Neurotransmitter signals like dopamine are transduced by cAMP. The cyclic nucleotide signaling cascade regulates a number of downstream signaling events as part of the physiological processes, including visual transduction, cell proliferation and differentiation, gene expression, inflammation, apoptosis and metabolic pathways (Conti & Beavo, 2007; Francis *et al.*, 2011; Keravis & Lugnier, 2012), as well as neuronal functions like neurodevelopment, apoptosis, neuronal excitability, synaptic transmission and neuroplasticity and, ultimately, behavior (Xu *et al.*, 2011). Synthesis of the two major cyclic nucleotides, cyclic adenosine monophosphate (cAMP) and cyclic guanosine monophosphate (cGMP), is catalyzed by adenylyl-cyclases (AC) and guanylyl-cyclases (GC) respectively, which convert ATP or GTP to their respective 3',5'-cyclic nucleotide monophosphate and pyrophosphate.

The focus of this thesis will be on the action of phasic release of dopamine onto the striatal medium-sized spiny neurons (MSNs), and how this signal is integrated through cAMP/PKA signaling pathway.

1.1. Signals integration through cAMP/PKA signaling pathway

There are five G-protein coupled receptors (GPCRs) that mediate dopamine signaling ($D_1 - D_5$). D_1 and D_5 (D_1 -like) receptors stimulate stimulatory G protein alpha-subunit (G_s and G_{olf}), whereas D_2 , D_3 , and D_4 (D_2 -like) receptors stimulate inhibitory G protein alpha-subunit (G_o and G_i) (Missale *et al.*, 1998; Neve *et al.*, 2004). All five dopamine receptors are expressed in the striatum, but D_1 and D_2 receptors are by far the most abundant. D_2 receptors are highly expressed in cholinergic interneurons and afferent fibers, but in this thesis we will focus on MSNs. As described below, these two receptors are segregated in direct- and indirect-pathway MSNs: D_1 receptors are expressed by direct-pathway MSNs, whereas D_2 receptors are expressed by indirect-pathway MSNs. D_1 receptors are positively coupled to the cAMP/PKA signaling pathway, via $G_{s/olf}$, while D_2 receptors are negatively coupled to the same pathway via $G_{i/o}$, which inhibit AC (Figure 1) (Stoof & Keibadian, 1984).

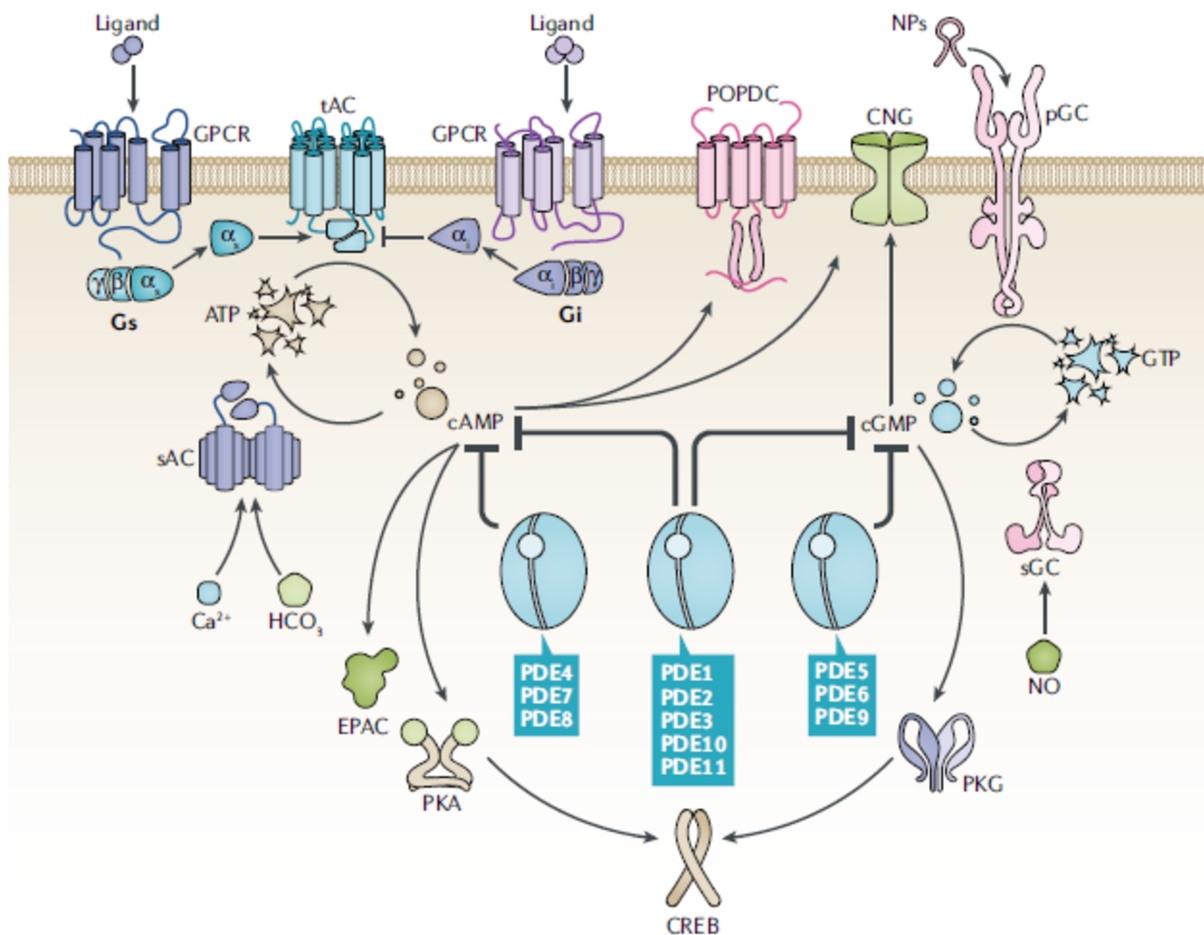


Figure 1 - Cyclic nucleotide signaling pathways. Both of the canonical cyclic nucleotide signalling pathways (cAMP and cGMP) are composed of numerous molecules responsible for the synthesis, execution and breakdown of their signals. cAMP is synthesized by transmembrane adenylyl cyclases (tACs) that are activated by *G_s*/olf and inhibited by *G_i*/o as well as soluble adenylyl cyclases (sACs) that are activated by bicarbonate and calcium. cGMP is synthesized by particulate guanylyl cyclases (pGCs) that are activated by natriuretic peptides (NPs) and soluble guanylyl cyclases (sGCs) that are activated by nitric oxide (NO). Both cAMP and cGMP activate cyclic nucleotide gated channels (CNGs) and modulate the activity of some phosphodiesterases (PDEs) (PDE2, PDE3, PDE5, PDE6, PDE10 and PDE11). cGMP stimulates protein kinase G (PKG), whereas cAMP activates protein kinase A (PKA) and exchange protein activated by cAMP (Epac). Signalling through either the cAMP or cGMP pathways ultimately leads to phosphorylation of a myriad of downstream targets, including the transcription factor cAMP responsive element binding protein (CREB). Abbreviations: GPCR, G protein-coupled receptor. From (Baillie *et al.*, 2019).

G_s and *G_{olf}* proteins stimulate AC, which induces the synthesis of cAMP, elevating intracellular levels of cAMP that transduce signal-encoded information by acting through a number of cellular effectors. cAMP binds and activates cAMP-dependent protein kinase (protein kinase A, PKA) leading to a series of phosphorylation events that result in the regulation of ion channels, enzymes, and changes in transcriptional and translational activities (Figure 1). Another effector of cAMP is a family of two cAMP-activated guanine nucleotide exchange proteins (exchange protein directly activated by cAMP 1 (EPAC1) and EPAC2), which were identified as activators of guanine nucleotide exchange factor Rap1 and shown to be involved in synapse remodeling upon dopamine signaling (Kawasaki *et al.*, 1998; de Rooij *et al.*, 1998; Woolfrey *et al.*, 2009). Cyclic nucleotide-gated ion channels (CNG) mediate

cyclic nucleotide signaling in photoreceptor and olfactory receptor neurons and are also recognized to regulate other functions in the CNS (Podda & Grassi, 2014). Phosphodiesterase (PDE) 10A, which contains an allosteric cyclic nucleotide-binding site in addition to its catalytic site, may also be a target of cAMP signaling (Jäger *et al.*, 2012).

1.2. Overview of the cGMP signaling pathway

cGMP signaling pathway is not activated by dopamine receptors, but since both cAMP and cGMP exhibit similarities, and are both degraded by PDEs, this other cyclic nucleotide signaling pathway is also briefly described here.

Activation of soluble guanylyl cyclases (sGCs) by nitric oxide (NO) is the main source of cGMP in the striatum (Figure 1). sGC is highly expressed in the striatum (Ding *et al.*, 2004; Ariano *et al.*, 1982; Matsuoka *et al.*, 1992), whereas particulate guanylyl cyclase (pGC) does not appear to be expressed in striatal spiny neurons (Herman *et al.*, 1996). NO is produced by a fraction of striatal interneurons that are highly expressing NO synthase (Vincent & Kimura, 1992; Rushlow *et al.*, 1995; Kawaguchi, 1997).

cGMP signaling, similarly to cAMP, regulates a number of neurobiological processes (Garthwaite, 2008), which largely depend on its targets. One of these targets is cGMP-dependent protein kinases (protein kinase G, PKG), but brain regions such as the hippocampus and the striatum which express high levels of sGC (Matsuoka *et al.*, 1992; Ding *et al.*, 2004), only express moderate levels of PKG protein (el-Husseini *et al.*, 1995; El-Husseini *et al.*, 1999; de Vente *et al.*, 2001). cGMP also opens the CNG, however, CNG expression has not been reported in the striatum (Savchenko *et al.*, 1997; Wei *et al.*, 1998). Another target of cGMP are cGMP-regulated PDEs, such as cGMP-activated PDEs (PDE2, PDE5, PDE6 and PDE11) and cGMP-inhibited PDE (PDE3) (Maurice *et al.*, 2014), and there are high levels of PDE2A expression in the striatum and hippocampus (Lakics *et al.*, 2010; Kelly *et al.*, 2014; Repaske *et al.*, 1993; Van Staveren *et al.*, 2003). This suggests that the major role of cGMP in the striatum may be to regulate cAMP levels via PDE2A activation, rather than to directly activate PKG or CNG. This hypothesis is clearly supported by the experiments which show that one major functional effect of NO-triggered cGMP production is the activation of PDE2A which then strongly reduce the cAMP response in both D1 and D2 neurons (Polito *et al.*, 2013). How PDE2A could modulate the cAMP response to dopamine in striatal neuron is therefore one question explored in my thesis work.

1.3. Cyclic nucleotide degradation by phosphodiesterases

The termination of the signals mediated by cyclic nucleotides requires a mechanism to eliminate these molecules. There are negative controls of cyclic nucleotides like multi-drug resistant proteins (MRP) and passive permeation through the membrane, but these processes do not seem to play any critical role in the neurons that we studied (unpublished data). The main mechanism remains PDEs, which are responsible for the hydrolysis of the 3',5' phosphodiester bond of cAMP or cGMP to yield 5'-AMP or 5'-GMP (Keravis & Lugnier, 2012; Maurice *et al.*, 2014; Baillie *et al.*, 2019).

General features of phosphodiesterases

The PDE superfamily consists of 11 gene families, with most families containing several genes giving rise to a total of 21 coding PDE genes (Figure 2), which together generate close to 100 PDE variants by alternative mRNA splicing or transcriptional processing. PDE variants display diverse enzymatic characteristics, primary structures, affinities for cAMP and cGMP, catalytic properties and responses to specific activators, inhibitors and effectors, as well as in their mechanisms of regulation and sub-cellular localization (Conti & Beavo, 2007; Francis *et al.*, 2011; Keravis & Lugnier, 2012). Each cell may express several of these different isozymes, and this combinatorial complexity of PDEs, creates a cell type-specific cAMP processing profile, which determines how cAMP signal is integrated at the subcellular level and their biological effects.

PDEs can either selectively hydrolyse cAMP or cGMP, as well as both cyclic nucleotides (Figure 2) (Conti & Beavo, 2007; Francis *et al.*, 2011; Keravis & Lugnier, 2012).

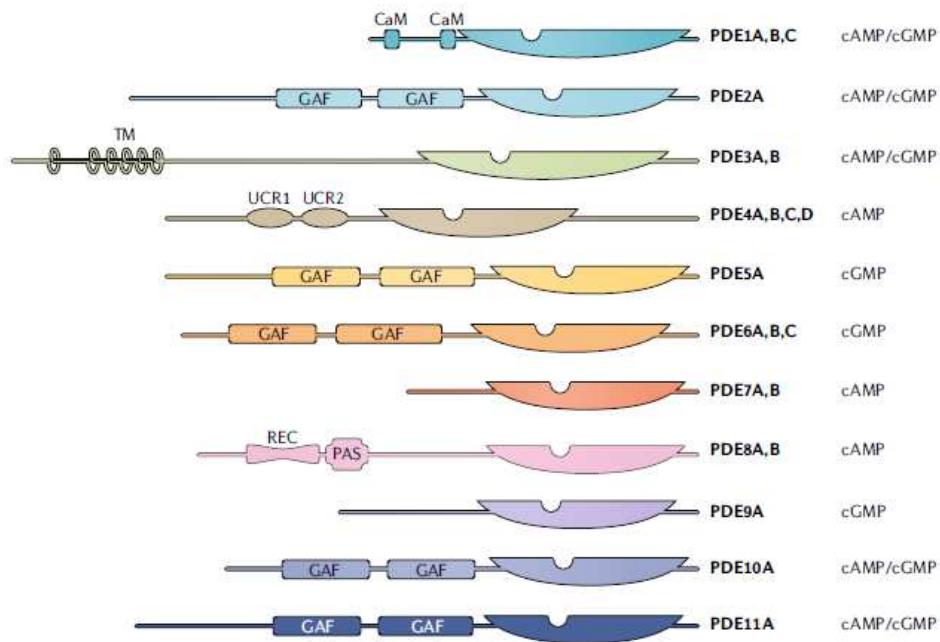


Figure 2 - Structure and domain organization of 11 mammalian PDE families. The substrate specificity of each family is shown in the right of each PDE family. Family designation is based on the homology of the conserved catalytic domain, located in the C-terminal (represented as a semi-ellipse). Due to alternate promoters and splicing events, each PDE family has multiple isoforms that differ in terms of the length and complexity of their N-terminal regulatory domains (depicted with different shapes), such as GAF domains, transmembrane domains, targeting domains, UCRs, PAS domains and REC domains) and N-terminal hydrophobic regions that are important in subcellular localization, in the incorporation of PDEs into compartmentalized signalosomes, in interactions with signalling molecules and molecular scaffolds, and in the regulation of substrate affinity and catalytic activity. GAF domains regulate the allosteric binding of cGMP (PDE2, PDE5, PDE6 and PDE11), the allosteric binding of cAMP (PDE10) and the regulation of catalytic activity (PDE2, PDE5 and PDE6) (Maurice *et al.*, 2014). Illustrations represent the longest isoform for gene A of each PDE family. Abbreviations: CaM, calmodulin; GAF, cGMP-binding PDEs *Anabaena* adenylyl cyclases and *Escherichia coli* FhlA; PAS, Per-Arnt-Sim domain; PDE, phosphodiesterase; PKA, protein kinase A; REC, signal receiver domain; TM, transmembrane domain; UCR, upstream conserved region. From (Baillie *et al.*, 2019).

The regulatory domain and the compartmentation of PDEs

The 11 PDEs families exhibit a common structural organization and are grouped based on their conserved carboxy-terminal catalytic core, but each PDE family has multiple isoforms that differ in their amino-terminal regulatory domains (Figure 2).

The N-terminal regulatory regions of PDEs contain structural elements that target individual PDEs to different sub-cellular locations and signalosomes (Houslay *et al.*, 2007; Kritzer *et al.*, 2012; Lee *et al.*, 2013), and also allow individual PDEs to specifically respond to different post-translational modifications, regulatory molecules and signals. These structural elements include dimerization domains, auto-inhibitory modules, binding sites for ligands and allosteric effectors, phosphorylation sites and other covalent modification sites, domains for isoform-specific protein-protein interactions with specific scaffolds and regulatory partners.

The incorporation of different types of PDEs into specific signalosomes contributes to both the fine-tuning and specificity of compartmented cyclic nucleotide signalling (Conti & Beavo, 2007; Francis *et al.*, 2011; Keravis & Lugnier, 2012). Sub-cellular compartmentation of cyclic nucleotide signaling is established via unique combinations of AC and cyclic nucleotide effectors (PKAs, EPACs, CNGs or PKGs), other kinases, phosphatases and individual or subsets of PDEs. The compartmentation of cyclic nucleotide signaling modulates the diffusion of cyclic nucleotide gradients within spatially restricted and temporally regulated compartments, which enables a single cell to integrate multiple distinct cellular signals and allow crosstalk between cyclic nucleotides and other signaling networks and systems (Stangherlin *et al.*, 2011; Mongillo *et al.*, 2006; Wilson *et al.*, 2011; Rampersad *et al.*, 2010; Terrin *et al.*, 2012). Indeed, the use of real-time approaches such as patch-clamp and biosensor imaging together with biochemical approaches, has confirmed that cells regulate their intracellular levels of cAMP or cGMP in a highly compartmentalized manner and generate functionally separate intracellular cyclic nucleotide pools (Castro *et al.*, 2010; Jurevicius & Fischmeister, 1996; Zaccolo *et al.*, 2000; Maurice, 2011; Stangherlin *et al.*, 2011; Mongillo *et al.*, 2006; Stangherlin & Zaccolo, 2012).

The catalytic domain of PDEs and the design of PDE inhibitors

PDEs are of particular interest because the structure of their catalytic site, with a distinctive cyclic-nucleotide binding pocket, makes it possible to create inhibitors with high affinity and selectivity, a property that has allowed the pharmaceutical industry to develop numerous drug candidates.

X-ray crystal structures revealed that the catalytic domains of several PDE families share a similar structure (Maurice *et al.*, 2014). The active site forms a deep hydrophobic pocket that contains a PDE-specific, histidine-containing signature motif and binding sites for two divalent metal ions that are essential for catalytic function (Ke *et al.*, 2011). Information from crystal structures of the catalytic sites of PDEs and PDE-inhibitor complexes suggest that the catalytic pocket is composed by highly conserved and invariant residues, including a highly conserved phenylalanine and an invariant glutamine, that forms crucial hydrogen bonds with cyclic nucleotides and inhibitors (Maurice *et al.*, 2014). The catalytic core also

contains variable determinants that determine PDE family specific affinities and selectivities for binding to substrate and inhibitors (Keravis & Lugnier, 2012; Manallack *et al.*, 2005; Bender & Beavo, 2006). Information from PDE structural biology, structure-function studies, advanced proteomics and X-ray crystallographic analysis improved the design of new inhibitors, more potent and selective, that are now generated by a structure-based design approach, being chemically synthesized after structure-informed virtual screening and computational design (Ke & Wang, 2007; Card *et al.*, 2004; Manallack *et al.*, 2005; Lee *et al.*, 2013; Maurice *et al.*, 2014).

Phosphodiesterases inhibition as therapeutic strategies

The dysregulation of intracellular cyclic nucleotide signaling pathways contributes to numerous diseases affecting the nervous system, particularly cognitive decline associated with aging and/or neuropsychiatric diseases involving dopaminergic dysregulation, such as drug addiction, Parkinson's disease, schizophrenia or Alzheimer's disease (Neves-Zaph, 2017; Xu *et al.*, 2011; Reneerkens *et al.*, 2009; Maurice *et al.*, 2014). Considering the crucial biological function of PDEs and the possibility to create selective PDE inhibitors, these enzymes constitute an interesting therapeutic target. The level of interest in PDE inhibitors can be readily appreciated from the large number of clinical trials registered on the ClinicalTrials.gov website. However, despite significant efforts targeting the inhibition of all PDE families, only inhibitors for PDEs 1, 3, 4, 5 and 10 have reached the market (Baillie *et al.*, 2019).

Non-selective first-generation PDE inhibitors such as xanthine derivatives, including theophylline and caffeine, were clinically used as bronchodilators in the treatment of pulmonary diseases, diuretics and inotropic agents, even before they were identified as PDE inhibitors (inhibit all PDE families, except PDE8 and PDE9) (Schudt *et al.*, 2011; Barnes, 2013).

Several **second-generation family-selective competitive PDE inhibitors** were developed using classical medicinal chemistry approaches (Card *et al.*, 2004; Manallack *et al.*, 2005). This strategy identified by screening the lead compounds with modest potency and selectivity to compete with the binding of cyclic nucleotide substrates at the catalytic sites of PDEs. These lead compounds served as scaffolds for systematic derivatization and chemical optimization to produce family selective, competitive inhibitors with greater affinity, selectivity, specificity and favorable pharmacokinetics and safety profiles with fewer side effects (Maurice *et al.*, 2014).

Conversely, some off-target effects of family-selective PDE inhibitors can positively affect their efficacy and safety profile. For example, it has been suggested that the PDE5 inhibitor, sildenafil, also induced PDE1 inhibition, which may be responsible for some effects in treating heart failure (Movsesian & Kukreja, 2011; Kukreja *et al.*, 2011). Thus, dual PDE1 and PDE5 inhibition might be beneficial in treating human cardiovascular diseases. Targeting multiple PDEs (combining several PDE inhibitors or with inhibitors that target multiple PDEs) in several target cells can theoretically produce additive or synergistic effects and lead to more effective therapies, with more favourable risk-benefit profiles (Maurice *et al.*, 2014). Moreover, the administration of lower doses of PDE inhibitors with ineffective doses can result in an effective combined dose only in tissues and subcellular compartments where both

molecules are present (Baillie *et al.*, 2019).

The enormous clinical success of the orally administered PDE5 inhibitors in treating erectile dysfunction (Francis & Corbin, 2011) and, more recently, pulmonary arterial hypertension (Ghofrani *et al.*, 2006; Kukreja *et al.*, 2011; Archer & Michelakis, 2009), highly contributed to the expanding pharmaceutical interest in PDEs as promising therapeutic targets for many diseases (Maurice *et al.*, 2014; Baillie *et al.*, 2019). Currently there are four PDE5 inhibitors FDA approved and two PDE5 inhibitors marketed outside the USA (Baillie *et al.*, 2019), with the first being sildenafil (Viagra; marketed as Revatio by Pfizer).

Several recent clinical trials have explored additional disease indications that might benefit from the vasodilatory properties of PDE5 inhibitors. PDE5 inhibitors such as sildenafil, tadalafil and vardenafil are currently approved for the treatment of pulmonary hypertension (Ghofrani *et al.*, 2006; Kukreja *et al.*, 2011; Archer & Michelakis, 2009). Similar to their effects on pulmonary circulation, PDE5 inhibitors may improve cerebral circulation and oxygenation and thus protect the brain against stroke (Kukreja *et al.*, 2011; Maurice *et al.*, 2014).

Expression of PDEs in the brain is particularly complex, with PDE isoforms differentially expressed across circuits, cell types and subcellular domains. Thus, the challenge in evaluating the clinical potential for the next generation of PDE-modulating drugs is to gain novel insights about nervous system disease-related changes in PDE structure, function and regulation to understand how PDEs should be selectively targeted in a brain region- and compartment-specific manner for therapeutic gain (Kelly *et al.*, 2014; Baillie *et al.*, 2019).

Numerous PDE-targeted therapeutics are currently **under development** by the pharmaceutical industry for multiple indications (Maurice *et al.*, 2014; Baillie *et al.*, 2019).

Despite the therapeutic success of a few PDE inhibitors, the presence of undesirable side effects resulting from the inability to target individual isoforms is the major limiting factor to success. For example, the PDE4 inhibitors rolipram and cilomilast failed in clinical trials because of their gastrointestinal side effects, especially nausea, emesis and diarrhoea possibly caused by PDE4D inhibition in the area postrema, the emetic centre in the brain (Schudt *et al.*, 2011; Tenor *et al.*, 2011).

Alternative therapeutic strategies targeting PDEs

The majority of PDE-targeted therapeutics on the market are simply competitive blockers of substrate binding at the catalytic site that lack the ability to selectively target a specific isozyme within a single PDE family or subfamily (Baillie *et al.*, 2019). Promising preclinical data of many PDE inhibitors failed in human clinical trials, suggesting that therapeutic approaches targeting PDEs need to extend beyond occlusion of the enzyme's catalytic site.

The design of novel selective agents is being developed by structural information from modern proteomics and X-ray crystallography about the unique allosteric interactions between the regulatory and catalytic domains of PDEs (Pandit *et al.*, 2009), as well as

between individual PDEs and their specific interacting partners. Innovative and technological strategies are currently being explored to increase the selectivity and specificity to target PDE function, including PDE activators (enhancing catalytic activity), signalosome disruptors to normalize altered compartmentation, modulating post-translational modifications (phosphorylation of some PDEs by PKA or PKG, that directly regulate PDE activity and location, Ubiquitylation, SUMOylation (small ubiquitin-like modifier), S-nitrosylation and proline hydroxylation) and gene therapy approaches, as well as the potential use of PDEs as disease biomarkers for diagnosis and/or patient selection (Baillie *et al.*, 2019).

PDE activation can be obtained by:

- targeting GAF (cGMP-specific and stimulated PDE, *Anabaena* adenylyl cyclases and *Escherichia coli* FhlA) domains. In mammals, GAF domains are only found in the PDE 2, 5, 6, 10 and 11 families, which increases their interest as a drug target. The binding of cyclic nucleotides to GAF domains is thought to cause structural changes that relieve auto-inhibition of the PDEs. Importantly, mammalian GAF domains are sufficiently structurally divergent between PDE families to allow selective pharmacological targeting of individual PDE families.
- targeting upstream conserved region (UCR)-based regulation, preventing trans-capping. For example, catalytic activity of PDE4 is inhibited when the UCR2 regulatory domain “trans-caps” the catalytic site, thus blocking cAMP access to the enzymatic core (Wang *et al.*, 2007; Keravis & Lugnier, 2012; Bender & Beavo, 2006).
- targeting protein-protein binding interactions.

The compartmentation of cyclic nucleotide signaling is achieved by virtue of PDEs being tethered to a precise cellular location via binding partners. Thus, promoting or disrupting isoform-specific protein-protein interactions may prove a viable approach to therapeutically target PDEs in an isoform-specific manner (Baillie *et al.*, 2019).

- Dominant-negative PDEs, which are catalytically inactive mutants that would displace their endogenous PDE. In fact, nature has developed its own dominant-negative approach with PDE4A7, a PDE isoform that is targeted to specific subcellular compartments but is catalytically dead (Johnston *et al.*, 2004).
- Disrupting PDE homodimerization, may also prove an effective way to target PDE function in a domain-specific manner. In fact, nature also takes advantage of dimerization as a mechanism to regulate PDE trafficking, for example when PDE10A2 heterodimerizes with PDE10A19, PDE10A2 is prevented from trafficking to the membrane as it normally does under conditions of homodimerization (MacMullen *et al.*, 2016).

Phosphodiesterases as disease biomarkers

PDEs are also being explored as both diagnostic and patient-selection biomarkers. Imaging compounds can be engineered with relative ease to selectively target a given PDE family/subfamily *in vivo*. Thus, PDEs can be explored as biomarkers in brain diseases (Baillie *et al.*, 2019).

PDE10A is widely reported as downregulated in both the striatum and the cortex of patients with Huntington's disease, with the extent of PDE10A loss corresponding to the

genetic burden associated with the disease (Russell *et al.*, 2016; Russell *et al.*, 2014; Ahmad *et al.*, 2014; Wilson *et al.*, 2016). A loss of PDE10A expression has also been observed in the basal ganglia of patients with Parkinson disease (Niccolini *et al.*, 2015). Highly-specific PDE10A positron emission tomography (PET) tracers show that PDE10A expression in patients with Huntington disease continues to decline over the years (Russell *et al.*, 2016). Thus, PET imaging of PDE10A could be a useful biomarker for assessing the initial diagnosis and subsequent progression of these neurodegenerative diseases (Boscutti *et al.*, 2019). PET ligands also exist for PDEs 2, 4, 5 and 7 (Schröder *et al.*, 2016).

Striatal phosphodiesterases

My primary goal in my thesis was to understand how the diversity of PDEs found in neurons contributes to the control of the amplitude and duration of cAMP signaling, and how regulation of PDEs activities can further modulate the integration of dopamine signals through cAMP processing in neurons.

PDE mRNA expression in the striatum is ~ 2-10 fold higher than in prefrontal cortex, hippocampus, cerebellum, hypothalamus or spinal cord (Kelly *et al.*, 2014; Lakics *et al.*, 2010). Both in situ hybridization (Figure 3) and quantitative polymerase chain reaction (qPCR) (Figure 4) approaches confirm a particularly robust striatal mRNA expression of PDE1B, PDE2A, PDE7B and PDE10A, in human (Lakics *et al.*, 2010) and rodents, and a more moderate expression of PDE4B and PDE8B (Kelly *et al.*, 2014). Another particularity is the strikingly selective mRNA expression of PDE1B and PDE10A in the caudate nucleus, which is 20-fold higher than in any other brain and peripheral tissues (Lakics *et al.*, 2010). PDE7B mRNA is highly expressed, but no protein has been detected in the striatum (unpublished information from Pfizer). PDE8B also present at a moderate mRNA level has not been reported at the protein level in the striatum. It is important to note that there is a high degree of protein homology and a conserved PDE expression patterns between human and rodents (Kelly *et al.*, 2014), which gives confidence that knowledge obtained in rodent studies can be transversal to the human brain.

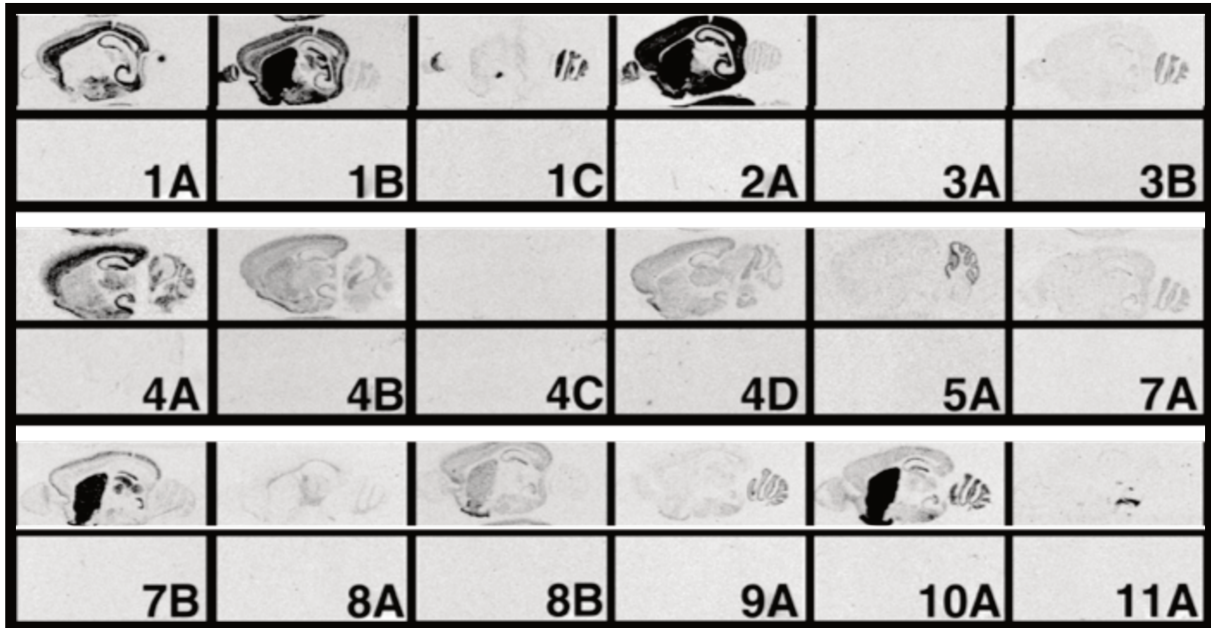


Figure 3 - PDE isoform expression patterns in mouse brain. Visualization of PDE isoforms by in situ hybridization in sagittal sections from mouse brain. From (Kelly et al., 2014).

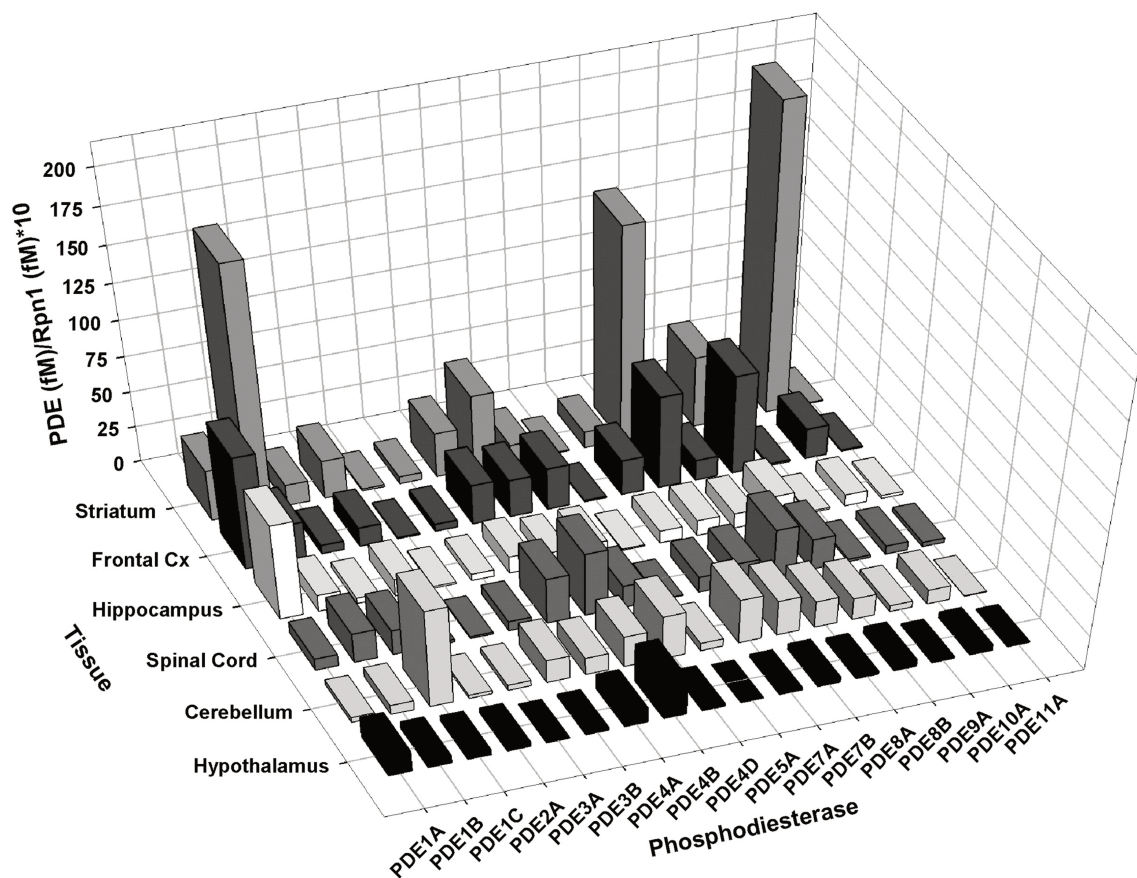


Figure 4 - PDE expression in the mouse brain is most robust in the striatum. PDE mRNA expression was quantified by qPCR. Rpn1 is the housekeeping gene Ribophorin1. PDE4C and all PDE6 isoforms are below the limit of detection. From (Kelly et al., 2014).

PDE1

Molecular features

The PDE1 family is encoded by 3 genes. Alternative promoters give rise to several protein isoforms by alternative splicing: PDE1A (nine variants), PDE1B (two variants) and PDE1C (five variants) (Maurice *et al.*, 2014). The molecular weights ranges from 58 to 86 kDa (Keravis & Lugnier, 2012).

Expression in the brain

PDE1B mRNA is highly expressed in the striatum, as well as, more marginally, in some other brain regions (Lakics *et al.*, 2010; Kelly *et al.*, 2014; Yan *et al.*, 1994; Polli & Kincaid, 1994). PDE1B expression is very similar across mice, rats (Kelly *et al.*, 2014) and humans (Lakics *et al.*, 2010). The high levels of PDE1B mRNA in caudate and nucleus accumbens (NAc) suggests that it may play an important role in signal transduction in these brain regions. At the cellular level, PDE1B is specifically and abundantly expressed in MSNs (Repaske *et al.*, 1993; Omori & Kotera, 2007; Fidock *et al.*, 2002). The importance of its functional role in the caudate has been demonstrated in PDE1B knockout mice, which exhibit locomotor hyperactivity and increased sensitivity to amphetamines (Reed *et al.*, 2002; Ehrman *et al.*, 2006).

Activity and regulation

All PDE1 isoforms hydrolyze both cAMP and cGMP. PDE1A and PDE1B preferentially hydrolyse cGMP, while PDE1C equally hydrolyses cAMP and cGMP (Bender & Beavo, 2006). PDE1B has a higher affinity (K_m) for cGMP (5 μ M) than for cAMP (33 μ M) (Poppe *et al.*, 2008).

PDE1 is the unique PDE family that is Ca^{2+} -dependently regulated via calmodulin (CaM, a 16 kDa Ca^{2+} -binding protein) complexed with four Ca^{2+} . The regulation of its activity by Ca^{2+} /CaM binding onto its N-terminal regulatory domain (which contains two Ca^{2+} /CaM binding domains), changes PDE1 conformation and increases the rate of cyclic nucleotide hydrolysis (V_{max}) without altering the affinity for cyclic nucleotides (Figure 5) (Keravis & Lugnier, 2012).

The N-terminal regulatory domain contains two phosphorylation sites: phosphorylation of PDE1B1 by calcium/calmodulin-dependent protein kinase II (CaMKII) decrease their calmodulin and Ca^{2+} sensitivities, resulting in a decrease of PDE1 activity.

Pharmacology

PDE1 inhibitors like isobutylmethylxanthine, zaprinast and vinpocetine have been used to try to determine the functional contribution of PDE1. The selectivity of these series of drugs is quite limited (Sitges & Nekrassov, 1999; Lugnier, 2006; Medina, 2011). The highly selective PDE1 inhibitors ITI-214 was moved into the clinic, with potential applications for cognitive deficits associated with schizophrenia and Parkinson disease (Table 1) (2011; Baillie *et al.*, 2019; Maurice *et al.*, 2014; Snyder *et al.*, 2016; Pekcec *et al.*, 2018). Other highly selective PDE1A inhibitors with some isoform selectivity Lu AF58027, Lu AF64196,

Lu AF66896 and Lu AF67897 were used to examine PDE1 isoforms function in the control of vascular smooth muscle cell relaxation (Khammy *et al.*, 2017). One of these novel inhibitors, Lu AF64196, was used in our study of PDE1B function in the striatum (Article #1). Lu AF64196 has a slightly higher potency for inhibiting PDE1B (K_i of 14 nM) than PDE1A (K_i of 58 nM) and PDE1C (K_i of 47 nM). Lu AF64196 also presents very low affinity towards other PDE enzymes with K_i values above 10 μ M (Khammy *et al.*, 2017).

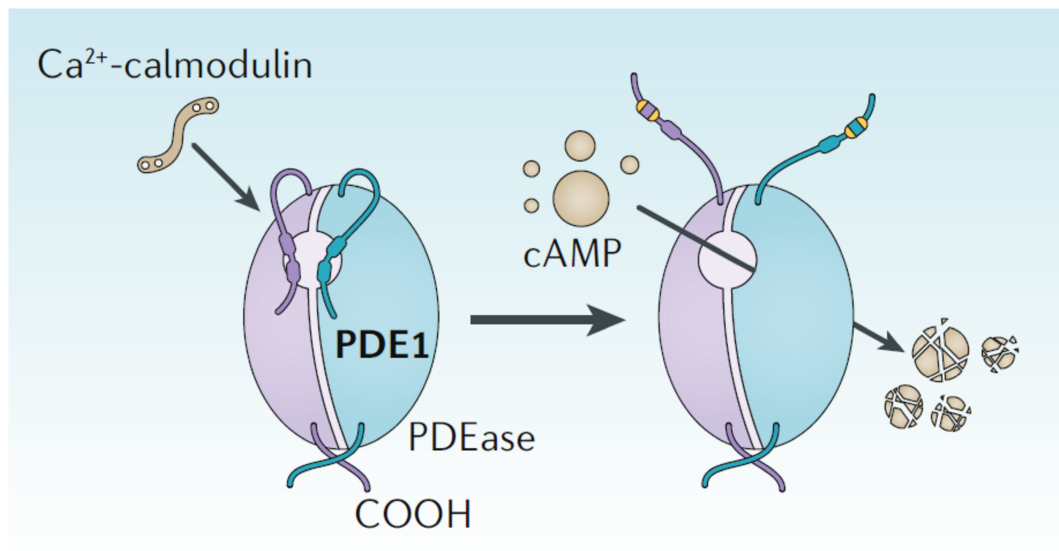


Figure 5 - Mechanism that activate PDE1 catalytic activity. Calcium-calmodulin (CaM) binding to the CaM domains of PDE1 relieves N-terminal auto-inhibition of the catalytic site, thereby promoting enzymatic activity. From (Baillie *et al.*, 2019).

Table 1 - Potential therapeutic applications of PDE inhibition, side effects and impact of knockout in mice.

PDE family	Potential therapeutic applications	Side effects of PDE inhibition	Knockout mouse phenotypes
PDE1	<ul style="list-style-type: none"> - Cerebral vascular disorders - Cognition enhancement - Ischaemic stroke - Memory impairment - Parkinson's disease - Schizophrenia 	<ul style="list-style-type: none"> - Flushing - Minor gastrointestinal disturbances - Rashes 	<ul style="list-style-type: none"> - PDE1B: increased exploratory behaviour, learning deficits, hyperactivity - PDE1C: regulation of olfaction
PDE2A	<ul style="list-style-type: none"> - Cognition and learning - Migraine - Schizophrenia 	-	<ul style="list-style-type: none"> - Embryonic death (E17)
PDE4	<ul style="list-style-type: none"> - Age-associated memory impairment - Alzheimer's disease - Anxiety - Cognition enhancement - Cognition (dementia) - Cognitive deficits in schizophrenia - Depression - Fragile X syndrome - Huntington's disease - Parkinson's disease 	<ul style="list-style-type: none"> - Decreased appetite - Diarrhoea - Dry mouth - Fainting - Headache - Hypersensitivity reactions of the skin - Insomnia - Mood changes - Nausea - Vomiting - Weight loss 	<ul style="list-style-type: none"> - PDE4A: no phenotype - PDE4B: reduced TNF response to LPA - PDE4D: delayed growth, impaired ovulation, reduced postnatal viability and refractory to muscarinic cholinergic stimulation
PDE10A	<ul style="list-style-type: none"> - Cognition enhancement - Schizophrenia - Huntington's disease 	<ul style="list-style-type: none"> - Diarrhoea - Dystonia - Flushing - Headache - Somnolence - Ventricular tachycardia - Vertigo 	<ul style="list-style-type: none"> - Decreased exploratory behaviour - Delayed acquisition of conditioned avoidance behaviour - Hypoactivity - Female PDE10A-null mice are smaller

Adapted from (Baillie *et al.*, 2019; Maurice *et al.*, 2014; Keravis & Lugnier, 2012). Abbreviations: E17, embryonic day 17; LPA, lysophosphatidic acid; TNF, tumour necrosis factor.

PDE2

Molecular features

PDE2A is the single gene in this family, with 3 alternatively spliced variants. The splice variants PDE2A2 and PDE2A3 are membrane-bound, and PDE2A1 is cytosolic (Keravis & Lugnier, 2012). Other localizations are documented for PDE2A: nuclear envelopes (Lugnier *et al.*, 1999) and the Golgi apparatus (Geoffroy *et al.*, 1999). The PDE2A has a GAF-A and a GAF-B domains. The GAF-A domain allows the dimerization of PDE2A (Martinez *et al.*, 2002).

Expression in the brain

PDE2A mRNA and protein are present at high levels in the striatum (Repaske *et al.*, 1993; Van Staveren *et al.*, 2003) and functionally active (Polito *et al.*, 2013; Wykes *et al.*, 2002; Lin *et al.*, 2010). Several human studies by Western blot, in situ hybridization, immunohistochemistry and real-time qPCR showed that the highest PDE2A levels are found in striatum, cortex and hippocampus compared with the lower expression in other brain regions (Sadhu *et al.*, 1999; Reyes-Irisarri *et al.*, 2007; Stephenson *et al.*, 2009; Stephenson *et al.*, 2012; Lakics *et al.*, 2010).

Activity and regulation

PDE2A has dual enzymatic activity, degrading both cAMP and cGMP levels (Erneux *et al.*, 1981; Martins *et al.*, 1982).

PDE2A hydrolyze cAMP (K_m of 110 μM) and cGMP (K_m of 31 μM) with similar reaction rates ($V_{\max} \sim 200 \mu\text{mol}/\text{min}/\text{mg}$) for both cyclic nucleotides (Poppe *et al.*, 2008).

A characteristic feature of PDE2A is the positive cooperativity of the substrate cGMP. Unliganded PDE2A GAF domains (GAF-A and GAF-B) of the N-terminal regulatory domain are arranged to form a parallel dimer that blocks the access of substrates to both catalytic domains of the dimeric PDE2A complex (Figure 6) (Pandit *et al.*, 2009; Wang *et al.*, 2010). The binding of sub-micromolar cGMP to the GAF-B domain of PDE2A (K_d of 10-30 μM) promotes the rotation of the monomeric catalytic domains, the removal of GAF-dependent steric hindrance and subsequent binding of the substrate (Pandit *et al.*, 2009; Wang *et al.*, 2010; Keravis & Lugnier, 2012; Bender & Beavo, 2006), resulting in a 5 to 40-fold increase in cAMP hydrolysis rate (Martins *et al.*, 1982; Martinez *et al.*, 2002; Jäger *et al.*, 2010). PKC can also phosphorylate PDE2, and thus increase its catalytic activity (Geoffroy *et al.*, 1999).

The interplay between cAMP and cGMP signals through PDE2A has been well characterized mainly in the cardiovascular system (Maurice, 2005; Nikolaev *et al.*, 2005), where cGMP-mediated allosteric regulation of cAMP hydrolysis occurs in a spatially confined cellular compartment and depends on the source of cGMP (Castro *et al.*, 2006; Stangherlin *et al.*, 2011). Regulation of cyclic nucleotides by PDE2A has already been shown in thalamic (Hepp *et al.*, 2007) and striatal neurons (Lin *et al.*, 2010; Polito *et al.*, 2013), although in the striatum the role of PDE2A at the cellular level remained to be analyzed in more detail.

PDE2A is an important target of cGMP in the striatum, and its increased activity by cGMP effectively modulates the integration of cAMP and PKA signals into MSNs (Polito *et al.*, 2013).

Pharmacology

There are several selective PDE2A inhibitors. EHNA has been used in the past, but this drug has an inhibitory action on adenosine deaminase, with a K_i of 1.5 nM.

BAY607550 (Boess *et al.*, 2004) is a selective PDE2A inhibitor (IC_{50} of 2-5 nM). BAY607550 presents a 50-fold selectivity for PDE2 compared to PDE1 and more than 100-fold selectivity compared to PDE5 and the other PDEs tested (PDE3B, PDE4B, PDE7B, PDE8A, PDE9A, PDE10A, PDE11A). BAY607550 did not show any effects on adenosine deaminase at concentrations of up to 10 μ M (Boess *et al.*, 2004). BAY607550 is commonly used in our brain slice preparations (Polito *et al.*, 2013). Inhibition of PDE2A in the brain is currently being considered for the treatment of cognitive disorders (Table 1) (Blokland *et al.*, 2006). However, this drug has fairly poor pharmacokinetics properties and passes poorly the blood brain barrier. More recent PDE2A inhibitors have been developed by Lundbeck (Redrobe *et al.*, 2014; Redrobe *et al.*, 2015). TAK-915, with some preclinical evidence of antipsychotic activity (Nakashima *et al.*, 2018) entered phase I trials.

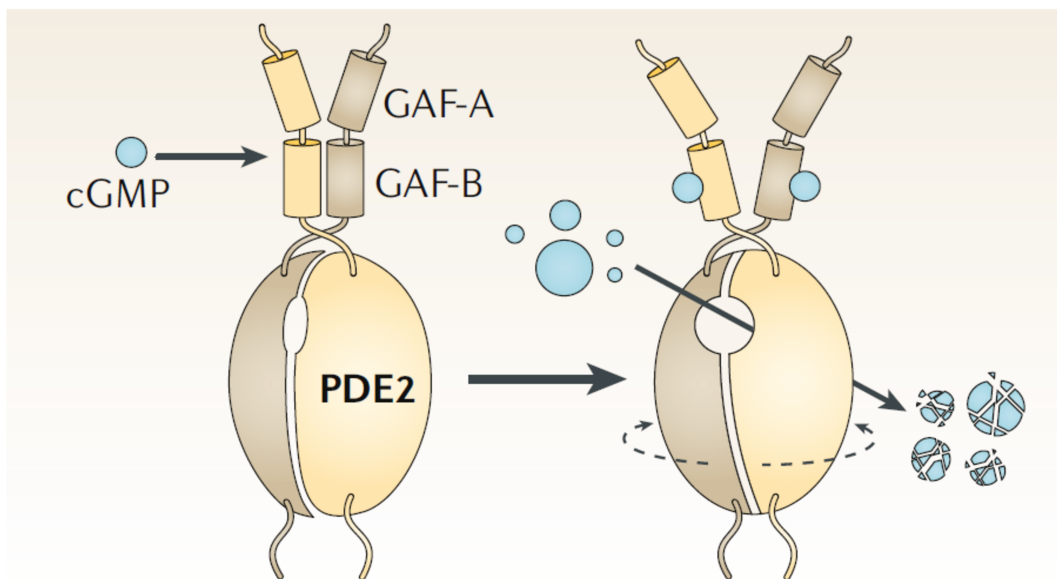


Figure 6 - Mechanism that activate PDE2 catalytic activity. cGMP binding to GAF-B domain of PDE2 are thought to promote catalytic activity by inducing an outward rotation of the catalytic domains and, thus, enabling access to substrates. Abbreviations: GAF, cGMP-binding PDEs *Anabaena* adenylyl cyclases and *Escherichia coli* FhlA. From (Baillie *et al.*, 2019).

PDE4

Molecular features

Four genes code for the PDEs of this family: PDE4A (seven variants), PDE4B (four variants), PDE4C (seven variants) and PDE4D (nine variants) (Maurice *et al.*, 2014), with a molecular weight between 50 and 125 kDa (Houslay & Adams, 2003; Bolger *et al.*, 2006). PDE4s are distinguished from other PDEs by the presence of unique N-terminal regulatory sequences, called UCR 1 and UCR 2 (Bolger *et al.*, 1993). The long isoforms of PDE4 express both UCR1 and UCR2 sequences. Short PDE4 isoforms do not express the UCR1 region, and super short isoforms express only half of the UCR2 region (Houslay *et al.*, 2007).

Long isoforms of PDE4 containing the UCR1 and UCR2 sequences can dimerize through interactions of UCR regions (Richter & Conti, 2004). These domains also determine the interaction with A kinase anchoring proteins (AKAPs), and therefore their subcellular localization (Skroblin *et al.*, 2010; Welch *et al.*, 2010; Dodge *et al.*, 2001).

Expression in the brain

In-situ hybridization studies described widespread distribution of PDE4A, B and D in human brain (Pérez-Torres *et al.*, 2000; Lakics *et al.*, 2010; Kelly *et al.*, 2014). PDE4B shows moderate expression in the striatum where its activity has been demonstrated (Nishi *et al.*, 2008).

Activity and regulation

The UCR1 region contains a phosphorylation site for PKA that upon phosphorylation prevents interaction between the UCR1 and UCR2 regions, leading to an increase in catalytic activity (factor 2) (Lim *et al.*, 1999; Beard *et al.*, 2000) (Figure 7). This PKA regulation mechanism would be a negative feedback to attenuate and limit cAMP signals. The C-terminal catalytic domain of PDE4, except for PDE4A, contains a phosphorylation site for extracellular signal-regulated kinase (ERK), which once phosphorylated allows the activation of PDE4 short isoforms and the inhibition of long isoforms (Baillie *et al.*, 2000). This bidirectional control of PKA and ERK kinases on the activity of PDE4 (long isoforms) makes it a key node in intracellular inter-signal communication: the simultaneous phosphorylation of PDE4 by PKA cancels the inhibitory effect of ERK on catalytic activity, and allows the return to a state of basal activity. More recently, additional regulators (Cdk5 and CaMKII) of PDE4 activity have been described, and support the idea that PDE4 plays a central role in the integration of cAMP / Ca²⁺ signals (Mika & Conti, 2016; Plattner *et al.*, 2015).

Pharmacology

PDE4 has been the focus of intense pharmacological research, and a number of highly selective inhibitors are available (Bender & Beavo, 2006). Among these, rolipram is selective for all PDE4 and was originally developed as a possible antidepressant or procognitive agent (Table 1) (Wachtel & Schneider, 1986; Schwabe *et al.*, 1976; Lugnier *et al.*, 1986; Lugnier *et al.*, 1993). Its clinical utility is limited by its intolerable side effects (nausea, vomiting, diarrhoea). These adverse effects can be circumvented by local application: three PDE4 inhibitors (roflumilast, apremilast and crisaborole) (Baillie *et al.*, 2019; Hatzelmann *et al.*,

2010) are currently FDA approved in the local treatment of inflammatory and respiratory diseases.

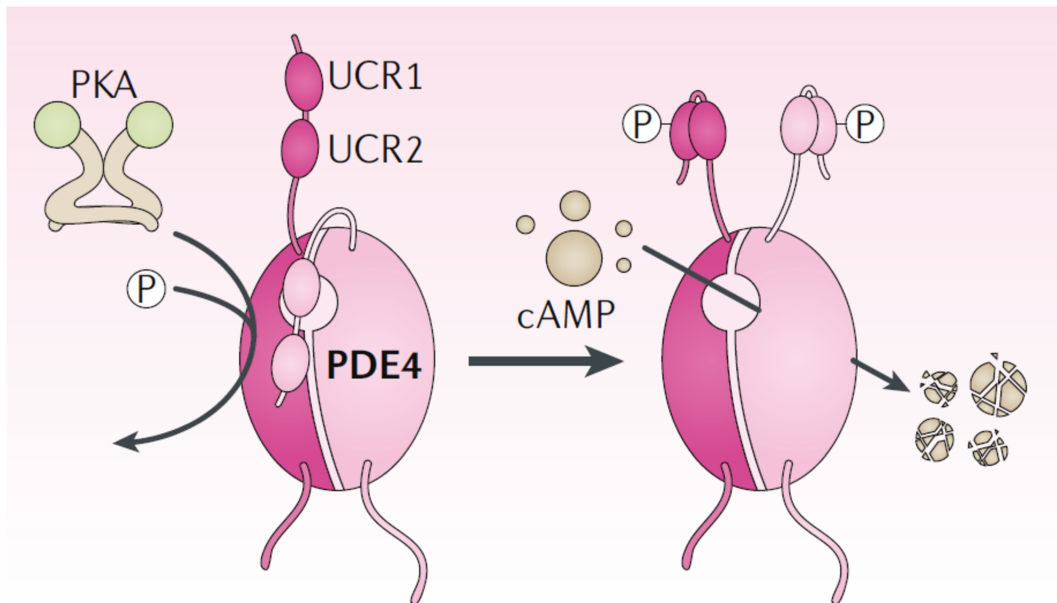


Figure 7 - Mechanism that activate PDE4 catalytic activity. Phosphorylation by protein kinase A (PKA) or protein kinase G (PKG) activates several PDEs. In the case of PDE4D, phosphorylation of the UCR1 domain by PKA causes UCR1 to bind its own UCR2 domain instead of the catalytic site of the other monomer, thereby locking the enzyme in an active state. Abbreviations: UCR, upstream conserved region. From (Baillie *et al.*, 2019).

PDE10

Molecular features

The PDE10 family is encoded by a single gene, PDE10A (Fujishige *et al.*, 1999; Fujishige *et al.*, 2000; Bender & Beavo, 2006). The PDE10A gene has 18 alternative splicing variants (PDE10A1-18) (88 kDa) (Strick *et al.*, 2006). These variants primarily differ in their N-terminal amino-acid sequence, which can result in alterations in their subcellular localization (Charych & Brandon, 2014). Preparations from striatal tissues have consistently shown that the PDE10A protein is enriched in membrane preparations (Charych *et al.*, 2010; Kotera *et al.*, 2004; Schülke *et al.*, 2014). This membrane insertion is dependent on a particular N-terminal amino acid sequence containing a CFRRLT motif, which is present in particular PDE10A variants (Figure 8). It has been shown that PDE10A is palmitoylated on Cys11 of the CFRRLT motif, which serves as an anchor for the membrane localization. Furthermore, membrane insertion is dependent on the phosphorylation status of threonine residue at position 16 (Thr16) (Charych *et al.*, 2010; Kotera *et al.*, 2004).

PDE10A2 in human (Q9Y233-2), the variant containing the N-terminal CFRRLT sequence, has been shown in many studies to be the major splice variant of PDE10A and suggests that primarily membrane-bound PDE10A contributes to cyclic nucleotide

metabolism in the striatum (Charych *et al.*, 2010; Kotera *et al.*, 2004).

A PDE10A gene product with a unique N-terminal sequence was only identified in primates (Figure 8) (MacMullen *et al.*, 2016). This isoform, named PDE10A19, lacks the N-terminal cysteine residue for membrane localization and was shown to be localized in the cytosol. Based on the number of next-generation sequencing reads, the PDE10A19 isoform is expressed to similar levels than PDE10A2, while RT-PCR experiments in the same study showed PDE10A19 to be expressed at lower levels compared to PDE10A2.

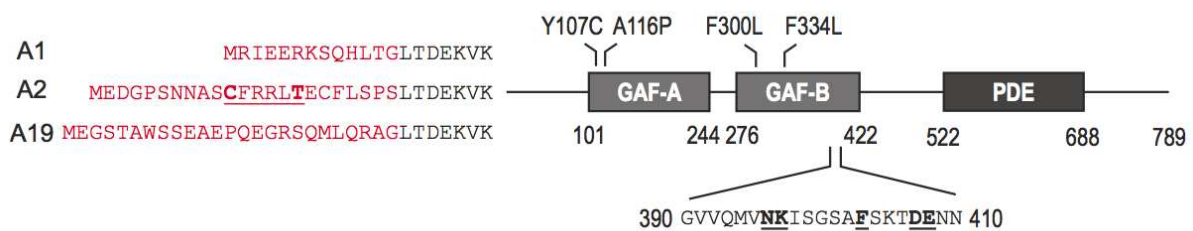


Figure 8 - Schematic representation of PDE10A. The N-terminal sequence variation in the different isoforms PDE10A1 in rat (Q9QYJ6-1), PDE10A2 in human (Q9Y233-2) and the novel, primate specific isoform PDE10A19 (MacMullen *et al.*, 2016) are highlighted in red. Cysteine 11 residue that can be palmitoylated and the threonine 16 phospho-residue within the CFRRLT sequence are highlighted in bold (Charych *et al.*, 2010). From (Schülke & Brandon, 2017).

Expression in the brain

PDE10A expression is highly similar across species and shows a unique expression pattern in the whole organism: it is found almost exclusively in the striatum (*sensus lato*) of human and rodents (Lakics *et al.*, 2010; Kelly *et al.*, 2014; Seeger *et al.*, 2003; Hebb *et al.*, 2004; Nishi *et al.*, 2008; Strick *et al.*, 2010). There is some debate as to whether there is any PDE10A expression in other CNS regions since antibodies may have some non-specific binding (Lakics *et al.*, 2010; Kelly *et al.*, 2014; Seeger *et al.*, 2003; Heiman *et al.*, 2008). Within the striatum, PDE10A is particularly highly expressed by MSNs (Seeger *et al.*, 2003; Xie *et al.*, 2006; Coskran *et al.*, 2006), and mainly located in the membrane of dendrites and spines (Charych *et al.*, 2010; Kotera *et al.*, 2004; Xie *et al.*, 2006). PDE10A is excluded from all classes of striatal interneurons (Xie *et al.*, 2006).

Activity and regulation

PDE10A hydrolyzes both cAMP and cGMP. The K_m of PDE10A for cAMP (0.25 μ M) is lower than for cGMP (1.1 μ M), and its maximum cGMP hydrolysis rate is twice that of cAMP (Poppe *et al.*, 2008). For these reasons, the hydrolysis of cGMP by PDE10A is inhibited by cAMP (competitive inhibition) (Keravis & Lugnier, 2012).

The protein sequence of PDE10A includes two N-terminal GAF domains. Unlike other PDEs, the GAF-A domain of PDE10A only seems to bind cAMP (Soderling & Beavo, 2000). A publication indicates that PDE10A is activated upon cAMP binding to the GAF-A domain (Jäger *et al.*, 2012), promoting cyclic nucleotide hydrolysis via allosteric regulation of

the distant C-terminal catalytic domain. However, another publication shows that binding of cyclic nucleotides to the PDE10 GAF domains does not stimulate catalytic activity (Matthiesen & Nielsen, 2009).

PDE10A2, contains a Thr16 that can be phosphorylated by PKA and dephosphorylated by phosphatase protein 2A (PP2A) and/or phosphatase protein 1 (PP1) but not phosphatase protein 2B (PP2B, calcineurin) (Kotera *et al.*, 1999; Russwurm *et al.*, 2015). Under basal conditions, PDE10A2 phosphorylation on Thr16 is low but can be induced by PKA. This phosphorylation by PKA at Thr16 does not change the enzymatic activity of PDE10A2 to hydrolyze cAMP, but prevents membrane localization of newly synthesized PDE10A2, due to the reduced affinity of PDE10A for AKAP150 that promote the dissociation from synaptic proteins AKAP150, NR2A, NR2B and PDS95 (Charych *et al.*, 2010; Russwurm *et al.*, 2015).

Pharmacology

Based on its selective distribution and high expression level, PDE10A has been considered a potential therapeutic target for diseases of the basal ganglia (Table 1) (Wilson & Brandon, 2015).

The PDE10 inhibitor papaverine is the historical inhibitor of PDE10, with an IC₅₀ of 36 nM (Siuciak *et al.*, 2006). However, papaverine presents relatively poor potency and selectivity and a very short exposure half-life after systemic administration (Schmidt *et al.*, 2008).

TP-10 (PF-03188212) is a potent and specific inhibitor of PDE10A (IC₅₀ of 0.3 nM), developed by Pfizer. TP-10 presents a minimal selectivity of 3000-fold for PDE10A based on IC₅₀s of greater than 1 μM for other 10 PDE families. Moreover, the minimal selectivity of TP-10 for PDE10A over other CNS targets is greater than 2500-fold (Schmidt *et al.*, 2008). It produced clear behavioral effects, and has been tested in preclinical for the treatment of schizophrenia (Schmidt *et al.*, 2008). *In vivo* administration of TP-10 increased cAMP and cGMP levels in a dose dependent manner with the cyclic nucleotide signal reaching its maximum 1 h post injection (Schmidt *et al.*, 2008). Phosphorylation of cAMP-responsive element binding protein (CREB) upon PDE10A inhibition reached its maximum after 30 min supporting the mechanism that signal transduction through dopamine and cAMP-regulated phosphoprotein of 32 kDa (DARPP-32) potentiates the effect on downstream substrates (Schmidt *et al.*, 2008). TP-10 also significantly induced expression of a CREB reporter gene *in vivo* and increased phosphorylation of histone H3-Ser10, pERK and pMEK (Kleiman *et al.*, 2011; Polito *et al.*, 2015). The effect on cAMP-PKA substrates was also shown *ex vivo* by using another tool inhibitor of PDE10A.

MP-10 (PF-2545920) is a TP-10 N-methyl analog similarly potent (IC₅₀ of 0.18 nM) (Verhoest *et al.*, 2009; Schmidt *et al.*, 2008) and has been tested in several phase II clinical trials for schizophrenia (Grauer *et al.*, 2009), both as a monotherapy and as adjunctive treatment (ClinicalTrials.gov: NCT01175135, NCT01939548). In all studies it failed to meet its primary endpoint (Verhoest *et al.*, 2009). MP-10 enhances striatal and cortical functions in a mouse model of Huntington's disease (Giampà *et al.*, 2010), and PDE10A has been shown to play a key role in the pathophysiology of Parkinson's disease (Giorgi *et al.*, 2011).

FRM-6308 (Forum) was also under evaluation in human clinical trials (Yoshikawa *et al.*, 2015).

TAK-063 was developed by Takeda (Harada *et al.*, 2015; Kunitomo *et al.*, 2014). It has potent inhibitory activity (IC₅₀ of 0.30 nM), excellent selectivity (>15 000-fold selectivity over other PDEs), and favorable pharmacokinetics in mice, including high brain penetration. TAK-063 has been evaluated in clinical trials for the treatment of schizophrenia (Yoshikawa *et al.*, 2015), but also failed to provide positive effects.

Many other highly selective and high affinity PDE10A inhibitors have been developed for the treatment of Huntington's disease, Parkinson's disease and Schizophrenia in the past 15 years by the pharmaceutical industry (Siuciak *et al.*, 2006; Menniti *et al.*, 2007; Chappie *et al.*, 2009; Chappie *et al.*, 2012; Kehler & Nielsen, 2011). However, despite encouraging results from pre-clinical models, PDE10A inhibitors failed to show efficacy as an antipsychotic in several clinical trials (Table 2) (Schülke & Brandon, 2017).

Table 2 - Clinical trials to test the efficacy of the PDE10A inhibitors in CNS diseases.

Drug name (Company)	Conditions	ClinicalTrials.gov Identifier, Phase - Status
MP-10, PF-02545920 (Pfizer)	Healthy	NCT01918202, Phase 1 - Completed (2014) NCT01244880, Phase 1 - Terminated (2012) NCT01103726, Phase 1 - Completed (2011)
	Schizophrenia	NCT01939548, Phase 2 - Terminated* (2014) NCT00570063, Phase 2 - Terminated (2008) NCT01829048, Phase 1 - Completed (2013) NCT00463372, Phase 1 - Completed (2007) NCT01175135, Phase 2 - Completed (2011)
	Huntington's Disease	NCT02342548, Phase 2 - Terminated* (2017) NCT02197130, Phase 2 - Completed (2016) NCT01806896, Phase 2 - Completed (2015)
RO5545965 (Roche)	Healthy	NCT01864226, Phase 1 - Completed (2014) NCT01711801, Phase 1 - Completed (2013)
	Schizophrenia	NCT01923025, Phase 1 - Completed (2013) NCT02019329, Phase 1 - Completed (2014) NCT02824055, Phase 1 - Completed (2017)
TAK-063 (Takeda)	Healthy	NCT02370602, Phase 1 - Completed (2014)
	Schizophrenia	NCT02477020, Phase 2 - Completed (2016) NCT01879722, Phase 1 - Completed (2014)
	Psychotic-like Symptoms	NCT01892189, Phase 1 - Completed (2014)
EVP-6308 (FORUM Pharmaceuticals)	Healthy	NCT02001389, Phase 1 - Completed (2014)
	Schizophrenia	NCT02037074, Phase 1 - Completed (2014)
Papaverine (University of Copenhagen)	Schizophrenia	NCT01813955, Early Phase 1 - Terminated** (2013)
PBF-999 (Palobiofarma SL)	Huntington's Disease	NCT02907294, Phase 1 - Terminated*** (2016)
		NCT02208934, Phase 1 - Completed (2015)

Reported on ClinicalTrials.gov (accessed July 2019).

Completed: The study has ended normally, and participants are no longer being examined or treated.

Terminated: The study has stopped early and will not start again. Participants are no longer being examined or treated.

*: The decision was not based on any safety concerns. **: Patient recruitment insufficient. ***: Change in the therapeutic indication.

PF-02545920: 2-[4-(1-Methyl-4-pyridin-4-yl-1H-pyrazol-3-yl)-phenoxy]methyl]-quinoline hydrochloride

TAK-063: [1-[2-fluoro-4-(1H-pyrazol-1-yl)phenyl]-5-methoxy-3-(1-phenyl-1H-pyrazol-5-yl)-pyridazin-4(1H)-one]

Papaverine: 6,7-Dimethoxy-1-veratrylisoquinoline hydrochloride

2. Dopamine and noncanonical GPCR signaling pathways

During my thesis I was interested in dopamine non-canonical signaling because several studies have revealed that dopamine receptors are also linked to other signaling pathways (Beaulieu *et al.*, 2004; Beaulieu *et al.*, 2005; Hasbi *et al.*, 2009), and these alternative signaling pathways may be involved in the therapeutic action of antipsychotic drugs (Bockaert *et al.*, 2010; Beaulieu *et al.*, 2015). Such mechanisms may involve alternate G protein coupling or non-G protein mechanisms involving ion channels, receptors tyrosine kinases (RTKs) or proteins such as β -arrestins (β arr) that are classically involved in GPCR

desensitization (Beaulieu *et al.*, 2015). Among these, I was particularly interested in the dopamine D₂ receptor which was reported to control Akt/GSK3-β via the recruitment of βarr (Figure 9) (Beaulieu *et al.*, 2004; Beaulieu *et al.*, 2005; Beaulieu *et al.*, 2008; Urs *et al.*, 2012). Of note, all these reports have been issued mainly from a same laboratory. Arrestins are a family of four molecular adaptor proteins that were originally characterized for their role in mediating GPCR desensitization and internalization. In addition to these functions, the two ubiquitous arrestins, βArr1 and βArr2, have also been shown to act as molecular scaffolds for signaling molecules such as kinases and phosphatases (Beaulieu *et al.*, 2005).

There are evidences that point towards the contribution of a βArr-mediated mechanism in the regulation of the serine/threonine kinases Akt and GSK3 by dopamine. Akt is involved in several cellular processes such as glucose metabolism, gene transcription, cell proliferation, migration and neurotrophin action through the stimulation of RTKs (Beaulieu *et al.*, 2015). Activation of RTKs activates phosphatidylinositol 3-kinase (PI3K), which converts phosphatidylinositol-2-phosphate (PIP2) to phosphatidylinositol-3-phosphate (PIP3). This newly formed PIP3 interacts with the pleckstrin homology domain of Akt, inducing the recruitment of Akt to the plasma membrane. This, in turn, results in the phosphorylation of Akt at the Thr308 and Ser473 residues by two phosphatidylinositol-dependent kinases, PDK1 and PDK2/ricator-mTOR respectively. Once activated, Akt phosphorylates several substrates including GSK3. Mammalian cells express two isoforms of GSK3, GSK3α and GSK3β, which are constitutively active and can phosphorylate several cellular substrates (Kaidanovich-Beilin & Woodgett, 2011). Phosphorylation by Akt inhibits both isoforms of GSK3 in response to growth factors and hormones, including insulin, IGF, and brain-derived neurotrophic factor (BDNF) (Altar *et al.*, 2008). Specifically, Akt phosphorylates Ser21 on GSK3α and Ser9 on GSK3β, which are located on their N-terminal domains (Beaulieu *et al.*, 2015).

The role of βArr2 in mediating the regulation of Akt and GSK3 by D₂ receptors is supported by direct *in vivo* biochemical observations in pharmacological and genetic models of enhanced dopaminergic neurotransmission (Beaulieu *et al.*, 2004; Beaulieu *et al.*, 2005).

The formation of the Akt : βArr2 : PP2A signalling complex in response to D₂ receptor activation represents a mechanism through which dopamine can trigger the inactivation of PI3K/Akt signalling. Moreover, the Akt : βArr2 : PP2A signaling complex dissociates in response to lithium, thus providing a probable explanation for the early behavioural observations of the antagonistic effect of lithium on dopaminergic behaviours as well as a reasonable mechanism for the activation of Akt by lithium (Beaulieu & Caron, 2008). The details of the mechanisms by which lithium triggers this dissociation are not yet fully understood (Beaulieu *et al.*, 2015).

This question is particularly interesting since biased agonism of D₂ receptors seems to be involved in the therapeutic efficacy of antipsychotic drugs (Urs *et al.*, 2017).

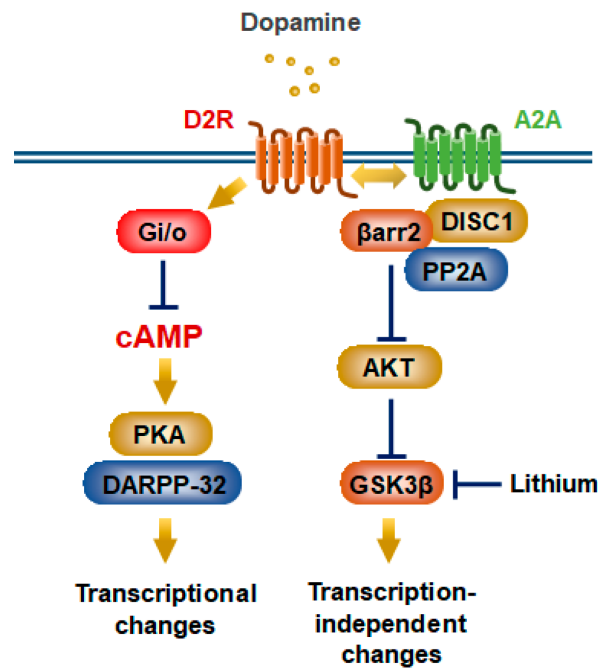


Figure 9 - Non-canonical G protein-coupled receptor (GPCR) signaling. D₂ dopamine receptor (D2R) activation stimulates a G_{i/o} protein that decreases intracellular cAMP in striatopallidal medium-sized spiny neurons (MSNs). This negatively regulates protein kinase A (PKA)/dopamine and cAMP-regulated phosphoprotein of 32 kDa (DARPP-32) signaling, eventually leading to transcriptional changes. D2R activation also facilitates its interaction with adenosine A_{2A} receptor (A_{2A}) and DISC1 (disrupted in schizophrenia 1) and induces β -arrestin2 (β arr2) signaling via heterodimeric D2R/A_{2A}, which inhibit protein kinase B (Akt) activity. Akt phosphorylates glycogen synthase kinase 3 beta (GSK3 β) to prohibit its activation. Mood stabilizer lithium negatively regulates GSK3 β activation and interferes with interaction between β arr2 and Akt. From (Komatsu *et al.*, 2019).

Activation of dopamine D₁ receptors also leads to phosphorylation of a variety of other cellular targets and activation of the mitogen activated protein kinase / extracellular signal-regulated kinase (MAPK/ERK) pathway through disinhibition of MEK by PP1 (Valjent *et al.*, 2001; Valjent *et al.*, 2005; Pascoli *et al.*, 2014). PKA activation can lead to the phosphorylation of Erk1-Thr202/Tyr204, Erk2-Thr185/Tyr187, CaMKII-Thr286. ERK was selectively activated in D1R-expressing MSNs of the NAc (shell/core) and dorsal striatum after acute or repeated administration of cocaine (Bertran-Gonzalez *et al.*, 2008), amphetamine (Gerfen *et al.*, 2008), MDMA (Doly *et al.*, 2009) or GBR12783, a selective DA reuptake inhibitor (Valjent *et al.*, 2010; Gangarossa *et al.*, 2019). ERK activation in neurons expressing D2R may be obtained by pharmacological blockade of D2Rs by haloperidol or raclopride, which also induces histone H3 phosphorylation in the dorsal striatum (Bertran-Gonzalez *et al.*, 2008; Bertran-Gonzalez *et al.*, 2009). The effects of D2R antagonists suggest that stimulation of D2Rs by basal or psychostimulant-induced DA release prevents the activation of ERK signaling events in neurons containing these receptors.

We were intrigued by reports indicating that D₂ receptor activation led to an increase in Erk activity in heterologous cellular systems (Luo *et al.*, 1998; Oak *et al.*, 2001) as well as in D2 MSNs in brain slices (Shioda *et al.*, 2017).

Interestingly, the formation of a complex between dopamine D₁ and NMDA receptors

leads to the activation of ERK, an effect which is prevented if this physical interaction is blocked. This places ERK as a critical detector of dopamine and glutamate coincidence, which is of huge importance in the theories of reward-based learning (Cahill *et al.*, 2014a; Cahill *et al.*, 2014b).

3. Genetically encoded biosensors to monitor dopamine signals

Modern-days genetically-encoded biosensors have gone through two decades of very complex evolution developed in parallel in many labs around the world. A large diversity of genetically-encoded reporter constructs are extensively applied in biological research for real-time visualization and tracking cellular events, such as small-molecule-messenger dynamics, enzyme activation and protein-protein interactions (Miyawaki, 2003; Umezawa, 2005). This chapter focuses on some biosensors specifically developed to monitor calcium, cyclic nucleotides and kinase-mediated phosphorylation events.

3.1. A sensor domain to detect a biological signal of interest

The measurement of a specific biological signal first depends on a protein domain which is selectively sensitive to this biological event, and changes its conformation in response to this event. Sensor domains for calcium were obtained and then engineered from calmodulin (Miyawaki *et al.*, 1997) and troponin C (Mank *et al.*, 2008; Thestrup *et al.*, 2014). Sensor domains for cAMP were derived from PKA (Zaccolo *et al.*, 2000) or Epac (Ponsioen *et al.*, 2004; DiPilato *et al.*, 2004; Nikolaev *et al.*, 2004), while sensor domains for cGMP derived from PKG (Honda *et al.*, 2001; Russwurm *et al.*, 2007). In Article #1, we describe a novel cGMP biosensor which uses a tandem of cGMP binding sites from PKG (Betolngar *et al.*, 2019).

A strategy for generating a genetically encoded reporter for any kinase and phosphatase is to have a substrate sequence for the protein kinase as a sensor domain, and a phosphoamino acid binding domain (PAABD) that recognizes the phosphorylated substrate sequence. The kinase of interest can phosphorylate the substrate peptide sequence, and upon phosphorylation, the PAABD forms an intramolecular complex with the phosphorylated peptide, thus inducing a large conformational change (Zhang *et al.*, 2001). Dephosphorylation of the peptide sequence by a phosphatase reverses this conformational change. Thus, this kind of biosensors report the equilibrium between phosphorylation by the kinase of interest and dephosphorylation by phosphatases. In our laboratory, we have several versions of A kinase activity reporter (AKAR), Akt activity reporter (AktAR) and Erk activity reporter (EKAR).

Other types of sensor domain can respond to protease activity, being simply a peptide link with a (moderate) selectivity towards a protease. Bacterial periplasmic proteins with a venus-flytrap shape also provided a number of sensor domain for sugars, amino-acids (Deuschle *et al.*, 2005). Sensor for measuring mechanical traction using vinculin have also known interesting developments (Grashoff *et al.*, 2010). Once the adequate sensor domain has been validated, its conformational change must somehow be detected. Fluorescence appeared to be a practical method to detect such conformational change.

3.2. Single-fluorophore biosensors

In several situations, a change in fluorescence could be obtained with a single fluorophore biosensor, such as the genetically encoded calcium indicators (GECIs) (Figure 10) (Nakai *et al.*, 2001; Mank & Griesbeck, 2008; Baird *et al.*, 1999) that allow imaging intracellular calcium transients.

Calcium-sensitive sensors GCaMPs

Among GECIs, the single-wavelength GFP-based GCaMPs (Nakai *et al.*, 2001), are the most widely used because of their high sensitivity and rapid response to changes in intracellular calcium concentrations. GCaMPs biosensors consists of circularly permuted GFP (cpGFP) fused to calmodulin and a Ca²⁺/CaM-binding myosin light chain kinase peptide (M13).

Several versions of the original GCaMP sensor (Nakai *et al.*, 2001) have been published (Ohkura *et al.*, 2005; Tallini *et al.*, 2006; Akerboom *et al.*, 2009). Recent advances in GCaMP engineering, through protein structure determination, targeted mutagenesis, high-throughput screening, and *in vitro* assays, have significantly enhanced the sensitivity by increasing the dynamic range of the fluorescence response, the Ca²⁺-saturated brightness, Ca²⁺ affinity and the signal-to-noise ratio (Tian *et al.*, 2009; Chen *et al.*, 2013).

High-performance GECIs in common usage can also function as “photoactivatable GECIs”, allowing the specification of target cell populations or organelles for functional imaging. Thus, two of the most useful features of fluorescent proteins can be combined in single reagents (Ai *et al.*, 2015).

The **strengths** of single-fluorophore biosensors with a single-wavelength detection are:

- the protein is small, which can be an advantage in viral transfection;
- some biosensors have a large signal change;
- changes in fluorescence at a single wavelength are easy to measure;
- imaging is easy and cheap to implement in any confocal or wide-field microscope;
- allows an acquisition time from tens of ms to seconds with a wide-field microscope, providing a high temporal resolution;
- it offers the possibility to combine several biosensors with different fluorescence wavelength in a same experiment;
- photoconversion of the single chromophore can be used for additional features, such as *in vivo* calcium imaging of spatially-specified subsets of neurons (or other cells) (Hoffman & Yang, 2006).

The **weaknesses** are:

- difficult to quantify: the signal changes if the light pathway is perturbed, for example when the focus changes, the preparation moves or the illumination is not stable or uniform; the quantification also depends from the biosensor concentration;
- calibration of the imaging instrument is difficult.

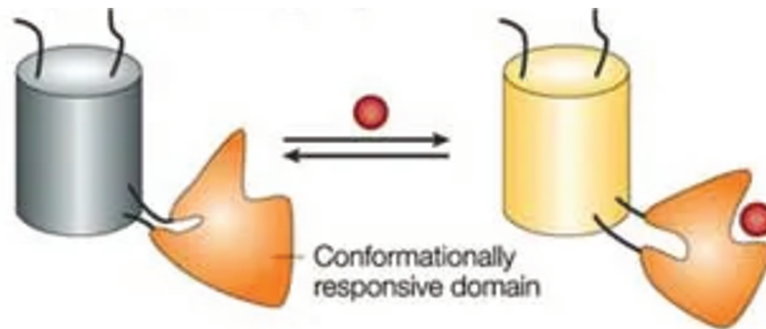


Figure 10 - Single-fluorophore biosensor. Biochemical modulation of aequorea fluorescent protein (AFP) fluorescence can be engineered to be sensitive to a conformationally responsive domain, in which fluorescence is modulated by the conformational change. From (Zhang *et al.*, 2002).

Such biosensors are difficult to use for calcium quantification in tissues since focus change and other similar experimental artifacts induce signal fluctuations. Thus, there are also GECIs to report calcium changes based on dual-fluorophore biosensors with Förster (fluorescence) resonance energy transfer (FRET), such as D3cpVenus (D3cpV) (Palmer *et al.*, 2006), YC3.60 (Nagai *et al.*, 2004), TN-XXL (Mank *et al.*, 2008) and Twitch-2B (Thestrup *et al.*, 2014).

3.3. Dual-fluorophore biosensors

Förster resonance energy transfer (FRET) to detect a conformational change

Historically, protein conformational changes were detected by labelling specific amino-acids with fluorophores such as fluorescein and rhodamine, and then measuring FRET changes between these two fluorophores as an indicator of a change in distance and/or orientation (Figure 11). FRET is a physical process whereby the energy of an excited fluorophore (the donor) is transferred by resonance to a neighboring fluorophore (the acceptor), a phenomenon that strongly depends on the relative distance and/or orientation between the donor and acceptor (Wouters *et al.*, 2001; Jares-Erijman & Jovin, 2003; Padilla-Parra & Tramier, 2012).

The Förster distance is the distance between the donor and acceptor at which 50% of FRET efficiency occurs, generally ranges between 2 and 8 nm (Padilla-Parra & Tramier, 2012).

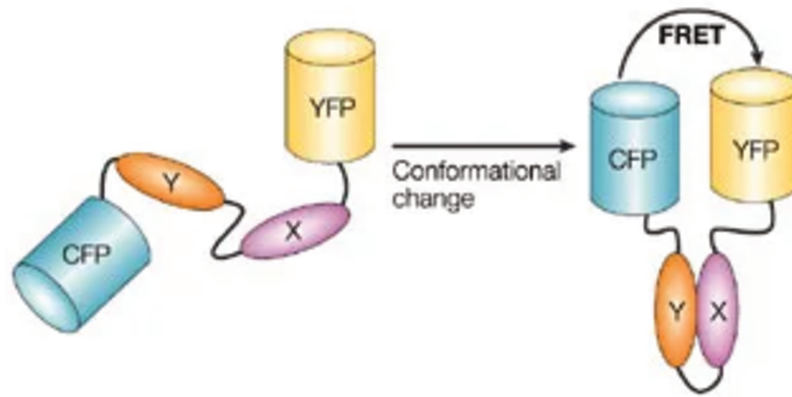


Figure 11 - Intramolecular genetically encoded FRET biosensors with two fluorophores. The conformational change of the sensor domain (here, association of X and Y domains) reduce the distance between the two fluorophores and increases FRET from the donor (CFP) to the acceptor (YFP). Abbreviations: CFP, cyan fluorescent protein; FRET, Förster Resonance Energy Transfer; YFP, yellow fluorescent protein. From (Zhang *et al.*, 2002).

A large number of biosensors use this principle: a domain sensitive to the biological signal of interest is inserted between two fluorophores, the donor and the acceptor. The biological signal triggers a conformational change of the sensor moiety, which modifies the extent of FRET from donor to acceptor upon donor excitation.

Measuring FRET changes

There are different methodological approaches to measure FRET between a donor and an acceptor, of which only two are reliable enough to be routinely used for live imaging of biosensor signals, in living cells: ratiometric FRET and fluorescence life-time imaging microscopy (FLIM).

Ratiometric approach to measure FRET

The FRET between donor and acceptor fluorophores is monitored upon donor excitation: FRET induces a reduction of the donor fluorescence intensity and an increase in acceptor fluorescence intensity. Thus the FRET process can be followed by ratiometric measurement of acceptor intensity divided by donor intensity (ratio = I_A / I_D). In this way, the ratio changes between R_{min} (the ratio for the biosensor in the conformation with the lowest FRET) and R_{max} (ratio when all the biosensor is in the activated conformation). The biosensor can thus be calibrated *in vitro* with known ligand concentrations, like we did for cGMP biosensor cyGNAL (Figure 1B, C, D in article #1).

The **strengths** of FRET detection based on intensity approaches are:

- ratiometric imaging is independent from biosensor concentration, the light pathway or the instrument employed, as long as donor and acceptors are in constant ratio, because ratiometric measurements cancels artifacts related to uneven illumination, focus change...;
- calibration of the system is easy, as long as R_{min} and R_{max} can be measured (see "Quantification and pitfalls" below)

- allows an acquisition time from tens of ms to seconds with a wide-field microscope, providing a high temporal resolution;
- low exposure duration reduces the bleaching of the fluorophores, allowing the recording of hundreds of data points on a same preparation.
- imaging is easy and cheap to implement in any confocal or wide-field microscope.

The main **weaknesses** is:

- an absolute measurement of FRET efficacy is difficult.

In conclusion, the ratio measurement can be used efficiently for intra-molecular FRET biosensors and also for inter-molecular FRET biosensors if the relative concentration of donor and acceptor is in a well-controlled molar ratio of 1:1.

Fluorescence life-time imaging microscopy (FLIM) to measure FRET

Fluorescence takes place when a molecule excited by light returns to its ground state releasing its energy through the emission of one photon. Fluorescence is a transient phenomenon taking place on a very short time (from picosecond to nanosecond range) in which the molecules stay in the excited state S1 (Figure 12).

When FRET occurs, since the energy of the donor is rapidly transferred to the acceptor, the population of excited donor declines faster, which translates into a decreased fluorescence lifetime of the donor. Since the fluorescence decay profile is independent from the concentration, FRET can be characterized by comparing the fluorescence decay of the donor alone and the fluorescence decay of the donor in FRET condition from different live samples. Thus, FLIM, by monitoring the change in fluorescence life-time of the donor fluorophore, directly reports FRET efficacy (Padilla-Parra & Tramier, 2012).

The **strengths** of FRET detection based on lifetime approaches are:

- it directly provides an absolute measurement of FRET efficiency;
- lifetime measurements are independent from biosensor concentration, even if donor and acceptors are in different stoichiometric ratio, allowing quantification of inter-molecular, as well as of intra-molecular FRET;
- the measurement is absolute and independent from the biosensor concentration, the light pathway or the instrument employed. Totally insensitive to uneven illumination, focus change...;
- since the life-time measurement is performed only at the wavelength of the donor, it offers the possibility to combine several biosensors with different fluorescence wavelength in a same experiment (Bertolin *et al.*, 2019).

The **weaknesses** are:

- signal to noise ratio is less than optimal;
- high levels of expertise required to analyze and interpret results;
- long acquisition time: several minutes with time-correlated single photon counting; several seconds with the frequency domain method;
- expensive instrumentation.

In conclusion, FLIM can be useful when a precise measurement of FRET efficacy is required, like during the process of biosensor optimization, or in the case of biosensors with

intermolecular FRET.

In my thesis work it was important to use a system with fast acquisition time providing a high temporal resolution in order to detect the fast changes in cAMP levels during phasic dopamine signals; it was also important to use a system allowing the recording of hundreds of data points on a same preparation, without the photo-destruction of the fluorophores; and, of course, it is even better if is easy and cheap to implement in a simple wide-field microscope. This is why we chose to monitor FRET-based biosensors with the ratiometric analysis.

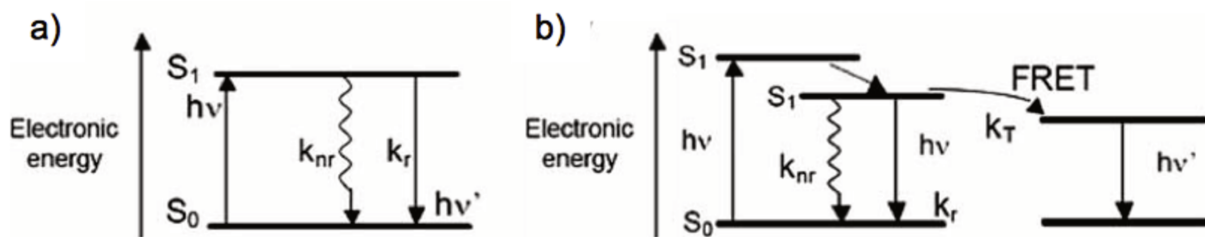


Figure 12 - Fluorescence and energy transfer through resonance. a) Modified Perrin-Jablonski diagrams showing photonic processes: after initial excitation, fluorescence occurs as a result of a photon being emitted during the decay of an excited electron from S_1 to the ground level (S_0) with a particular radiative kinetic constant. Note that other non-radiative phenomena for relaxation are also possible. b) The process of FRET is described in this diagram; the process of energy transfer is indicated with a horizontal arrow (k_T). In this case there is competition between three pathways of relaxation: energy transfer, fluorescence and nonradiative phenomena. From (Padilla-Parra & Tramier, 2012).

3.4. Biosensors for the cAMP/PKA signaling pathway

It is possible to find many fluorescent biosensors at the Fluorescent Biosensor Database (<https://biosensordb.ucsd.edu/index.php>).

FRET-based biosensors to detect cAMP

Historically, Roger Y. Tsien exploited PKA's ability to selectively bind cAMP to create the first FRET biosensor. The catalytic subunit of PKA was labelled with fluorescein (donor) and the regulatory subunit was labelled with rhodamine (acceptor): dissociation of the regulatory and catalytic subunit upon cAMP binding was monitored as a decrease in FRET between the two fluorophores (Adams *et al.*, 1991). This biosensor called FICRhR was used in invertebrate neurons (Bacskai *et al.*, 1993; Hempel *et al.*, 1996) and embryonic spinal neurons (Gorbunova & Spitzer, 2002). However, this first biochemical sensor remained impractical to use in vertebrate neurons due to the difficulty of injecting the recombinant and labeled holoenzyme into living cell, a difficult task but not impossible (Vincent & Bruscianno, 2001; Goillard & Vincent, 2002).

A great leap forward was made when genetically-encoded fluorophores became

available for making biosensors that were fully encoded genetically. The first proof of concept was designed by Atsushi Miyawaki, again in Roger Y. Tsien's lab. This biosensor used the binding of calmodulin to a M13 peptide to monitor intracellular calcium concentration (Miyawaki *et al.*, 1997). Thereafter, the first genetically encoded indicator for cAMP used the same design as FICRrhR, replacing the chemical fluorophores fluorescein and rhodamine with CFP and YFP (Zaccolo *et al.*, 2000; Lissandron *et al.*, 2005). This sensor reports the dissociation of the regulatory and catalytic subunits of PKA by a decrease in inter-molecular FRET between the fluorophores. This sensor can be targeted to different subcellular domains via AKAPs (Zaccolo *et al.*, 2006; Di Benedetto *et al.*, 2008). However, this type of sensor needs a precisely equal expression of both subunits to form the holoenzyme in the transfected cells, and any imbalance in this equilibrium can complicate ratiometric analysis and/or kill the cell. Moreover, PKA activity in this sensor could not be killed by mutation.

Both problems were solved with a single-gene genetically encoded FRET biosensors (biosensors with intra-molecular FRET) devoid of catalytic activity, which used the cAMP-binding domain B of RII β subunit of PKA as cAMP sensing domain (PKA-camps sensor) (Nikolaev *et al.*, 2004). In parallel, other sensors were developed using either the whole Epac protein or truncated forms harboring its cAMP binding domain (Nikolaev *et al.*, 2004; DiPilato *et al.*, 2004; Ponsioen *et al.*, 2004). For example Nikolaev and co-workers developed a cAMP sensor composed of a single cAMP binding domain of either Epac1 or Epac2, fused to CFP and YFP to generate Epac1-camps and Epac2-camps sensors, respectively (Nikolaev *et al.*, 2004). Epac2-camps exhibits a slightly higher cAMP sensitivity than Epac1-camps (0.9 μ M versus 2.4 μ M) and both exhibit significantly faster kinetics than the sensor based on PKA holoenzyme. A transgenic mouse line was then created with ubiquitous expression of the Epac1-camps sensor, allowing the study of the cAMP signaling in more physiological conditions (Calebiro *et al.*, 2009). Epac2-camps was further modified by mutating the cAMP binding domain to increase its sensitivity to cAMP. This sensor, called Epac2-camps300 (Norris *et al.*, 2009) has an EC₅₀ for cAMP of 0.3 μ M and is suitable for measurements of the very low cAMP levels present in mature neurons (Castro *et al.*, 2010). Another cAMP sensor was derived from the cAMP binding domain of the hyperpolarization-activated cationic channel HCN2 (Nikolaev *et al.*, 2006). This sensor called HCN2-camps, has a fairly low cAMP sensitivity with an EC₅₀ of 6 μ M.

While most biosensors use the traditional CFP/YFP pair of fluorophores, or their improved derivatives (Aquamarine, mTurquoise, Citrine, Venus...), it may be needed to perform recordings at other wavelength. Various versions of Epac-based sensors have been created with GFP donor and various yellow and red acceptors (van der Krogt *et al.*, 2008; Hong *et al.*, 2011). Some limitations of biosensor imaging include sensitivity to photobleaching, pH, and temperature, and it is therefore desirable to use the brightest as well as the most stable fluorophores in biosensor constructs. Thus, taking advantage of the CFP-derived donor fluorophore mTurquoise and using the Epac1 backbone, ¹Epac^{VV} showed improved photostability and outstanding ratio changes upon cAMP activation (Klarenbeek *et al.*, 2011). This sensor was further improved by replacing the donor with mTurquoise2 and the acceptor with a single cp174Citrine. Its sensitivity for cAMP was increased by introducing the Q270E mutation in the cAMP binding domain, yielding Epac-S^{H150} (Polito *et al.*, 2013) (Figure 13). More recently, this family of Epac-based biosensors was further improved at the level of fluorophores and linkers (Klarenbeek *et al.*, 2015).

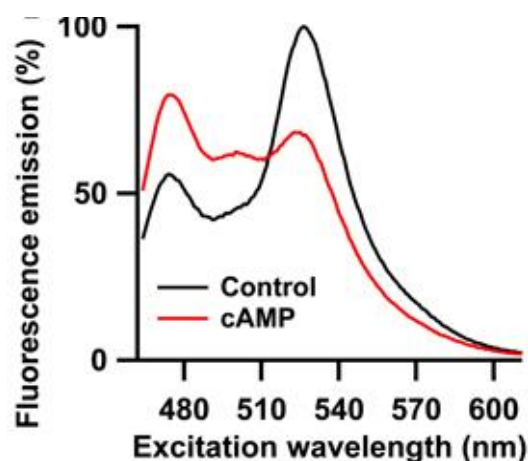


Figure 13 - The Epac-S^{H150} sensor report cAMP signals in D1 and D2 MSNs. Emission spectrum of Epac-S^{H150} in the absence and in the presence of saturating (100 μ M) cAMP. From (Polito *et al.*, 2013).

FRET-based sensors to detect PKA-dependent phosphorylation

Downstream of cAMP, PKA activity can be investigated using biosensors of a different scheme, which were actually created earlier than cAMP biosensors. The AKAR is a family of FRET biosensors composed of CFP-like as FRET donor, a PAABD, a PKA-specific substrate and YFP-like as FRET acceptor. When this protein is phosphorylated by PKA, the PAABD binds onto the phosphorylated PKA substrate, driving a conformational change which increases FRET between donor and acceptor. After the initial proof of concept of AKAR1, which lacked reversibility (Zhang *et al.*, 2001), AKAR2 (Zhang *et al.*, 2005) was a well usable reporter, rapidly superseded by AKAR3, where the acceptor was changed for a circularly permuted citrine (Allen & Zhang, 2006). Changing the CFP donor by the brighter Cerulean yielded AKAR4 (Depry *et al.*, 2011) while Aquamarine as donor led to AqAKARCit with improved photostability (Erard *et al.*, 2013).

Although commonly dubbed "PKA sensors", one must keep in mind that the phosphorylation level of the biosensor results from the equilibrium between PKA-dependent phosphorylation and dephosphorylation performed by phosphatases, and is therefore a reporter of the phosphorylation level of a PKA substrate.

3.5. Biosensors for other kinase activities

A similar strategy was followed to monitor the phosphorylation level of other kinase substrates. Among these, I was interested in observing changes in the Akt/GSK3 pathway, and in the MAPK pathway.

FRET-based sensors to detect Akt-dependent phosphorylation

The first reporter of Akt-dependent phosphorylation was the biosensor Aktus (Sasaki *et al.*, 2003). Then several FRET-based Akt biosensors were developed: BKAR (Kunkel *et al.*, 2005;

Belal *et al.*, 2014), Akind (Yoshizaki *et al.*, 2007), AktAR (Gao & Zhang, 2008; Zhou *et al.*, 2015) and Eevee-Akt (Komatsu *et al.*, 2011; Miura *et al.*, 2014). More recent versions are AktAR2 (Zhou *et al.*, 2015) and Eevee-iAkt (Miura *et al.*, 2014). AktAR2 presents an enhanced dynamic range and was generated with a brighter variant of CFP, the Cerulean3. Eevee-iAkt has the particularity to contain a long EV linker, a system that allows to have no FRET in basal conditions.

FRET-based sensors to detect ERK-dependent phosphorylation

The first FRET biosensor for ERK was EKAR (Harvey *et al.*, 2008). The original version of EKAR contained EGFP (donor), WW domain of human cdc25, an ERK substrate peptide fused with a docking domain and mRFP1 (acceptor). When activated, ERK phosphorylates the threonine in the substrate peptide (PDVPRTPVGK), which is recognized by the WW domain in the biosensor. Then several changes were done in order to improve the sensitivity and dynamic range of the biosensor. The FP pair was changed to ECFP/YPet and a longer linker (116 aa, EV-linker) was added originating EKAR-EV (Komatsu *et al.*, 2011). Changing the FP pair to mTurquoise2/ YPet originated EKAR3 (Sparta *et al.*, 2015). In my work we decided to use the biosensor EKAR-EV and an improved version with faster dephosphorylation rate for a faster read-out from ERK signaling cascade, called EKAR-EV GW4.0 biosensor developed and provided by Franck Riquet.

3.6. Quantification and pitfalls

Calibration of a ratiometric biosensor

Theoretically, the optical response of a dual wavelength (ratiometric) sensor can be calibrated to convert the ratio value into an absolute ligand concentration. This was initially established for chemical calcium dyes (Grynkiewicz *et al.*, 1985) and the same equations apply to cAMP sensors (Violin *et al.*, 2008; Mironov *et al.*, 2009; Börner *et al.*, 2011). This calibration uses the EC_{50} and Hill coefficients, determined *in vitro* for most published cAMP sensors. In addition, the conversion of ratio measurements into cAMP concentrations requires the determination of R_{min} and R_{max} , which are the ratio values in the absence and in the presence of saturating concentrations of cAMP, respectively. R_{max} is obtained by maximally stimulating ACs with forskolin together with inhibiting PDEs with IBMX, or using a membrane permeant cAMP analogue like 8-Br-2'-O-Me-cAMP-AM. This is why all our experiments are terminated by the application of a forskolin and IBMX application. R_{min} may be obtained by inhibiting ACs with dideoxy-adenosine, SQ22536 or MDL-12,330A (Castro *et al.*, 2013; Polito *et al.*, 2015; Mironov *et al.*, 2009; Börner *et al.*, 2011). In MSNs, SQ22536 (200 μ M) slightly decreased the basal ratio of the Epac-S^{HI50} biosensor, indicating a basal cAMP concentration in the range of 100 nM.

Buffering effect

Biosensor concentration may complicate the interpretation of biosensor measurements: if biosensor molecules are present in large excess compared to cAMP, only a

small fraction of the biosensor will be activated and the ratio will report a lower cAMP concentration than what would have occurred if the biosensor was at lower concentration. In parallel, excessive biosensor concentration, by buffering cAMP, also prevents cAMP from acting on its physiological targets.

Biosensor concentration is usually in the sub-micromolar range, a concentration that should not affect the biological signal. However, biosensor concentrations of several tens of micromolar can be reached easily (van der Wal *et al.*, 2001; Drobac *et al.*, 2010), where it certainly impacts the concentration measurement. While determining accurately the concentration of a biosensor inside a living cell is technically delicate, it is quite easy to verify the impact of biosensor concentration on the cAMP responses by plotting the amplitude of the cAMP response versus the biosensor fluorescence level: low fluorescence intensity, indicative of low biosensor expression level, should be associated with responses of larger amplitude whereas high fluorescence intensities, indicative of large biosensor concentrations, potentially buffering effect, should be associated with ratio responses of smaller amplitude. This negative trend was not observed in pyramidal cortical neurons showing that a buffering effect did not affect the responses in these precise conditions (Castro *et al.*, 2013). However, the buffering effect was clearly measured in vascular smooth muscle cells, with a statistically lower cAMP response in the cells expressing the biosensor at the highest level (Figure 5 in (Vallin *et al.*, 2018)). Simulations using a model built from our biosensor recordings showed that this buffering effect is negligible in MSNs (Yapo *et al.*, 2017).

4. Striatum as a target of dopamine inputs

During my thesis I was particularly interested in how MSNs from dorsomedial striatum respond to dopamine inputs.

4.1. Anatomy of the striatum

The striatum is the largest nucleus of the basal ganglia and can be anatomically divided into functionally distinct regions that differ in their connectivity and modulatory inputs (cortical, thalamic and dopaminergics) (Nicola, 2007):

- the **dorsal striatum** receives dopaminergic inputs from the SNc and is involved in coordination of motor function. The dorsomedial striatum (DMS, caudate nucleus in primates) receives glutamatergic inputs primarily from association cortices (from motor cortex, participates in spatial learning and executive functions) whereas the dorsolateral striatum (DLS, putamen in primates) receives glutamatergic inputs from sensorimotor cortex, and participates in procedural learning, conditioned responses learning, “habituation” and sensorimotor control.
- the **ventral striatum** (or NAc) receives glutamatergic inputs from frontal cortex and limbic regions and dopaminergic inputs from the VTA. The ventral striatum is involved in attention, motivation and reward behavior. It can be further subdivided into core and shell regions.

4.2. Striatal neurons

Despite the existence of different functional territories, the striatal tissue appears homogeneous, and neurons share a number of common cellular features. Of note, the striatum lacks intrinsic glutamatergic neurons.

Striatal neurons have been characterized at the anatomical, biochemical and physiological levels (Kawaguchi *et al.*, 1995; Wilson, 1993).

Medium-sized spiny neurons (MSNs)

Common features of MSNs

Anatomy

Spiny projection neurons are also known as medium-sized spiny neurons (MSNs), due to the medium size of their soma and numerous dendritic spines. MSNs represent the vast majority (>95%) of all striatal neurons (Kemp & Powell, 1971a). The total number of MSNs within the striatum seems to be similar between different rodent species, being about 5.58 million for the rat (Oorschot, 1996). In the human there are thought to be 100 million MSNs (Lange *et al.*, 1976). MSNs have a cell body diameter of 20 μm in Human (Lanciego *et al.*, 2012) and about 12 μm in rodents (Oorschot, 1996). MSNs are multipolar stellate cells (rounded or polygonal cell bodies) with radially oriented four to eight spine-free primary dendrites (Lanciego *et al.*, 2012). These dendrites usually branch within 30 μm of the soma, giving rise to secondary dendrites of more variable length (Wilson & Groves, 1980). These dendrites are covered by small postsynaptic specializations called dendritic spines (Lanciego *et al.*, 2012). Dendritic spines appear at distances more than 20 μm from the cell body, and maintained a high density throughout the remainder of the dendritic length. Third- and fourth-order dendrites were traced to their terminations at distances of up to 280 μm from the cell body. The main branch of the axon could be followed for a distance of over 500 μm from the cell body of origin (Wilson & Groves, 1980).

Biochemistry

Adenylyl cyclase type 5 (AC5) is the predominant AC isoform in MSNs, that integrate signals from multiple receptors including D_1 , D_2 , and A_{2A} through the production (or not) of the second messenger cAMP (Lee *et al.*, 2002; Doyle *et al.*, 2019).

A particularity of striatum is that the G-protein that stimulates AC5 is $G_{\alpha_{\text{olf}}}$ instead of $G_{\alpha_{\text{s}}}$. $G_{\alpha_{\text{olf}}}$ G-protein is activated by D_1 and A_{2A} receptors. Once activated, $G_{\alpha_{\text{olf}}}$ binds to AC5. The duration of the AC5 activation due to $G_{\alpha_{\text{olf}}}$ is limited by the GTPase activity of the G-protein, which acts as the deactivation mechanism of the G-protein. The binding of $G_{\alpha_{\text{olf}}}$ with AC5 induces cAMP production.

All MSNs use GABA as a neurotransmitter (GABAergic), thus they act by inhibiting their targets. In contrast to most other brain regions, in the striatum, the GABAergic MSNs form the sole output to downstream basal ganglia nuclei.

Electrophysiology

Electrophysiologically, D1 and D2 MSNs exhibit similar properties, and many studies have considered them as a single cell type (Kreitzer, 2009). Under resting conditions MSNs are hyperpolarized and silent due to a high potassium conductance (Tepper & Bolam, 2004). Increased activity of many convergent corticostriatal neurons (and possibly thalamostriatal neurons as well) depolarizes MSNs to the up state, from which additional excitatory inputs, an alteration in the strength of the synapses or an alteration in the balance of excitatory and inhibitory inputs leads to the firing of action potentials (Tepper & Bolam, 2004).

MSNs can be divided into two approximately equally sized subpopulations (D1 and D2 MSNs) based on their **(1) anatomical** connectivity (axonal projection targets) to other basal ganglia nuclei (as represented in figure 14), their **(2) biochemical and physiological properties**, like selective expression of different neuropeptides and receptors, their opposite **(3) dopamine modulation** on the direct and indirect pathways (Figure 15), which plays a pivotal role in their **(4) motor control**.

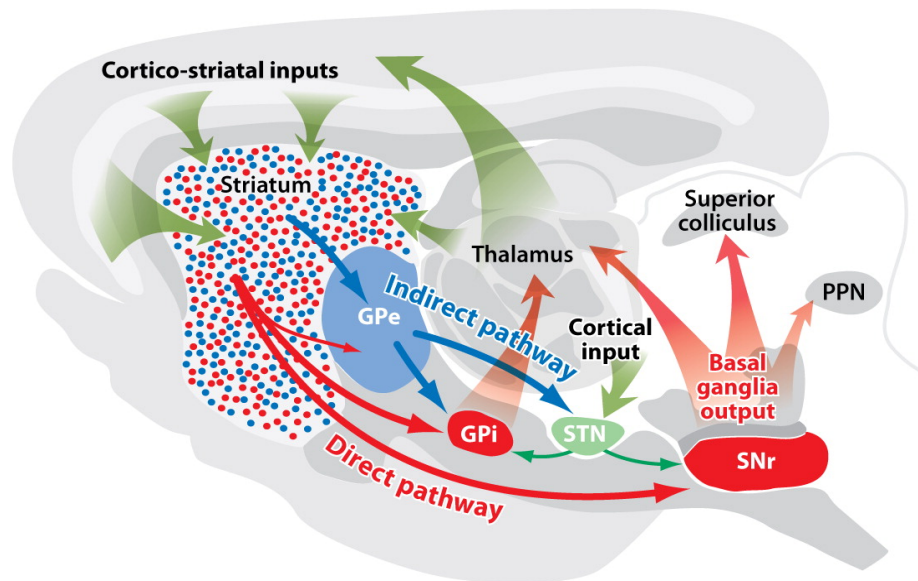
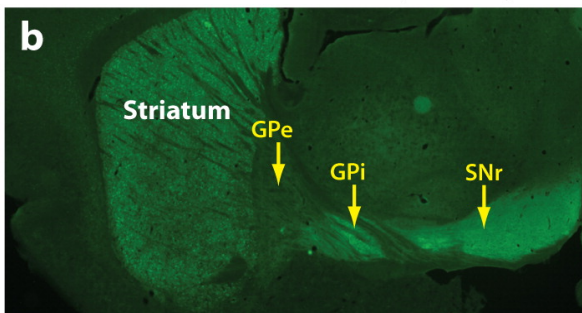
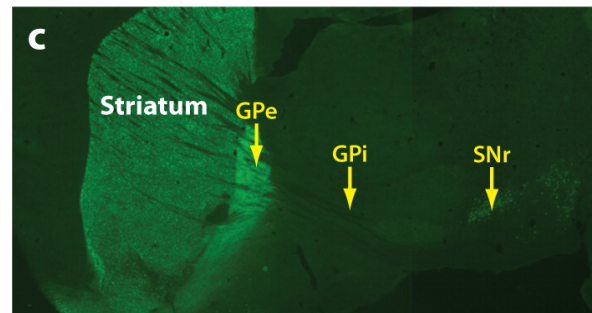
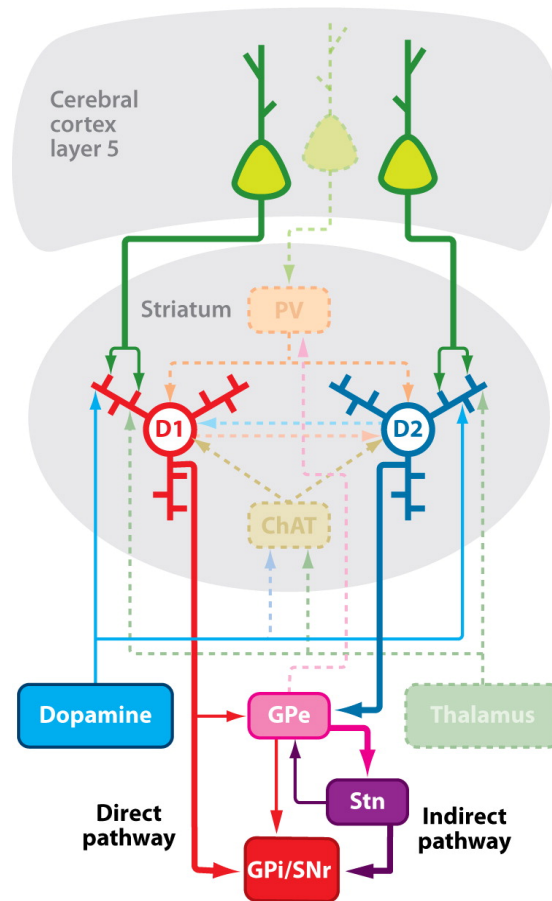
a**Basal ganglia circuits****Drd1a BAC-EGFP (direct pathway)****Drd2 BAC-EGFP (indirect pathway)**

Figure 14 - Mouse basal ganglia circuit organisation. Basal ganglia nuclei and their major connections in mouse, shown in a sagittal section. The direct pathway is shown in red, the indirect pathway in blue. Green arrows represent connections shared by multiple pathways. Red and blue dots represent direct pathway- and indirect pathway-medium spiny neurons, respectively. (a) The striatum receives excitatory corticostriatal and thalamic inputs. Outputs of the basal ganglia arise from the GPi and SNr, which are directed to the thalamus, superior colliculus and PPN. The direct pathway originates from D1-expressing MSNs that project to the GPi and SNr output nuclei. The indirect pathway originates from D2-expressing MSNs that project only to the GPe, which together with the STN contain transsynaptic circuits connecting to the basal output nuclei. The direct and indirect pathways provide opponent regulation of the basal ganglia output interface. (b) Fluorescent imaging of a brain section from a mouse expressing enhanced green fluorescent protein (eGFP) under regulation of the *Drd1a* promoter shows *Drd1a*-expressing MSNs in the striatum that project axons through the GPe, which terminate in the GPi and GPe. (c) Fluorescent imaging of a *Drd2*-eGFP mouse shows that labeled MSNs provide axonal projections that terminate in the GPe but do not extend to the GPi or SNr. Abbreviations: GPe, external segment of the globus pallidus; GPi, internal segment of the globus pallidus; MSNs, medium-sized spiny neurons; PPN, pedunculopontine nucleus; SNr, substantia nigra pars reticulata; STN, subthalamic nucleus. From (Gerfen & Surmeier, 2011).



Corticostriatal and direct/indirect pathway canonical striatal microcircuits

Figure 15 - Basal ganglia microcircuits. Cortico-striatal and direct/indirect pathway canonical circuits. Layer 5 cortical pyramidal neurons provide excitatory glutamatergic inputs to the spines of Drd1a (D1) and Drd2 (D2) medium-sized spiny neurons (MSNs). D1 MSNs give rise to striatal direct-pathway projections to the output nuclei of the basal ganglia GPi/SNr, whereas D2 MSNs give rise to striatal indirect-pathway projections to basal ganglia output nuclei. Dopamine input through the nigrostriatal pathway is directed to the spine necks of D1 and D2 bearing MSNs to modulate corticostriatal inputs. In gray is represented feedforward, feedback, and intrinsic striatal circuits. One feedforward circuit involves fast-spiking, PV GABAergic interneurons that provide perisomatic synapses on both D1 and D2 MSNs. These PV neurons receive excitatory inputs from layer 5 corticostriatal neurons and are inhibited by the GPe. Intralaminar thalamic nuclei provide inputs to D1 and D2 MSNs as well as contribute to a feedforward circuit involving thalamostriatal inputs to ChAT interneurons that provide input to both D1 and D2 MSNs. Cholinergic neuron activity is also affected by dopamine inputs. Feedback striatal microcircuits involve interconnections between local axonal collaterals of D1 and D2 MSNs that make synaptic contact with other MSNs. Abbreviations: ChAT, cholinergic; GPe, external segment of the globus pallidus; GPi, internal segment of the globus pallidus; PV, parvalbumin; SNr, substantia nigra pars reticulata; STN, subthalamic nucleus. From (Gerfen & Surmeier, 2011).

D1 MSNs: striatonigral MSNs in direct pathway

Anatomy

D1 MSNs correspond to approximately half of MSNs that project directly to the main output nuclei of the basal ganglia, the GPi (in primates; or medial globus pallidus, MGP or entopeduncular nucleus in rodents) and SNr (Gerfen, 1992b; Smith *et al.*, 1998);

Biochemistry

They are classically characterized by the expression of type 1 dopamine receptors (D1R) and M4 muscarinic receptor (Chrm4) (Harrison *et al.*, 1996; Ince *et al.*, 1997; Beckstead, 1988; Gerfen *et al.*, 1990); these neurons also express neuropeptides substance P and dynorphin (Chesselet & Graybiel, 1983; Beckstead & Kersey, 1985; Le Moine & Bloch, 1995; Hersch *et al.*, 1995; Gerfen, 1992a; Bertran-Gonzalez *et al.*, 2008; Bateup *et al.*, 2008; Matamales *et al.*, 2009).

Dopamine modulation

In D1 MSNs, dopamine activates D1Rs, which are coupled to G_{olf} that activate AC5 activity, increasing the second messenger cAMP and excitability in direct pathway MSNs. Symmetrically, activation of muscarinic M4 receptors efficiently decreases cAMP and opposes the D1 response (Nair *et al.*, 2019).

The cAMP/PKA signaling pathway potentiates glutamatergic synapses responsible for the transition to the up-state, and the ion channels controlling spiking. In the somatic region where spikes are generated, D_1 receptor stimulation and PKA activation increases Cav1 L-type Ca^{2+} channel currents and decreases somatic K^+ currents (Galarraga *et al.*, 1997; Gao *et al.*, 1997; Kitai & Surmeier, 1993; Surmeier *et al.*, 1995). In addition, D_1 receptor signaling decreases the opening of Cav2 Ca^{2+} channels that control activation of Ca^{2+} -dependent, small-conductance K^+ (SK) channels that slow repetitive spiking in MSNs (Surmeier *et al.*, 1995; Vilchis *et al.*, 2000). These effects induce the increase spiking of direct-pathway MSNs with somatic depolarization. A number of studies also show that D_1 receptor, in contrast to D_2 receptor, has positive effects on AMPA and NMDA receptor function and trafficking. For example, D_1 receptor activation of PKA enhances surface expression of both AMPA and NMDA receptors (Hallett *et al.*, 2006; Snyder *et al.*, 2000; Sun *et al.*, 2005).

Motor control

Activation of direct pathway neurons disinhibits the striatonigral pathway by reducing the activity of inhibitory GABAergic neurons in the SNr (Chevalier *et al.*, 1985; Deniau & Chevalier, 1985). Consistent with its role in controlling movement, optogenetic stimulation of the direct pathway neurons increased locomotor activity (Kravitz *et al.*, 2010). Hence, direct activation of direct pathway neurons facilitates intended movement (**go pathway**) (Graybiel, 2000).

D2 MSNs: striatopallidal MSNs in indirect pathway

Anatomy

D2 MSNs correspond to the other half of MSNs that only connect indirectly to basal ganglia output nuclei through a polysynaptic pathway. These MSNs project to the GPe (in

primates; or lateral globus pallidus, LGP in rodents). The GPe neurons project to the glutamatergic neurons of the STN (Gerfen, 1992b; Smith *et al.*, 1998). Activity within this indirect-pathway circuit is also modulated by excitatory cortical input to the STN.

Biochemistry

They express the type 2 dopamine receptor (D2R) and adenosine A_{2A} receptors (A_{2A}) (Schiffmann *et al.*, 1991; Fink *et al.*, 1992; Schiffmann & Vanderhaeghen, 1993; Beckstead, 1988; Gerfen *et al.*, 1990), and contain the neuropeptide enkephalin (Chesselet & Graybiel, 1983; Beckstead & Kersey, 1985; Le Moine & Bloch, 1995; Hersch *et al.*, 1995; Gerfen, 1992a; Bertran-Gonzalez *et al.*, 2008; Bateup *et al.*, 2008; Matamalas *et al.*, 2009).

Dopamine modulation

In D2 MSNs, dopamine activates D2Rs, which are coupled to G_i that block AC5 activity, decreasing the second messenger cAMP and reduce activity of the indirect pathway (Zhuang *et al.*, 2000). In contrast, adenosine increases cAMP through the activation of G_{o1r}-coupled A_{2A} purinergic receptors (Yapo *et al.*, 2017).

In contrast to D1 MSNs, D₂ receptor signaling impedes the up-state transition and diminishes up-state spiking in indirect-pathway MSNs (Surmeier *et al.*, 2007). D₂ receptors exert almost diametrically opposing effects on indirect-pathway MSNs. Activation of D₂ receptor signaling reduces inward, depolarizing currents through Cav1 (L-type) Ca²⁺ channels and Nav1 Na⁺ channels, while increasing outward, hyperpolarizing K⁺ channel currents (Greif *et al.*, 1995; Hernandez-Lopez *et al.*, 2000; Kitai & Surmeier, 1993; Olson *et al.*, 2005; Schiffmann *et al.*, 1998; Surmeier *et al.*, 1992). D₂ receptor stimulation also decreases dendritic Ca²⁺ entry through voltage-dependent ion channels (Day *et al.*, 2008; Higley & Sabatini, 2010), reduces glutamatergic signaling (Bamford *et al.*, 2004). Activation of D₂ receptors also decreases AMPA receptor currents of MSNs (Cepeda *et al.*, 1993; Hernández-Echeagaray *et al.*, 2004), through D₂ receptor-triggered dephosphorylation of GluR1 subunits, which should promote trafficking of AMPA receptors out of the synaptic membrane (Håkansson *et al.*, 2006).

Motor control

Activation of indirect pathway neurons resulted in inhibition of movement (Kravitz *et al.*, 2010) and suppresses movement (**no-go pathway**) (Graybiel, 2000).

Thus, the standard model of the basal ganglia is built on the segregation of information processing in the direct and indirect pathways, which act in opposing directions to control movement. The D1 and D2 MSNs activity is associated with either the initiation of movement or action suppression, respectively (Graybiel, 2000).

Co-expression of D₁ and D₂ receptors in MSNs

While the segregation of D₁ and D₂ receptors on two types of MSNs is now widely accepted (Gerfen *et al.*, 1990; Gertler *et al.*, 2008; Valjent *et al.*, 2009), co-expression of D₁ and D₂ receptors occurs in a few striatal MSNs. D1/D2 MSNs from mice are morphologically distinct from the D1 and D2 MSNs: they have a smaller cell body, a less profusely arborized dendritic tree with fewer dendritic spines than those of the D1 and D2 MSNs (Gagnon *et al.*,

2017). They are uniformly scattered throughout the striatum, where they represent approximately 2% of the total number of MSNs, but heterogeneously distributed and more abundant in the NAc, where their proportion ranged from 7 to 15% of all MSNs (Gagnon *et al.*, 2017). These proportion is in agreement with figures reported in other studies conducted in bacterial artificial chromosome (BAC) transgenic mice (Thibault *et al.*, 2013; Bertran-Gonzalez *et al.*, 2008; Escande *et al.*, 2016).

Imaging levels of PKA-mediated phosphorylation in MSNs from dorsomedial striatum of mouse brain slices by two-photon microscopy showed that 53% of striatal cells responded to D₁ receptor agonist, 40% responded to the A_{2A} receptor agonist, 5% responded to neither agonist and 2% responded to both D1 and A_{2A} agonists (Castro *et al.*, 2013). However, the imaging of cAMP levels never showed a MSN responding simultaneously to D1 and D2 agonist (Yapo *et al.*, 2017).

Interneurons

MSNs receive synapses from interneurons as well as axon collaterals from other MSNs (Tepper *et al.*, 2004).

Aspiny interneurons (Figure 16) are rare in number, comprising altogether ~5% of striatal neurons (Rymar *et al.*, 2004; Kawaguchi, 1997; Bolam *et al.*, 2000; Tepper & Bolam, 2004; Tepper *et al.*, 2008; Kreitzer, 2009; Kawaguchi *et al.*, 1995), and can be categorized anatomically into:

- **medium-sized aspiny GABAergic interneurons** (Table 3), that represent 2-3% in rodent of all neostriatal neurons (Rymar *et al.*, 2004), and possibly up to 23% in primates (Graveland *et al.*, 1985). The diversity of striatal interneurons is far greater than originally thought. In addition to the three classically described striatal GABAergic interneurons (parvalbumin, somatostatin, calretinin) there are at least four additional cell types: tyrosine hydroxylase (TH)-expressing interneurons (THIN), neurogliaform (NGF) interneuron, fast adapting interneurons (FAI) and spontaneously active bursty interneurons (SABI); and it is likely that all of them were not yet found (Tepper *et al.*, 2018).
- **large aspiny cholinergic interneurons**, that can be physiologically characterized by their significant hyperpolarization-activated currents and spontaneous activity under physiological conditions (Wilson *et al.*, 1990). They are also known by giant aspiny interneurons, because they are the largest neurons in the striatum, with a somatic diameter that can be in excess of 40 μm . They are also called tonically active neurons (TANs), due to their characteristic pattern of activity (typically firing slowly and regularly, with action potentials of long duration and lengthy and slow spike after-hyperpolarizations) (Wilson *et al.*, 1990).

Table 3 - Main characteristics of striatal GABAergic interneurons.

Striatal GABAergic interneurons	Markers	Connectivity with MSNs
FS , fast spiking interneurons	PV	high ~80%
LTS , low-threshold spiking interneurons	NPY/NOS/SOM	low ~20%
CR , calretinin-expressing interneurons	CR	?
TH , tyrosine hydroxylase-expressing interneurons	TH	low ~20% reciprocal
NFG , neurogliaform interneurons	NPY	high ~80%
FA , fast adapting interneurons	Htr3a	high ~50%
SAB , spontaneously active bursty interneurons	Htr3a	No (4%)

Adapted from (Tepper *et al.*, 2018). Abbreviations: CR, calretinin; FS, fast spiking; Htr3a, ionotropic serotonin receptor 5HT3a; SOM, somatostatin; NPY, neuropeptide Y; NOS, nitric oxide synthase; PV, parvalbumin; TH, tyrosine hydroxylase.

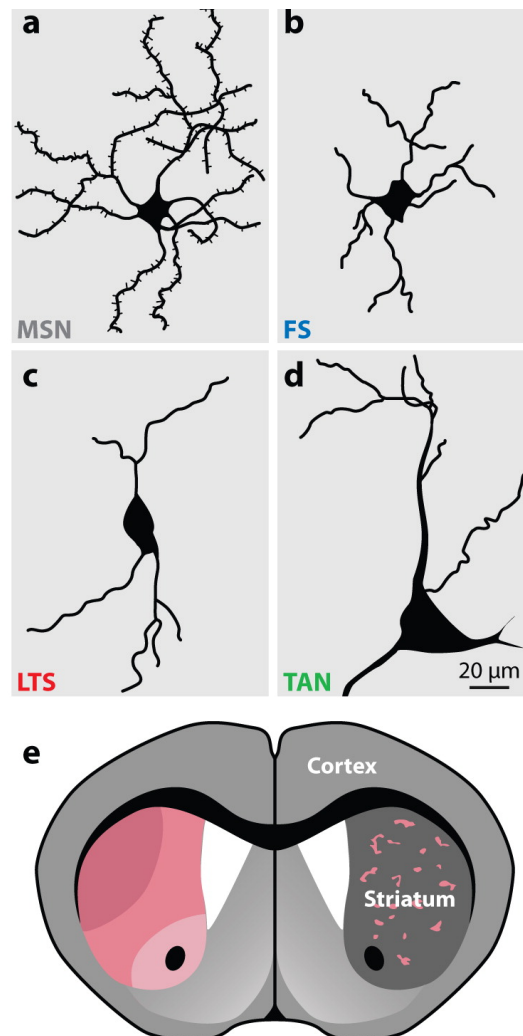


Figure 16 - Cell types and functional organization of the rodent striatum. Schematic representations of (a) a striatal medium spiny neuron (MSN), (b) a fast spiking (FS) interneuron, (c) a low-threshold spiking (LTS) interneuron, and (d) a cholinergic tonically active neuron (TAN). Drawings based on images from (Kawaguchi, 1993). (e) A coronal schematic of the mouse forebrain depicting the cortex and striatum. Striatal patches (pink) are illustrated in the right hemisphere, and the dorsolateral, dorsomedial, and ventral divisions of the striatum are schematically illustrated in the left hemisphere. From (Kreitzer, 2009).

The GABAergic interneurons produces a strong inhibitory postsynaptic potential in MSNs, the function of which is probably to influence the precise timing of action potential firing in either individual or ensembles of MSNs (Tepper & Bolam, 2004). By contrast, the role of cholinergic interneurons is to modulate the sub- and supra-threshold responses of MSNs to cortical and/or thalamic excitation, particularly in reward-related activities (Tepper & Bolam, 2004).

4.3. Neuromodulatory inputs to MSNs

The GABAergic MSNs as well as GABAergic interneurons can release GABA in the striatum. MSNs receive glutamatergic excitatory inputs from cortex and neuromodulatory inputs: dopaminergic from SNc and VTA as described above, as well as serotonergic from raphe nucleus. There are many more neurotransmitters and neuromodulators in the striatum, but in this thesis I focused on dopamine. I was also interested in glutamate and NO as activators of PDE1 and PDE2, respectively.

Dopamine

The striatum is heavily innervated by dopaminergic inputs from different midbrain regions (Prensa & Parent, 2001). MSNs are a target of midbrain dopaminergic neuron axons that can form synapses on MSNs dendrites and spine necks (Smith *et al.*, 1994). However, most of the dopamine input is released by varicosities on axon branches without a specific synaptic structure, leading to massive "volume transmission" (Wickens & Arbuthnott, 2005).

All midbrain dopamine (DA) neurons share a core genetic program to produce the neurotransmitter dopamine. However, DA neurons have diverse functions that can in part be explained by their heterogeneity. DA neuron subtypes may have unique axonal projections, synaptic inputs, physiological properties, or functional roles (Poulin *et al.*, 2018). Several dopamine neuron subtypes were identified and classified, with distinct molecular, anatomical, and functional properties.

Anatomical classification of DAergic neurons is based in three midbrain clusters located in the VTA, the SNc, and a third smaller cluster, found in the retrorubral area (RR) (Björklund & Dunnett, 2007). However, these regions are composed of molecularly heterogeneous DA neuron populations (Poulin *et al.*, 2014; Poulin *et al.*, 2018).

At molecular level, heterogeneous expression of markers in the dopamine system has been reported (Poulin *et al.*, 2018; Gerfen *et al.*, 1987; Fu *et al.*, 2012). Several markers related to distinct DA neurons were identified and localized in the adult mouse brain by single-cell gene expression profiling (Poulin *et al.*, 2014). Each DA subpopulation has specific expression profiles of transcription factors, channels, receptors, DA related genes, neuropeptides and secretory factors (Poulin *et al.*, 2014).

DA neuron subtypes possess distinct but partly overlapping projection patterns, even within a given target region. They present distinct DAergic pathways arising from the SNc and from the VTA that innervate specific regions of the caudate putamen, NAc and amygdala (Poulin *et al.*, 2014; Poulin *et al.*, 2018).

Besides dopamine, neurons from SNc can also release GABA, which may modulate the response to dopamine.

Other inputs

MSNs receive massive glutamatergic inputs from the cortex and thalamus that terminate predominantly on spines (Redgrave *et al.*, 2010; Kemp & Powell, 1971b).

The glutamate binds and opens two main types of glutamate-gated ion channels: α -amino-3-hydroxy-5-methyl-4-isoxazolepropionic acid receptors (AMPA) and N-methyl-D-aspartate receptors (NMDARs). In addition, metabotropic glutamate receptors are also highly expressed by MSNs.

Inhibitory GABAergic MSNs also receive feedback inputs from other MSNs. More GABAergic input is provided by interneurons: FS and FA interneurons form strong inhibitory connections on MSNs.

Furthermore, cholinergic interneurons have robust tonic activity and release acetylcholine on MSNs (Abudukeyoumu *et al.*, 2019). Acetylcholine activates M4 muscarinic receptor in D1 MSNs, which powerfully inhibits cAMP response to dopamine (Nair *et al.*, 2015; Nair *et al.*, 2019).

It is commonly accepted that NO produced by NOS interneurons diffuses throughout the striatal complex and increases corticostriatal and dopaminergic synaptic transmission via a sGC-cGMP dependent mechanism (West *et al.*, 2002; West & Grace, 2004; West & Tseng, 2011). In addition, NO diffuses into the dendrites of MSNs modulating corticostriatal synaptic plasticity *in vitro* (Calabresi *et al.*, 1999; Calabresi *et al.*, 2000) and *in vivo* (West & Grace, 2004).

5. Striatal function and disorders

In rats and mice, dopaminergic neuronal cell bodies exhibit two kinds of discharge activity: single spikes or bursts of two to six action potentials. Individual dopaminergic neurons can switch from one pattern to another and sensory stimuli favor the bursting pattern in unrestrained rats. The single spike pattern of activity is due to the intrinsic properties of dopaminergic neurons. In contrast, the bursting activity is due to excitatory afferents and is mediated by NMDA receptors.

When the dopamine release is evoked by an electrical stimulation mimicking one burst (i.e. 4 pulses at 15 Hz, whole duration 200 ms), an excitatory response can be recorded in a subpopulation of striatal neurons. This response mediated by D₁ receptors, lasts for 0.5 s and is delayed as compared to the evoked dopamine overflow: it starts 0.3 s after the beginning of the stimulation train, i.e. when the released dopamine has been almost completely eliminated by reuptake. This delayed excitatory response fully develops when D₁ receptors are stimulated by dopamine for a sufficient duration (i.e. by a burst) since single pulse stimulations are much less effective (Gonon *et al.*, 2000).

The relevant phasic signal in the transmission mediated by D₂ receptors, occurs when the tonic activity of dopaminergic neurons is interrupted by brief (200 ms) silent periods which seem to code errors in the temporal prediction of reward (Hollerman & Schultz, 1998).

Dopaminergic transmission in the striatum occurs outside synaptic clefts. The dopamine signal in the striatum has a delay below 3 ms due to dopamine diffusion outside the synaptic cleft (Gonon *et al.*, 2000).

The maximal distance to which dopamine can diffuse from release sites to outside the synaptic cleft is limited by reuptake via the dopamine transporter (DAT) and ranges between 7 and 10 μm , which regulates the duration of this stimulation (Gonon *et al.*, 2000). The dopamine half-life in the striatal extracellular space was found to be in the range of 60 to 100 ms. However, these experimental values represent an overestimate of the dopamine half-life, because in the living tissue the kinetics of the dopamine overflow can be faster than those observed by carbon fiber electrodes. Thus the dopamine clearance by reuptake can occur within less than 50 ms (Gonon *et al.*, 2000).

5.1. Reward-based learning

Midbrain dopamine signals are widely thought to report reward prediction errors that drive learning in the basal ganglia (Figure 17). Phasic, sub-second responses in the majority of midbrain dopamine neurons code a reward prediction error. Their activity is increased for one hundred or two hundred milliseconds when a reward or reward predicting stimulus is better than predicted, their activity is unchanged when these events have the same reward value as their prediction, and their activity is briefly depressed when these events have lower reward value than predicted (Schultz, 2019).

However, dopamine neurons are more diverse than previously thought (Watabe-Uchida & Uchida, 2018). Dopamine neurons projecting to the posterior “tail” of the striatum are activated by a subset of negative events including threats from a novel object, send prediction errors for external threats, and reinforce avoidance behaviors. Thus, there are at least two axes of dopamine mediated reinforcement learning in the brain: one learning from canonical reward prediction errors (Figure 17) and another learning from threat prediction errors (Watabe-Uchida & Uchida, 2018). Dopamine is also implicated in encoding uncertainty and controlling exploration. Dopamine signalling can reinforce learning framework (Gershman & Uchida, 2019).

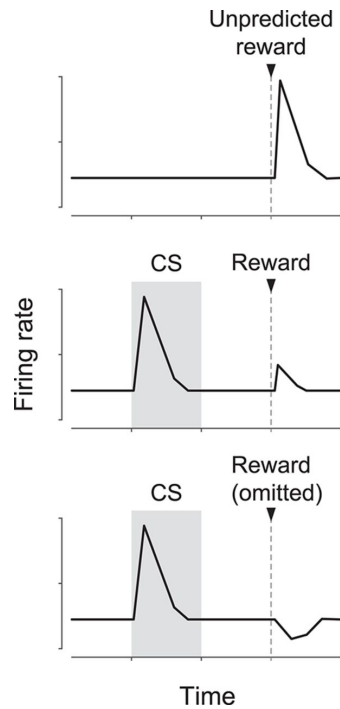


Figure 17 - Schema of the canonical reward prediction error signals. Firing rate of dopamine neurons. Dopamine neurons code for an error in the prediction of reward. (top) The dopamine neuron is activated by the unpredicted occurrence reward. (middle) After learning, the conditioned stimulus predicts reward, and the reward occurs according to the prediction, hence no error in the prediction of reward. The dopamine neuron is activated by the reward-predicting stimulus but fails to be activated by the predicted reward. (bottom) After learning, the conditioned stimulus predicts a reward, but the reward fails to occur because of a mistake in the behavioral response. The activity of the dopamine neuron is depressed exactly at the time when the reward would have occurred. The depression occurs more than 1 s after the conditioned stimulus without any intervening stimuli, revealing an internal representation of the time of the predicted reward. Abbreviations: CS, conditioned reward-predicting stimulus. From (Watabe-Uchida & Uchida, 2018).

5.2. Direct- and indirect-pathways and action selection

Despite advances in our understanding of basal ganglia circuitry, the relationship between the direct- and indirect-pathways and the generation of actions is still unclear (Cui *et al.*, 2013; Klaus *et al.*, 2019).

Findings in human basal ganglia diseases, like movement disorders, combined with literature of animal studies describing neuroanatomy, neurophysiology, neurochemistry and connectivity of the basal ganglia, led to the development of the main model about the functional neuroanatomical organisation of basal ganglia: the Rate Model. This model was formulated by several investigators (Albin *et al.*, 1989; DeLong, 1983; DeLong, 1990; Penney & Young, 1983) and has evolved since then (Nelson & Kreitzer, 2014).

This model of basal ganglia function proposes that direct and indirect pathways have opposing effects on movement: while activity of direct-pathway MSNs purportedly facilitates movement, activity of indirect-pathway MSNs inhibits movement (Figure 18a) (Albin *et al.*, 1989; DeLong, 1990). According to this model, movements occur during pauses in the tonic inhibitory activity of the basal ganglia output interface, generated by activity in the direct

pathway (Gerfen & Surmeier, 2011; Chevalier *et al.*, 1985; Deniau & Chevalier, 1985; Hikosaka & Wurtz, 1983). The opposing role of the indirect pathway in suppressing movements was originally proposed on the basis of studies in animal models of Parkinson's disease (Gerfen & Surmeier, 2011).

Studies using genetic approaches for selectively targeting direct and indirect pathway neurons supports the general Rate model hypotheses (Hikida *et al.*, 2010; Kravitz *et al.*, 2010). Ablation of direct pathway neurons by selective expression of diphtheria toxin resulted in bradykinesia (Drago *et al.*, 1998), while ablation of indirect pathway neurons led to an increase in locomotion (Sano *et al.*, 2003; Durieux *et al.*, 2009; Durieux *et al.*, 2012). Deletion of key signaling proteins such as DARPP-32 from either direct or indirect pathway MSNs also resulted in divergent motor behaviors: disrupting the function of direct-pathway MSNs led to loss of hyperkinetic behaviors and disrupting the function of indirect-pathway MSNs increased locomotion (Bateup *et al.*, 2010). However, neuronal ablation or blocking neurotransmission, even with rapid techniques, may lead to plasticity in basal ganglia microcircuits. To determine whether altering the balance of activity in the two pathways could achieve similar results, several groups have employed optogenetics, which allows millisecond timescale manipulations. Selective optical activation of direct pathway MSNs increases locomotor activity, while activation of indirect pathway neurons causes freezing (Kravitz *et al.*, 2010).

While optogenetic studies in rodents have shown that direct and indirect pathway activation is sufficient to cause opposing behaviors (Kravitz *et al.*, 2010; Tai *et al.*, 2012), they have not shown that such imbalances are necessary to produce behavior. Studies have suggested that the basal ganglia system is more complicated than initially assumed and this model fails to account for the great diversity and complexity of the decision-making process in action selection (Cisek & Kalaska, 2010). At the time that the Rate Model was described, the authors highlighted limitations and caveats, but the simplicity of the model has proven to be of considerable clinical value for clinicians and fundamental scientists. Although current researchers continue to identify inconsistencies in the Rate Model, it has been a useful tool for research that has promoted greater knowledge of basal ganglia function as well as a more methodical approach (Nelson & Kreitzer, 2014).

Other models

Another model proposes that the activation of direct pathway neurons promote the desired/wanted motor programs while the activation of indirect pathway neurons inhibit competing motor programs (Mink, 2003; Nambu, 2008; Hikosaka *et al.*, 2000). This model predicts that during ongoing behavior, there will be increased activity in neuronal ensembles that are part of direct- and indirect-pathway circuits, rather than one or the other. The execution of a movement sequence would then generate a complex pattern of activity in specific neuronal ensembles (Turner & Anderson, 1997; Turner & Anderson, 2005). Consistent with such data, current models propose that the striatum performs a computation on sensorimotor, cognitive, and emotional/motivational information provided by the cerebral cortex to facilitate the selection of an appropriate action out of a collection of possibilities (Balleine *et al.*, 2007; Cisek & Kalaska, 2010; Nambu, 2008). Distinct cortico-basal ganglia

loops may play different roles in the acquisition and stabilization of context-dependent action selection. For example, work by Costa's group suggests that the dorsomedial striatum-associative cortex loop plays an important role in the early phases of skill acquisition, whereas the dorsolateral striatum-sensorimotor cortex loop is more involved once the skill has been established and the action program becomes more automated and inflexible (Costa, 2007; Yin *et al.*, 2009; Vicente *et al.*, 2016).

Contrary to the data supporting a prokinetic/antikinetic dichotomy in direct versus indirect pathways, more recent models propose that the coordinated activation of both pathways is critical for action selection, or for the appropriate timing/synchrony of basal ganglia circuits during movement (Figure 18b) (Brown, 2007; Chan *et al.*, 2005; Goldberg & Fee, 2012; Klaus *et al.*, 2019).

In-vivo optical recording of the activity of MSNs, using deep brain-inserted fiber optics in freely moving mice to monitor changes in the intracellular calcium transients in D1 and D2 MSNs revealed transient increases in neuronal activity in both direct- and indirect-pathway MSNs predicting the occurrence of specific movements within 500 ms. A clear co-activation of both direct- and indirect-pathway MSNs preceded movement initiation, and both pathways were inactive when the animal was not moving (Cui *et al.*, 2013).

Although this model is consistent with most of what we know, the role of the striatal microcircuits is almost completely undefined in this model (Gerfen & Surmeier, 2011). Also, it is commonly assumed that direct- and indirect- pathway MSNs receive the same cortical information. This assumption is being debated in the literature (Ballion *et al.*, 2008; Lei *et al.*, 2004; Parthasarathy & Graybiel, 1997) but will not be easy to resolve, given the complex architecture of the striatum (Gerfen & Surmeier, 2011). It would fundamentally change our ideas about what each pathway was doing to control behavior (Gerfen & Surmeier, 2011). It is also far from clear how the timing of activity in the direct and indirect pathways shapes the activity in the circuitry controlling actual movement (Nambu, 2008). In diseases of the basal ganglia, such as Parkinson's disease, the timing of activity, rather than the overall level of activity, appears to be the most important determinant of movement choice and initiation (Bevan *et al.*, 2002).

The view of basal ganglia function organisation may have implications for understanding the origin of motor symptoms in basal ganglia disorders.

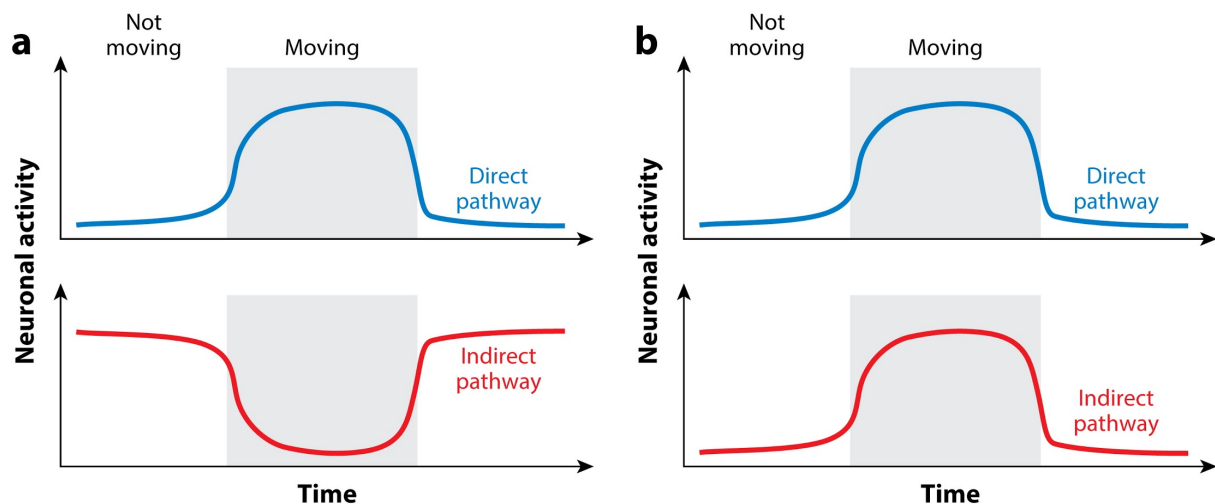


Figure 18 - Potential scenarios of how activity in direct and indirect pathway MSNs in the striatum is related to movement. (a) The prokinetic versus antikinetic model suggests that D1 MSNs activity is higher during movement and D2 MSNs activity is lower during movement, and vice versa during immobility. (b) Other models suggest that both pathways are more active during movement to select the particular desired movement; and are less active during immobility. From (Klaus *et al.*, 2019).

5.3. Basal ganglia disorders

Basal ganglia circuits are involved in a variety of neurological diseases like dystonia, neurodegenerative diseases such as Parkinson's disease and Huntington's disease (Nelson & Kreitzer, 2014) and also psychiatric conditions like schizophrenia, autism-spectrum disorders, Tourette syndrome, obsessive-compulsive disorder and addiction (Hyman *et al.*, 2006; DeLong & Wichmann, 2007; Breakefield *et al.*, 2008; Graybiel, 2008; Kreitzer, 2009). In my thesis I was particularly interested in psychiatric conditions, more precisely schizophrenia and autism-spectrum disorders (Fragile X syndrome).

Schizophrenia

Schizophrenia is a devastating psychiatric disease, which results in persistent cognitive and emotional impairments, associated with psychotic episodes. Several studies with advanced technologies have been made in recent years, identifying genetic and signaling pathways associated with the risk factors for major psychiatric disorders, such as schizophrenia, bipolar disorder and depression (Komatsu *et al.*, 2019). However, not even a single gene has been identified to provokes any of the psychiatric symptoms (Komatsu *et al.*, 2019). There has been a marked reduction in the development of new psychiatric drugs worldwide. This is mainly due to the complex causes, like genetic as well as environmental and epigenetic risk factors that underlie these diseases (Komatsu *et al.*, 2019). Furthermore, the rational design of multitarget drugs such as multi-acting receptor targeted antipsychotics (MARTA) has encountered considerable challenges in optimizing multiple structure-activity relationships while maintaining drug-like properties (Gandal *et al.*, 2018; Teroganova *et al.*, 2016; Hopkins, 2008).

GPCRs are the most common targets of antipsychotics such as quetiapine and aripiprazole, and play pivotal roles in controlling brain function by regulating multiple downstream signaling pathways (Komatsu *et al.*, 2019). Progress in our understanding of GPCR signaling has opened new possibilities for selective drug development (Komatsu *et al.*, 2019). The biased ligands can modulate some, but not all, of a given receptor downstream signaling pathways. GPCRs, especially D₂ receptors, are well known therapeutic targets for the disorders. Classical and atypical antipsychotic agents share the property of inhibiting D₂ receptors (Ginovart & Kapur, 2012) and thus increasing PKA-dependent phosphorylation selectively in D2 MSNs (Bateup *et al.*, 2008; Bertran-Gonzalez *et al.*, 2008; Bertran-Gonzalez *et al.*, 2009). In contrast, psychostimulants, which are psychotomimetic, activate many signaling responses in D1 MSNs (Bateup *et al.*, 2008; Bertran-Gonzalez *et al.*, 2008; Bertran-Gonzalez *et al.*, 2009).

However, all D2 antagonists are not antipsychotics, and it was hypothesized that the antipsychotic activity was related to drug action on the non-canonical signaling pathways regulated by D₂ receptors (Urs *et al.*, 2017). This raises the possibility that the biased GPCR ligands can provide therapeutically desirable outcomes to treat mental disorders with fewer adverse side effects (Komatsu *et al.*, 2019). However, this application requires a detailed understanding of the mode of action of antipsychotics, the mechanistic bases for multiple signaling modes and the potential of the biased modulators that drive distinct pharmacologies (Komatsu *et al.*, 2019).

Another therapeutic strategy was based on PDE10A inhibitors, which were shown to increase cAMP levels in the striatum (Schmidt *et al.*, 2008) and could be expected to mimic the effects of both antipsychotic and psychotomimetic compounds.

Autism-spectrum disorders

Autism-spectrum disorders (ASD) are the most prevalent neurodevelopmental disorders. ASD define a clinically heterogeneous group of disorders, that generally exhibits two core symptoms: impaired social communication and repetitive behaviors (Bhat *et al.*, 2014; Fakhoury, 2015).

Many studies have reported structural and functional alterations in the caudate and putamen of human patients with ASD (Rothwell, 2016; Sears *et al.*, 1999; Eliez *et al.*, 2001; Levitt *et al.*, 2003; Hollander *et al.*, 2005; Haznedar *et al.*, 2006; Silk *et al.*, 2006; Turner *et al.*, 2006; Voelbel *et al.*, 2006; Langen *et al.*, 2007; Langen *et al.*, 2012; Takarae *et al.*, 2007; Di Martino *et al.*, 2011). Recent studies associate various dopamine system genes with ASD. However, how dopamine system dysfunction induces ASD remains unknown (Lee *et al.*, 2018).

A large number of risk genes that are associated with ASD pathogenesis have been implicated in an altered axonal growth, an imbalance of the neuronal network excitation/inhibition ratio, and an altered long-term synaptic plasticity in the corticostriatal pathway (Fuccillo, 2016; Golden *et al.*, 2018; Kuo & Liu, 2019; Shepherd, 2013). The high-confidence ASD-associated genes include: *FMRI*, *KMT2A*, *GRIN2B*, *SCN2A*, *NLGNI*, *NLGN3*, *MET*, *CNTNAP2*, *FOXP2*, *TSHZ3*, *SHANK3*, *PTEN*, *CHD8*, *MECP2*, *DYRK1A*, *RELN*, *FOXP1*,

SYNGAP1, and *NRXN* (Li & Pozzo-Miller, 2019; Nakanishi *et al.*, 2019; Verma *et al.*, 2019).

During my thesis I studied a *Fmr1*-KO mouse model, a widely used animal model to study Fragile X syndrome, which presents some key aspects of ASD (Bagni & Oostra, 2013).

Mutations in the human fragile X mental retardation 1 (*FMRI*) gene leads to Fragile X Syndrome (FXS). FXS is a genetic developmental condition causing the most common inherited form of intellectual disability often presented as a monogenic cause of autism spectrum disorder (Bagni & Oostra, 2013). Currently, there is no cure or approved medication for the treatment of the underlying causes of FXS (Zafarullah & Tassone, 2019).

In addition to intellectual disability, the clinical symptoms of FXS individuals include a range of neurological alterations: autistic-like behavior, seizures, cognitive impairment (learning and memory impairments), delayed language development, hyperactivity, anxiety, impulsivity, insomnia, epilepsy, repetitive behavior, social withdrawal and physical features such as hypotonia, flat feet, hyperextensible joints, and macroorchidism (Zafarullah & Tassone, 2019).

In the normal population, the *FMRI* gene (Figure 19), located on the X chromosome (Loci Xq27.3), contains a CGG repeat in the 5'-untranslated region (UTR). The CGG repeat is polymorphic and ranges from 5 to 55 CGGs with an average length of 30 CGG units (Fu *et al.*, 1991).

FXS is a trinucleotide repeat disorder caused by the abnormal expansion of the CGG repeat to more than 200 repeats (Figure 19). This expansion is known as the full mutation (FM). This trinucleotide repeat expansion mutation causes the hypermethylation of the repeat and the promoter region of the *FMRI* gene (Oberlé *et al.*, 1991; Verkerk *et al.*, 1991; Sutcliffe *et al.*, 1992). As a consequence the transcription of the *FMRI* gene is silenced, leading to the loss of expression of the fragile X mental retardation 1 protein (FMRP) and to the diagnosis of FXS (Verheij *et al.*, 1993; Verkerk *et al.*, 1991; Oberlé *et al.*, 1991; Pieretti *et al.*, 1991).

Individuals carrying expansion of 55-200 CGG repeat are pre-mutation carriers and at risk of developing the late-onset neurodegenerative syndrome, fragile X-associated tremor/ataxia syndrome (FXTAS), the fragile X-associated primary ovarian insufficiency (FXPOI) and the fragile X-associated neuropsychiatric disorders (FXAND) (Figure 19) (Zafarullah & Tassone, 2019).

The *FMRI* gene encodes the FMRP. The *FMRI* gene can generate by alternative splicing twelve different protein isoforms with a molecular weight ranging between 70 and 80 kDa (Verkerk *et al.*, 1993; Brackett *et al.*, 2013). FMRP isoforms are expressed in many tissues and organs with a tissue-specific relative abundance (Kaufmann *et al.*, 2002; Xie *et al.*, 2009). FMRP is abundantly expressed in the cortex and striatum (Bonaccorso *et al.*, 2015; Li & Pozzo-Miller, 2019).

FMRP is involved in mRNA transport to synapses where protein synthesis occurs. FMRP is also an RNA-binding protein that regulates the translation of a large number of mRNAs encoding synaptic proteins, many of which are involved in the maintenance and development of neuronal synaptic function and plasticity. Depending on the considered gene, FMRP acts as a translational activator or repressor of its mRNA targets.

FMRP loss-of-function results in immature dendritic spines, excitation/inhibition imbalance, and altered mGluR-mediated LTD in many brain regions in mouse models of FXS, including the hippocampus and cerebellum (Dahlhaus, 2018).

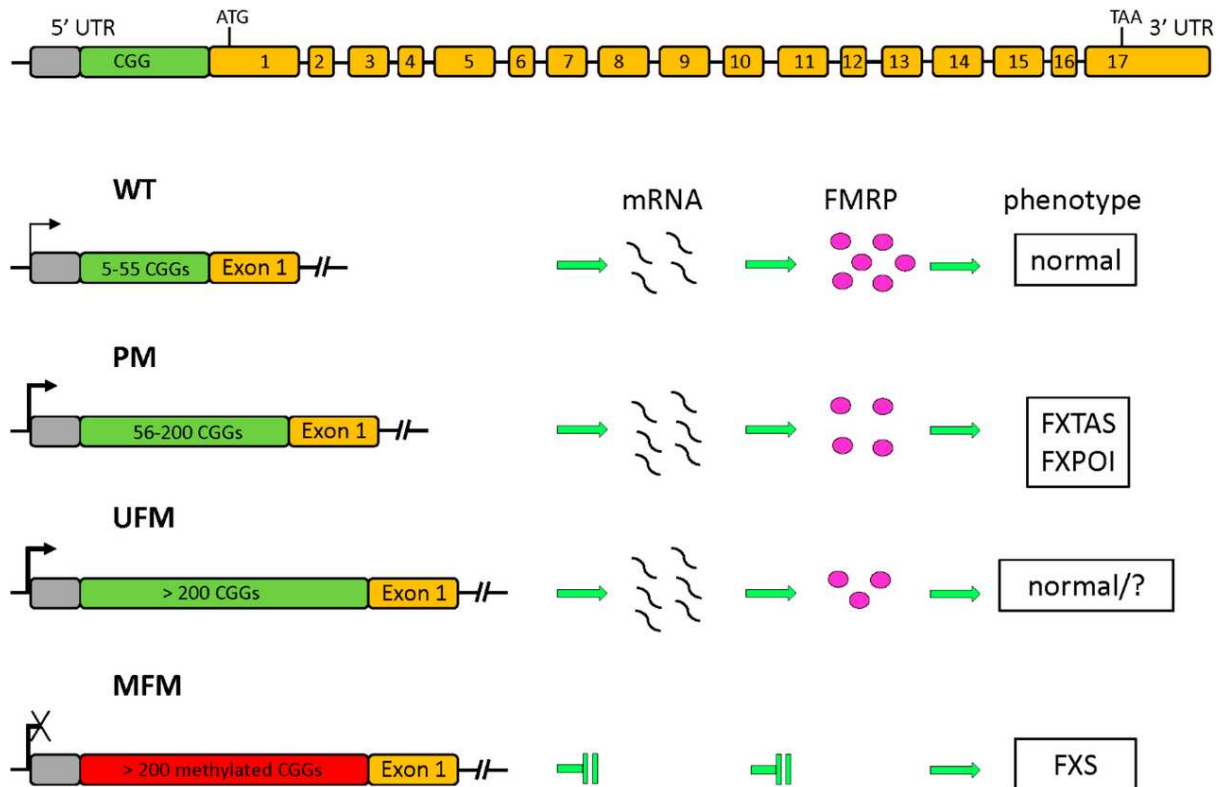


Figure 19 - *Fragile X mental retardation 1 (FMR1)* gene and its various allelic forms. The polymorphic CGG sequence is placed upstream of exon 1 in the 5'-untranslated region (UTR) (top). Based on the CGG expansion four different classes of alleles are shown, with their transcriptional activity indicated by the arrow: normal (WT); premutated (PM) with a higher transcription (bold arrow) and slight decrease of translation associated to the fragile X-associated tremor/ataxia syndrome (FXTAS) end fragile X-associated primary ovarian insufficiency (FXPOI) phenotypes; unmethylated full mutation (UFM), similar to PM for transcription and translation, without an apparent phenotype; methylated full mutation (MFM) leading to absence of transcript and fragile X mental retardation protein (FMRP) and consequently to fragile X syndrome (FXS). From (Tabolacci *et al.*, 2016).

Maurin *et al.* (Maurin *et al.*, 2018a) identified by high-throughput sequencing-crosslinking immunoprecipitation (HITS-CLIP) PDE2A as a prominent mRNA target of FMRP. Our team had a collaboration with them in a project where I studied the activity of PDE2A in single neurons of the CA1 region of hippocampus of *Fmr1*-KO mice (Figure 1 in article #3) (Maurin *et al.*, 2018b).

6. Objective

MSNs integrate neuromodulatory signals like dopamine through the cAMP signalling pathway in the striatum (Figure 20). The intracellular level of cyclic nucleotides is controlled by the balance between synthesis by ACs and GCs, and degradation by PDEs.

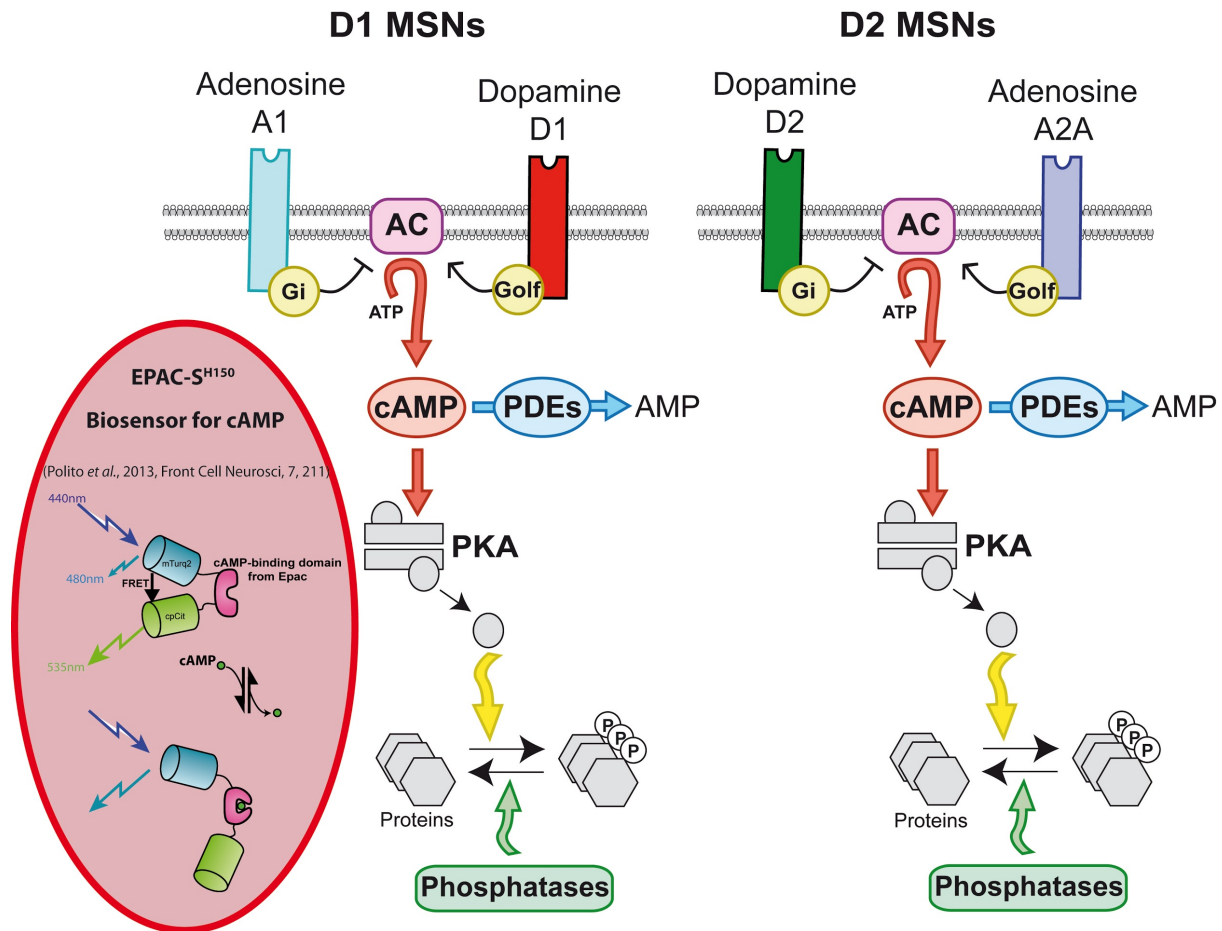


Figure 20 - The cAMP/PKA signaling cascade of the two types of MSNs in the Striatum. The genetically-encoded FRET biosensor Epac-S^{H150} allows imaging the changes in cAMP concentration at the level of individual neurons.

My thesis work focused on the effects of dopamine through D₁ and D₂ receptors, and in particular the role played by PDEs in shaping these two types of dopamine responses. Transient activation of D₁ receptors produces a transient increase in cAMP, and the amplitude and duration of this cAMP signal depends on PDE activities. Activation of the D₂ receptor decreases cAMP production, and PDE activities are required to decrease this cAMP and thus integrate the dopamine signal. Besides the PDEs which are continuously active such as PDE10A and PDE4, I also tested the effect on dopamine of other neuromodulators which regulate PDE activities, like NO, which increases cGMP and activates PDE2, and glutamate, which increases calcium and activates PDE1. Besides the cAMP/PKA signaling pathway, the D₂ dopamine receptor is also coupled to non-canonical signaling pathways and I also wanted to monitor these signals using biosensors to monitor Akt and ERK activities. This part of the project however did not bring clear conclusions.

7. Protocol to monitor D1 and D2 dopamine responses in MSNs

Based on the above description of FRET measurement methods, our choice is the ratiometric method on wide-field imaging. A protocol was previously designed in the laboratory to record the response to dopamine at the single-cell level simultaneously in several neurons, in striatal brain slices (Yapo *et al.*, 2017). A transient stimulation of dopamine was obtained with the photorelease of caged dopamine (NPEC-DA), leading to a quasi-instantaneous increase in dopamine concentration throughout the imaging volume. This uncaging was shown to be complete, and therefore the concentration of active dopamine was considered identical to the known concentration of the caged precursor added to the bath.

Upon dopamine uncaging stimulation both dopamine D₁ and D₂ receptors were activated equally for the same duration. Before dopamine release, D1 MSNs present a basal level, where the dynamic equilibrium between biological cAMP sources/production and cAMP degradation by PDEs is such that cAMP concentration is close to zero. When dopamine is transiently released there is a transient activation of AC, which leads to a fast increase of cAMP levels that rises to the maximal D₁ receptor activation, ie, the same cAMP level obtained with D1 agonist (SKF-81297, 100 nM) (Castro *et al.*, 2013). During this fast production of cAMP, PDEs are not sufficient to control and degrade such enormous cAMP production. When dopamine concentration decays, cAMP production stops and cAMP degradation by PDEs is immediately and quickly visible, that corresponds to the recovery to the level before uncaging, ie, to the basal cAMP level.

Since D₂ receptors are negatively coupled to cAMP production and tonic production of cAMP is low in slices at basal conditions, intracellular cAMP production was first increased to a higher steady-state selectively in D2 MSNs by applying the A_{2A} receptor agonist CGS 21680 (CGS, 1 μM) in the presence of the A1 antagonist PSB36 (100 nM). In fact, this steady-state can correspond to a biological situation, since it was previously reported that the basal level of phospho-Thr-34 DARPP-32 is higher in D2 MSNs than in D1 MSNs (Nishi *et al.*, 1997; Bateup *et al.*, 2008; Polito *et al.*, 2015). While A_{2A} adenosine receptors are activated, there is a dynamic equilibrium between cAMP production by AC via G_{s/olf} and cAMP degradation by PDEs. During dopamine release, the ACs are inhibited, which means that there is no more cAMP production and there is only a fast cAMP degradation by PDEs, ie, a decrease in cAMP level down to the lowest level of cAMP, that can allow the PKA deactivation. As dopamine washes out of the preparation, there is a progressive cAMP increase because AC is no longer inhibited.

The response to the same dopamine challenge could thus be monitored simultaneously in D1 and D2 MSNs, which allowed the comparison of dopamine receptor sensitivity.

The same response could be elicited several times, and this type of protocol was used to analyze the functional contribution of PDEs in the integration of dopamine responses.

Thus, when the cAMP level rises to the highest level upon dopamine D₁ receptor activation, PDE activity is important in order to degrade cAMP and return to the basal level. Symmetrically, when cAMP production stops after activation of dopamine D₂ receptor, PDEs activity is required to degrade cAMP.

II - Materials and Methods

1. Cloning biosensor sequences in a pSinRep5 vector for virus preparation

The Sindbis virus was used as a vector to induce expression of the biosensors after overnight incubation (Ehrengruber *et al.*, 1999). The coding sequences of the cAMP biosensor Epac-S^{H150} (Polito *et al.*, 2013), PKA/phosphatase equilibrium reporter AKAR4 (Depry *et al.*, 2011), cGMP biosensor cyGNAL, calcium biosensor Twitch-2B (Thestrup *et al.*, 2014), Akt biosensor AktAR2 (Zhou *et al.*, 2015), Akt biosensor Eevee-iAkt (Miura *et al.*, 2014), ERK biosensor EKAR-EV (Komatsu *et al.*, 2011) or ERK biosensor EKAR-EV GW4.0 (article in preparation) were inserted into the plasmid vector pSinRep5 (Invitrogen, San Diego, CA). The linear pSinRep5 and the DH(26S) helper DNA (which contains the structural proteins required for packaging of the Sindbis viral genome) were used to prepare recombinant RNA *in vitro*. The capped and polyadenylated RNA transcripts (from DH(26 S) and pSinRep5) were co-transfected into baby hamster kidney (BHK) cells to produce the pseudovirions.

2. Biosensor construct and validation

The Epac-S^{H150} biosensors (Polito *et al.*, 2013) and AKAR4 (Depry *et al.*, 2011) were used to record intracellular cAMP and PKA signals in brain slice preparations. FRET biosensors consist of a sensor domain, either sensitive to intracellular levels of cAMP (biosensors of the Epac family) or to PKA-mediated phosphorylation (and phosphatase dephosphorylation, AKAR biosensors), between two fluorophores derived from GFP, a donor derived from CFP and an acceptor derived from YFP, excited at the specific wavelength of the donor. When a change in the biological signal occurs (for example, when the intracellular cAMP levels increase or decrease), the sensor domain undergoes a conformational change. As a result, the donor and acceptor fluorophores move toward or away from each other and/or change their relative orientation, ultimately leading to a change in FRET efficiency. The latter is measured in real time by fluorescence microscopy, and quantified according to ratiometric methods (Polito *et al.*, 2014). More information on slice preparation methods (optimized for neuron survival for nearly 24 hours), acquisition of cAMP and PKA signals (full-field and dual-photon fluorescence imaging), and neuron transfection (via sindbis virus) can be found in the methods of Articles 1 and 2.

All constructs were checked by sequence analysis.

3. Viral infection

A transgene vector derived from sindbis virus (single-stranded, positive-polarity RNA alphavirus capable of replicating in virtually all eukaryotic cells) was used to allow the expression of Epac and AKAR biosensors in our neuron preparations (Ehrengruber *et al.*,

1999). The coding sequences of the biosensors were inserted into a plasmid pSinRep5 (Invitrogen, San Diego, California) and the virions produced in BHK cells. The viral vector obtained has a good neuronal tropism (little infection of glial cells), and makes it possible to obtain a strong translation and a rapid expression (from 8 hours of incubation) of the transgene, specifically and homogeneously in the neurons, without altering their morphology. Infection of the slices is carried out by the deposition of virus solution (1 to 2 μ L of diluted solution, containing close to 10^5 viral particles), then incubation at 35 °C in a humidified atmosphere in the presence of 5 % CO₂- 95% O₂.

4. Brain slice preparation

Wild-type C57Bl/6J mice (3-6 g) were obtained from Janvier (Le Genest Saint Isle, France). Mice were maintained in a 12 h light/dark cycle, in stable conditions of temperature (22 ± 1 °C), controlled humidity ($55 \pm 10\%$) with food and water available ad libitum. All the experiments were performed according to guidelines for the care and use of laboratory animals established by the Animal Experiments Committee ("Darwin") and the French Ministry of Agriculture and Forestry guidelines for handling animals.

Brain slices were prepared from mice aged from 7 to 12 days. The brain was removed and coronal brain slices of 300 μ m thickness were cut with a VT1200S microtome (Leica, Germany). Slices were prepared in an ice-cold solution of the following composition: 125 mM NaCl, 0.4 mM CaCl₂, 1 mM MgCl₂, 1.25 mM NaH₂PO₄, 26 mM NaHCO₃, 20 mM glucose, 2.5 mM KCl, 5 mM sodium pyruvate and 1 mM kynurenic acid, saturated with 5% CO₂ and 95% O₂. The slices were incubated in this solution for 30 min and then placed on a Millicell-CM membrane (Millipore) in culture medium (50% Minimum Essential Medium, 50% Hanks' Balanced Salt Solution, 6.5 g/l glucose, penicillin-streptomycin, Invitrogen).

Compared to our previous work (Castro *et al.*, 2013), the viral vector was diluted to decrease the number of infected neurons and thus facilitate individual cell measurement. Slices were incubated overnight for biosensor expression. Before the experiment, slices were incubated for 30 min in the recording solution (identical to the solution used for cutting, except that the calcium concentration was 2 mM and kynurenic acid was omitted). During recordings, brain slices were continuously perfused with this solution saturated with 5% CO₂/95% O₂, at a rate of 2 ml/min, in a recording chamber of ~1 ml volume maintained at 32°C. The viability of the neurons in these experimental conditions have been checked by patch-clamp recording, which showed electrical activity to be normal (Gervasi *et al.*, 2007; Castro *et al.*, 2010).

5. Optical recordings on brain slices

Recordings were made on MSNs, that constitute 95% of neurons in the striatum. Large neurons, presumably cholinergic interneurons, were excluded (i.e., diameter larger than 14 μ m). Wide-field images were obtained with an Olympus BX50WI or BX51WI upright microscope with a 40 \times 0.8 NA water-immersion objective and an ORCA-AG camera

(Hamamatsu). Images were acquired with iVision (Biovision, Exton, PA, USA). The excitation and dichroic filters were D436/20 and 455dcxt. Signals were acquired by alternating the emission filters, HQ480/40 for CFP, and D535/40 for YFP, with a filter wheel (Sutter Instruments, Novato, CA, USA). All filters were obtained from Chroma Technology (Brattleboro, VT, USA). Image acquisition was triggered manually, except for kinetics measurement where images were acquired automatically with 3-5 s intervals.

Images were analyzed with custom routines written in the IGOR Pro environment (Wavemetrics, Lake Oswego, OR, USA).

The emission ratio was calculated for each pixel: F535/F480 for AKAR and F480/F535 for Epac-S^{H150} or cyGNAL. Pseudocolor images display the ratio value coded in hue and the fluorescence intensity coded in intensity. A calibration square indicates the intensity values from left to right and the ratio values from bottom to top. The size of the square indicates the scale of the image in microns. No correction for bleed-through or direct excitation of the acceptor was applied and the ratio changes in our conditions therefore appear smaller than those reported by other studies in which such corrections were applied.

6. Fast drug release

Dopamine was released from a photo-sensitive compound, NPEC-dopamine, by a flash of UV light. Previous work has demonstrated that the UV power was sufficient to release all the dopamine within the imaging volume and therefore the concentration of free dopamine in the imaging volume was set by the concentration of the caged precursor that was added in the bathing solution (Yapo *et al.*, 2017).

The UV light source was a 360 nm LED purchased Mightex, delivering a power of 10 mW light at the exit of the objective. Image acquisition in these fast wide-field recordings was automatic at a frequency ranging from 0.2 to 0.3Hz. Image acquisition was otherwise triggered manually by the user.

7. Data analysis and statistics

Ratiometric quantification was performed with a ratio value between the R_{min} and R_{max} values, which correspond to the minimal ratio value (no biological signal) and maximal response (saturated biosensor) (Grynkiewicz *et al.*, 1985; Börner *et al.*, 2011). The baseline ratio in control conditions was considered to be equal to R_{min} because adenylyl cyclase inhibition with 50 μ M SQ22536 and guanylyl cyclase inhibition with 10 μ M ODQ yielded no ratio decrease with Cygnet2 biosensor. The maximal response (R_{max}, corresponding to biosensor saturation) was determined for each neuron at the end of the recording. This level was determined by applying 13 μ M forskolin (for cAMP) or SNAP (for cGMP) in the presence of the broad-spectrum PDE inhibitor IBMX (200 μ M). Absolute ratio values differed between cells (as shown with the mutant biosensor in (Castro *et al.*, 2013)), so the amplitude of the response to receptor stimulation was quantified for each neuron as the fractional change

in ratio from its own baseline (Rmin) and maximal final ratio response (Rmax).

Measurements were performed on regions of interest (ROIs) and some of the signal measured on a region of interest comes from out-of-focus neurons. Regions of interest which displayed clear responses to both SKF38393 and CGS21680 and which therefore contained fluorescence signal from out of focus cells were discarded from our analysis.

Kinetic parameters (amplitude, tmax and $t_{1/2\text{off}}$) were determined using IGOR Pro environment (Wavemetrics, Lake Oswego, OR, USA). tmax values were determined as the time to reach the peak of the response and the $t_{1/2\text{off}}$ represents the time to reach a half of the recovery of the response.

We analyzed at least four neurons per brain slice, with n indicating the number of independent neurons tested. Unpaired two-tailed student's t-tests were used for statistical comparisons. Differences were considered significant when $P < 0.001$.

8. Pharmacological stimulation of receptors

The neurons in which the imaging measurements are made are pharmacologically stimulated by various drugs (Table 4), applied via an infusion bath of recording solution 125 mM NaCl, 2 mM CaCl₂, 1 mM MgCl₂, 1.25 mM NaH₂PO₄, 26 mM NaHCO₃ and 25 mM glucose, saturated with 5% CO₂ and 95% O₂. The transient dopaminergic stimuli are carried out by the dopamine uncaging technique (photorelease of dopamine), detailed in the methods of articles 1, 2 and 4.

Table 4 - Drugs used in biosensor imaging recordings.

Drug	Concentrations	Pharmacodynamics
NPEC-dopamine	1 μ M to 10 μ M	D ₁ and D ₂ receptor agonist
MNI-NMDA	100 μ M	NMDA receptor activation
SKF-81297	1 μ M	D ₁ receptor agonist
quinpirole	1 to 5 μ M	D ₂ receptor agonist
haloperidol	100 nM	D ₂ receptor antagonist
CGS 21680	1 μ M	A _{2A} receptor agonist
PSB36	100 nM	A1 receptor antagonist
TTX	200 nM	Na ⁺ channels blocker
atropine	1 μ M	Muscarinic receptor antagonist
CGP 55845A	100 nM	GABA B receptor antagonist
AM 251	100 nM	CB-1 receptor antagonist
naloxone	500 nM	Opioid receptor antagonist
forskolin	63 nM to 13 μ M	Adenylyl cyclases activator
IBMX	200 μ M	Non selective PDE inhibitor
TP-10	1 μ M	PDE10A inhibitor (iPDE10)
BAY607550	200 nM	PDE2A inhibitor (iPDE2)
rolipram	100 nM	PDE4 inhibitor (iPDE4)
Lu AF64196	1 nM to 10 μ M	PDE1 inhibitor (iPDE1)
cantharidine	30 to 50 μ M	PP1 and PP2A inhibitor
fostricéine	200 nM	PP2A inhibitor
FK506	5 to 10 μ M	PP2B inhibitor
cyclosporine A	5 μ M	PP2B inhibitor
DEANO	10 μ M	NO donor for cGMP elevation
SQ22536	200 μ M	Adenylyl cyclases inhibitor

III - Results

Article 1: PDE1 - dopamine and glutamate coincidence

Phosphodiesterase 1 bridges glutamate inputs with NO- and dopamine-induced cyclic nucleotide signals in the striatum.

Betolngar DB, Mota É, Fabritius A, Nielsen J, Hougaard C, Christoffersen CT, Yang J, Kehler J, Griesbeck O, Castro LRV, Vincent, P.

Cerebral Cortex. 2019

DOI: 10.1093/cercor/bhz041.

(Betolngar *et al.*, 2019)

PDE1B is highly expressed in the striatum, at least at the mRNA level, but its functional role was difficult to study because of lack of specific inhibitor. Through a collaboration with Lundbeck, we obtained a novel highly selective inhibitor Lu AF64196. The aim of this project was to determine whether PDE1 was functionally present in MSNs, and how it contributed to the regulation of cyclic nucleotides in these neurons.

First, a novel biosensor for cGMP was created, to improve our measurements compared to previously existing cGMP sensors. This novel cyGNAL sensor was characterized and showed the required sensitivity and selectivity to be used in this project.

We designed novel protocols, using NMDA stimulation to induce transient and reproducible calcium signals to activate PDE1 in a consistent way. A genetically-encoded FRET biosensor for cAMP (Epac-S^{H150}) or cGMP (cyGNAL) was expressed by viral transfection in brain slice preparations to image changes in cyclic nucleotide concentration at the level of individual neurons. As a control, we also monitored the calcium signal after NMDA uncaging using the genetically-encoded FRET biosensor Twitch-2B, to show that during our protocol the NMDA release induces a transient stimulation of NMDA receptors, which increases intracellular calcium. We believe that this calcium transient triggers a decrease in cGMP and cAMP mediated by PDE1 action in striatal MSNs.





In this article, we showed that:

- PDE1 is active only in the presence of intracellular calcium, ie PDE1 is not active in basal condition;
- PDE1 degrades both cAMP and cGMP, as expected from biochemical data;
- PDE1 moderates the cAMP response during the coincident activation of NMDA receptors and dopamine D₁ receptors;
- co-release of NMDA with dopamine leads to cAMP responses of lower amplitude;
- this effect negatively affects synaptic plasticity.

Conclusion: PDE1 down-regulates the dopamine-induced cAMP signal when there is a coincidence of dopamine and glutamate neurotransmission.

ORIGINAL ARTICLE

Phosphodiesterase 1 Bridges Glutamate Inputs with NO- and Dopamine-Induced Cyclic Nucleotide Signals in the Striatum

Dahdjim B. Betolngar¹, Élia Mota ¹, Arne Fabritius², Jacob Nielsen³, Charlotte Hougaard³, Claus T. Christoffersen³, Jun Yang⁴, Jan Kehler³, Oliver Griesbeck ², Liliana R.V. Castro ¹ and Pierre Vincent ¹

¹Sorbonne Université, CNRS, Biological Adaptation and Ageing, F-75005 Paris, France, ²Max Planck Institute for Neurobiology, Tools for Bio-Imaging, Am Klopferspitz 18, 82152 Martinsried, Germany, ³H. Lundbeck A/S, Ottiliavej 9, DK-2500 Valby, Denmark and ⁴Shanghai Chempartner Co. Ltd., Shanghai, China

Address correspondence to Pierre Vincent, Sorbonne Université, CNRS, Biological Adaptation and Ageing, Mailbox #256, UMR8256, 7 Quai Saint Bernard, F-75005 Paris, France. Email: pierre.vincent@upmc.fr  orcid.org/0000-0002-8479-1908

Abstract

The calcium-regulated phosphodiesterase 1 (PDE1) family is highly expressed in the brain, but its functional role in neurones is poorly understood. Using the selective PDE1 inhibitor Lu AF64196 and biosensors for cyclic nucleotides including a novel biosensor for cGMP, we analyzed the effect of PDE1 on cAMP and cGMP in individual neurones in brain slices from male newborn mice. Release of caged NMDA triggered a transient increase of intracellular calcium, which was associated with a decrease in cAMP and cGMP in medium spiny neurones in the striatum. Lu AF64196 alone did not increase neuronal cyclic nucleotide levels, but blocked the NMDA-induced reduction in cyclic nucleotides indicating that this was mediated by calcium-activated PDE1. Similar effects were observed in the prefrontal cortex and the hippocampus. Upon corelease of dopamine and NMDA, PDE1 was shown to down-regulate the D₁-receptor mediated increase in cAMP. PDE1 inhibition increased long-term potentiation in rat ventral striatum, showing that PDE1 is implicated in the regulation of synaptic plasticity. Overall, our results show that PDE1 reduces cyclic nucleotide signaling in the context of glutamate and dopamine coincidence. This effect could have a therapeutic value for treating brain disorders related to dysfunctions in dopamine neuromodulation.

Key words: biosensor imaging, calcium, cAMP, cGMP, synaptic plasticity

Introduction

Cyclic nucleotide signaling is an important regulator of neuronal excitability. The intracellular level of cyclic nucleotides is controlled by the balance between synthesis by adenylate and guanylate cyclases (AC and GC), and degradation by 3′/5′-cyclic nucleotide phosphodiesterases (PDEs). There are 11 families of PDEs in mammals that can hydrolyze cAMP and/or cGMP (Keravis & Lugnier 2012). PDE1 hydrolyzes both cAMP and cGMP,

and is the only PDE that is activated by Ca²⁺-calmodulin (CaM) (Hansen & Beavo 1986; Lugnier et al. 1986; Goraya & Cooper 2005), suggesting it can mediate a crosstalk between the intracellular calcium and cyclic nucleotide signaling pathways. In particular, while glutamate increases cGMP production via NMDA receptors and nNOS-dependent NO production (Vallebuona & Raiteri 1995; Piedrafita et al. 2007; Garthwaite 2019), PDE1 could oppose this effect by promoting cGMP breakdown in such

conditions of elevated calcium. 3 PDE1 genes have been identified (PDE1A-C), which are all expressed in the central nervous system. PDE1A is primarily expressed in CA1–3 of the hippocampus and layer 5–6 of the cortex. PDE1B is highly expressed in the striatum and in the dentate gyrus of the hippocampus. In addition, PDE1B is expressed at lower levels in many other brain areas including the cortex. PDE1C is mostly expressed in the cerebellum (Polli & Kincaid 1994; Yan et al. 1994; Lakics et al. 2010; Kelly et al. 2014). Overall, the expression pattern in the central nervous system is very similar in humans and rodents (Lakics et al. 2010).

Medium-sized spiny neurons (MSNs) are GABA-ergic projection neurons that constitute more than 90% of all neurons in the striatum. They integrate glutamate, nitric oxide and dopamine inputs through the calcium, cGMP and cAMP signaling pathways, respectively. The high expression of PDE1B in these neurons suggests that it plays an important role in the integration of these inputs. MSNs express either D₁ dopamine receptors, or both D₂ dopamine and A_{2A} adenosine receptors, and will be hereafter called D1 or D2 MSNs, respectively (Valjent et al. 2009; Bertran-Gonzalez et al. 2010; Yapo et al. 2017). Since PDE1B is reported to be expressed in the majority of striatal neurons (Polli & Kincaid 1994), it is expected to be present in both D1 and D2 MSN. Suppression of PDE1B in knockout mice enhanced D1-mediated phosphorylation of PKA substrates (Reed et al. 2002), but PDE1B function in D2 MSNs was not studied. The functional role of PDE1B was confirmed *in vivo*: spontaneous locomotor activity was increased in male and female PDE1B knockout mice (Siuciak et al. 2007), and the induction of locomotor activity by dopamine releasing agents was exacerbated (Reed et al. 2002; Ehrman et al. 2006; Siuciak et al. 2007).

In 6-OHDA lesioned mouse model of Parkinson's disease, increased PDE1B expression was associated with complex changes in cyclic nucleotide signaling (Sancesario et al. 2004), suggesting that PDE1B might be a target for treatment of the disease and the dyskinesias that result from its treatment with levodopa (Giorgi et al. 2008; Sancesario et al. 2014). Although PDEs have been evaluated as therapeutic targets for a wide variety of pathologies (Keravis & Lugnier 2012; Ahmad et al. 2015) including neuropsychiatric disorders (Menniti et al. 2006; Reneerkens et al. 2009; Schmidt 2010), the lack of specificity of early PDE1 inhibitors such as zaprinast and vinpocetine rendered uncertain the actual involvement of PDE1 in the effects reported in preclinical and clinical pharmacological studies (Ahn et al. 1989; Vemulapalli et al. 1996; Sitges & Nekrassov 1999; Sitges et al. 2005; Lugnier 2006; Medina 2011). More recently, selective PDE1 inhibitors have been developed (Maurice et al. 2014): the PDE1 inhibitor ITI-214 was shown to enhance memory processes and cognitive performance (Snyder et al. 2016; Pekcec et al. 2018), while Lu AF64196 was used to examine PDE1 function in the control of vascular smooth muscle cell relaxation (Khammy et al. 2017).

Although these studies have shown an impact of PDE1 modulation on animal behavior, the mechanistic details of its effect remain unclear. Cyclic nucleotide and calcium signals in living neurons are transient and to catch PDE1 in action has been a challenge so far. In this report, we have used biosensor imaging to monitor transient changes in cAMP and cGMP at the single cell level in brain slice preparations. In the first part of this work, the experiments were designed to reveal the action of PDE1 on artificially elevated steady-state cyclic nucleotide levels: a transient increase in intracellular calcium triggered by uncaging NMDA transiently reduced both cAMP and cGMP. We used the recently

developed selective PDE1 inhibitor, Lu AF64196 (Khammy et al. 2017) to show that this effect was mediated by PDE1. The second part of this work shows a functional inhibitory effect of PDE1 on the transient cAMP response to dopamine and on long-term potentiation (LTP). This suggests that PDE1 inhibitors may be useful for treating brain disorders related to dysfunctions in dopamine neuromodulation.

Materials and Methods

Construction of the cyGNAL Biosensor

We synthesized (GeneArt, Thermo Fischer Scientific) the CNB-A and CNB-B region of bovine cGMP dependent protein kinase I alpha (PKG I) *de novo*, starting from residue Q79 to residue K344, analog to (Russwurm et al. 2007), and placed it between different combinations of cyan fluorescent proteins as donors and yellow fluorescent proteins as acceptors in pRSET B (Invitrogen). CNB-B was amplified starting from residue P225 to residue Y335 of PKG I and reinserted inside the sensing domain, replacing CNB-A starting from residue E108 to E211, leaving only a 29 amino acid stretch at the N-terminus of the sensor domain intact.

Recombinant Expression and Protein Purification

Protein over-expression and purification was performed according to the protocol presented in (Fabritius et al. 2018). In brief, His-tagged proteins were over-expressed in E.coli BL21 (Invitrogen) in 50 mL cultures of auto inductive LB. Harvested cells were lysed via physical and enzymatic methods (freeze thaw cycle, lysozyme and sonication) with protease inhibitors (4 mM PMSF, 20 µg/mL Pepstatin A, 4 µg/mL Leupeptin, Sigma Aldrich, Germany). It was taken care not to include detergents such as Triton X100 within the purification protocol, as we found this to negatively impact *in vitro* sensor performance. Proteins were then purified from cleared lysate using Ni-NTA agarose resin (Jena Bioscience, Germany) and eluted through completion with imidazole (elution buffer: 20 mM Na₂PO₄, 300 mM NaCl, 300 mM imidazole).

Biosensor Imaging in Brain Slice Preparations

Mice (C57BL/6J; Janvier labs) were housed under standardized conditions with a 12 h light/dark cycle, stable temperature (22 ± 1 °C), controlled humidity (55 ± 10%) and food and water *ad libitum*. All animal procedures were performed in accordance with the Sorbonne University animal care committee regulations. Brain slices were prepared from mice aged from 7 to 11 days. Coronal (striatum and hippocampus) and sagittal (prefrontal cortex) brain slices were cut with a VT1200S microtome (Leica). Slices were prepared in an ice-cold solution of the following composition: 125 mM NaCl, 0.4 mM CaCl₂, 1 mM MgCl₂, 1.25 mM NaH₂PO₄, 26 mM NaHCO₃, 20 mM glucose, 2.5 mM KCl, 5 mM sodium pyruvate, and 1 mM kynurenic acid, saturated with 5% CO₂ and 95% O₂. The slices were incubated in this solution for 30 min and then placed on a Millicell-CM membrane (Millipore) in culture medium (50% Minimum Essential Medium, 50% Hanks' Balanced Salt Solution, 5.5 g/L glucose, penicillin-streptomycin, Invitrogen). We used the Sindbis virus as a vector to induce expression of the biosensors after overnight incubation (Ehrengruber et al. 1999). The coding sequences of the cAMP biosensor Epac-S^{H150} (Polito et al. 2013), calcium biosensor Twitch-2B (Thestrup et al. 2014) or cGMP biosensor cyGNAL were inserted into the plasmid vector pSinRep5 (Invitrogen, San Diego, CA). The linear pSinRep5 and the DH(26 S)

helper DNA (which contains the structural proteins required for packaging of the Sindbis viral genome) were used to prepare recombinant RNA *in vitro*. The capped and polyadenylated RNA transcripts (from DH26S) and pSinRep5) were co-transfected into BHK cells to produce the pseudovirions. This viral vector was added on the brain slices ($\sim 5 \times 10^5$ particles per slice), and the infected slices were incubated overnight at 35 °C under an atmosphere containing 5% CO₂. Before the experiment, slices were incubated for 30 min in the recording solution (125 mM NaCl, 2 mM CaCl₂, 1 mM MgCl₂, 1.25 mM NaH₂PO₄, 26 mM NaHCO₃, 20 mM glucose, 2.5 mM KCl and 5 mM sodium pyruvate saturated with 5% CO₂ and 95% O₂). Recordings were performed with a continuous perfusion of the same solution at 32 °C.

All experiments were performed in the presence of 200 nM tetrodotoxin (TTX) to block electrical activity. Wide-field images were obtained with an Olympus BX50WI or BX51WI upright microscope with a 40 × 0.8 NA water-immersion objective and an ORCA-AG camera (Hamamatsu). Images were acquired with iVision (Biovision, Exton, PA, USA). The excitation and dichroic filters were D436/20 and 455dcxt. Signals were acquired by alternating the emission filters, HQ480/40 for CFP, and D535/40 for YFP, with a filter wheel (Sutter Instruments, Novato, CA, USA). Filters were obtained from Chroma Technology and Semrock.

Photo-release of caged compounds was performed using high power 360 nm LED sources mounted on the epifluorescence port of the microscopes, providing 14 mW at the exit of the microscope objective (0.5 s flash duration) or 7.5 mW (1 s flash duration). The combination of LED sources at 360 nm (for uncaging) and 420 nm (off-peak light source for 436 nm excitation filter for imaging) was purchased from Mightex (Toronto, Canada). The frequency of data acquisition, usually 1 image pair every 30/50 s, was increased to 0.6 Hz in order to resolve peak dynamics, starting 10 data points before MNI-NMDA and/or NPEC-DA uncaging.

Image Analysis

Images were analyzed with custom routines written in the IGOR Pro environment (Wavemetrics, Lake Oswego, OR, USA). No correction for bleed-through or direct excitation of the acceptor was applied to keep the benefit of ratiometric cancellation of optical artefacts. Biosensor activation level was quantified by ratiometric imaging: donor fluorescence divided by acceptor fluorescence for Epac-S^{H150} and cyGAL; acceptor divided by donor for Twitch-2B. The emission ratio was calculated for each pixel and displayed in pseudocolor images, with the ratio value coded in hue and the fluorescence of the preparation coded in intensity. Wide-field imaging of Epac-S^{H150} allowed for the separation of D1 and D2 MSNs, provided that the infection level was kept low and no fluorescence overlap between neighboring neurones was observed. The optical cross-contamination resulting from out of focus light was evaluated by the response to CGS 21680, an agonist of the adenosine A_{2A} receptors, and SKF-81297, a selective agonist of dopamine D₁ receptors: cells were rejected from analysis if the cross-contamination was above 30%. Cells were also excluded from the analysis when basal ratio was elevated, when the response to forskolin was lacking or when the neuronal morphology was altered (uneven cell contours).

LTP Measurements

Male Wistar rats (7–9 weeks old) from Shanghai Laboratory Animal Center (Shanghai, China) were used. The rats were

housed under 12 h light/dark cycle at a temperature of 23 ± 3 °C and a humidity of 40–70%. Food and water was available *ad libitum*. All procedures were conducted with approval from the Danish Animal Experimentation Inspectorate (journal no. 2014 15 0201 00 339) and in accordance with the ChemPartner Institutional Animal Care and Use Committee. Rats were anesthetized by isoflurane and perfused transcardially with an ice-cold sucrose saline solution (in mM): 110 sucrose, 60 NaCl, 3 KCl, 28 NaHCO₃, 1.25 NaH₂PO₄, 0.5 CaCl₂, 7 MgCl₂ and 5 glucose (pH 7.4; saturated with 95% O₂/5% CO₂). After decapitation, brains were removed, placed in chilled sucrose solution and parasagittal slices (350 μm) containing the Nucleus Accumbens (NAc) were cut using a VT1200S vibratome (Leica Microsystems Inc., Bannockburn, Illinois, USA). Slices were incubated in regular artificial cerebrospinal fluid (ACSF) containing (in mM): 119 NaCl, 2.5 KCl, 1.2 Na₂HPO₄, 25 NaHCO₃, 2.5 CaCl₂, 1.3 MgCl₂ and 10 glucose (pH 7.4; saturated with 95% O₂/5% CO₂) at 30 °C for the first 60 min and then transferred to room temperature prior to recordings.

Multi-electrode array (MEA) MED64 Quad 2 systems (AlphaMed Scientific, Japan) were used for extracellular recordings. The MEA probes were composed of 16 platinum electrodes on the surface of a carrier substrate. The electrodes (each 50 × 50 μm²) were arranged in a 4 × 4 matrix, 150 μm apart from each other. Slices were left in the probe for at least 30 min prior to recordings and continuously perfused with oxygenated ACSF (4 mL/min, 32 °C). In most recordings, the synaptically evoked population spike/field excitatory postsynaptic potential (fEPSP, N₂) which is mediated by endogenous glutamate release and concomitant activation of AMPA receptors, was preceded by a nonsynaptic compound action potential (N₁) that is independent of glutamate release and activation of glutamate receptors. fEPSPs were obtained in the presence of the GABA_A antagonist Gabazine (SR95531, 10 μM). 0–80 μA biphasic pulses (100 μs each) with a 5 μA step were applied to evoke fEPSPs and input/output relations were measured. The stimulation intensity evoking a half-maximal response was used for LTP experiments. Electrical stimulation was applied at the NAc core, 100–400 μm from the border between the cortex and the NAc core, to stimulate primarily infralimbic and prelimbic afferents. fEPSPs were recorded from a neighboring electrode 150 μm caudal of the stimulation electrode and reported as fEPSP slopes (10–90% of the rising phase of the response).

Following a 30 min-long stable baseline recording, slices were exposed to either DMSO (control) or 3 μM Lu AF64196 for the remaining of the experiments. And 30 min after DMSO or Lu AF64196 application, LTP was induced by applying a theta burst stimulation (TBS) (Hawes et al. 2013): 10 bursts were delivered at 200 ms interval—each burst consisting of 4 pulses delivered at 50 Hz. The protocol was repeated 10 times at 15 s intervals.

Drugs

Solutions were prepared from powders purchased from Sigma-Aldrich (St Quentin-Fallavier, Isère, France). TTX was from Latoxan (Valence, France). All other drugs were from Tocris Bio-technique (Lille, France). NPEC-DA: (N)-1-(2-nitrophenyl)ethyl-carboxy-3,4-dihydroxyphenethylamine. MNI-NMDA: 4-methoxy-7-nitroindolyl-caged N-methyl-D-aspartic acid. DEANO: 2-(N,N-diethylamino)-diazeneolate 2-oxide sodium salt hydrate.

SKF-81297, a selective agonist of dopamine D₁ receptors, was used to identify MSNs of the D1 type, while CGS 21680, an agonist of the adenosine A_{2A} receptors was used to identify MSNs of the D2 type (Fig. 3). All drugs except TTX and

DEDMSO were added to the bath solution from a stock solution in DMSO; final DMSO concentration in the bath solution remained below 1%.

Statistical Analysis

For biosensor imaging experiments, the responses obtained from all neurons were averaged together and statistics were calculated per experiment (i.e., brain slice). N indicates the number of repeats of the same experiment, and n indicates the total number of neurons. Statistical analysis (unpaired t-tests, except for data in Fig. 6 where paired t-test was used) were performed using Igor Pro (Wavemetrics, Lake Oswego, OR, USA). Degrees of freedom were calculated assuming a possible difference in variance between the samples, resulting in noninteger degrees of freedom values (reported between brackets). For LTP quantification, statistics were calculated per cell, assuming a same variance for all samples. Shading on traces represent standard error of the mean (SEM).

Results

A New Biosensor for cGMP

Several existing FRET biosensors for cGMP are based on dim fluorescent proteins, usually CFP and YFP, or display a limited cGMP selectivity, therefore limiting their use in living cells (Russwurm & Koesling 2018), and we therefore undertook the development of a novel fluorescence resonance energy transfer (FRET) biosensor for optimal measurement of changes in intracellular cGMP in brain slice preparations. We selected the cGMP binding domain of the bovine PKG I. Even though CNB-A of PKG I has high affinity to cGMP, it only displays poor selectivity between cGMP and cAMP (Kim et al. 2011; Huang et al. 2014). We reasoned that under physiological conditions, given comparatively high cAMP concentrations, CNB-A would not contribute much to the required conformational change within the FRET sensor, because its binding site would be saturated. We therefore replaced the CNB-A binding site within the sensor with a copy of the structurally very similar CNB-B binding site, leading to a tandem of CNB-B domains with a high selectivity for cGMP over cAMP. In our hands, sensors using 2 CNB-B binding sites displayed a 2-fold increase in response over sensors using CNB-A and CNB-B binding sites.

We incorporated the brightest available fluorescent proteins in the relevant wavelength ranges, namely mCerulean3 (Markwardt et al. 2011) as the donor and Ypet (Nguyen & Daugherty 2005) as the acceptor fluorescent proteins. We optimized the positioning of fluorescent proteins within the sensor and found that the best overall performance was achieved by having mCerulean3 in a C-terminal position and by removing 11 amino acids from the C-terminus of a N-terminally positioned Ypet (Fig. 1A). This novel biosensor, called cyGNAL, is responding to an increase in cGMP with an inverted change in donor and acceptor fluorescence (Fig. 1B), indicative of a decreased FRET upon cGMP binding. This is similar to the effect of cAMP on T Epac^{vv} and the Epac-S^H series (Polito et al. 2013; Klarenbeek et al. 2011, 2015). The dose-response curve of cyGNAL for cGMP could be fitted to a Hill equation with a K_d of 465 ± 69 nM and a Hill coefficient of 0.801 ± 0.075 , while the dose-response curve for cAMP showed an EC_{50} in the millimolar range (Fig. 1C). This biosensor thus shows a large selectivity for cGMP against cAMP. The ratio was stable at physiological pH and displayed an increase in ratio below 7 (Fig. 1D). Since

the fluorophores have a pK_a in a much lower range, this suggests a pH sensitivity in other domains of the protein.

The properties of the biosensor were further tested in brain slice preparations using viral transfer. In striatal medium spiny neurons, cGMP elevation by bath application of the NO donor DEANO (10 μ M) produced a steady-state F480/F535 ratio increase in all recorded striatal neurons as expected. This response was not saturating since application of the nonspecific PDE inhibitor IBMX at the end of the recording increased the ratio further to a higher steady-state level (Fig. 1E). As commonly accepted (Russwurm & Koesling 2018), we assumed this final level to correspond to biosensor maximal response, that is, saturation of the biosensor with cGMP.

NMDA Receptor Activation Transiently Decreases cGMP in the Striatum

Since PDE1 is highly expressed in the striatum, we first examined its functional role in the control of cGMP in striatal slices in which the cyGNAL biosensor was sparsely expressed via viral transduction. To reduce variability resulting from endogenous electrical activity in the brain slice, action potentials were suppressed by the continuous application of TTX (200 nM) in all experiments. As previously described, tonic production of cGMP is low in slices at basal conditions (Polito et al. 2013) and cGMP production was first increased to a higher steady-state level by applying the NO donor DEANO (10 μ M). PDE1 activity is calcium dependent, and we aimed at increasing intracellular calcium with a transient activation of NMDA receptors while monitoring changes in intracellular cGMP (Fig. 2A,B). To this end, a caged-derivative of NMDA, MNI-NMDA (100 μ M), was applied during the steady-state cGMP level, which had no effect by itself. After a few minutes to allow for the diffusion of the compound into the brain slice, the uncaging protocol was performed: acquisition frequency was increased to 0.6 Hz and a flash of UV light was applied to release NMDA in the brain slice. Immediately following the flash, the cGMP level showed a multiphasic change with an initial decrease for about 1 min, then a recovery overshooting the initial level and finally a progressive return to the level before uncaging after 3 min (Fig. 2B). At the end of the recording, the nonselective PDE inhibitor IBMX (200 μ M) was added to reach the maximal ratio response of the biosensor, and that level was used for normalization. PDE9A which is not inhibited by IBMX and expressed at a low level in the brain, has low K_m and V_{max} for cGMP (Rybalkin et al. 2013; Dornier-Ciossek et al. 2017) and therefore unlikely to prevent reaching the saturation level of the biosensor in that final condition. The decrease in ratio value after MNI-NMDA uncaging was of $-41.8 \pm 8.5\%$ (mean \pm SD, $N = 5$, $n = 38$) of the maximal ratio response.

To check for photophysical effects of the UV flash on the biosensor, the same experiment was performed in the absence of MNI-NMDA; this had negligible effect (Supplementary Fig. S1A). To control whether MNI-NMDA exerted effects independently of NMDA receptors upon uncaging, the same experiment was performed in the presence of the NMDA receptor antagonist D-APV (40 μ M), which strongly reduced the effect of MNI-NMDA uncaging (Supplementary Fig. S1B).

With each molecule of biosensor binding 2 molecules of cGMP, it might be possible that the biosensor exerts a buffering effect on the response to be measured. To test for this effect, the fluorescence emission of the YFP channel in baseline condition was used as a proxy for biosensor concentration and was measured for every neuron that was well in focus, measuring

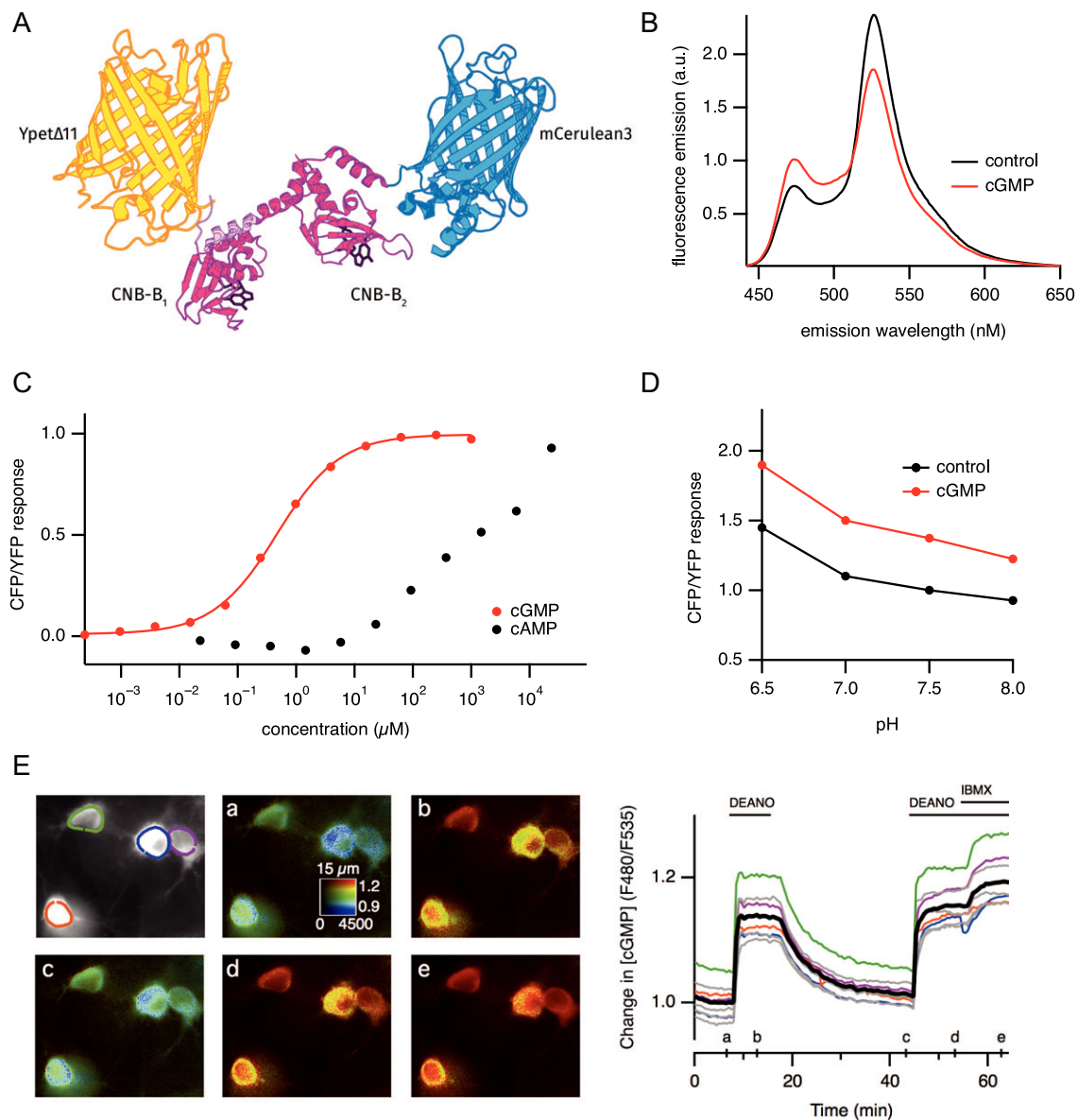


Figure 1. A novel biosensor for imaging cGMP. (A) Structure of the FRET-based cGMP sensor cyGNAL. The sensor domain is constituted of a tandem of the CNB-B domain from bovine type I PKG placed in between Ypet Δ 11 (acceptor) and mCerulean3 (donor). (B) Emission spectrum of cyGNAL without (control) and with 1 mM cGMP. (C) cGMP and cAMP titration of the ratio response. The cGMP curve is fitted to a Hill equation with a K_d of $0.465 \pm 0.069 \mu\text{M}$ and a Hill coefficient of 0.801 ± 0.075 . Half-maximal activation of cyGNAL was obtained with a concentration of 1.4 mM cAMP. (D) pH dependency of the ratio in control condition or with 1 mM cGMP. (E) The cyGNAL biosensor was expressed in striatal brain slices and imaged with wide-field microscopy. Raw fluorescence of the acceptor is displayed in gray and donor/acceptor fluorescence ratio is displayed in pseudocolor, coded from blue (low F480/F535 ratio, i.e., low cGMP) to red (high cGMP). Ratio images (a–e) correspond to the time points indicated in the bottom graph. Changes in ratio were measured during time and plotted besides: each trace indicates the F480/F535 emission ratio measurement on regions indicated by the color contour drawn on the gray image. Gray traces correspond to regions of interest outside this region of the image. The thick black trace represents the average. Horizontal bars indicate the bath application of DEANO (10 μM) and IBMX (200 μM).

the average fluorescence intensity of the 10% brightest pixels in the region of interest. Supplementary Figure S2A shows all the responses to NMDA uncaging with a color coding that reflects fluorescence intensity. Intensity values cover a range from 4 to 120 counts/pixel/s. There is no overt relationship between fluorescence intensity and the shape of the NMDA-induced decreases in cGMP concentration. The amplitude of negative peak and onset slope plotted against fluorescence intensity (Supplementary Fig. S2B and C) show a tendency towards response of smaller amplitude and slower onset for the highest

biosensor expression levels. However, this tendency appears modest, and affects only a minority of neurones.

We then used the selective PDE1 inhibitor Lu AF64196 (Khammy et al. 2017) to determine the contribution of PDE1 on the change in cGMP level induced by NMDA uncaging (Fig. 2C). The addition of 10 μM Lu AF64196 to DEANO had no effect on the steady-state cGMP levels, showing that PDE1 does not control cGMP in that condition. However, Lu AF64196 suppressed the transient decrease observed with NMDA uncaging: in the presence of 10 μM Lu AF64196, the ratio decrease in response to

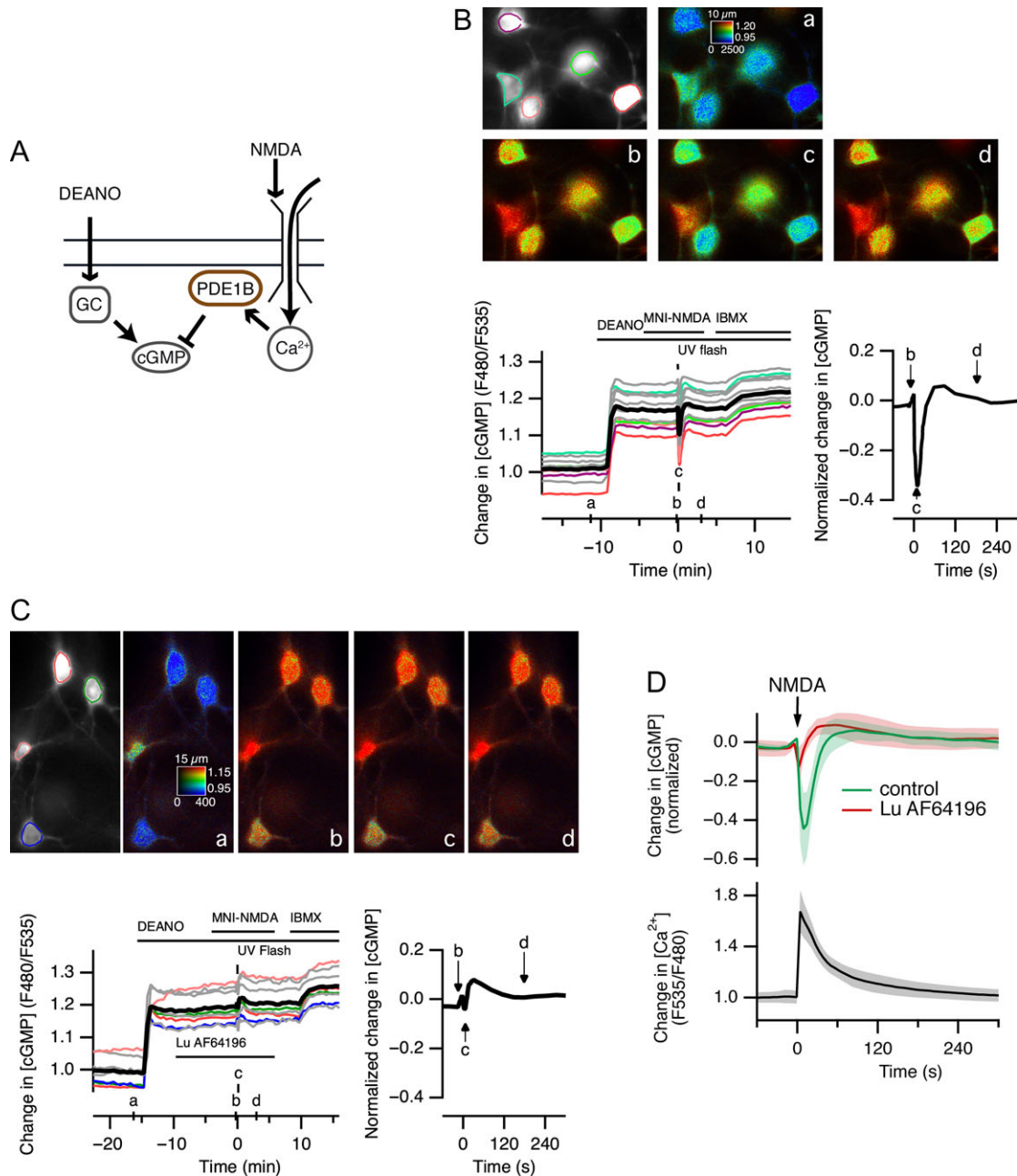


Figure 2. NMDA uncaging transiently decreases cGMP in striatal neurons, in a PDE1 dependent manner. (A) DEANO (10 μ M) was applied to activate the soluble cyclase and trigger cGMP production. NMDA was released from caged NMDA (MNI-NMDA, 100 μ M) by a flash of UV light. NMDA receptors allow for a calcium influx that activates PDE1. (B) Wide-field imaging of mouse striatal brain slices expressing the cyGNAL biosensor for cGMP. Raw fluorescence of the acceptor is displayed in gray and donor/acceptor fluorescence ratio is displayed in pseudocolor, coded from blue (low F480/F535 ratio, i.e., low cGMP) to red (high cGMP). Changes in ratio are plotted below, left: each trace indicates the F535/F480 emission ratio measured over the region of interest of corresponding color shown on the gray image. Traces in gray correspond to regions of interest outside the displayed part of the field. The black trace represents the average. Drugs were applied in the bath for the duration indicated by the horizontal bars. Ratio images correspond to the time points indicated on the horizontal axis. The graph on the right shows the normalized average ratio change for all the regions of interest in this experiment. Time 0 was the time of the UV flash; amplitude 0 is the average of the 10 data points that precede the UV flash; the ratio was normalized to the maximal ratio change obtained with DEANO plus IBMX (200 μ M). (C) Same as (B) except that 10 μ M Lu AF64196 was applied before and during NMDA uncaging. (D) Similar experiments were averaged, with shading indicating SEM. Top: Response to NMDA uncaging measured with the cyGNAL biosensor for cGMP in control condition (green: $n = 33$, $N = 4$) and in the presence of 10 μ M Lu AF64196 (red: $n = 48$, $N = 6$). Bottom: changes in intracellular calcium during the same NMDA uncaging protocol measured with Twitch-2B (black: $n = 37$; $N = 3$).

the UV flash was $-3.3 \pm 4.3\%$ (mean \pm SD, $N = 6$, $n = 47$) of the maximal ratio response, similar to the response obtained in the absence of MNI-NMDA or with NMDA receptor antagonists, and significantly different from the control response in the absence of the inhibitor ($t[3.4] = 5.7$, $P = 0.007$, Fig. 2D, top traces).

In the presence of 10 μ M DEANO and before the flash of UV light, the steady-state ratio value measured with the cyGNAL biosensor was $79.6 \pm 5.3\%$ (mean \pm SD, $N = 12$, $n = 89$) of the maximal ratio response; considering the K_d and Hill coefficient described for the cyGNAL biosensor, this level corresponds to a

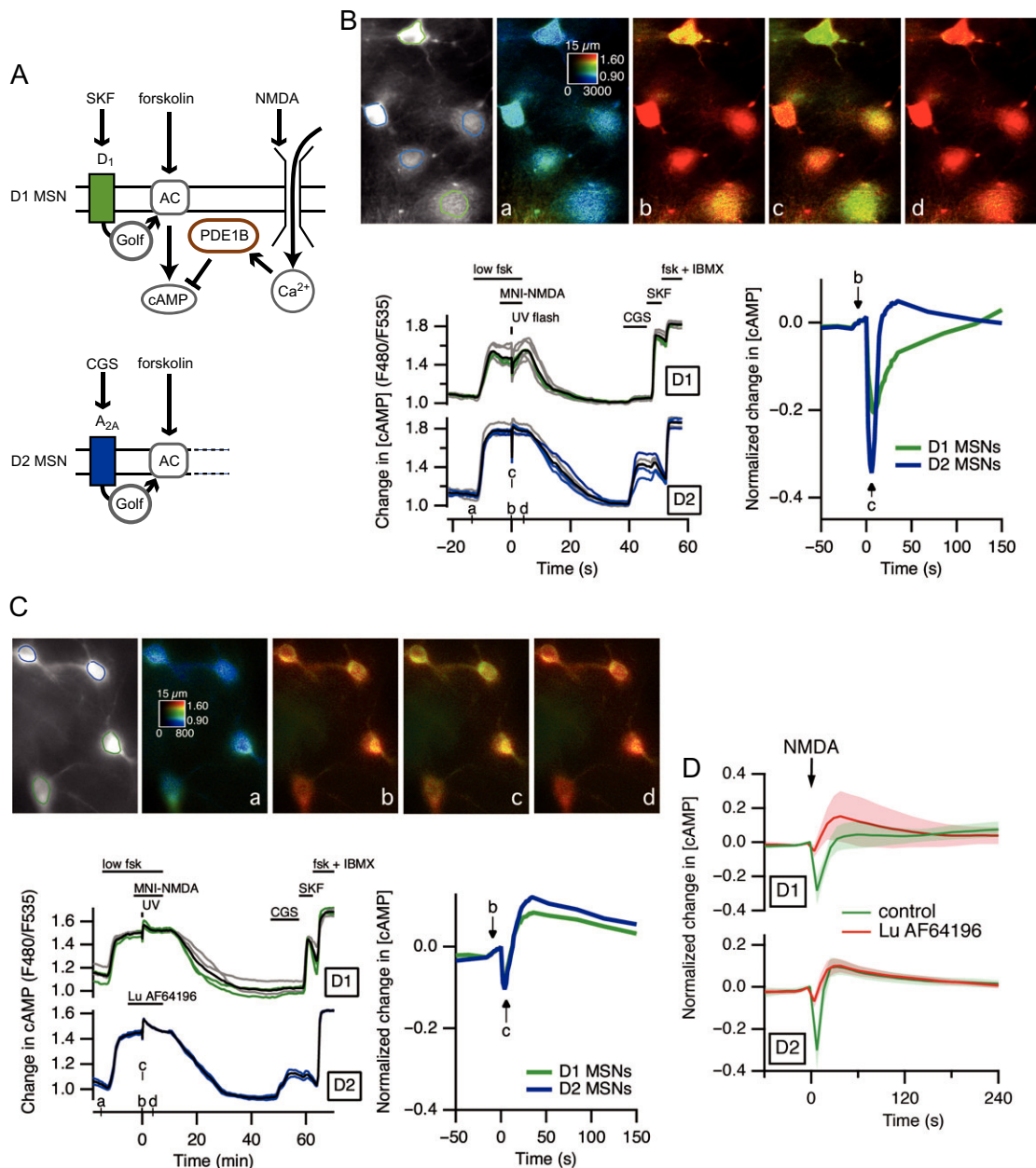


Figure 3. NMDA uncaging transiently decreases cAMP in striatal neurons, an effect blocked by the PDE1 inhibitor Lu AF64196. (A) A low concentration of forskolin (500 nM) was used to sub-maximally activate cAMP production. NMDA was released from caged NMDA (MNI-NMDA, 100 μ M) by a flash of UV light, triggering a calcium influx to activates PDE1. MSNs were identified as D1 or D2 from their response to either SKF-81297 (SKF, 1 μ M, agonist of D1 dopamine receptors) or CGS 21680 (CGS, 1 μ M, A_{2A} adenosine receptor). Maximal ratio was determined at the end of the experiment using 13 μ M forskolin and 200 μ M IBMX. (B) Wide-field imaging of mouse striatal brain slices expressing the Epac-S^{H150} biosensor for cAMP. Raw fluorescence of the acceptor is displayed in gray and donor/acceptor fluorescence ratio is displayed in pseudocolor, coded from blue (low F480/F535 ratio, i.e., low cAMP) to red (high cAMP). Changes in ratio are plotted below, left: each trace indicates the F480/F535 emission ratio measured over the region of interest of corresponding color shown on the gray image. Traces in gray correspond to regions of interest outside the displayed part of the field. The black trace represents the average. Ratio images correspond to the time points indicated by the horizontal axis. Drugs were applied in the bath for the duration indicated by the horizontal bars. The graph on the right shows the normalized average ratio change for all the regions of interest in this experiment. Time 0 was the time of the UV flash; amplitude 0 is the average of the 10 data points that precede the UV flash; amplitude was normalized to the maximal ratio change (fsk + IBMX). (C) Same as (B), except that 10 μ M Lu AF64196 was applied before and during NMDA uncaging. (D) Similar experiments were averaged, with shading indicating SEM. Top: Response to NMDA uncaging measured in D1 neurons in control condition (green: $n = 28$, $N = 4$) and in the presence of 10 μ M Lu AF64196 (red: $n = 27$, $N = 5$). Bottom: Response to NMDA uncaging measured in D2 neurons in control condition (green: $n = 13$, $N = 4$) and in the presence of 10 μ M Lu AF64196 (red: $n = 16$, $N = 5$).

cGMP concentration of approximately 2.5 μ M in a range from 1.7 to 4.0 μ M.

Finally, we also monitored the calcium signal after NMDA uncaging using the genetically encoded FRET biosensor Twitch-

2B (Thestrup et al. 2014): MNI-NMDA (100 μ M) uncaging was immediately followed by a large ratio increase, which declined progressively (Fig. 2D, bottom trace), over a time-course that roughly matched the transient decrease in cGMP levels.

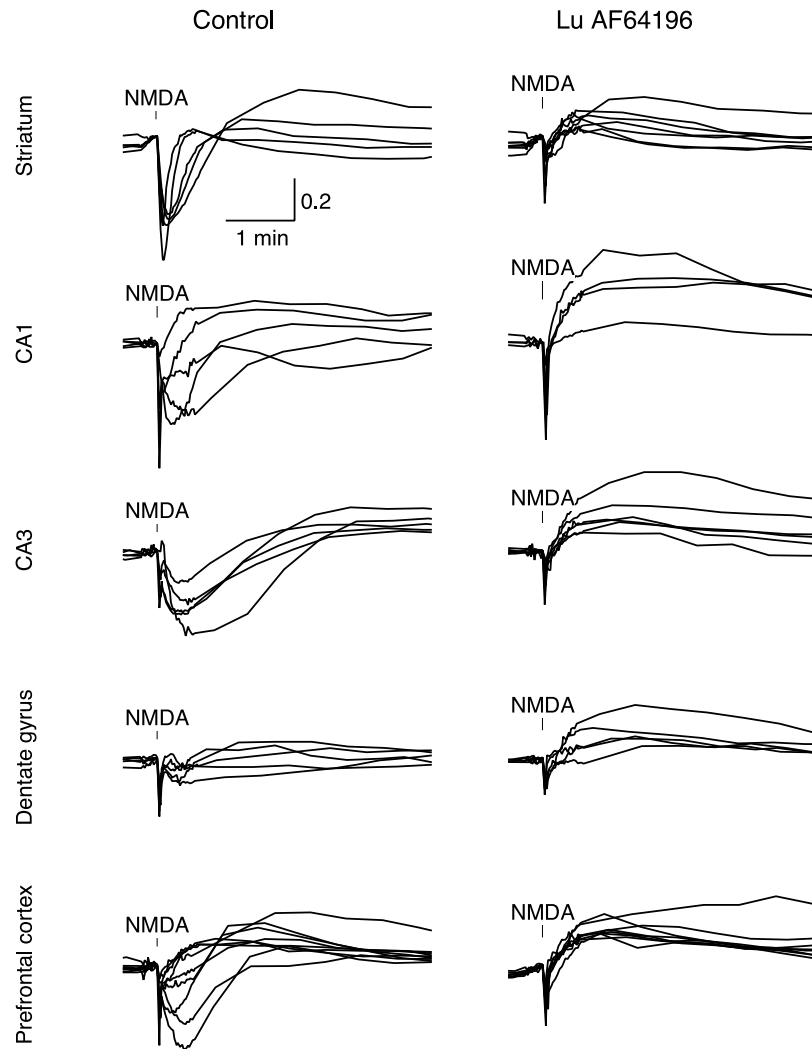


Figure 4. PDE1 effect on cGMP in various regions in mouse brain slices. NMDA was uncaged while monitoring cGMP with the cyGfAL biosensor, using the protocol shown in Figure 2. The experiment was performed in the absence (left column) or in the presence of 10 μ M Lu AF64196 (right column). Each trace represents the average ratio of one experiment comprising 1–13 neurones. Traces are normalized between baseline and maximal response to DEANO (10 μ M) and IBMX (200 μ M). The vertical bar indicates the uncaging of NMDA (100 μ M). The experiments were performed in striatum (same data as in Fig. 2), hippocampus (CA1 and CA3), dentate gyrus and prefrontal cortex. Calibration bars: horizontally, 1 min; vertically: 20% of the maximal ratio change.

These data show that a transient stimulation of NMDA receptors, which increases intracellular calcium, triggers a decrease in cGMP mediated by PDE1 action in striatal MSNs. In addition, these data show that PDE1 does not contribute significantly to cGMP control in these neurones in basal condition.

NMDA Uncaging Transiently Decreases cAMP in the Striatum

PDE1 can also hydrolyze cAMP, and to test if PDE1 controlled cAMP responses similarly to cGMP, we used the Epac-S^{H150} biosensor to monitor cAMP in striatal neurones (Fig. 3). We used a protocol for NMDA uncaging similar to that used for monitoring cGMP, except that a steady-state cAMP level was obtained with the application of 500 nM of forskolin (low fsk). MSNs were sorted in 2 groups, D1 or D2 MSNs, according to their positive cAMP response to either a D₁ agonist (SKF-81297, 100 nM) or an A_{2A} agonist (CGS 21680, 1 μ M), (Fig. 3A,B) as published previously (Yapo et al. 2017; Nair et al. 2018). At the end of the recording, the nonselective PDE inhibitor IBMX (200 μ M) was added to reach the maximal ratio response of the biosensor,

and that level was used for normalization. PDE8B is not inhibited by IBMX but its expression level is low in the brain. In addition, PDE8 has a low K_m and moderate V_{max} for cAMP compared with the highly expressed PDE2A (Rybalkin et al. 2013), and therefore PDE8 is unlikely to prevent reaching the saturation level of the biosensor. Similar to the cGMP responses, NMDA release triggered a transient decrease in cAMP in both D1 and D2 MSNs (Fig. 3B). This decrease was $-28.1 \pm 8.0\%$ (mean \pm SD, $N = 4$, $n = 28$) of the maximal ratio response in D1 MSNs, and of $-30.7 \pm 8.7\%$ (mean \pm SD, $N = 4$, $n = 13$) of the maximal ratio response in D2 MSNs, not significantly different between D1 and D2 MSNs. The recovery of the NMDA response appeared faster in D2 than in D1 MSNs, but this may be related to higher cAMP level reached in the former upon forskolin stimulation.

Similarly to cGMP, PDE1 inhibition with Lu AF64196 (10 μ M) had no effect when added to forskolin-induced cAMP steady-state level, showing a lack of PDE1 activity in the absence of a calcium signal (Fig. 3C). However, Lu AF64196 completely suppressed the transient decrease in cAMP triggered by NMDA: the decrease in cAMP level was of $-4.4 \pm 3.3\%$ (mean \pm SD, $N = 5$,

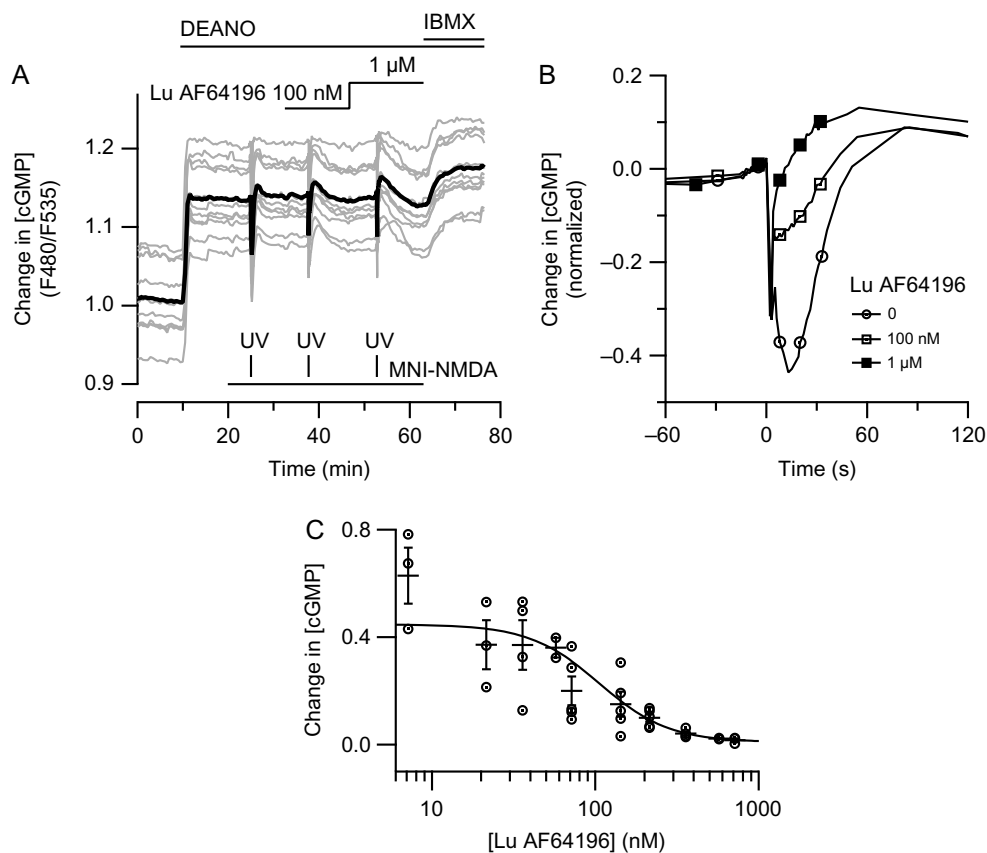


Figure 5. Dose-dependency of Lu AF64196 effect on striatal PDE1 activity in cGMP regulation. The cGMP biosensor cyGNAL was expressed in mouse striatal slices. (A) Protocol example: after elevating cGMP level with DEANO (10 μ M), 3 successive NMDA uncaging were performed. The first and third were used for normalization and were carried out at 0 and 1 μ M AF64196, respectively. The Lu AF64196 test dose was applied during the second NMDA uncaging. (B) Means of the 3 responses are overlaid for comparison. (C) Dose–response curve of the inhibitory effect of AF64196. The protocol was performed as shown in (A), testing different doses. Only one dose was tested per brain slice, represented by a circle on the plot. These data were fitted to a Hill equation with IC_{50} of 105 ± 19 nM and a Hill coefficient of 2 ± 0.6 .

$n = 27$) of the maximal ratio response in D1 MSNs, and of $-5.9 \pm 2.8\%$ (mean \pm SD, $N = 5$, $n = 16$) of the maximal ratio response in D2 MSNs. This decrease was significantly different from that measured in the absence of Lu AF64196 ($t[3.8] = 5.5$, $P = 0.0059$ for D1 MSNs, and $t[3.5] = 5.5$, $P = 0.0078$ for D2 MSNs, Fig. 3D). In contrast to the decrease obtained in control condition, NMDA uncaging in the presence of the PDE1 inhibitor led to a large rebound increase that lasted about 1 min in both D1 and D2 MSNs, possibly resulting from the activation of calcium-dependent adenylyl cyclases (Fig. 3D).

The Epac-S^{H150} ratio steady-state level reached before the UV flash was $58.0 \pm 20.3\%$ (mean \pm SD, $N = 9$, $n = 55$) of the maximal ratio response in D1 MSNs, and of $78.7 \pm 6.2\%$ (mean \pm SD, $N = 9$, $n = 29$) of the maximal ratio response in D2 MSNs. Considering a K_d of 4.4 μ M and Hill coefficient of 0.77 (Polito et al. 2013), these ratio values correspond to cAMP concentrations of 7 μ M, in a range from 3 to 20 μ M. In D2 MSNs, this level is 25 μ M in a range from 15 to 40 μ M.

These data show that PDE1 efficiently degrades cAMP following the activation of NMDA receptors. However, like for cGMP, PDE1 shows no cAMP degradation in the absence of NMDA stimulation.

PDE1 in Other Brain Regions

Besides the high expression level of PDE1B in the striatum, PDE1 is also highly expressed in cortex and hippocampus. To assess whether PDE1 is also engaged in cyclic nucleotide regulation

outside the striatum, we explored the effect of NMDA uncaging in the prefrontal cortex and in the hippocampus (CA1, CA3 and DG) using the same protocols as for measuring cGMP with the cyGNAL biosensor in the striatum (Fig. 2). This revealed a powerful action of PDE1 on cGMP level (Fig. 4) in the CA1 and CA3 regions of the hippocampus: the release of NMDA was followed by a marked decrease in cGMP concentration, which was replaced by an increase in cGMP when PDE1 was blocked by Lu AF64196 (10 μ M). The minimal ratio amplitude was measured over a temporal window from 6 to 50 s after uncaging, and expressed as a fraction of the maximal ratio response. In CA1, the ratio decrease was $-2.5 \pm 2.2\%$ (mean \pm SD, $N = 4$, $n = 7$) in the presence of Lu AF64196 versus $-22.7 \pm 11.7\%$ (mean \pm SD, $N = 5$, $n = 11$) in control condition, statistically different ($t[4.3] = 3.7$, $P = 0.017$). In CA3, the ratio decreases was $-2.8 \pm 2.5\%$ ($N = 6$, $n = 20$) versus $-31.5 \pm 16.5\%$ ($N = 5$, $n = 18$), statistically different ($t[4.2] = 3.8$, $P = 0.017$). In the cortex, some experiments showed a large decrease in cGMP after NMDA release, whereas other experiments showed minimal decrease in cGMP. In the presence of Lu AF64196, no experiment in the cortex showed any decrease in cGMP, but all displayed a sustained rebound increase in cGMP. The ratio level in the 6–50 s time range after uncaging was also higher in the presence of Lu AF64196 than in control condition, with $-3.7 \pm 4.6\%$ ($N = 8$, $n = 36$) versus $-14.9 \pm 12.2\%$ ($N = 9$, $n = 26$; $t[10.4] = 2.5$, $P = 0.028$), showing that PDE1 can down-regulate cGMP in cortical neurones, or at least in a subset thereof. The contribution of PDE1 in the degradation of cGMP in the dentate gyrus was clearly

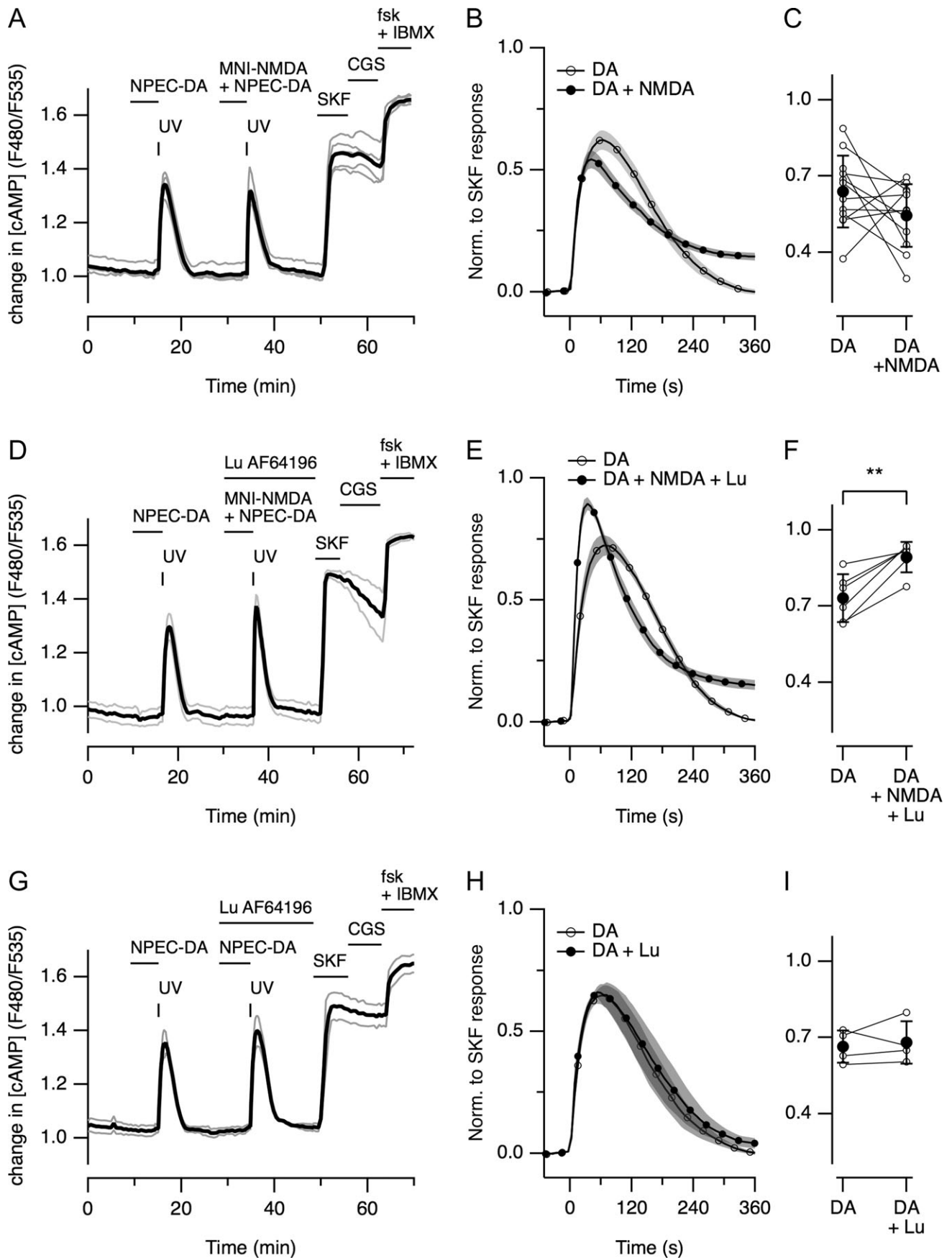


Figure 6. PDE1 opposes the potentiation of the cAMP response to dopamine induced by NMDA. Striatal brain slices from mouse expressing the Epac-S^{H150} biosensor. (A) NPEC-DA (3 μ M) was applied in the bath, and dopamine was released by a flash of UV light to trigger the control cAMP response. After recovery to baseline, a second uncaging episode was performed in the presence of both NPEC-DA (3 μ M) and MNI-NMDA (100 μ M). (B) Average of the first and second peak from 12 similar experiments. Shading indicates SEM. (C) Amplitude of the first and second cAMP peak for all experiment. Average \pm SEM is represented by the filled circle. (D–F) Same as A–C except that Lu AF64193 (1 μ M) was added during and after the second uncaging episode. (G–I) Same as A–C, except that no MNI-NMDA was applied.

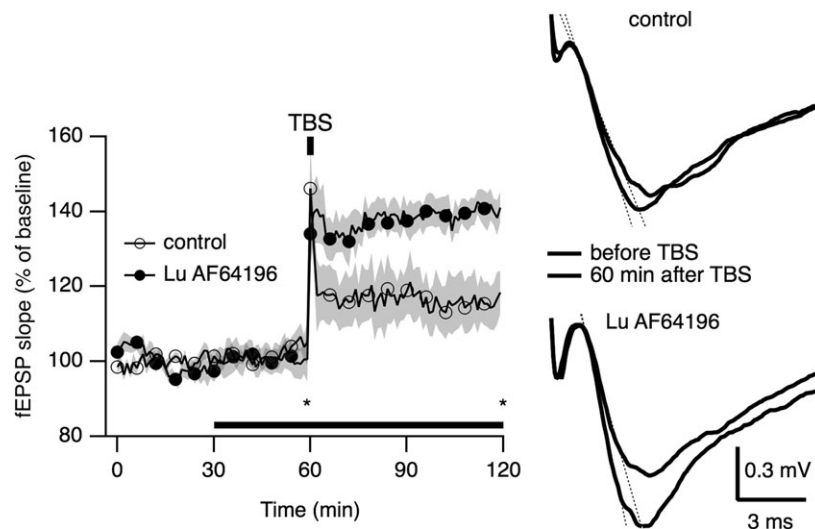


Figure 7. Lu AF64196 potentiates the LTP response. Rat brain slices were prepared from ventral striatum. Left: Normalized fEPSP slope as a function of time. Bath application of Lu AF64196 ($3\ \mu\text{M}$, $n = 8$, $N = 5$) increased the fEPSP slope following theta burst stimulation (TBS) when compared with DMSO treated (control) slices ($n = 9$, $N = 5$). Gray shading indicates SEM. The horizontal bar indicates the period during which Lu AF64196 or DMSO were added to the perfusing ACSF. TBS was applied at time 60 min: 10 bursts delivered at 200 ms interval—each burst consisting of 4 pulses at 50 Hz, repeated 10 times at 15 s intervals. Right: Traces show representative fEPSP traces before and after TBS (at times indicated by * on the left graph) in the absence (control) or in the presence of Lu AF64196. Dotted lines indicate the linear fit of response onset, which slope was used to quantify fEPSP.

visible on the shape of the ratio traces (Fig. 4), but the amplitude measured in the 6–50 s time range did not show a statistically significant difference, mainly because of the small absolute ratio changes. This is consistent with these neurons being highly hyperpolarised (Staley et al. 1992), therefore keeping NMDA receptor blocked with magnesium. To better account for decrease in cGMP concentration mediated by PDE1, the slope of the ratio trace was calculated over a 6–20 s time range. This slope, expressed as a fraction of normalized ratio per second was $+5.38 \pm 3.3\%$ (mean \pm SD, $N = 5$, $n = 22$) with Lu AF64196 versus $-2.0 \pm 2.3\%$ ($N = 5$, $n = 24$) in control condition ($t[7.1] = 4.1$, $P = 0.004$).

A similar experimental protocol was applied with the Epac-S^{H150} cAMP biosensor on the same brain regions. While the effect of Lu AF64196 was visible qualitatively, the results were more complex to analyze, with a large variability of the NMDA-induced response (Supplementary Fig. S3).

Overall, these experiments reveal a clear contribution of PDE1 in the regulation of cGMP in the striatum, hippocampus and cortex after the transient activation of NMDA receptors. An effect of PDE1 on cAMP was also clear in the striatum, but more refined protocols are required to quantify its role on cAMP in other brain regions.

Dose-Response Analysis in the Striatum With cGMP

To determine the dose-dependency of the Lu AF64196 effect on PDE1 activity in mouse brain slice preparations, we focused on its action on cGMP in the striatum. Since the amplitude of the PDE1-mediated decrease in cGMP varied from cell to cell, the effect of each dose of Lu AF64196 was quantified using 3 successive NMDA uncaging episodes (Fig. 5): an initial control uncaging was performed without Lu AF64196, a second uncaging was done in the presence of Lu AF64196 at the test concentration and a third uncaging was performed in the presence of a maximal dose of Lu AF64196 ($1\ \mu\text{M}$). We verified that 3 consecutive episodes of NMDA uncaging produced similar decreases in cGMP (Supplementary Fig. S4A), and that $1\ \mu\text{M}$ Lu AF64196 was sufficient to completely block the decrease in cGMP (Supplementary Fig. S4B). The effect of the Lu AF64196 test

concentration (second uncaging event) was normalized to the uncaging events with no and maximal ($1\ \mu\text{M}$) Lu AF64196 (Fig. 5A,B). This protocol was repeated for Lu AF64196 doses ranging from 7 to 730 nM in the striatum. A single dose was tested in each experiment. The peak amplitude of the cGMP response to NMDA were averaged for each experiment, and provided a dose-response curves which was fitted to a Hill equation with IC_{50} of 105 nM (Fig. 5C).

Dopamine—NMDA Coincidence in the Striatum

Coincidence of dopamine and glutamate neurotransmission is considered to be a key mechanism underlying learning processes in the striatum (Surmeier et al. 2007; Kreitzer & Malenka 2008; Cerovic et al. 2013), and we wanted to determine whether the cAMP signal produced by dopamine D₁-like receptors in the striatum are affected by PDE1 activity triggered by the concomitant release of NMDA. To this end, we used NPEC-dopamine (NPEC-DA, “caged dopamine”), which has previously been shown to consistently induce large increases in cAMP in D1 MSNs (Yapo et al. 2017). Experiments were performed on mouse striatal slices expressing the cAMP biosensor Epac-S^{H150} (Fig. 6A). These experiments were performed with TTX (200 nM), atropine ($1\ \mu\text{M}$), CGP 55845A (100 nM), AM251 (100 nM), naloxone (500 nM) and eticlopride (100 nM) to block voltage-dependent sodium channels, muscarinic, GABA_B, CB₁, opioid, and dopamine D₂-like receptors, respectively. D1 and D2 MSNs were identified at the end of the experiment from their response to either D₁ or A_{2A} receptor agonists SKF-81297 (100 nM) or CGS 21680 ($1\ \mu\text{M}$), respectively (Yapo et al. 2017) and as illustrated in Figure 3A, and only D1 MSNs were analyzed. A first reference dopamine response was measured with the uncaging of NPEC-DA ($3\ \mu\text{M}$); a second response was measured with the simultaneous uncaging of NPEC-DA ($3\ \mu\text{M}$) and MNI-NMDA ($100\ \mu\text{M}$). The same experiment was repeated and Figure 6B shows the average of the first and second peaks. The recovery kinetics appeared somewhat slower on the second peak. The amplitude of the cAMP responses were similar ($64 \pm 4\%$ of the response to SKF for the first peak vs. $54 \pm 4\%$, mean \pm SEM for the

second peak, $N = 12$, $n = 59$, not significantly different) ($t[11]=1.5$, $P=0.15$; peak amplitudes are shown in Fig. 7C).

To test the involvement of PDE1 in the regulation of the dopamine-induced cAMP peak, a second set of similar experiments was performed in which Lu AF64196 (1 μM) was applied a few minutes before and maintained during and after the co-release of dopamine and NMDA (Fig. 6D). In contrast to the control condition, the amplitude of the cAMP response produced by co-release of NMDA and dopamine was increased when PDE1 was inhibited (Fig. 6E,F): the amplitude of the first peak was $73 \pm 4\%$ versus $89 \pm 2\%$, $N = 6$, $n = 23$ for the second peak, significantly different (paired t -test, $t[5] = 5.2$, $P = 0.003$). As a control, we verified that Lu AF64196 had no effect on the dopamine response in the absence of NMDA (Fig. 6G–I, paired t -test, $t[3] = 0.51$, $P = 0.65$).

These experiments show that PDE1 modulates the amplitude of a dopamine-induced cAMP signal in the context of coincidental activation of NMDA and D_1 receptors.

PDE1 Action in Synaptic Plasticity

The cAMP/PKA signaling pathway, activated by D_1 receptors in D_1 MSNs and adenosine A_{2A} receptors in D_2 MSNs, is required for LTP induction (Kreitzer & Malenka 2008; Surmeier et al. 2009; Cerovic et al. 2013), and since we observed that PDE1 opposed the dopamine-induced cAMP signal, we wondered whether PDE1 action might reduce LTP induction. The effect of Lu AF64196 (3 μM) on LTP in the ventral striatum (NAc) was tested using field recordings in rat brain slices (Fig. 7). To isolate the response to glutamatergic synapses, GABA_A receptor activity was blocked by supplying Gabazine (10 μM) to the perfusing ACSF. Slices were subjected to Lu AF64196 or DMSO for 30 min prior to theta-burst stimulation (TBS) and during this period fEPSP slopes remained largely unaffected by the presence of compound, indicating that basal cAMP/cGMP levels and/or intracellular Ca^{2+} concentration are too low to observe an effect of PDE1 activity under these conditions. TBS induced an increase in the fEPSP slope, which remained elevated during the time course of the experiment, both in the absence and the presence of Lu AF64196 (3 μM). Lu AF64196 increased the average fEPSP slope 50–60 min after TBS to $140 \pm 4.5\%$ (mean \pm SEM, $N = 5$, $n = 8$) relative to prestimulation levels, which is significantly higher than in DMSO controls ($113 \pm 5.4\%$, mean \pm SEM, $N = 5$, $n = 9$, $t(15) = 3.785$, $P = 0.002$). Thus, PDE1 inhibition results in an increased LTP response in NAc, consistent with PDE1 opposing the cAMP signals which are required for LTP induction.

Discussion

PDE1 is highly expressed in the brain, but there are little mechanistic data on its functional impact in neurons. Using the selective PDE1 inhibitor Lu AF64196 and biosensors for cyclic nucleotides, we describe PDE1 action on both cAMP and cGMP in mouse brain slice preparations. Our experiments reveal that, upon activation of NMDA receptors, PDE1 degrades cAMP and cGMP in the striatum, cortex, and hippocampus. Our results also show that PDE1 is implicated in the regulation of synaptic plasticity, and that it regulates the effect of dopamine when NMDA receptors are stimulated at the same time.

While the palette of biosensors for cAMP now includes bright sensors with high signal change (Polito et al. 2013; Klarenbeek et al. 2011, 2015), biosensors for cGMP with similarly high ratio changes and good photostability have been missing. From the first cygnet family of biosensors for cGMP developed by W. Dostman (Honda et al. 2001, 2005), a number of more recent sensors were created with various cGMP sensing

domains and architecture, like cGES-DE5 (Nikolaev et al. 2006) or the cGi series (Russwurm et al. 2007). All these cGMP biosensors are discussed in detail in a recent review (Russwurm & Koesling 2018). Since PDE1 can hydrolyze both cAMP and cGMP, it was critical that our biosensors had a high selectivity for each cyclic nucleotide. The Epac-S^{H150} biosensor has already been reported to be unresponsive to the high cGMP levels obtained in striatal neurons by application of NO donors (Polito et al. 2013). The cyGNAL biosensor developed here showed a high selectivity for cGMP against cAMP. With a K_d of 465 nM for cGMP, high selectivity against cAMP, a large ratio change and bright fluorophores, this biosensor proved suitable for measuring cGMP in brain slice preparations.

Increased intracellular calcium—and in particular through the activation of NMDA receptors—can stimulate the synthesis of cyclic nucleotides through various mechanisms. This effect can be direct, for example via the calcium-activated adenylyl cyclase AC1 and AC8. In addition, the activation of local neurons can lead to the release of neuromodulatory compounds such as NO (Garthwaite 2019). In the cortex, we have already shown that VIP, CRF and PACAP can trigger powerful cAMP signals (Hu et al. 2011), and NMDA stimulation may release such neuropeptides locally. How PDE1 could oppose such changes in cyclic nucleotide signal has been so far difficult to characterize, for lack of measurement methods with sufficient sensitivity and temporal resolution. Using biosensor imaging, we first tested whether PDE1 could revert an artificially induced high steady-state level of cyclic nucleotide, in conditions of action potential inhibition. Transient activation of NMDA receptors efficiently decreased both cGMP and cAMP levels, effects that were blocked by the PDE1 inhibitor Lu AF64196, and therefore attributable to PDE1 action. The transient decrease roughly matched the kinetics of the increase in intracellular calcium, on the time-scale of a minute. Such transient decrease was observed in all the brain regions that were included in our studies in which PDE1A and/or PDE1B are expressed (although it was not present in all neurons in the prefrontal cortex). Interestingly, full PDE1 inhibition revealed an increase in cyclic nucleotide level that follows the calcium signal, although on a slightly slower time-scale. The precise mechanisms underlying these increases remain to be identified and may involve calcium-induced activation of adenylyl cyclases AC1 or AC8 in the case of cAMP, and an increase in NO concentration resulting from NMDA-dependent activation of nNOS. TTX may also be insufficient to prevent the release of endogenous neuropeptides. PDE1 action thus opposes the NMDA-induced increase in cyclic nucleotide levels. While these 2 opposite effects may seem physiologically inconsistent, it potentially opens for a richer array of integrative properties. Indeed, further work is needed to determine the precise spatial and temporal features of these cyclic nucleotide events at the level of single synapses where it determines plasticity.

In striatal MSNs where PDE1B is highly expressed, we observed that the application of Lu AF64196 alone had no effect on cyclic nucleotide levels showing that PDE1 has no functional activity in the absence of a calcium signal (Figs 2C and 3C). This is consistent with a tight control of calcium–calmodulin in living neurons, sufficient to maintain PDE1 activity below our detection threshold. This contrasts with striatal PDE2A which, although activated by cGMP, displays a clear activity even in the absence of elevated cGMP (Polito et al. 2013). Among the regulated PDEs, PDE1 thus appears to strictly require calcium to operate, which suggests a tight link between PDE1 function and neuronal activity or excitatory synaptic input.

Our experiments in the striatum show that PDE1 efficiently degrades both cAMP and cGMP. PDEs have different K_m values for cyclic nucleotides which determines the concentration of cyclic nucleotide onto which it operates (Neves-Zaph 2017): in cells expressing a combination of PDEs, cyclic nucleotide signals in different concentration ranges are controlled by different PDEs. This has been illustrated in HEK293 cells in which PDE3 and PDE10A control cAMP signals elicited by minimal stimulation, whereas PDE4 action is only visible for more powerful stimulations (Matthiesen & Nielsen 2011). The high K_m value of PDE1B for cGMP and cAMP (5 and 33 μM , respectively) (Poppe et al. 2008) suggests that PDE1 would be efficient on high concentrations of cyclic nucleotides. Indeed, in MSNs, the steady-state cyclic nucleotide levels before NMDA uncaging (around 2 μM cGMP and 7–25 μM cAMP) at which a consistent PDE1-mediated response was observed, were in the same order of magnitude as the respective K_m of PDE1B. Biosensor imaging has already shown that cAMP levels could rise to particularly high level in the striatum compared with the cortex (Castro et al. 2013), which could explain why PDE1 exerted such powerful effect in MSNs. In contrast, the lower cAMP level reached in the cortex may in part explain why the action of PDE1 was observed less consistently in this brain region. Indeed, PDE4 has already been shown to be critical in controlling large cAMP signals in this part of the brain (Castro et al. 2010; Kuroiwa et al. 2012), and PDE4 action may be masking a comparatively smaller PDE1 contribution. However, other factors such as differences in PDE1 expression in a brain region with higher neuronal diversity are also likely to contribute.

PDE2A and PDE10A are also dual specificity enzymes, and constitute with PDE1B the major PDE types expressed in MSNs. PDE2A also displays a high K_m for cGMP and cAMP (31 and 112 μM , respectively) (Poppe et al. 2008), and PDE2A was also shown to degrade high cAMP and cGMP levels (Polito et al. 2013). This suggests that PDE1B and PDE2A simultaneously regulate high cyclic nucleotide levels in MSNs. However, their action differ in the ways they are regulated, with PDE1B strictly depending on glutamatergic inputs, and PDE2A being activated by NOergic interneurons, but also having a notable activity in the absence of cGMP (Polito et al. 2013). In contrast, PDE10A shows no or modest regulation by cAMP (Matthiesen & Nielsen 2009; Jager et al. 2012), has a high affinity for cAMP (K_m of 0.67 μM) (Poppe et al. 2008), and was shown to regulate the sub-micromolar cAMP level resulting from basal cAMP production (Polito et al. 2015). In summary, our experiments clarify the functional conditions in which PDE1B operates in the striatum: dual specificity, performing on high cyclic nucleotide levels and requiring a calcium signal such as that triggered by glutamatergic inputs.

Both cAMP and cGMP play important roles in synaptic plasticity and transmission in general (Kandel 2001; Garthwaite 2008) and particularly in the striatum (Lovinger 2010; Threlfell & West 2013; Padovan-Neto & West 2017). In the case of cGMP, in vivo studies have demonstrated the importance of NO production by interneurons, which control both the excitability of MSNs and the efficacy of cortico-striatal synaptic transmission (Padovan-Neto et al. 2015), while in addition, cGMP and calcium induce LTD (Calabresi et al. 1999). In parallel, direct glutamatergic inputs from the cortex increase calcium in MSNs, which activates PDE1B and opposes the NO-induced increase in cGMP. The efficacy of cortico-striatal synaptic transmission will thus result from a complex balance between these effects, and more experimental work is required to determine the contribution of PDE1B in the various schemes of synaptic regulation. In the case of cAMP, dopamine through D_1 receptors has been shown

to play a critical role in reward-mediated learning in the striatum, and LTP induction requires the activation of D_1 receptors (Kreitzer & Malenka 2008; Surmeier et al. 2009; Lovinger 2010; Cerovic et al. 2013). We report here that the positive cAMP response elicited by D_1 receptors is reduced by the co-activation of NMDA receptors. This is consistent with the observed potentiation of LTP upon PDE1 inhibition, in which PDE1 opposes the rise in cAMP which is needed for synaptic plasticity.

Collectively, these observations highlight PDE1 as a negative regulator of cyclic nucleotide signaling operating at the cross-road between calcium and cyclic nucleotide signaling pathways, and therefore endowed with a critical function in fine-tuning synaptic plasticity. By showing that PDE1 is involved in the coincidence detection of glutamate-mediated calcium signals with dopamine or NO signals, our study strongly supports that PDE1 inhibitors could have a therapeutic value, in particular in conditions related to hypodopaminergia.

Supplementary Material

Supplementary material is available at *Cerebral Cortex* online.

Funding

Lundbeck A/S and by the “Investissements d’Avenir” program managed by the ANR under reference ANR-11-IDEX-0004-02.

Note

We would like to thank Drs Régis Blaise and Jean-Christophe Poncer for helpful comments on the article. O.G. and P.V. received a funding for cooperation from “Bayerisch-Französisches Hochschulzentrum.” O.G. was an invited scientist of Ecole des Neurosciences de Paris. The group of E.M., P.V., and L.R.V.C. is member of the Bio-Psy Labex. *Conflicts of interests:* J.N., C.H., C.T.C., and J.K. are employed by H. Lundbeck A/S. J.Y. has worked as a consultant for the company H. Lundbeck A/S. The PDE1 inhibitor used in this study has been generated by Lundbeck.

References

- Ahmad F, Murata T, Shimizu K, Degerman E, Maurice D, Manganiello V. 2015. Cyclic nucleotide phosphodiesterases: important signaling modulators and therapeutic targets. *Oral Dis.* 21:e25–e50.
- Ahn HS, Crim W, Romano M, Sybertz E, Pitts B. 1989. Effects of selective inhibitors on cyclic nucleotide phosphodiesterases of rabbit aorta. *Biochem Pharmacol.* 38:3331–3339.
- Bertran-Gonzalez J, Hervé D, Girault JA, Valjent E. 2010. What is the degree of segregation between striatonigral and striatopallidal projections. *Front Neuroanat.* 4:136.
- Calabresi P, Gubellini P, Centonze D, Sancesario G, Morello M, Giorgi M, Pisani A, Bernardi G. 1999. A critical role of the nitric oxide/cGMP pathway in corticostriatal long-term depression. *J Neurosci.* 19:2489–2499.
- Castro LR, Brito M, Guiot E, Polito M, Korn CW, Herve D, Girault JA, Paupardin-Tritsch D, Vincent P. 2013. Striatal neurones have a specific ability to respond to phasic dopamine release. *J Physiol.* 591:3197–3214.
- Castro LR, Gervasi N, Guiot E, Cavellini L, Nikolaev VO, Paupardin-Tritsch D, Vincent P. 2010. Type 4 phosphodiesterase plays different integrating roles in different cellular domains in pyramidal cortical neurons. *J Neurosci.* 30:6143–6151.

- Cerovic M, d'Isa R, Tonini R, Brambilla R. 2013. Molecular and cellular mechanisms of dopamine-mediated behavioral plasticity in the striatum. *Neurobiol Learn Mem.* 105:63–80.
- Dorner-Ciossek C, Kroker KS, Rosenbrock H. 2017. Role of PDE9 in cognition. *Adv Neurobiol.* 17:231–254.
- Ehrengruber MU, Lundstrom K, Schweitzer C, Heuss C, Schlesinger S, Gähwiler BH. 1999. Recombinant Semliki Forest virus and Sindbis virus efficiently infect neurons in hippocampal slice cultures. *Proc Natl Acad Sci U S A.* 96:7041–7046.
- Ehrman LA, Williams MT, Schaefer TL, Gudelsky GA, Reed TM, Fienberg AA, Greengard P, Vorhees CV. 2006. Phosphodiesterase 1B differentially modulates the effects of methamphetamine on locomotor activity and spatial learning through DARPP32-dependent pathways: evidence from PDE1B-DARPP32 double-knockout mice. *Genes Brain Behav.* 5:540–551.
- Fabritius A, Ng D, Kist AM, Erdogan M, Portugues R, Griesbeck O. 2018. Imaging-based screening platform assists protein engineering. *Cell Chem Biol.* 25:1554–1561.e8.
- Garthwaite J. 2008. Concepts of neural nitric oxide-mediated transmission. *Eur J Neurosci.* 27:2783–2802.
- Garthwaite J. 2019. NO as a multimodal transmitter in the brain: discovery and current status. *Br J Pharmacol.* 176:197–211.
- Giorgi M, D'Angelo V, Esposito Z, Nuccetelli V, Sorge R, Martorana A, Stefani A, Bernardi G, Sancesario G. 2008. Lowered cAMP and cGMP signalling in the brain during levodopa-induced dyskinesias in hemiparkinsonian rats: new aspects in the pathogenetic mechanisms. *Eur J Neurosci.* 28:941–950.
- Goraya TA, Cooper DM. 2005. Ca²⁺-calmodulin-dependent phosphodiesterase (PDE1): current perspectives. *Cell Signal.* 17:789–797.
- Hansen RS, Beavo JA. 1986. Differential recognition of calmodulin-enzyme complexes by a conformation-specific anti-calmodulin monoclonal antibody. *J Biol Chem.* 261:14636–14645.
- Hawes SL, Gillani F, Evans RC, Benkert EA, Blackwell KT. 2013. Sensitivity to theta-burst timing permits LTP in dorsal striatal adult brain slice. *J Neurophysiol.* 110:2027–2036.
- Honda A, Adams SR, Sawyer CL, Lev-Ram V, Tsien RY, Dostmann WRG. 2001. Spatiotemporal dynamics of guanosine 3',5'-cyclic monophosphate revealed by a genetically encoded, fluorescent indicator. *Proc Natl Acad Sci USA.* 98:2437–2442.
- Honda A, Sawyer CL, Cawley SM, Dostmann WR. 2005. Cygnets: in vivo characterization of novel cGMP indicators and in vivo imaging of intracellular cGMP. *Methods Mol Biol.* 307:27–43.
- Hu E, Demmou L, Cauli B, Gallopin T, Geoffroy H, Harris-Warrick RM, Paupardin-Tritsch D, Lambollez B, Vincent P, Hepp R. 2011. VIP, CRF, and PACAP act at distinct receptors to elicit different cAMP/PKA dynamics in the neocortex. *Cereb Cortex.* 21:708–718.
- Huang GY, Kim JJ, Reger AS, Lorenz R, Moon EW, Zhao C, Casteel DE, Bertinetti D, Vanschouwen B, Selvaratnam R, et al. 2014. Structural basis for cyclic-nucleotide selectivity and cGMP-selective activation of PKG I. *Structure.* 22:116–124.
- Jager R, Russwurm C, Schwede F, Genieser HG, Koesling D, Russwurm M. 2012. Activation of PDE10 and PDE11 phosphodiesterases. *J Biol Chem.* 287:1210–1219.
- Kandel ER. 2001. The molecular biology of memory storage: a dialogue between genes and synapses. *Science.* 294:1030–1038.
- Kelly MP, Adamowicz W, Bove S, Hartman AJ, Mariga A, Pathak G, Reinhart V, Romegialli A, Kleiman RJ. 2014. Select 3',5'-cyclic nucleotide phosphodiesterases exhibit altered expression in the aged rodent brain. *Cell Signal.* 26:383–397.
- Keravis T, Lugnier C. 2012. Cyclic nucleotide phosphodiesterase (PDE) isozymes as targets of the intracellular signalling network: benefits of PDE inhibitors in various diseases and perspectives for future therapeutic developments. *Br J Pharmacol.* 165:1288–1305.
- Khammy MM, Dalsgaard T, Larsen PH, Christoffersen CT, Clausen D, Rasmussen LK, Folkersen L, Grunnet M, Kehler J, Aalkjaer C, et al. 2017. PDE1A inhibition elicits cGMP-dependent relaxation of rat mesenteric arteries. *Br J Pharmacol.* 174:4186–4198.
- Kim JJ, Casteel DE, Huang G, Kwon TH, Ren RK, Zwart P, Headd JJ, Brown NG, Chow DC, Palzkill T, et al. 2011. Co-crystal structures of PKG I β (92–227) with cGMP and cAMP reveal the molecular details of cyclic-nucleotide binding. *PLoS One.* 6:e18413.
- Klarenbeek JB, Goedhart J, Hink MA, Gadella TW, Jalink K. 2011. A mTurquoise-based cAMP sensor for both FLIM and ratio-metric read-out has improved dynamic range. *PLoS One.* 6:e19170.
- Klarenbeek J, Goedhart J, van Batenburg A, Groenewald D, Jalink K. 2015. Fourth-generation Epac-based FRET sensors for cAMP feature exceptional brightness, photostability and dynamic range: characterization of dedicated sensors for FLIM, for ratiometry and with high affinity. *PLoS One.* 10:e0122513.
- Kreitzer AC, Malenka RC. 2008. Striatal plasticity and basal ganglia circuit function. *Neuron.* 60:543–554.
- Kuroiwa M, Snyder GL, Shuto T, Fukuda A, Yanagawa Y, Benavides DR, Nairn AC, Bibb JA, Greengard P, Nishi A. 2012. Phosphodiesterase 4 inhibition enhances the dopamine D1 receptor/PKA/DARPP-32 signaling cascade in frontal cortex. *Psychopharmacology (Berl).* 219:1065–1079.
- Lakics V, Karran EH, Boess FG. 2010. Quantitative comparison of phosphodiesterase mRNA distribution in human brain and peripheral tissues. *Neuropharmacology.* 59:367–374.
- Lovinger DM. 2010. Neurotransmitter roles in synaptic modulation, plasticity and learning in the dorsal striatum. *Neuropharmacology.* 58:951–961.
- Lugnier C. 2006. Cyclic nucleotide phosphodiesterase (PDE) superfamily: a new target for the development of specific therapeutic agents. *Pharmacol Ther.* 109:366–398.
- Lugnier C, Schoeffter P, Le Bec A, Strouthou E, Stoclet JC. 1986. Selective inhibition of cyclic nucleotide phosphodiesterases of human, bovine and rat aorta. *Biochem Pharmacol.* 35:1743–1751.
- Markwardt ML, Kremers GJ, Kraft CA, Ray K, Cranfill PJ, Wilson KA, Day RN, Wachter RM, Davidson MW, Rizzo MA. 2011. An improved cerulean fluorescent protein with enhanced brightness and reduced reversible photoswitching. *PLoS One.* 6:e17896.
- Matthiesen K, Nielsen J. 2009. Binding of cyclic nucleotides to phosphodiesterase 10 A and 11 A GAF domains does not stimulate catalytic activity. *Biochem J.* 423:401–409.
- Matthiesen K, Nielsen J. 2011. Cyclic AMP control measured in two compartments in HEK293 cells: phosphodiesterase K(M) is more important than phosphodiesterase localization. *PLoS One.* 6:e24392.
- Maurice DH, Ke H, Ahmad F, Wang Y, Chung J, Manganiello VC. 2014. Advances in targeting cyclic nucleotide phosphodiesterases. *Nat Rev Drug Discov.* 13:290–314.
- Medina AE. 2011. Therapeutic utility of phosphodiesterase type I inhibitors in neurological conditions. *Front Neurosci.* 5:21.
- Menniti FS, Faraci WS, Schmidt CJ. 2006. Phosphodiesterases in the CNS: targets for drug development. *Nat Rev Drug Discov.* 5:660–670.
- Nair AG, Castro LRV, El Khoury M, Gorgievski V, Giros B, Tzavara ET, Hellgren-Kotaleski J, Vincent P. 2018. The high efficacy of muscarinic M4 receptor in D1 medium spiny neurons reverses striatal hyperdopaminergia. *Neuropharmacology.* 146:74–83.

- Neves-Zaph SR. 2017. Phosphodiesterase diversity and signal processing within cAMP signaling networks. *Adv Neurobiol.* 17:3–14.
- Nguyen AW, Daugherty PS. 2005. Evolutionary optimization of fluorescent proteins for intracellular FRET. *Nat Biotechnol.* 23:355–360.
- Nikolaev VO, Gambaryan S, Lohse MJ. 2006. Fluorescent sensors for rapid monitoring of intracellular cGMP. *Nat Methods.* 3:23–25.
- Padovan-Neto FE, Sammut S, Chakroborty S, Dec AM, Threlfell S, Campbell PW, Mudrakola V, Harms JF, Schmidt CJ, West AR. 2015. Facilitation of corticostriatal transmission following pharmacological inhibition of striatal phosphodiesterase 10 A: role of nitric oxide-soluble guanylyl cyclase-cGMP signaling pathways. *J Neurosci.* 35:5781–5791.
- Padovan-Neto FE, West AR. 2017. Regulation of striatal neuron activity by cyclic nucleotide signaling and phosphodiesterase inhibition: implications for the treatment of Parkinson's disease. *Adv Neurobiol.* 17:257–283.
- Pekcec A, Schülert N, Stierstorfer B, Deiana S, Dörner-Ciossek C, Rosenbrock H. 2018. Targeting the dopamine D₁ receptor or its downstream signalling by inhibiting phosphodiesterase-1 improves cognitive performance. *Br J Pharmacol.* 175:3021–3033.
- Piedrafita B, Cauli O, Montoliu C, Felipo V. 2007. The function of the glutamate-nitric oxide-cGMP pathway in brain in vivo and learning ability decrease in parallel in mature compared with young rats. *Learn Mem.* 14:254–258.
- Polito M, Guiot E, Gangarossa G, Longueville S, Doulazmi M, Valjent E, Hervé D, Girault JA, Paupardin-Tritsch D, Castro LR, et al. 2015. Selective effects of PDE10A inhibitors on striatopallidal neurons require phosphatase inhibition by DARPP-32. *eNeuro.* 2:1–15.
- Polito M, Klarenbeek J, Jalink K, Paupardin-Tritsch D, Vincent P, Castro LR. 2013. The NO/cGMP pathway inhibits transient cAMP signals through the activation of PDE2 in striatal neurons. *Front Cell Neurosci.* 7:211.
- Polli JW, Kincaid RL. 1994. Expression of a calmodulin-dependent phosphodiesterase isoform (PDE1B1) correlates with brain regions having extensive dopaminergic innervation. *J Neurosci.* 14:1251–1261.
- Poppe H, Rybalkin SD, Rehmann H, Hinds TR, Tang XB, Christensen AE, Schwede F, Genieser HG, Bos JL, Døskeland SO, et al. 2008. Cyclic nucleotide analogs as probes of signaling pathways. *Nat Methods.* 5:277–278.
- Reed TM, Repaske DR, Snyder GL, Greengard P, Vorhees CV. 2002. Phosphodiesterase 1B knock-out mice exhibit exaggerated locomotor hyperactivity and DARPP-32 phosphorylation in response to dopamine agonists and display impaired spatial learning. *J Neurosci.* 22:5188–5197.
- Reneerkens OA, Rutten K, Steinbusch HW, Blokland A, Prickaerts J. 2009. Selective phosphodiesterase inhibitors: a promising target for cognition enhancement. *Psychopharmacology (Berl).* 202:419–443.
- Russwurm M, Koesling D. 2018. Measurement of cGMP-generating and -degrading activities and cGMP levels in cells and tissues: focus on FRET-based cGMP indicators. *Nitric Oxide.* 77:44–52.
- Russwurm M, Mullershausen F, Friebe A, Jäger R, Russwurm C, Koesling D. 2007. Design of fluorescence resonance energy transfer (FRET)-based cGMP indicators: a systematic approach. *Biochem J.* 407:69–77.
- Rybalkin SD, Hinds TR, Beavo JA. 2013. Enzyme assays for cGMP hydrolyzing phosphodiesterases. *Methods Mol Biol.* 1020:51–62.
- Sancesario G, Giorgi M, D'Angelo V, Modica A, Martorana A, Morello M, Bengtson CP, Bernardi G. 2004. Down-regulation of nitrenergic transmission in the rat striatum after chronic nigrostriatal deafferentation. *Eur J Neurosci.* 20:989–1000.
- Sancesario G, Morrone LA, D'Angelo V, Castelli V, Ferrazzoli D, Sica F, Martorana A, Sorge R, Cavaliere F, Bernardi G, et al. 2014. Levodopa-induced dyskinesias are associated with transient down-regulation of cAMP and cGMP in the caudate-putamen of hemiparkinsonian rats: reduced synthesis or increased catabolism. *Neurochem Int.* 79:44–56.
- Schmidt CJ. 2010. Phosphodiesterase inhibitors as potential cognition enhancing agents. *Curr Top Med Chem.* 10:222–230.
- Sitges M, Galván E, Nekrassov V. 2005. Vinpocetine blockade of sodium channels inhibits the rise in sodium and calcium induced by 4-aminopyridine in synaptosomes. *Neurochem Int.* 46:533–540.
- Sitges M, Nekrassov V. 1999. Vinpocetine selectively inhibits neurotransmitter release triggered by sodium channel activation. *Neurochem Res.* 24:1585–1591.
- Siuciak JA, McCarthy SA, Chapin DS, Reed TM, Vorhees CV, Repaske DR. 2007. Behavioral and neurochemical characterization of mice deficient in the phosphodiesterase-1B (PDE1B) enzyme. *Neuropharmacology.* 53:113–124.
- Snyder GL, Prickaerts J, Wadenberg ML, Zhang L, Zheng H, Yao W, Akkerman S, Zhu H, Hendrick JP, Vanover KE, et al. 2016. Preclinical profile of ITI-214, an inhibitor of phosphodiesterase 1, for enhancement of memory performance in rats. *Psychopharmacology (Berl).* 233:3113–3124.
- Staley KJ, Otis TS, Mody I. 1992. Membrane properties of dentate gyrus granule cells: comparison of sharp microelectrode and whole-cell recordings. *J Neurophysiol.* 67:1346–1358.
- Surmeier DJ, Ding J, Day M, Wang Z, Shen W. 2007. D1 and D2 dopamine-receptor modulation of striatal glutamatergic signaling in striatal medium spiny neurons. *Trends Neurosci.* 30:228–235.
- Surmeier DJ, Plotkin J, Shen W. 2009. Dopamine and synaptic plasticity in dorsal striatal circuits controlling action selection. *Curr Opin Neurobiol.* 19:621–628.
- Thestrup T, Litzlbauer J, Bartholomäus I, Mues M, Russo L, Dana H, Kovalchuk Y, Liang Y, Kalamakis G, Laukat Y, et al. 2014. Optimized ratiometric calcium sensors for functional in vivo imaging of neurons and T lymphocytes. *Nat Methods.* 11:175–182.
- Threlfell S, West AR. 2013. Review: modulation of striatal neuron activity by cyclic nucleotide signaling and phosphodiesterase inhibition. *Basal Ganglia.* 3:137–146.
- Valjent E, Bertran-Gonzalez J, Herve D, Fisone G, Girault JA. 2009. Looking BAC at striatal signaling: cell-specific analysis in new transgenic mice. *Trends Neurosci.* 32:538–547.
- Vallebuona F, Raiteri M. 1995. Age-related changes in the NMDA receptor/nitric oxide/cGMP pathway in the hippocampus and cerebellum of freely moving rats subjected to transcerebral microdialysis. *Eur J Neurosci.* 7:694–701.
- Vemulapalli S, Watkins RW, Chintala M, Davis H, Ahn HS, Fawzi A, Tulshian D, Chiu P, Chatterjee M, Lin CC, et al. 1996. Antiplatelet and antiproliferative effects of SCH 51866, a novel type 1 and type 5 phosphodiesterase inhibitor. *J Cardiovasc Pharmacol.* 28:862–869.
- Yan C, Bentley JK, Sonnenburg WK, Beavo JA. 1994. Differential expression of the 61 kDa and 63 kDa calmodulin-dependent phosphodiesterases in the mouse brain. *J Neurosci.* 14:973–984.
- Yapo C, Nair AG, Clement L, Castro LR, Hellgren Kotaleski J, Vincent P. 2017. Detection of phasic dopamine by D1 and D2 striatal medium spiny neurons. *J Physiol.* 595:7451–7475.

Article 2: PDE - dopamine

PDE10A is required for dopamine action in D2-expressing striatal medium spiny neurons.

Mota É, Castro LRV, Vincent P.

in preparation.

An important part of the signal transduction process is the rapid degradation of the cyclic nucleotides by cyclic nucleotide PDEs, and we wanted to determine how the main striatal PDEs participate in the integration of the dopamine signal. We showed in the previous paper (Betolngar *et al.*, 2019) that PDE1B in the striatum is active only in the presence of calcium, and we showed that PDE1B down-regulates the cAMP response during the coincidence of dopamine and glutamate/NMDA in D1 MSNs. Using similar approaches, we wanted to analyze here how the other main striatal PDEs, PDE2A, PDE4 and PDE10A, participate in the degradation of cAMP during the response to dopamine.

To this end, we used the protocol of transient stimulation with dopamine uncaging, already described in (Yapo *et al.*, 2017). Since we observed that successive dopamine uncagings on the same preparation produced identical cAMP responses in MSNs, we compared the dopamine responses in the absence, and then in the presence of selective PDE inhibitors. This approach revealed that PDE2A, PDE4 and PDE10A are all able to control elevated cAMP levels, in the micromolar concentration range. These PDEs therefore regulate the amplitude of the positive D1 response.

In D2 MSNs, we observed that only PDE10A was able to reduce cAMP down to the lowest level. Since PKA is activated by low cAMP levels, dopamine action through the D₂ receptor requires a profound and durable decrease in cAMP concentration, as was illustrated by simulations performed in the laboratory.

This suggested that PDE10A action was required to de-activate PKA and therefore allow for a dephosphorylation of PKA targets in D2 MSNs. To test this hypothesis, we used the genetically-encoded FRET biosensor AKAR4 for PKA/phosphatase equilibrium to monitor the dephosphorylation induced by D₂ dopamine receptor activation, and we tested again the contribution of the main striatal PDEs. Indeed, we observed that PKA substrates could not be dephosphorylated when PDE10A was inhibited, whereas inhibition of both PDE2A and PDE4 still allowed for a transduction of the D2 signal at the phosphorylation level.

Conclusion: Dopamine signaling in D2 MSNs requires PDE10A activity to transduce a dopamine signal into a dephosphorylation of PKA substrates.

PDE10A is required for dopamine action in D2-expressing striatal medium spiny neurons.

Authors

Élia Mota¹, Liliana R.V. Castro¹ and Pierre Vincent¹.

Author affiliation

¹: Sorbonne Université, CNRS, Biological Adaptation and Ageing, F-75005 Paris, France.

Running title: PDE10A: a critical mediator of dopamine action

Corresponding Author

Pierre Vincent: pierre.vincent@upmc.fr; mailbox #256; UMR8256; 7 quai Saint-Bernard; 75005 Paris, France

ORCID numbers

Élia Mota: 0000-0003-4393-5781

Liliana Castro: 0000-0001-8902-089X

Pierre Vincent: 0000-0002-8479-1908

Keywords

Striatum; dopamine; cAMP/PKA signaling; phosphodiesterases; biosensor

Abstract

Dopamine in the striatum plays a crucial role in reward processes and action selection. Dopamine signals are transduced by D1 and D2 dopamine receptors which trigger mirror effects through the cAMP/PKA signaling cascade in D1 and D2 medium spiny neurons (MSNs). Phosphodiesterases, which determine the profile of cAMP signals, are highly expressed in MSNs, but their functional roles on dopamine signal integration remain poorly understood. We expressed genetically-encoded FRET biosensors to monitor at the single cell level changes in the cAMP/PKA signaling pathway in mouse striatal brain slices. The functional contribution of PDE2A, PDE4 and PDE10A on the response to dopamine was evaluated using specific inhibitors. We found that PDE2A and PDE4 only operate on high cAMP levels such as those elicited by D1 or A2A receptor stimulation. In contrast, PDE10A degrades cAMP over a wide range of concentrations, and is required to reduce cAMP down to baseline during a D2 response. At the level of PKA-dependent phosphorylation, we observed that PDE10A activity was required to obtain a negative effect during sustained D2 receptors activation. These data highlight PDE10A as a key determinant for transducing dopamine signals through the D2 receptor down to the level of PKA-dependent phosphorylation, and further confirms that PDE10A inhibitors may be useful for treating brain disorders related to dysfunctions in dopamine neuromodulation.

Abbreviations

AC, adenylate cyclase; **AKAR4**, cAMP-dependent protein kinase activity reporter; **cAMP**, cyclic adenosine 3', 5'-monophosphate; **D1 MSN**, direct pathway MSN; **D1R**, dopamine D1 receptor; **D2 MSN**, indirect pathway MSN; **D2R**, dopamine D2 receptor; **FRET**, Förster resonance energy transfer; **MSN**, medium-sized spiny neuron; **PDE**, phosphodiesterase; **PKA**, cAMP-dependent protein kinase A.

Introduction

Dopamine neurotransmission is a key mechanism underlying learning and reward processes in the striatum (Surmeier *et al.*, 2007; Kreitzer & Malenka, 2008; Cerovic *et al.*, 2013). Dopamine is released in the striatum by midbrain dopaminergic neurons which exhibit two distinct modes of firing: a pacemaker firing pattern which results in tonic release of dopamine, and a burst firing pattern associated with phasic release of dopamine. In the striatum, the phasic release of dopamine is associated with reward-predicting stimulus (Gonon *et al.*, 2000; Schultz, 1998), whereas omission of an expected reward, along with punishments, result in a dip in tonic dopamine concentration (Schultz & Romo, 1987; Schultz, 2007; Matsumoto & Hikosaka, 2009). The striatum comprises ~90% of medium-sized spiny neurons (MSNs), which express either D1 or D2 dopamine receptors, and hereafter called D1 MSNs and D2 MSNs, respectively. The D1 dopamine receptor is coupled positively to adenylyl cyclase, whereas the D2 receptor receptor inhibits adenylyl cyclase through Gi/o (Valjent *et al.*, 2019). D2 MSNs also express adenosine A2A receptors positively coupled to cAMP production. Striatal neurons also express a set of specific signaling proteins that determine the profile of the cAMP/PKA signaling pathway (Castro *et al.*, 2013). Among these, DARPP-32 (32-kDa dopamine and cAMP-regulated phosphoprotein), a multifunctional protein regulating phosphatase and kinase activities. For example, when phosphorylated by PKA at threonine 34 residue (Thr34), DARPP-32 becomes a potent inhibitor of serine/threonine protein phosphatase-1 (PP-1) (Hemmings *et al.*, 1984; Svenningsson *et al.*, 2004), and increases the duration of PKA-dependent signals (Castro *et al.*, 2013).

The segregation between D1 and D2/A2A expressing neurons, now clearly established (Valjent *et al.*, 2009; Bertran-Gonzalez *et al.*, 2010), was also visualized using

cAMP and PKA biosensors (Castro *et al.*, 2013; Yapo *et al.*, 2017). When cAMP was first elevated, for example by activating A2A adenosine receptors, the negative response mediated by D2 receptors could be monitored as a decrease in cAMP level. Using UV-mediated release of dopamine from a caged precursor, biosensor imaging thus reported in real time the transient cAMP change in response to D1 and D2 receptor activation. In this experimental setup, it appeared that the same range of dopamine concentration was sensed by D1 and D2 receptor (EC₅₀ of 0.4 and 0.7 μ M, respectively), in contradiction with the commonly accepted higher sensitivity of D2 receptors (Yapo *et al.*, 2017). In D1 MSNs, the positive cAMP signal triggered by D1 receptors was efficiently transduced down the cascade at the level of PKA-dependent phosphorylation. However, in D2 MSNs, the transduction of a decrease in cAMP into a decrease in PKA-dependent phosphorylation was much less efficient, and modeling indicates that the phosphorylation of DARPP-32 on the threonine 34, which inhibits PP1, can explain the slow dephosphorylation of PKA substrates upon D2 receptor activation (Yapo *et al.*, 2017). Simulations further suggest that, in a context of combined A2A and D2 receptor activation, D2 MSNs would respond positively to a transient lack of dopamine (Yapo *et al.*, 2017).

The proper integration of these complex dopamine signals also depend on a precise regulation of cAMP levels by cyclic-nucleotide phosphodiesterases (PDE). In situ hybridization and qPCR report a particularly robust mRNA expression of PDE1B, PDE2A, PDE7 and PDE10A, and a more marginal expression of PDE4B and PDE8B (Lakics *et al.*, 2010; Kelly *et al.*, 2014). High levels of PDE2A protein have been reported in the striatum (Stephenson *et al.*, 2009; Stephenson *et al.*, 2012). PDE2A degrades both cAMP and cGMP and is activated by cGMP binding to its GAF domains, increasing its activity up to 40 fold

(Martins *et al.*, 1982; Martinez *et al.*, 2002; Jäger *et al.*, 2010). PDE2A can thus mediate a cross-talk between cGMP and cAMP pathways, and cGMP-induced activation of PDE2A was shown to efficiently regulate cAMP in both D1 and D2 MSNs (Polito *et al.*, 2013). The high K_m of PDE2A for cAMP suggests that PDE2A mainly regulates high cAMP levels. Behavioral studies indicate that PDE2A inhibitors may be of interest for treating cognitive impairments including those associated with schizophrenia (Boess *et al.*, 2004; Redrobe *et al.*, 2014; Redrobe *et al.*, 2015). More recently, it was shown in a mouse model of fragile-X syndrome that PDE2A expression was increased, and pup treatment with PDE2A inhibitors reversed the deficits (Maurin *et al.*, 2018b; Maurin *et al.*, 2018a).

PDE4 protein is also present in MSNs (Cherry & Davis, 1999; Perez-Torres *et al.*, 2000; Nishi *et al.*, 2008; Nishi & Snyder, 2010). PDE4B is the main isoform expressed in the striatum, with more expression in D2 MSNs than in D1 MSNs (Nishi & Snyder, 2010; Nishi *et al.*, 2008). The PDE4 family specifically degrades cAMP with a K_m in the micromolar range. PDE4 inhibitors have been the center of intense work aiming at reducing cognitive decline (Hansen & Zhang, 2017).

The PDE10A protein is present almost exclusively and at very high levels in MSNs (Seeger *et al.*, 2003; Coskran *et al.*, 2006; Lakics *et al.*, 2010), suggesting an important functional role and raising great hope as a therapeutic target (Schülke & Brandon, 2017). We observed that, although PDE10A inhibition increased intracellular cAMP in both D1 and D2 MSNs, activation of PKA and phosphorylation of its targets occurred exclusively in D2 MSNs (Polito *et al.*, 2015). Our work suggests that these differences resulted from an asymmetrical regulation of phosphatase activity by DARPP-32 protein which allowed D2 MSNs to respond to tonic cAMP signal. This functional effect of PDE10A inhibitors mimics

the action of antipsychotic agents, and centered the interest of PDE10A in treatment of schizophrenia and Huntington's disease (Kehler *et al.*, 2007; Menniti *et al.*, 2007; Chappie *et al.*, 2009).

Two other PDEs were not included in this study. PDE1B is highly expressed in MSNs (Yan *et al.*, 1994; Polli & Kincaid, 1994) but is only active in conditions of increased intracellular calcium (Betolngar *et al.*, 2019). PDE7B messenger is highly expressed, but the presence of PDE7 protein has not been reported in the striatum so far.

In this work, we analyzed the functional contribution of PDE2A, PDE4 and PDE10A in the dynamics of the cAMP/PKA response to transient dopamine. Selective pharmacological inhibition of these PDEs revealed that PDE2A and PDE4 preferentially regulate high cAMP levels, while PDE10A operates over a wide range of cAMP concentrations. At the PKA level, PDE10A appears to be required for dopamine action through D2 receptors, and PDE10A inhibition leads to a global blunting of dopamine responsiveness in both D1 and D2 MSNs.

Materials and Methods

Biosensor imaging in brain slice preparations

Mice (C57BL/6J; Janvier labs) were housed under standardised conditions with a 12 hours light/dark cycle, stable temperature ($22 \pm 1^\circ\text{C}$), controlled humidity ($55 \pm 10\%$) and food and water ad libitum. All animal procedures were performed in accordance with the Sorbonne University animal care committee regulations. Brain slices were prepared from mice aged from 7 to 11 days. Coronal striatal brain slices were cut with a VT1200S microtome (Leica). Slices were prepared in an ice-cold solution of the following composition: 125 mM NaCl, 0.4 mM CaCl₂, 1 mM MgCl₂, 1.25 mM NaH₂PO₄, 26 mM NaHCO₃, 20 mM glucose, 2.5 mM KCl, 5 mM sodium pyruvate and 1 mM kynurenic acid, saturated with 5% CO₂ and 95% O₂. The slices were incubated in this solution for 30 minutes and then placed on a Millicell-CM membrane (Millipore) in culture medium (50% Minimum Essential Medium, 50% Hanks' Balanced Salt Solution, 5.5 g/L glucose, penicillin-streptomycin, Invitrogen). The cAMP biosensor Epac-S^{H150} (Polito *et al.*, 2013) and AKAR4 reporter of PKA/phosphatase equilibrium (Depry *et al.*, 2011) were expressed using the Sindbis virus as vector (Ehrengruber *et al.*, 1999): the viral vector was added on the brain slices ($\sim 5 \times 10^5$ particles per slice), and the infected slices were incubated overnight at 35°C under an atmosphere containing 5% CO₂. Before the experiment, slices were incubated for 30 min in the recording solution (125 mM NaCl, 2 mM CaCl₂, 1 mM MgCl₂, 1.25 mM NaH₂PO₄, 26 mM NaHCO₃, 20 mM glucose, 2.5 mM KCl and 5 mM sodium pyruvate saturated with 5% CO₂ and 95% O₂). Recordings were performed with a continuous perfusion of the same solution at 32°C.

All experiments were performed in the presence of 200 nM tetrodotoxin (TTX) to

block electrical activity. Wide-field images were obtained with an Olympus BX50WI or BX51WI upright microscope with a 40x 0.8 NA water-immersion objective and an ORCA-AG camera (Hamamatsu). Images were acquired with iVision (Biovision, Exton, PA, USA). The excitation and dichroic filters were D436/20 and 455dcxt. Signals were acquired by alternating the emission filters, HQ480/40 for donor emission, and D535/40 for acceptor emission, with a filter wheel (Sutter Instruments, Novato, CA, USA). Filters were obtained from Chroma Technology and Semrock.

Photo-release of caged compounds was performed using high power 360 nm LED sources mounted on the epifluorescence port of the microscope, providing 14 mW at the exit of the microscope objective (0.5 s flash duration) or 7.5 mW (1 s flash duration). The combination of LED sources at 360 nm (for uncaging) and 420 nm (off-peak light source for 436 nm excitation filter for biosensor imaging) was purchased from Mightex (Toronto, Canada). The frequency of data acquisition, usually 1 image pair every 30/60 seconds, was increased to 0.2 Hz in order to resolve peak dynamics, starting 10 data points before NPEC-DA uncaging.

Image analysis

Images were analysed with custom routines written in the IGOR Pro environment (Wavemetrics, Lake Oswego, OR, USA). No correction for bleed-through or direct excitation of the acceptor was applied to keep the benefit of ratiometric cancellation of artefacts. Biosensor activation level was quantified by ratiometric imaging: donor fluorescence divided by acceptor fluorescence for Epac-S^{H150}, and acceptor divided by donor for AKAR4. The emission ratio was calculated for each pixel and displayed in pseudo-colour images, with the ratio value coded in hue and the fluorescence of the preparation coded in intensity. Wide-field

imaging allowed for the separation of D1 and D2 MSNs, provided that the infection level was kept low and no fluorescence overlap between neighbouring neurones was observed. Cells were also excluded from the analysis when basal ratio was elevated, when the response to forskolin was lacking or when the neuronal morphology was altered (uneven cell contours).

Drugs

Solutions were prepared from powders purchased from Sigma-Aldrich (St Quentin-Fallavier, Isère, France). TTX was from Latoxan (Valence, France). All other drugs were from Tocris Bio-technie (Lille, France). NPEC-DA: (N)-1-(2-Nitrophenyl)ethylcarboxy-3,4-dihydroxyphenethylamine.

SKF-81297, a selective agonist of dopamine D1 receptors, was used to identify MSNs of the D1 type

CGS 21680, an agonist of the adenosine A2A receptors was used to increase cAMP in MSNs of the D2 type.

All drugs except TTX were added to the bath solution from a DMSO stock solution. Final DMSO concentration in the bath solution remained below 1‰.

Estimates of cAMP concentration

Ratiometric imaging can be used to determine absolute analyte concentrations (Grynkiewicz *et al.*, 1985). For Epac-S^{HI50}, we used a Kd of 4.4 μ M and a Hill coefficient of 0.77 (Polito *et al.*, 2013). Rmax was determined in every experiment by the final application of fsk + IBMX. The difference between basal ratio and Rmin was evaluated using the adenylyl cyclase inhibitor SQ22536 and reported \sim 5% (Polito *et al.*, 2015), corresponding to \sim 0.1 μ M cAMP.

Statistical analysis

For biosensor imaging experiments, the responses obtained from all neurones were averaged together and statistics were calculated per experiment (i.e. brain slice). N indicates the number of repeats of the same experiment (ie, independent brain slices), and n indicates the total number of neurones. Statistical analysis (paired t-tests) were performed using Igor Pro (Wavemetrics, Lake Oswego, OR, USA).

Results

Role of PDE2A in the cAMP response to transient dopamine

First, we investigated the functional contribution of PDE2A in determining the dynamics of transient cAMP responses in D1 and D2 MSNs. The genetically-encoded FRET biosensor Epac-S^{H150} (Polito *et al.*, 2013) was expressed by viral transfection in mouse striatal slice preparations and imaged with wide-field microscope to monitor in real time the intracellular changes in cAMP concentration following a transient dopaminergic stimulation, at the level of individual neurones (Figure 1). Since dopamine D2 receptors are negatively coupled to cAMP production and the basal level of cAMP is low (Polito *et al.*, 2015), intracellular cAMP production was first increased selectively in D2 MSNs by applying the adenosine A2A receptor agonist CGS 21680 (CGS, 1 μ M), mimicking the adenosine tone in the striatum. This stimulation was performed in the presence of the adenosine A1 receptor antagonist PSB36 (PSB, 100 nM). Once a steady-state cAMP level was reached in D2 MSNs, a caged-derivative of dopamine, NPEC-DA (3 μ M), was applied, which had no effect by itself on the cAMP level in D1 and D2 MSNs. After a few minutes to allow for the diffusion of the compound into the brain slice, a flash of UV light was applied to release dopamine. This transient dopamine stimulation decreased cAMP level in the D2 MSNs in the field of view. In parallel, cAMP increased in another neuronal population, thus identified as D1 MSNs.

These opposite changes in cAMP concentration in D1 and D2 MSNs have already been described and shown to be repeatable with the same amplitude (Yapo *et al.*, 2017; Betolngar *et al.*, 2019). A second transient response to dopamine could thus be performed in the presence of the PDE2A inhibitor BAY607550 (hereafter called iPDE2). Bath application

of iPDE2 (200 nM) increased the amplitude of the A2A-dependent cAMP steady-state level in D2 MSNs, but had no effect on the basal cAMP level in D1 MSNs. In the presence of iPDE2, dopamine uncaging produced again transient cAMP responses of opposite direction in D1 and D2 MSNs, that could thus be compared with the first control response for each individual MSNs (Figure 1B). At the end of the recording, the selective D1-like agonist SKF-81297 (SKF, 100 nM) was applied to confirm the identity of D1 MSNs. Then, the adenylyl cyclases activator forskolin (fsk, 13 μ M) together with the nonselective PDE inhibitor IBMX (200 μ M) were added to reach the maximal ratio response of the biosensor, and that level was used for normalization.

The same experiment was performed 4 times, and the average trace for each cell type in an experiment were averaged and displayed in Figure 1B (green for D1, blue for D2 MSNs). The amplitude of the dopamine response is plotted with connecting lines to show for each neuron the change in amplitude resulting from iPDE2 treatment. In D1 MSNs, the amplitude of the dopamine transient peak in control condition was 0.51 ± 0.07 as a fraction of maximal ratio response, vs 0.74 ± 0.12 with iPDE2, statistically different (mean \pm SD, Student's paired t-test, $n=24$, $t[23]=11.9$; $P=2.10^{-11}$).

In D2 MSNs, the application of iPDE2 increased the steady-state ratio level. The second dopamine uncaging in D2 MSNs in the presence of iPDE2 decreased cAMP level down to baseline, with a similar profile/kinetics to the first response: the minimal ratio level after the UV flash was 0.01 ± 0.05 of the maximal ratio response to fsk and IBMX, and was 0.02 ± 0.03 in the presence of iPDE2, not significantly different ($n=7$, $t[6]= 1.41$, $P = 0.21$).

These experiments show that PDE2A contribute to the degradation of cAMP during the positive cAMP response in D1 MSNs. In D2 MSNs, PDE2A contributes to the regulation

of the steady-state response to A2A receptor activation, but is not necessary to degrade cAMP after switching-off cAMP production via D2 receptors.

Role of PDE4 in the cAMP response to transient dopamine

We then tested the contribution of PDE4 using the same protocol, except that, instead of BAY, we used rolipram (iPDE4, 100 nM) to selectively inhibit PDE4 (Figure 2). PDE4 inhibition slightly increased the amplitude of the cAMP peak in D1 MSNs from 0.64 ± 0.09 as a fraction of maximal ratio response to 0.72 ± 0.06 . Although small, the difference was highly significant ($n=10$, $t[9]=6.2$, $P=2.10^{-4}$). In D2 MSNs, iPDE4 increased the steady-state ratio level, but the response to dopamine still reached the baseline in control condition (-0.08 ± 0.04) or with iPDE4 (-0.07 ± 0.03), not statistically different ($n = 5$, $t[4]=1.1$, $P=0.3$).

Role of PDE2A and PDE4, in the cAMP response to transient dopamine

It might be possible that PDE2A and PDE4 action compensate each other and we tested this hypothesis by simultaneously inhibiting both PDE2A and PDE4. iPDE2 (200 nM) and iPDE4 (rolipram, 100 nM) were applied together few minutes before and maintained during and after the release of dopamine (Figure 3A). This experiment was performed 4 times, and the average response for each cell type in an experiment were averaged (Figure 3B). In D1 MSNs, the amplitude of the dopamine transient peak in control condition was 0.52 ± 0.12 as a fraction of maximal ratio response, vs 0.82 ± 0.08 with iPDE2 and iPDE4, statistically different ($n=17$; $t[16]=14.7$, $P=1.10^{-10}$). In D2 MSNs, the application of iPDE2 and iPDE4 on top of the CGS response increased the ratio. Dopamine uncaging also decreased the ratio down to the baseline in the presence of iPDE2 and iPDE4, reaching a final level (0.02 ± 0.03) that was not statistically different from the level reached in control

condition (-0.02 ± 0.08 , $n=7$; $t[6]=1.4$; $P=0.21$).

To summarize, in D1 MSNs, PDE2A and PDE4 contribute to the negative control of the cAMP peak elicited by transient dopamine, and inhibition of these PDEs essentially increases the peak amplitude of the response. In D2 MSNs, PDE2A and PDE4 participate in the regulation of the high cAMP steady-state levels induced by A2A adenosine receptors; however, when cAMP production is stopped via D2 receptors, cAMP still decreases towards the basal level. This shows that, besides PDE2A and PDE4, another phosphodiesterase activity is sufficient to efficiently reduce cAMP level.

Role of PDE10A in the cAMP response to transient dopamine

PDE10A is highly and selectively expressed in the striatum, and previous work of our team has already revealed its action as regulator of basal cAMP level in MSNs (Polito *et al.*, 2015). To test its role on dopamine-induced changes in cAMP levels, another set of similar experiments was performed in which the selective inhibitor TP-10 (1 μ M), hereafter called iPDE10 was applied for a few minutes before and maintained during and after the release of dopamine (Figure 4). Contrary to what was observed with iPDE2 and iPDE4, application of iPDE10 alone increased the basal cAMP level in D1 MSNs, consistent with our previous findings (Polito *et al.*, 2015).

This protocol was repeated 4 times. In D1 MSNs, the amplitude of the first dopamine transient peak was 0.52 ± 0.12 of the maximal ratio response and 0.74 ± 0.12 in the presence of iPDE10 (second peak), statistically larger ($n=16$, $t[15]=-14.0$, $P=5.10^{-10}$). The recovery kinetics appeared much slower on the second dopamine transient peak (Figure 4). In D2 MSNs, iPDE10 also increased the levels during the steady-state cAMP level in response to A2A receptor agonist. Even though the steady-state cAMP level reached in the presence of

CGS and iPDE10 was lower with PDE10A inhibition than with combined iPDE2A and iPDE4, the negative cAMP response to dopamine in the presence of iPDE10 was far from reaching the baseline (0.33 ± 0.07 , a significantly higher level than in the control condition for the same neurons (0.01 ± 0.05 , $n=17$; $t[16]=15.2$, $P=6.10^{-11}$).

These experiments reveal that PDE10A exerts a powerful action on transient dopamine-induced cAMP signals in both D1 and D2 MSNs. More importantly, PDE10A activity is required in D2 MSNs to degrade cAMP to the lowest levels detectable with the Epac-S^{H150} biosensor. In other words, PDE2A and PDE4 (and possibly other less expressed PDEs) are not sufficient to degrade cAMP down to baseline during the negative transient dopamine-induced cAMP signals in D2 MSNs, while inhibition of PDE10A suppresses the ability to reduce cAMP down to baseline level.

PDE10A contribution for PKA/phosphatases equilibrium in response to dopamine

Since cAMP exerts its action in the striatum mostly through PKA, we then wondered how D2-mediated signals were transduced into PKA-dependent phosphorylation. Our previous work showed that the transient decrease in cAMP elicited by dopamine uncaging was too brief to lead to notable dephosphorylation of PKA substrates, possibly because of DARPP-32 mediated inhibition of PP1 (Yapo *et al.*, 2017). A new protocol was then designed using steady-state bath application of dopamine to provide a long enough inhibition of cAMP production to allow for the dephosphorylation of PKA substrates. Like in the previous protocols, cAMP production in D2 MSNs was first induced by the A2A receptor agonist CGS (1 μ M) in the presence of the A1 antagonist PSB (100 nM), which led to a steady-state PKA phosphorylation level. Dopamine (3 μ M) was then applied in the bath, which increased PKA phosphorylation level in D1 MSNs (Fig. 5 left, top trace) and decreased PKA

phosphorylation level in D2 MSNs (Fig. 5 left, bottom trace). After a few minutes, iPDE10 (1 μ M) was added, which produced a large ratio increase in D2 MSNs, while D1 MSNs remained at a high level. Final controls with SKF and fsk + IBMX did not further increase PKA-dependent phosphorylation, indicating that PDE10A inhibition together with the activation of A2A or D1 receptors pushed both D1 and D2 MSNs to the maximal phosphorylation level of the biosensor.

This experiment, repeated 4 times, shows that, in the presence of iPDE10, dopamine via D2 receptors is unable to maintain a low enough cAMP level to maintain PKA in the inactive state.

Previous experiments with cAMP imaging showed that cAMP could decrease to baseline level even when PDE2A and PDE4 were both inhibited (Figure 3). This suggested that dopamine via D2 receptors should still be able to maintain PKA-dependent phosphorylation at a low level. The same protocol was thus repeated, replacing iPDE10 with the application of both iPDE2 and iPDE4 (Figure 5, right). As expected, once dopamine had induced a marked decrease in AKAR4 ratio, addition of iPDE2 and iPDE4 had no effect. This experiment was repeated 4 times with the same observation, except a single D2 MSN which responded positively to iPDE2 + iPDE4.

These experiments show that PDE10A is required to mediate the action of dopamine through D2 receptors at the level of PKA/PP equilibrium, whereas PDE2A and PDE4 play no critical role.

Discussion

Our study highlights the specific action of PDE2A, PDE4 and PDE10A in the regulation of the cAMP response to dopamine in both D1 and D2 MSNs. PDE2A and PDE4 appear to control high cAMP levels such as those reached in D1 MSNs upon dopamine activation or in D2 MSNs after activating adenosine A2A receptors. These PDEs have no effect on the low cAMP levels. In contrast, PDE10A controls the low cAMP levels, and is therefore required for hydrolyzing cAMP down to the low concentrations (submicromolar) needed for PKA de-activation and transduction of a dopamine signal mediated by D2 receptors. Surprisingly, besides its action on low cAMP levels, PDE10A efficiently regulates high cAMP levels as well.

PDEs contribute differently, depending on their affinity for cAMP

Our results are quite consistent with the idea that PDE exhibit distinctive enzymatic properties that endows them with a specific functional role in striatal neurons (Neves-Zaph, 2017). In this review, the author highlights that PDE2A, which exhibits a K_m of 112 μM (Poppe *et al.*, 2008), essentially degrades the highest cAMP levels. In our experiments, we observed that PDE2A inhibition increased the peak cAMP response to dopamine in D1 MSNs, while it also increased the A2A-induced steady-state cAMP level in D2 MSNs. Both levels are in the mid-range of biosensor activation, ie correspond to micromolar and higher cytosolic cAMP concentration: this suggests that, even with a K_m of 112 μM , PDE2A efficiently controls micromolar levels of cAMP. PDE2A however is not involved in the regulation of basal (ie unstimulated) cAMP since its inhibition did not affect basal cAMP level in MSNs of both types (Polito *et al.*, 2013).

A characteristic feature of PDE2A is its positive regulation by the cGMP. Indeed,

NOS interneurons release NO, which increases cGMP in MSNs (West *et al.*, 2002; West & Grace, 2004; West & Tseng, 2011). Binding of cGMP to the GAF-B domain of PDE2A results in a strong increase in cAMP hydrolysis (Martinez *et al.*, 2002; Jäger *et al.*, 2010). Although this regulatory mechanism allows PDE2A to decrease cAMP levels in the micromolar range in both D1 and D2 MSNs, it was not sufficient to suppress PKA activity in response to transient dopamine in D1 MSNs (Polito *et al.*, 2013). In this work, we show that, when PDE10A is inhibited, PDE2A (and PDE4) action are insufficient to reduce cAMP level below the micromolar level, and therefore prevent PKA deactivation. It remains to be tested whether selective PDE2A activation with cGMP might further decrease cAMP, but this is quite unlikely considering the very high K_m of this enzyme.

Besides PDE2A, we observed a very similar contribution of PDE4 in the regulation of elevated cAMP concentrations. Simultaneous inhibition of both PDE2A and PDE4 essentially exacerbated the effect of the inhibition of either one or the other: no effect on basal cAMP level in D1 MSNs, but prolonged the transient cAMP response to D1 stimulation and potentiated the cAMP response to A2A receptor activation in D2 MSNs.

Previous work reported a lack of PDE4 activity in unstimulated D1 MSNs but a potentiation of the A2A response (Nishi *et al.*, 2008). The same study reported no potentiating effect of PDE4 inhibition on DARPP-32 phosphorylation induced by D1 receptor stimulation. However, the stimulation with 1 μ M SKF81297 probably produced a response that could not be further increased by rolipram. Similarly, PDE4 inhibition had no effect on PKA-dependent phosphorylation upon weak D1 receptor stimulation (Castro *et al.*, 2013), possibly because the cAMP level was too low. Our current work is consistent with PDE4 being functional in both D1 and D2 MSNs (even though expressed at a lower level in

D1 MSNs: (Nishi *et al.*, 2008)). With a K_m of 5.5 μM for cAMP (Poppe *et al.*, 2008), PDE4 thus regulates moderate to high cAMP levels, which is confirmed in computer simulations (Neves-Zaph, 2017).

PDE1B, also highly expressed in the striatum, has a K_m of 33 μM (Poppe *et al.*, 2008). Our previous work showed that PDE1 efficiently degrades cAMP in a micromolar concentration range, which probably underlies PDE1B involvement in LTP induction in these neurons (Betolngar *et al.*, 2019). How PDE1B might control the D2 response remains to be investigated in the context of increased intracellular calcium.

In contrast to these PDEs, PDE10A has a K_m of 0.25 μM (Poppe *et al.*, 2008), and is thus expected to mainly regulate the lowest cAMP levels. Indeed, we already reported that PDE10A inhibition in the absence of any stimulation increased cAMP from sub-micromolar to micromolar concentration (Polito *et al.*, 2015). Surprisingly, PDE10A also regulates high cAMP levels since its inhibition largely prolongs D1 responses and increases A2A-induced cAMP plateau in D2 MSNs. This is consistent with biochemical data which reported that PDE10A inhibition potentiated D1 responses and the phosphorylation of its downstream targets, such as DARPP-32 (Nishi *et al.*, 2008). By working on both low and high cAMP levels, PDE10A thus appears to play a predominant functional role in MSNs. This comes in very good agreement with previous biochemical studies which showed that PDE10A accounted for the large majority of cAMP hydrolyzing activity in striatal extracts (Russwurm *et al.*, 2015).

Subcellular compartmentation may complicate the interpretation

Intracellular compartmentation of PDEs may add another level of complexity. Indeed, the PDEs studied here can be targeted to various sub-cellular domains, a property that largely

depends on alternative splicing. PDE10A can thus be found in the cytosol or at the membrane (Kotera *et al.*, 2004). In the striatum, most of PDE10A activity co-immunoprecipitates within signaling complexes of high molecular weight, and PDE10A is released from these complexes in conditions of activated PKA following its phosphorylation (Russwurm *et al.*, 2015). PDE10A phosphorylation was also reported to be targeted to the membrane upon phosphorylation (Charych *et al.*, 2010). PDE2A exists in three different splice variants of the N-terminal domain which determine the cytosolic or membrane localization of the enzyme (Russwurm *et al.*, 2009). Finally, PDE4 come in a variety of splice variants, each of them with different capabilities of interacting with AKAPs (McCahill *et al.*, 2008). In this work, biosensor imaging reported global cAMP/PKA signals, ignoring possible sub-cellular compartmentation: high local cAMP levels may translate in a much lower concentration in the cytosol. A precise analysis of cAMP/PKA signaling within signaling microdomains requires experimental tools that remain to be validated in differentiated neurons.

PDE10A is required to transduce transient and tonic dopamine

Regardless of the underlying mechanisms, our work shows that PDE10A plays a central role, being able to regulate both high and low cAMP levels, and being required for lowering cAMP to a low enough level to de-activate PKA. In D2 MSNs, we saw that PDE10A inhibition suppressed the negative action of dopamine on PKA-dependent targets, which is consistent with the initial hypothesis that PDE10A inhibitors may work as antipsychotics (Menniti *et al.*, 2007; Chappie *et al.*, 2009). However, PDE10A inhibition also affects D1 MSNs, and the resulting D1/D2 imbalance may lead to unwanted effects. Indeed, PDE10A inhibition tends to "blurr" the response to dopamine in D1 MSNs. In a previous work, we have already observed that, in the absence of any exogenous neuromodulator,

PDE10A was responsible for controlling basal cAMP levels (Polito *et al.*, 2015). That work revealed the role played by the equilibrium between PP1 activity and DARPP-32 phosphorylation level. We showed that, in the absence of stimulation, DARPP-32 was much less phosphorylated in D1 MSNs than in D2 MSNs, and the high activity of PP1 in D1 MSNs prevented the rise of PKA-dependent phosphorylation. This is why, in that previous study, the moderate steady-state increase in cAMP resulting from PDE10A inhibition was insufficient to lead to any phosphorylation of PKA targets. Here, the situation is radically different, with the stimulation of D1 receptors rapidly switching on the phosphorylation of PKA targets including DARPP-32, thus turning off PP1 action and prolonging the effect of dopamine through D1 receptors (Castro *et al.*, 2013). This positive feed-forward control loop leads to all-or-none responses, an effect that was particularly visible in the nucleus (Yapo *et al.*, 2018). PDE10A inhibition moderately raises global cAMP but also amplifies and prolongs dopamine action (see Figure 3 and 4). In vivo, partial PDE10A inhibition would thus switch D1 MSNs to the DARPP-32 phosphorylated state which would then become highly excitable. Indeed, we found in vivo that PDE10A inhibition activated PKA in the dorsolateral striatum, possibly as a result of increased dopamine in that brain region (Polito *et al.*, 2015). By powerfully switching-on a fraction of D1 MSNs, PDE10A inhibition may cause some of the adverse effects observed in patients treated with MP-10 (ClinicalTrials.gov: NCT01175135).

Acknowledgements

The group of EM, LRVC and PV is member of the Bio-Psy Labex.

Conflicts of interests

No competing interests.

Funding

This work was supported by the “Investissements d’Avenir” program managed by the ANR under reference ANR-11-IDEX-0004-02, and called "Bio-Psy Labex". EM benefited from a PhD fellowship from this institution.

Author contributions

EM, LRVC and PV designed the experiments. EM prepared brain slices and conducted the imaging experiments; EM, LRVC and PV analyzed data. EM, LRVC and PV wrote the paper.

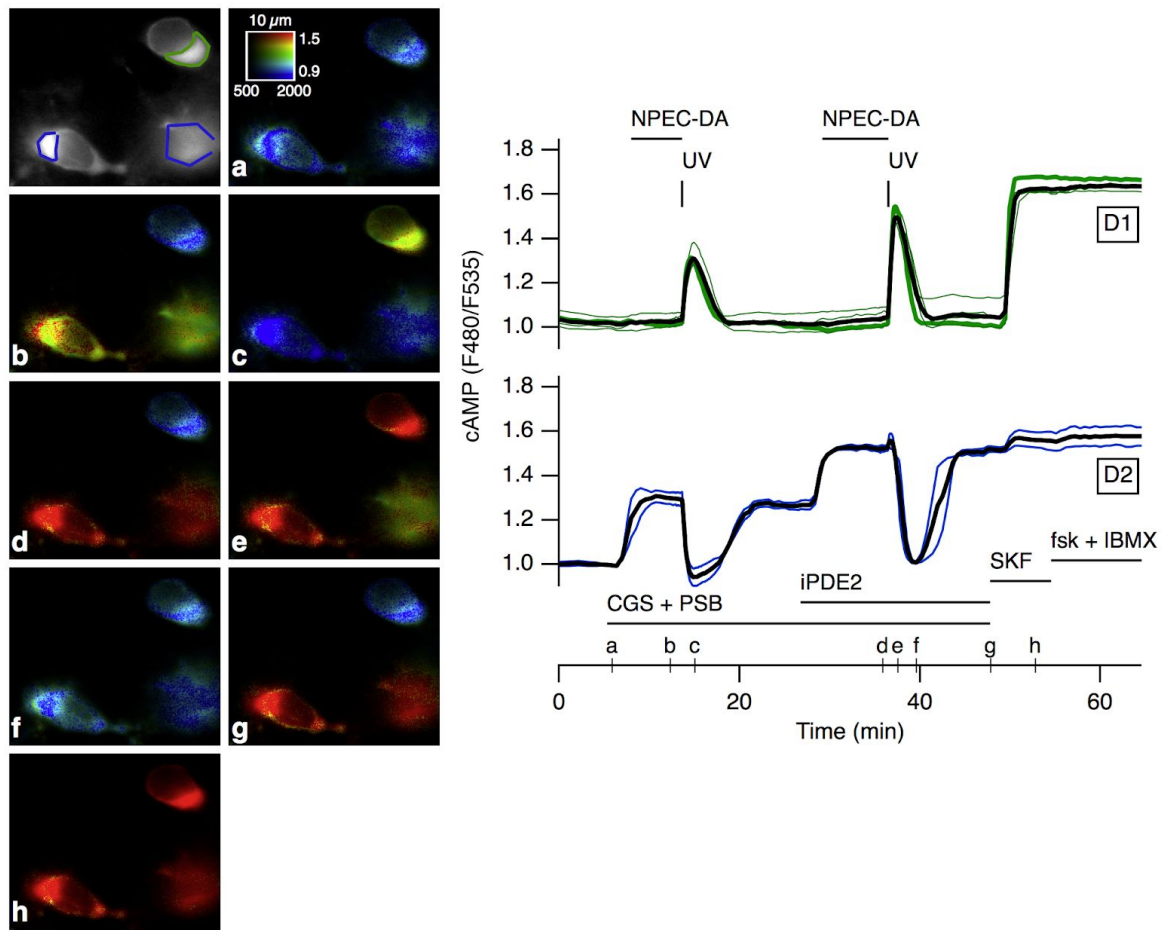
References

- Bertran-Gonzalez J, Hervé D, Girault JA & Valjent E (2010). What is the Degree of Segregation between Striatonigral and Striatopallidal Projections. *Front Neuroanat* **4**, 136.
- Betolngar DB, Mota É, Fabritius A, Nielsen J, Hougaard C, Christoffersen CT, Yang J, Kehler J, Griesbeck O, Castro LRV & Vincent P (2019). Phosphodiesterase 1 Bridges Glutamate Inputs with NO- and Dopamine-Induced Cyclic Nucleotide Signals in the Striatum. *Cereb Cortex* **In press**.
- Boess FG, Hendrix M, van der Staay FJ, Erb C, Schreiber R, van Staveren W, de Vente J, Prickaerts J, Blokland A & Koenig G (2004). Inhibition of phosphodiesterase 2 increases neuronal cGMP, synaptic plasticity and memory performance. *Neuropharmacology* **47**, 1081–1092.
- Castro LR, Brito M, Guiot E, Polito M, Korn CW, Herve D, Girault JA, Paupardin-Tritsch D & Vincent P (2013). Striatal neurones have a specific ability to respond to phasic dopamine release. *J Physiol* **591**, 3197–3214.
- Cerovic M, d’Isa R, Tonini R & Brambilla R (2013). Molecular and cellular mechanisms of dopamine-mediated behavioral plasticity in the striatum. *Neurobiol Learn Mem* **105**, 63–80.
- Chappie T, Humphrey J, Menniti F & Schmidt C (2009). PDE10A inhibitors: an assessment of the current CNS drug discovery landscape. *Curr Opin Drug Discov Devel* **12**, 458–467.
- Charych EI, Jiang LX, Lo F, Sullivan K & Brandon NJ (2010). Interplay of palmitoylation and phosphorylation in the trafficking and localization of phosphodiesterase 10A: implications for the treatment of schizophrenia. *J Neurosci* **30**, 9027–9037.
- Cherry JA & Davis RL (1999). Cyclic AMP phosphodiesterases are localized in regions of the mouse brain associated with reinforcement, movement, and affect. *J Comp Neurol* **407**, 287–301.
- Coskran TM, Morton D, Menniti FS, Adamowicz WO, Kleiman RJ, Ryan AM, Strick CA, Schmidt CJ & Stephenson DT (2006). Immunohistochemical localization of phosphodiesterase 10A in multiple mammalian species. *J Histochem Cytochem* **54**, 1205–1213.
- Depry C, Allen MD & Zhang J (2011). Visualization of PKA activity in plasma membrane microdomains. *Mol Biosyst* **7**, 52–58.
- Ehrengruber MU, Lundstrom K, Schweitzer C, Heuss C, Schlesinger S & Gähwiler BH (1999). Recombinant Semliki Forest virus and Sindbis virus efficiently infect neurons in hippocampal slice cultures. *Proc Natl Acad Sci U S A* **96**, 7041–7046.
- Gonon F, Burie JB, Jaber M, Benoit-Marand M, Dumartin B & Bloch B (2000). Geometry and kinetics of dopaminergic transmission in the rat striatum and in mice lacking the dopamine transporter. *Prog Brain Res* **125**, 291–302.
- Grynkiewicz G, Poenie M & Tsien RY (1985). A new generation of Ca²⁺ indicators with greatly improved fluorescence properties. *J Biol Chem* **260**, 3440–3450.
- Hansen RT & Zhang HT (2017). The Past, Present, and Future of Phosphodiesterase-4 Modulation for Age-Induced Memory Loss. *Adv Neurobiol* **17**, 169–199.
- Hemmings HCJ, Greengard P, Tung HY & Cohen P (1984). DARPP-32, a dopamine-regulated neuronal phosphoprotein, is a potent inhibitor of protein phosphatase-1. *Nature* **310**, 503–505.
- Jäger R, Schwede F, Genieser HG, Koesling D & Russwurm M (2010). Activation of PDE2 and PDE5 by specific GAF ligands: delayed activation of PDE5. *Br J Pharmacol* **161**, 1645–1660.
- Kehler J, Ritzén A & Greve DRPQ (2007). The potential therapeutic use of phosphodiesterase 10 inhibitors. *Expert Opin Ther Patents* **17**, 147–158.
- Kelly MP, Adamowicz W, Bove S, Hartman AJ, Mariga A, Pathak G, Reinhart V, Romegialli A & Kleiman RJ (2014). Select 3',5'-cyclic nucleotide phosphodiesterases exhibit altered expression in the aged rodent brain. *Cell Signal* **26**, 383–397.
- Kotera J, Sasaki T, Kobayashi T, Fujishige K, Yamashita Y & Omori K (2004). Subcellular localization of cyclic nucleotide phosphodiesterase type 10A variants, and alteration of the localization by cAMP-dependent protein kinase-dependent phosphorylation. *J Biol Chem* **279**, 4366–4375.
- Kreitzer AC & Malenka RC (2008). Striatal plasticity and basal ganglia circuit function. *Neuron* **60**, 543–554.

- Lakics V, Karran EH & Boess FG (2010). Quantitative comparison of phosphodiesterase mRNA distribution in human brain and peripheral tissues. *Neuropharmacology* **59**, 367–374.
- Martinez SE, Wu AY, Glavas NA, Tang XB, Turley S, Hol WG & Beavo JA (2002). The two GAF domains in phosphodiesterase 2A have distinct roles in dimerization and in cGMP binding. *Proc Natl Acad Sci U S A* **99**, 13260–13265.
- Martins TJ, Mumby MC & Beavo JA (1982). Purification and characterization of a cyclic GMP-stimulated cyclic nucleotide phosphodiesterase from bovine tissues. *J Biol Chem* **257**, 1973–1979.
- Matsumoto M & Hikosaka O (2009). Two types of dopamine neuron distinctly convey positive and negative motivational signals. *Nature* **459**, 837–841.
- Maurin T, Lebrigand K, Castagnola S, Paquet A, Jarjat M, Popa A, Grossi M, Rage F & Bardoni B (2018a). HITS-CLIP in various brain areas reveals new targets and new modalities of RNA binding by fragile X mental retardation protein. *Nucleic Acids Res* **46**, 6344–6355.
- Maurin T, Melancia F, Jarjat M, Castro L, Costa L, Delhaye S, Khayachi A, Castagnola S, Mota E, Di Giorgio A, Servadio M, Drozd M, Poupon G, Schiavi S, Sardone L, Azoulay S, Ciranna L, Martin S, Vincent P, Trezza V & Bardoni B (2018b). Involvement of Phosphodiesterase 2A Activity in the Pathophysiology of Fragile X Syndrome. *Cereb Cortex* **In press.**
- McCahill AC, Huston E, Li X & Houslay MD (2008). PDE4 associates with different scaffolding proteins: modulating interactions as treatment for certain diseases. *Handb Exp Pharmacol* 125–166.
- Menniti FS, Chappie TA, Humphrey JM & Schmidt CJ (2007). Phosphodiesterase 10A inhibitors: a novel approach to the treatment of the symptoms of schizophrenia. *Curr Opin Investig Drugs* **8**, 54–59.
- Neves-Zaph SR (2017). Phosphodiesterase Diversity and Signal Processing Within cAMP Signaling Networks. *Adv Neurobiol* **17**, 3–14.
- Nishi A, Kuroiwa M, Miller DB, O’Callaghan JP, Bateup HS, Shuto T, Sotogaku N, Fukuda T, Heintz N, Greengard P & Snyder GL (2008). Distinct roles of PDE4 and PDE10A in the regulation of cAMP/PKA signaling in the striatum. *J Neurosci* **28**, 10460–10471.
- Nishi A & Snyder GL (2010). Advanced research on dopamine signaling to develop drugs for the treatment of mental disorders: biochemical and behavioral profiles of phosphodiesterase inhibition in dopaminergic neurotransmission. *J Pharmacol Sci* **114**, 6–16.
- Perez-Torres S, Miro X, Palacios JM, Cortes R, Puigdomenech P & Mengod G (2000). Phosphodiesterase type 4 isozymes expression in human brain examined by in situ hybridization histochemistry and [³H]rolipram binding autoradiography. Comparison with monkey and rat brain. *J Chem Neuroanat* **20**, 349–374.
- Polito M, Guiot E, Gangarossa G, Longueville S, Doulazmi M, Valjent E, Hervé D, Girault JA, Paupardin-Tritsch D, Castro LR & Vincent P (2015). Selective Effects of PDE10A Inhibitors on Striatopallidal Neurons Require Phosphatase Inhibition by DARPP-32. *eNeuro* **2**, 1–15.
- Polito M, Klarenbeek J, Jalink K, Paupardin-Tritsch D, Vincent P & Castro LR (2013). The NO/cGMP pathway inhibits transient cAMP signals through the activation of PDE2 in striatal neurons. *Front Cell Neurosci* **7**, 211.
- Polli JW & Kincaid RL (1994). Expression of a calmodulin-dependent phosphodiesterase isoform (PDE1B1) correlates with brain regions having extensive dopaminergic innervation. *J Neurosci* **14**, 1251–1261.
- Poppe H, Rybalkin SD, Rehmann H, Hinds TR, Tang XB, Christensen AE, Schwede F, Genieser HG, Bos JL, Doskeland SO, Beavo JA & Butt E (2008). Cyclic nucleotide analogs as probes of signaling pathways. *Nat Methods* **5**, 277–278.
- Redrobe JP, Jørgensen M, Christoffersen CT, Montezinho LP, Bastlund JF, Carnerup M, Bundgaard C, Lerdrup L & Plath N (2014). In vitro and in vivo characterisation of Lu AF64280, a novel, brain penetrant phosphodiesterase (PDE) 2A inhibitor: potential relevance to cognitive deficits in schizophrenia. *Psychopharmacology (Berl)* **231**, 3151–3167.

- Redrobe JP, Rasmussen LK, Christoffersen CT, Bundgaard C & Jorgensen M (2015). Characterisation of Lu AF33241: A novel, brain-penetrant, dual inhibitor of phosphodiesterase (PDE) 2A and PDE10A. *Eur J Pharmacol*
- Russwurm C, Koesling D & Russwurm M (2015). Phosphodiesterase 10A Is Tethered to a Synaptic Signaling Complex in Striatum. *J Biol Chem* **290**, 11936–11947.
- Russwurm C, Zoidl G, Koesling D & Russwurm M (2009). Dual acylation of PDE2A splice variant 3: targeting to synaptic membranes. *J Biol Chem* **284**, 25782–25790.
- Schülke JP & Brandon NJ (2017). Current Understanding of PDE10A in the Modulation of Basal Ganglia Circuitry. *Adv Neurobiol* **17**, 15–43.
- Schultz W (1998). Predictive reward signal of dopamine neurons. *J Neurophysiol* **80**, 1–27.
- Schultz W (2007). Multiple dopamine functions at different time courses. *Annu Rev Neurosci* **30**, 259–288.
- Schultz W & Romo R (1987). Responses of nigrostriatal dopamine neurons to high-intensity somatosensory stimulation in the anesthetized monkey. *J Neurophysiol* **57**, 201–217.
- Seeger TF, Bartlett B, Coskran TM, Culp JS, James LC, Krull DL, Lanfear J, Ryan AM, Schmidt CJ, Strick CA, Varghese AH, Williams RD, Wylie PG & Menniti FS (2003). Immunohistochemical localization of PDE10A in the rat brain. *Brain Res* **985**, 113–126.
- Stephenson DT, Coskran TM, Kelly MP, Kleiman RJ, Morton D, O’Neill SM, Schmidt CJ, Weinberg RJ & Menniti FS (2012). The distribution of phosphodiesterase 2A in the rat brain. *Neuroscience* **226**, 145–155.
- Stephenson DT, Coskran TM, Wilhelms MB, Adamowicz WO, O’Donnell MM, Muravnick KB, Menniti FS, Kleiman RJ & Morton D (2009). Immunohistochemical localization of phosphodiesterase 2A in multiple mammalian species. *J Histochem Cytochem* **57**, 933–949.
- Surmeier DJ, Ding J, Day M, Wang Z & Shen W (2007). D1 and D2 dopamine-receptor modulation of striatal glutamatergic signaling in striatal medium spiny neurons. *Trends Neurosci* **30**, 228–235.
- Svenningsson P, Nishi A, Fisone G, Girault JA, Nairn AC & Greengard P (2004). DARPP-32: an integrator of neurotransmission. *Annu Rev Pharmacol Toxicol* **44**, 269–296.
- Valjent E, Bertran-Gonzalez J, Herve D, Fisone G & Girault JA (2009). Looking BAC at striatal signaling: cell-specific analysis in new transgenic mice. *Trends Neurosci* **32**, 538–547.
- Valjent E, Biever A, Gangarossa G & Puighermanal E (2019). Dopamine signaling in the striatum. *Adv Protein Chem Struct Biol* **116**, 375–396.
- West AR, Galloway MP & Grace AA (2002). Regulation of striatal dopamine neurotransmission by nitric oxide: effector pathways and signaling mechanisms. *Synapse* **44**, 227–245.
- West AR & Grace AA (2004). The nitric oxide-guanylyl cyclase signaling pathway modulates membrane activity states and electrophysiological properties of striatal medium spiny neurons recorded in vivo. *J Neurosci* **24**, 1924–1935.
- West AR & Tseng KY (2011). Nitric Oxide-Soluble Guanylyl Cyclase-Cyclic GMP Signaling in the Striatum: New Targets for the Treatment of Parkinson’s Disease? *Front Syst Neurosci* **5**, 55.
- Yan C, Bentley JK, Sonnenburg WK & Beavo JA (1994). Differential expression of the 61 kDa and 63 kDa calmodulin-dependent phosphodiesterases in the mouse brain. *J Neurosci* **14**, 973–84.
- Yapo C, Nair AG, Clement L, Castro LR, Hellgren Kotaleski J & Vincent P (2017). Detection of phasic dopamine by D1 and D2 striatal medium spiny neurons. *J Physiol* **595**, 7451–7475.
- Yapo C, Nair AG, Hellgren Kotaleski J, Vincent P & Castro LRV (2018). Switch-like PKA responses in the nucleus of striatal neurons. *J Cell Sci* **131**, jcs.216556.

A



B

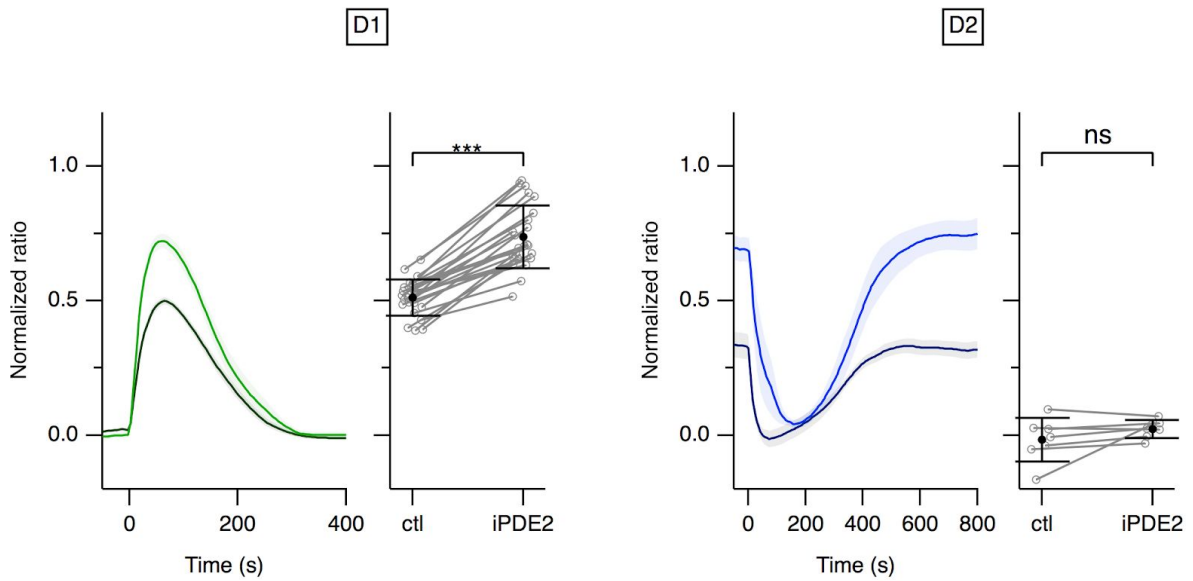
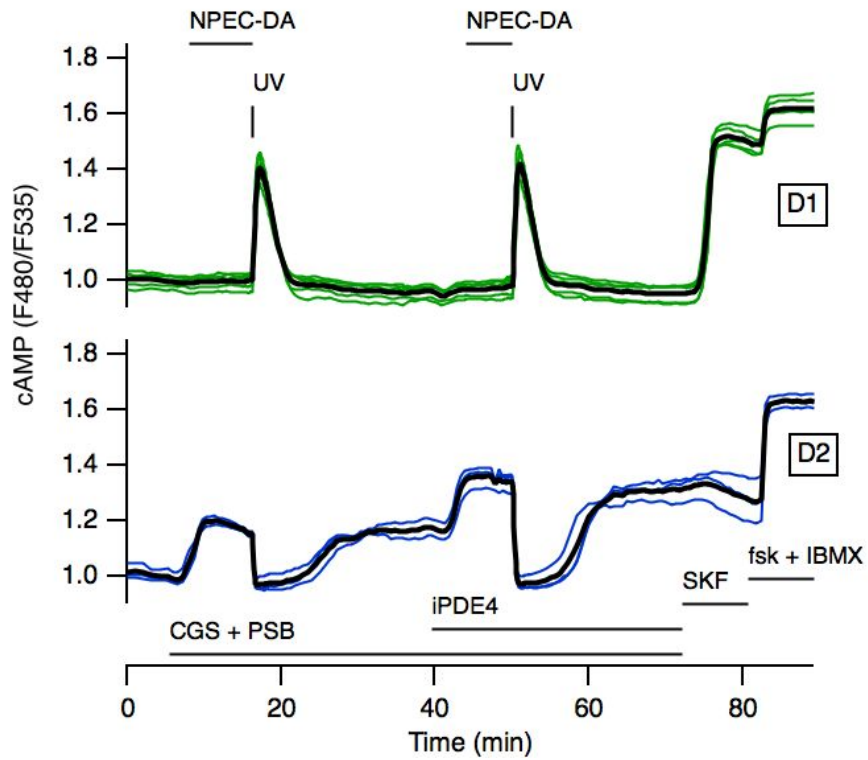


Figure 1

PDE2A contributes to the regulation of high cAMP levels obtained in responses to the stimulation by dopamine in D1 MSNs and adenosine A2A receptors stimulation in D2 MSNs.

The Epac-SH150 biosensor was expressed in mice striatal brain slices and imaged with wide-field microscopy. (A) Left: part of the field showing the raw fluorescence of the donor, displayed in grey, and the donor/acceptor fluorescence ratio, displayed in pseudo-colour. The regions of interest (ROI) around individual cells define the area used for measuring the ratio during time and shown on the graph. Images a–h show the ratio corresponding to the time points indicated on the graph. Right: the each trace on the graph indicates the emission ratio measured on the cell body of an individual neuron. Traces are grouped on the basis of their similar response pattern. Thick traces correspond to the cells presented on the left. The adenosine A2A receptor agonist CGS 21680 (CGS, 1 μ M), in the presence of the antagonist of adenosine A1 receptor PSB36 (100 nM), increased cAMP in D2 MSNs (blue traces). NPEC-DA (3 μ M) was applied in the bath and uncaged by a flash of UV light, increasing cAMP in D1 MSNs (green traces) and decreasing cAMP in D2 MSNs. The PDE2 inhibitor BAY607550 (iPDE2, 200 nM) further increased cAMP in D2 MSNs. A second NPEC-DA (3 μ M) was performed in the presence of iPDE2. The D1 receptor agonist SKF-81297 (SKF, 100 nM) increased cAMP in D1 MSNs. Forskolin (fsk, 13 μ M) and IBMX (200 μ M) increased the ratio measurement to the maximal level, used for normalization. (B) Average D1 and D2 responses for the first and second NPEC-DA uncaging of 4 similar experiments are overlaid for comparison.

A



B

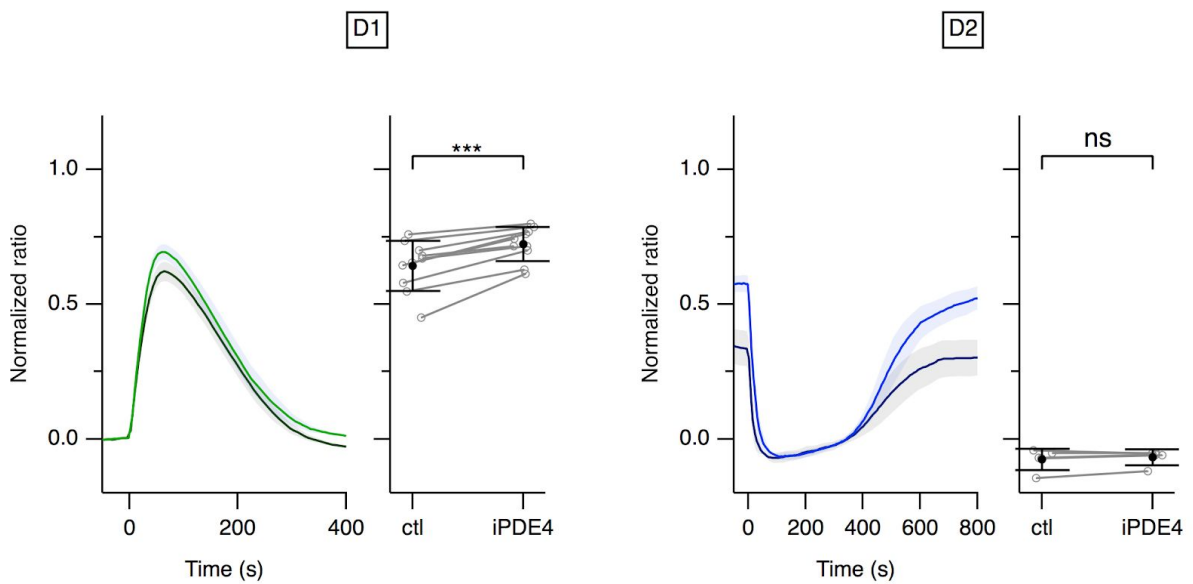
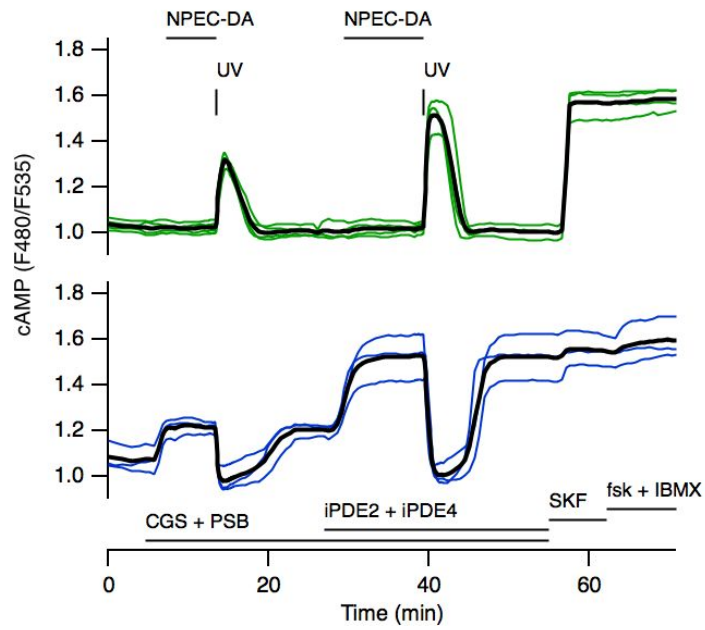


Figure 2

PDE4 reduces the cAMP responses to dopamine in D1 MSNs and to adenosine via A2A receptors in D2 MSNs in striatal brain slices from mice expressing the Epac-SH150 biosensor. Same protocol as in Figure 1 except that PDE4 was inhibited with rolipram (iPDE4, 100 nM).

A



B

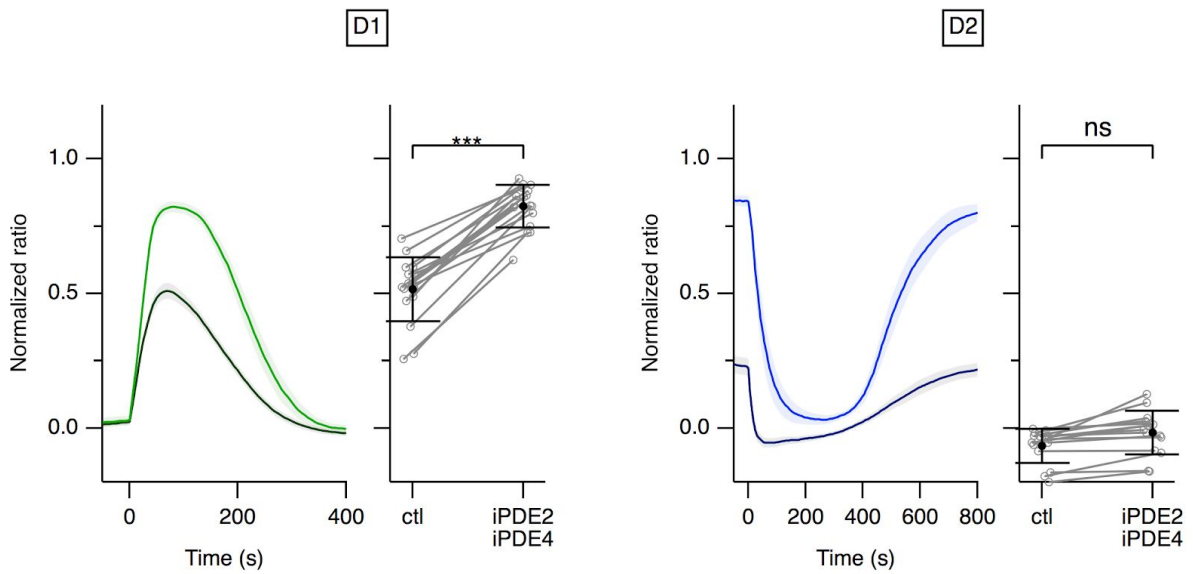
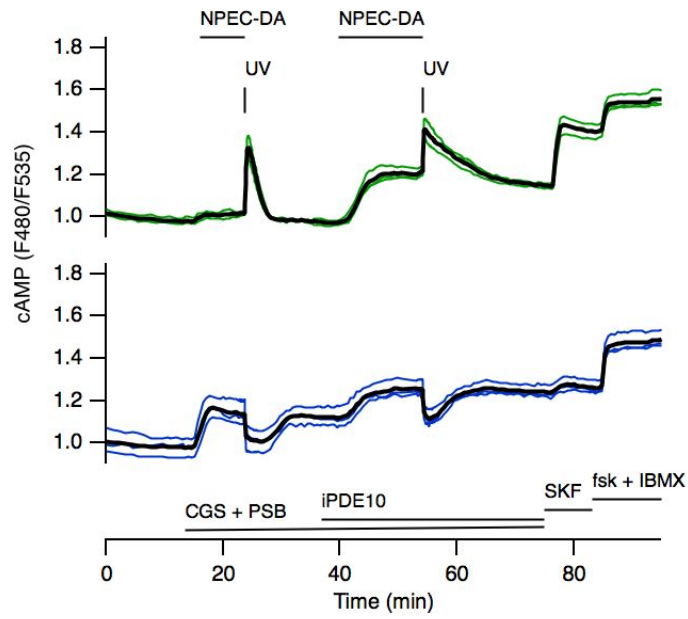


Figure 3

PDE2 and PDE4 together degrade only high levels of cAMP during dopamine release in D1 and during adenosine stimulation in D2 MSNs. Same protocol as Figure 2, except that PDE2A and PDE4 were both inhibited with BAY607550 (iPDE2, 200 nM) and rolipram (iPDE4, 100 nM).

A



B

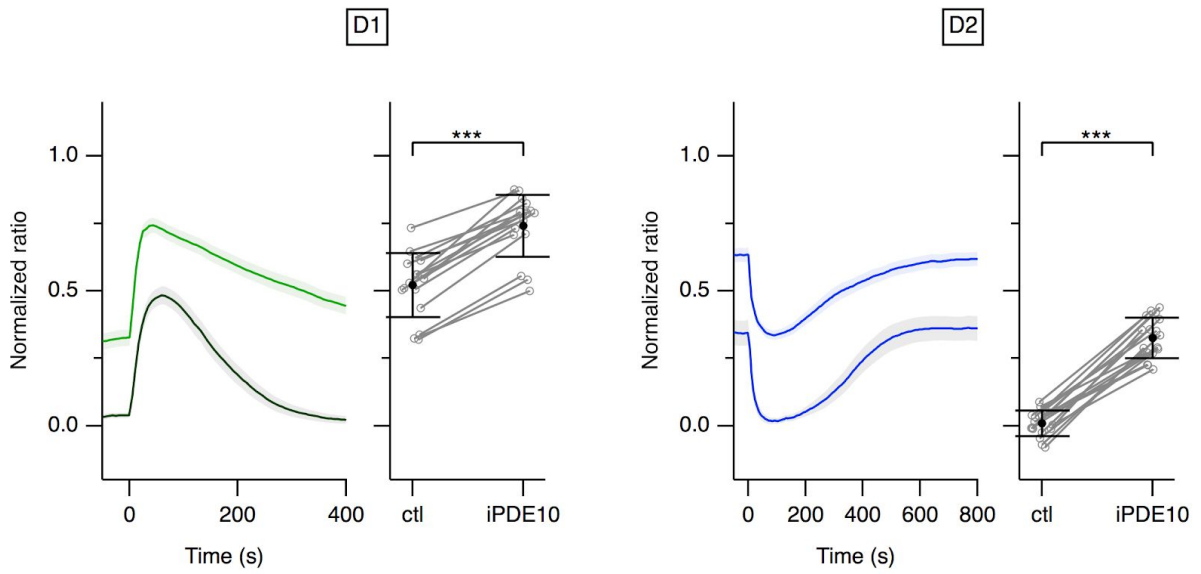


Figure 4

PDE10 activity is required to lower cAMP levels to the lowest cAMP concentration in D2 MSNs.

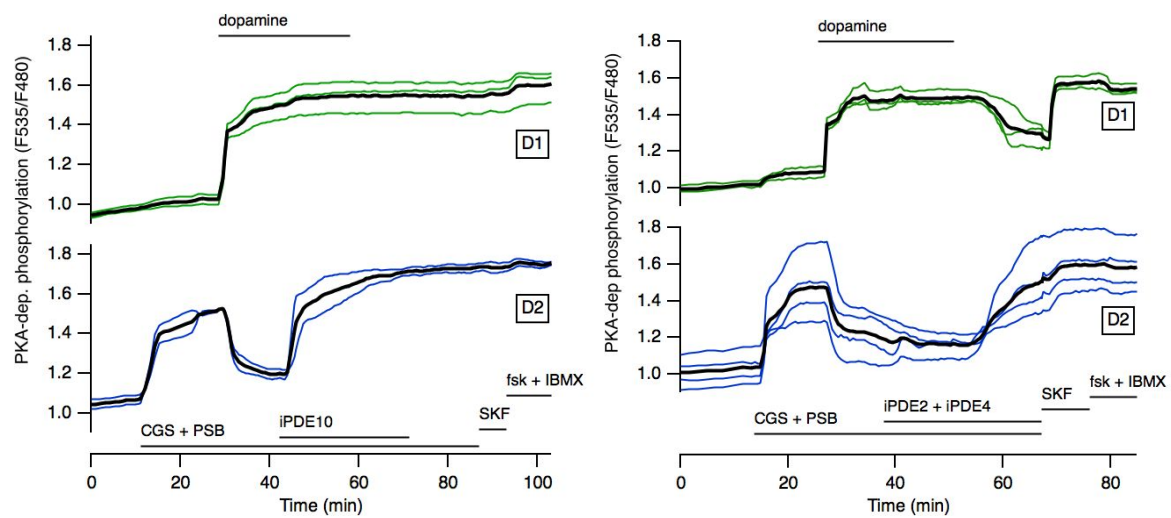


Figure 5

PDE10 is required to degrade and maintain cAMP concentration below the level required to de-activate PKA activity.

Article 3: PDE2A - Fragile X syndrome - hippocampus

Involvement of phosphodiesterase 2A activity in the pathophysiology of fragile X syndrome.

Maurin T, Melancia F, Jarjat M, Castro L, Costa L, Delhaye S, Khayachi A, Castagnola S, **Mota E**, Di Giorgio A, Servadio M, Drozd M, Poupon G, Schiavi S, Sardone L, Azoulay S, Ciranna L, Martin S, Vincent P, Trezza V, Bardoni B.

Cerebral Cortex. 2018

DOI: 10.1093/cercor/bhy192.

(Maurin *et al.*, 2018b)

Fragile X syndrome (FXS) is characterised as the most common form of inherited intellectual disability and the most common genetic cause of autism. The FXS is caused by the absence of expression of the *FMR1* gene that leads to the lack of fragile X mental retardation protein (FMRP). This protein is a translational modulator of synaptic proteins and a regulator of mRNA transport at the synapse. Thus, several pathways are dysregulated in *Fmr1*-KO neurons. In hippocampus and cortex, a prominent target of FMRP is the Pde2a mRNA, which encodes PDE2A (Maurin *et al.*, 2018a). In the absence of FMRP binding to Pde2a mRNA, the messenger translation is no longer repressed, leading to an increased level of PDE2A protein. This led to the hypothesis that this excessive PDE2A expression was a cause of some aspect of the symptoms.

Our contribution to this project was to assess whether the increased expression of PDE2A, detected at the biochemical level, translated into an increased PDE2A activity in living neurons. PDE2A can be activated through cGMP, and we increased cGMP level using a NO donor, DEANO.

Our observations:

- cAMP synthesis was first stimulated using forskolin, leading to a steady-state similar in WT and *Fmr1*-KO (Figure 1B, C in article #3);
- PDE2A was then activated using the NO donor DEANO, which decreased the cAMP levels. The *Fmr1*-KO neurons presented faster cAMP degradation than WT neurons (Figure 1C, D in article #3), which is consistent with an elevated PDE2A activity in the *Fmr1*-KO hippocampus;
- PDE2A activity was then blocked by the addition of the potent and specific PDE2A inhibitor BAY607550, which increased the cAMP levels, revealing the effective contribution of PDE2A in cAMP degradation (Figure 1B, C in article #3).

Conclusion: There is an elevated activity of PDE2A in hippocampal *Fmr1*-KO neurons, compared to wild-type mice.

Behavioral and cellular experiments presented in this article suggest that PDE2A might represent a novel therapeutic target to treat children affected by FXS. Inhibiting PDE2A in early developmental ages of *Fmr1*-KO animals restores:





- LTD in hippocampus;
- axonal length and dendritic spine maturation;

- interaction behaviors;
- social communications.


Moreover, the early treatment (from PND5 to PND21) of *Fmr1*-KO mice with a PDE2A inhibitor, reversed their social deficits at PND30, showing that the beneficial effects of early treatment are long-lasting.

ORIGINAL ARTICLE

Involvement of Phosphodiesterase 2A Activity in the Pathophysiology of Fragile X Syndrome

Thomas Maurin ^{1,2}, Francesca Melancia³, Marielle Jarjat^{1,2}, Liliana Castro ^{4,5}, Lara Costa⁶, Sébastien Delhaye^{1,2}, Anouar Khayachi¹, Sara Castagnola^{1,2}, Elia Mota^{4,5}, Audrey Di Giorgio⁷, Michela Servadio³, Malgorzata Drozd^{1,2}, Gwénola Poupon¹, Sara Schiavi³, Lara Sardone⁸, Stéphane Azoulay⁷, Lucia Ciranna⁸, Stéphane Martin⁹, Pierre Vincent ^{4,5}, Viviana Trezza³ and Barbara Bardoni ^{2,9}

¹Université Côte d'Azur, CNRS, IPMC, F-06560 Valbonne, France, ²CNRS LIA «Neogenex», F-06560 Valbonne, France, ³Department of Sciences, Università RomaTre, I-00145 Roma, Italy, ⁴Sorbonne Université, CNRS, Biological Adaptation and Ageing, F-75005 Paris, France, ⁵Labex BioPsy, F-75005 Paris, France, ⁶Department of Clinical and Experimental Medicine, University of Messina, I-98122 Messina, Italy, ⁷Université Côte d'Azur, CNRS, Institut de Chimie de Nice, F-06108 Nice, France, ⁸Department of Biomedical and Biotechnological Sciences, University of Catania, I-95123 Catania, Italy and ⁹Université Côte d'Azur, INSERM, CNRS, IPMC, F-06560 Valbonne, France

Address correspondence to Barbara Bardoni, Thomas Maurin, CNRS UMR7275, Institute of Molecular and Cellular Pharmacology, 660 Route des Lucioles, Sophia-Antipolis, 06560 Valbonne, France. Email: bardoni@ipmc.cnrs.fr (B.B.); maurin@ipmc.cnrs.fr (T.M.)  orcid.org/0000-0001-6411-1517

Fancesca Melancia and Marielle Jarjat equally contributed; Liliana Castro, Lara Costa and Sébastien Delhaye equally contributed to this work; Lucia Ciranna, Stéphan Martin, Pierre Vincent and Viviana Trezza equally contributed to this work

Abstract

The fragile X mental retardation protein (FMRP) is an RNA-binding protein involved in translational regulation of mRNAs that play key roles in synaptic morphology and plasticity. The functional absence of FMRP causes the fragile X syndrome (FXS), the most common form of inherited intellectual disability and the most common monogenic cause of autism. No effective treatment is available for FXS. We recently identified the *Phosphodiesterase 2A* (*Pde2a*) mRNA as a prominent target of FMRP. PDE2A enzymatic activity is increased in the brain of *Fmr1*-KO mice, a recognized model of FXS, leading to decreased levels of cAMP and cGMP. Here, we pharmacologically inhibited PDE2A in *Fmr1*-KO mice and observed a rescue both of the maturity of dendritic spines and of the exaggerated hippocampal mGluR-dependent long-term depression. Remarkably, PDE2A blockade rescued the social and communicative deficits of both mouse and rat *Fmr1*-KO animals. Importantly, chronic inhibition of PDE2A in newborn *Fmr1*-KO mice followed by a washout interval, resulted in the rescue of the altered social behavior observed in adolescent mice. Altogether, these results reveal the key role of PDE2A in the pathophysiology of FXS and suggest that its pharmacological inhibition represents a novel therapeutic approach for FXS.

Key words: autism spectrum disorder, *Fmr1*-KO mice, *Fmr1*-KO rats, fragile X syndrome, phosphodiesterase 2A

Introduction

Fragile X syndrome (FXS) is a rare genetic neurodevelopmental disorder with a prevalence of 1:4000 males and 1:7000 females representing the most common form of inherited intellectual disability (ID) and a leading genetic cause of autism spectrum disorder (ASD). Patients may also exhibit a range of disabling neurological problems including hyperactivity, attention deficit, anxiety and epileptic seizures in addition to facial dysmorphisms and physical abnormalities (Bassell and Warren 2008; Maurin et al. 2014; Castagnola et al. 2017). FXS is caused by the absence of expression of the *FMR1* gene, which ultimately leads to the lack of its product, the fragile X mental retardation protein (FMRP), a translational modulator of synaptic proteins and a regulator of mRNA transport at the synapse. Consequently, neurons of both FXS patients and *Fmr1*-KO mice exhibit abnormal dendritic spines associated with altered forms of synaptic plasticity (Bassell and Warren 2008; Maurin et al. 2014; Castagnola et al. 2017). Furthermore, altered volumes of specific brain structures that develop prenatally or early postnatally in young FXS children (Gothelf et al. 2008; Hoefft et al. 2010) and *Fmr1*-KO pups (Lai et al. 2016) have been described. The abundance of many synaptic proteins is altered in the absence of FMRP and, consequently, multiple molecular pathways are dysregulated in *Fmr1*-KO neurons (Maurin et al. 2018). However, despite the research efforts made both at preclinical and clinical levels, approved therapies are not yet available for FXS (Budimirovic et al. 2017; Castagnola et al. 2017; Erickson et al. 2017). Towards this goal, it is essential to have a better understanding of the pathophysiology of FXS and of the role played by FMRP during brain development. Therefore, we used High Throughput Sequencing-Cross Linking Immuno-Precipitation (HITS-CLIP) to identify FMRP RNA targets at postnatal day (PND) 13, an early developmental stage of mouse brain, when FMRP is most highly expressed and synaptogenesis peaks (Maurin et al. 2018). At this age, in hippocampus and in cortex a prominent target of FMRP is the *Phosphodiesterase 2A* (*Pde2a*) mRNA (Maurin et al. 2018), which encodes an enzyme involved in cAMP and cGMP degradation (Maurice et al. 2014). PDE2A levels and activity are increased (Maurin et al. 2018 and this study) in *Fmr1*-KO, resulting in reduced levels of cAMP and cGMP, 2 intracellular secondary messengers having key roles in neuronal differentiation, development and function (Shelly et al. 2010; Park et al. 2014). Here, we unravel the pathophysiological relevance of PDE2A activity in FXS by combining *in vitro*, *ex vivo*, and *in vivo* experiments and using 2 rodent models of FXS. We conclude that PDE2A represents a novel therapeutic target to treat children affected by FXS.

Materials and Methods

Neuronal Cultures and Spine Morphology Analysis

Primary cortical neurons were prepared from embryos at E15.5 obtained from pregnant C57BL/6 *Fmr1*-KO and wild type (WT) mice as previously described (Khayachi et al. 2018). Neurons (17 days *in vitro*) were treated with 0.2 μ M BAY607550 or DMSO (control) for 24 h in total. After 5 h of pharmacological treatment, neurons were transduced with attenuated Sindbis viral particles pSinRep5(nsP2726)-expressing GFP at a multiplicity of infection (MOI) of 0.1. Transduced neurons (18 days *in vitro*) were washed twice in PBS at room temperature (RT) after 19 h of transduction, and then fixed (Devader et al. 2015). Sequential confocal images (512 \times 220 pixels; Zoom 3.0; Average 4; Speed 7) of GFP-expressing neurons were acquired with a 63X oil-immersion lens (Numerical Aperture NA 1.4) on an inverted Zeiss LSM780

confocal microscope. Z-series of 7–8 images of randomly selected secondary dendrites (3 independent cultures, 24–30 neurons per condition) were analyzed using NeuronStudio software, which allows for the automated detection of immature and mature spines (Rodriguez et al. 2008; Devader et al. 2015).

The dendritic spine morphology analysis was scored and analyzed by trained observers who were unaware of treatment conditions.

cAMP and cGMP Detection

1) ELISA test: Frozen ground hippocampi from PND 13 mice, were resuspended in 10 volumes of 0.1 N HCl and centrifuged to remove debris. Supernatants were used directly for cGMP measurement. ELISA was then carried out according to the manufacturer's instructions (Direct cGMP ELISA kit; Enzo Life Science). 2) cAMP-Glo Max assay: Primary cortical neurons (17–21 days *in vitro*) cultured in 96 wells plates were stimulated in 2 biological replicates with 10 μ M Forskolin and 1 μ M BAY607550 in dPBS supplemented with CaCl₂ and MgCl₂ for 30 min at 37 °C. cAMP concentration was measured with the cAMP-Glo Max assay (Promega) according to the manufacturer's indications. 3) cAMP Biosensors: Brain slices were prepared from male mice at PND 7–11, transduced with Sindbis viral particles to express the cAMP biosensor Epac-S^{H150} (Polito et al. 2013). Wide-field images were obtained with an Olympus BX50WI or BX1WI upright microscope with a 40 \times 0.8 NA water-immersion objective and an ORCA-AG camera (Hamamatsu). Images were acquired with iVision (Biovision, Exton, PA, USA). The excitation and dichroic filters were D436/20 and 455dxc. Signals were acquired by alternating the emission filters with a filter wheel (Sutter Instruments, Novato, CA, USA), HQ480/40 for the donor, and D535/40 for the acceptor. Images were analyzed with custom routines according to the IGOR Pro environment (Wavemetrics, Lake Oswego, OR, USA). The emission ratio was calculated for each pixel as F480/F535. The pseudocolor images display the ratio value coded in hue and the fluorescence of the preparation coded in intensity. The amplitudes of responses were quantified for each neuron as the fractional change in ratio from its own baseline and maximal final ratio response (in the presence of forskolin and IBMX). Responses obtained from CA1 neurons were averaged for each experiment (i.e., brain slice). Data were analyzed with SPSS statistical software version 22.0 (Chicago, IL, USA). Normality in variable distributions and homogeneity of variances across groups were assessed with the Shapiro–Wilk and Levene tests, respectively.

Animals

The experiments were performed following the ARRIVE (Animals in Research: Reporting In Vivo Experiments) guidelines (Kilkenny et al. 2010). *Fmr1*-knockout (KO) and WT mice on a C57BL/6J congenic background were obtained from Prof. R. Willemsen (Mientjes et al. 2006), while *Fmr1*-KO and WT rats on a Sprague-Dawley background were purchased from Horizon Discovery (formerly SAGE Labs, USA). All animals were generated and housed in groups of 4 in standard laboratory conditions (22 °C, 55 \pm 10% humidity, 12-h light/12-h dark diurnal cycles) with food and water provided *ad libitum*.

Behavior

Experimental testing was performed between 12:00 and 16:30 each day during the 12-h light period. Only male mice and rats were used. Animal care was conducted in accordance with the

European Community Directive 2010/63/EU. The experiments were approved by the local ethics committee (Comité d'Ethique en Expérimentation Animale CIEPAL-AZUR N. 00788.01; APAFIS#4985-2 016 032 314 169 426 v4APAFIS#8100-2 016 112 217 148 206 v3), by the French Ministry of Research and by the Italian Ministry of Health. The number of animals used in each experiment is indicated in the figure legends.

Electrophysiology

Hippocampal slices were prepared from WT and *Fmr1*-KO mice on a C57BL/6J genetic background at PND 13 as previously described (Costa et al. 2012), following protocols approved by local ethics committee (OPBA, University of Catania) and by the Italian Ministry of Health (N. 35212016-PR). Data were acquired and analyzed with the Signal software (Cambridge Electronic Design, England). Excitatory Post Synaptic Current (EPSC) amplitude was measured as the difference between peak and baseline current. EPSC amplitude values were averaged over 1 min and expressed as % of baseline (mean EPSC amplitude calculated from EPSCs recorded during at least 15 min before [S]-3,5-Dihydroxyphenylglycine [DHPG] application). Different sets of values were compared using the appropriate statistical tests indicated in the corresponding figure legend. The amount of long-term depression (LTD) induced by metabotropic group I glutamate receptor (mGluR) was calculated 40 min after LTD induction by DHPG application and is expressed by indicating EPSC amplitude as percentage of baseline (% EPSC).

Drug Treatment

BAY607550 (Cayman) was dissolved in 10% DMSO/8.75% Tween 80/8.75% polyethylene glycol/saline. For the behavioral experiments, BAY607550 or Lu AF64280 (or their vehicles) were administered intraperitoneally (i.p.) 30 min before testing. BAY607550 was administered at the doses of 0.05 mg/kg at infancy and 0.1 mg/kg at adolescence, while Lu AF64280 was administered at 0.5 mg/kg. Drug doses and pretreatment intervals were based on literature (Boess et al. 2004; Masood et al. 2008, 2009; Ding et al. 2014; Redrobe et al. 2014; Wang et al. 2017) and our pilot data showing that, at the doses used in the present study, drugs did not affect the behavior of WT animals. In one experiment, chronic treatment was carried out by a daily i.p. injection of 0.05 mg/kg BAY607550 to mice from PND 5–21 and mice were tested for social interaction after a washout interval of 9 days. One pup per litter from different litters per treatment group was used in the behavioral experiments, to control for any potential litter effect. Animals were randomly allocated to each treatment group. Coding of the drug solutions ensured that both during experimentation and behavior analysis, the experimenter was unaware of the treatment of the animals. The number of animals per group is indicated in the figure legends.

The Isolation-Induced Ultrasonic Vocalizations Test

The test was performed as previously described (Servadio et al. 2016). Briefly, each pup (at PND 10 for mice and PNDs 5 and 9 for rats) was individually removed from the nest and placed into a black Plexiglas arena, located inside a sound-attenuating and temperature-controlled chamber. Pup ultrasonic vocalizations (USVs) were detected for 3 min by an ultrasound microphone (Avisoft Bioacoustics, Germany) sensitive to frequencies between 10 and 250 kHz and fixed at 10 cm above the arena. Pup axillary temperature was measured before and after the test by a digital thermometer. The emission of USVs was analyzed using Avisoft Recorder software (Version 5.1).

Homing Behavior Test

At PND 14, the litter was separated from the dam and kept for 30 min in a temperature-controlled holding cage. Then, each mouse pup was placed into a Plexiglas box whose floor was covered for 1/3 with bedding from the pup's home cage and for 2/3 with clean bedding. The pup was located at the side of the box covered by clean bedding, and its behavior was videorecorded for 4 min for subsequent analysis. The following parameters were scored using the Observer 3.0 software (Noldus Information Technology): latency (s) to reach the home-cage bedding area; total time (s) spent by the pup in the nest bedding area.

Social Interaction Test

The test was performed as previously described (Terranova and Laviola 2005; Jamain et al. 2008). The 28–30-day-old mice were individually habituated to the experimental apparatus (a Plexiglas cage measuring 30 × 30 × 30 cm³) for 5 min the day before testing. On the test day, the animals were isolated for 2 h before testing, to enhance their social motivation and thus facilitate the expression of social interaction during testing. The test consisted of placing 2 animals (same treatment and weight) into the test cage for 10 min.

The behavior of the animals was recorded using a video camera with zoom lens, DVD recorder and LCD monitor. Behavior was assessed per single animal and analyzed by a trained observer who was unaware of genotype and treatment conditions using the Observer XT software (Noldus, The Netherlands).

The following parameters were scored (Terranova and Laviola 2005; Jamain et al. 2008):

- a. Social activities:
 1. Social sniffing: sniffing any part of the body of the partner, including the anogenital area.
 2. Following: moving in the direction of or pursuing the partner, who moves away.
 3. Mutual circle: partners are mutually sniffing each other's anogenital region, while describing tight circles with their reciprocal following movements.
 4. Pushing past: the focal animal passes between the wall of the cage and the body of the partner by pushing its own body through the narrow space available.
 5. Crawling under/over: the focal animal crawls underneath or over the partner's body, crossing it transversely from one side to the other.
 6. Social grooming: chewing and licking the fur of the partner.
 7. Social rest: the focal animal is being groomed by the partner.
 8. Pushing under: the focal animal pushes its own snout or the whole anterior part of its body under the partner's body, and rests for at least 3 s.
 9. Social inactivity: the focal animal is lying flat or standing still (eyes closed or open) while maintaining close physical contact with the partner.
- b. Nonsocial activities:
 1. Running: the focal animal performs a sudden, rapid, vigorous, and erratic darting, characterized by frequent and sharp changes in direction and without any obvious target.
 2. Inactive: Self-explanatory.
 3. Exploring: Self-explanatory.

4. Digging: the focal animal is digging in the sawdust, pushing and kicking it around, using the snout and/or both the forepaws and hindpaws.

The average frequency of total social activities, quantified as number of events during the 10 min testing session, was graphed.

Statistical Analysis

Results are expressed as mean \pm standard error of the mean (SEM). All statistical analyses were based on biological replicates. Appropriate statistical tests used for each experiment are described in the corresponding figure legends. All statistical analyses were carried out using the GraphPad Prism Version 6.0e.

Results

PDE2A Dysregulation is Involved in the Physiopathology of FXS

Pde2a is expressed both in cortex and hippocampus (e.g., supragranular layer of neocortex, CA1 and CA3 regions of hippocampus) (Stephenson et al. 2009, 2012), with a high and homogenous expression in the mouse CA1. To assess whether the increased

abundance of the PDE2A protein in the absence of FMRP that we described (Maurin et al. 2018) is associated with its elevated activity in hippocampus, we measured cAMP levels in single neurons of the CA1 area in *Fmr1*-KO and WT mouse brain slices. For this purpose, we used the Epac-S^{H150} fluorescent biosensor that detects an increase in cAMP levels by a decrease in FRET between the donor and acceptor fluorophores (Polito et al. 2013). These changes were monitored in real-time by ratiometric fluorescence imaging. cAMP synthesis was first stimulated using forskolin, leading to a steady-state biosensor emission ratio. PDE2A was then activated using the NO donor DEANO, which decreased the biosensor ratio. PDE2A activity was then blocked by the addition of the potent and specific PDE2A inhibitor BAY607550 (Boess et al. 2004), which increased the biosensor ratio, revealing the effective contribution of PDE2A in cAMP degradation. A final application of forskolin and the nonselective phosphodiesterase inhibitor IBMX increased the biosensor ratio to its maximum. An example of this analysis in WT neurons is reported in Figure 1A, B. Then we performed these assays in hippocampal slices obtained from PND 7–11 WT and *Fmr1*-KO mice. cAMP levels elicited by forskolin and DEANO stimulation were significantly lower in the absence of *Fmr1* expression, consistent with an elevated PDE2A activity in the *Fmr1*-KO hippocampus (Fig. 1C). We confirmed these findings by a detailed analysis of cAMP

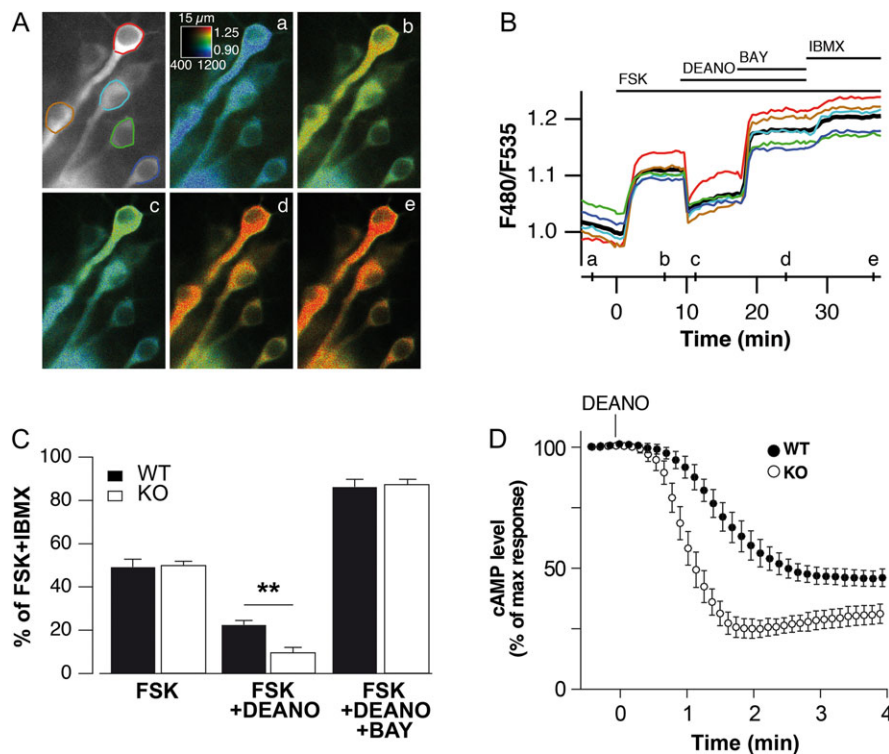


Figure 1. The increased activity of PDE2A results into decreased cAMP levels. (A) Hippocampal brain slices expressing the Epac-S^{H150} biosensor were imaged with wide-field fluorescence microscopy (here exemplified with a measure in a WT brain slice). Images show the raw fluorescence intensity at 535 nm (in gray scale) and the ratio (in pseudocolor), reporting changes in cAMP concentration before stimulation and at different times of the recording during the different treatments (a–e), as indicated by the corresponding lines on the graph in panel “B”. The calibration square on the pseudocolor image indicates from left to right increasing fluorescence intensity levels, and from bottom to top increasing ratio values. The width of the square is used as a scale bar. Its size is indicated above it in micrometers. (B) Each trace on the graph indicates the F480/F535 emission ratio measured on the regions (neuron) delimited by the color contour drawn on the gray scale image (upper left panel). The black trace corresponds to the mean of the 5 colored traces. (C) Quantification of cAMP in WT and *Fmr1*-KO hippocampal slices: the successive responses to forskolin, DEANO and BAY607550 were quantified as a fraction of the maximal response measured in the presence of IBMX. (D) Average ratio response to forskolin (10 μ M), forskolin + DEANO (10 μ M) and forskolin + DEANO + BAY607550 (0.2 μ M) for WT and *Fmr1*-KO. Mean \pm SEM is shown. In each experiment (i.e., brain slices tested, one slice per animal) a variable number of neurons have been considered (between 1 and 6). Results from $n = 12$ WT and $n = 16$ *Fmr1*-KO experiments are shown. Two-way ANOVA followed by Bonferroni multiple comparisons post hoc test revealed a significantly lower level of cAMP in *Fmr1*-KO slices for the FSK + DEANO condition ($F_{\text{treatment}(1,26)} = 640, P < 0.001$; $F_{\text{genotype}(1,26)} = 1.25, P = 0.278$; $F_{\text{genotype} \times \text{treatment}(1,26)} = 15.76, P = 0.001$) followed by Bonferroni multiple comparisons post hoc test (adjusted P value $**P < 0.01$). (D) Time course measurement of cAMP levels after DEANO application in the presence or in the absence of FMRP.

degradation kinetics in the presence and in the absence of FMRP upon PDE2A activation with DEANO: the decrease in biosensor ratio upon PDE2A stimulation with DEANO was significantly faster in *Fmr1*-KO neurons than in WT (Fig. 1D).

In addition, using an ELISA immuno-assay, we showed that cGMP levels are also significantly decreased in *Fmr1*-KO hippocampi (Supplementary Fig. S1). Collectively, these data indicate that there is an elevated activity of PDE2A in hippocampal *Fmr1*-KO neurons.

Blocking PDE2A Activity Suppresses the Exaggerated LTD in *Fmr1*-KO hippocampus

A hallmark of FXS is the exaggerated LTD induced by mGluR activation in the hippocampal CA3-CA1 synapses (Huber et al. 2002). To assess whether inhibition of PDE2A can prevent the exaggerated synaptic plasticity characterizing FXS hippocampi, we measured LTD expression in the presence and in the absence of BAY607550. AMPA receptor-mediated excitatory postsynaptic currents (EPSCs) were recorded from CA1 pyramidal neurons under whole-cell patch clamp following stimulation of Schaffer collaterals, in the continuous presence of D-AP5 (50 μ M) and bicuculline (5 μ M). Bath application of DHPG (100 μ M, 5 min), an agonist of group I mGluRs, induced a LTD of EPSC amplitude that in WT was not modified in the presence of BAY607550 (50 nM; Fig. 2A,C). The amount of mGluR-LTD is exaggerated in *Fmr1*-KO hippocampi (EPSC amplitude: $40 \pm 9\%$ vs. $78 \pm 9\%$ in WT vs. *Fmr1*-KO treated with BAY607550; Fig. 2B,C), as previously reported (Costa et al. 2012; Castagnola et al. 2017). Intracellular BAY607550 (50 nM) in *Fmr1*-KO mouse hippocampal neurons reverted the exaggerated mGluR-LTD to a level that is not statistically different from WT control recordings (EPSC % amplitude: $78 \pm 9\%$ vs. $86 \pm 7\%$ in WT vs. *Fmr1*-KO treated with BAY607550; Fig. 2B,C). Remarkably, BAY607550 treatment (50 nM) had no effect on mGluR-LTD in WT slices (Fig. 2A-C). These results clearly show the implication of PDE2A-mediated regulation of cAMP and cGMP in the exaggerated mGluR-dependent LTD in *Fmr1*-KO mice.

Inhibiting PDE2A Activity Restores Axonal Length and Spine Maturation in Cultured Cortical *Fmr1*-KO Neurons

The presence of abnormal immature dendritic spines in the brain of FXS patients and in primary neuronal cultures of mouse *Fmr1*-KO models of FXS (Comery et al. 1997; Irwin et al. 2000; Nimchinsky et al. 2001; Antar et al. 2005, 2006) is another hallmark associated with the functional absence of FMRP. Importantly, both cAMP and cGMP have been reported to exert an important role in axonal growth and dendritic spine maturation (Shelly et al. 2010; Shen and Cowan 2010; Averaimo and Nicol 2014; Akiyama et al. 2016). Therefore, to assess the involvement of PDE2A in synaptic morphology, we first analyzed cAMP levels in cultured cortical neurons in the absence or in the presence of PDE2A inhibitors (Supplementary Fig. S2). We then assessed the impact of an inhibition of PDE2A activity on the maturation of dendritic spines (Fig. 3) and on axonal growth (Fig. 4) in *Fmr1*-KO cultured cortical neurons. To quantify the activity of PDE2A in FXS neurons, we measured cAMP levels in cultured *Fmr1*-KO upon forskolin stimulation associated with pan-PDE inhibition with IBMX (Supplementary Fig. S2). This latter treatment led to a significant increase in cAMP levels both in the presence and in the absence of FMRP expression (Supplementary Fig. S2A), while treatment with Rolipram (a specific inhibitor of PDE4) did not (Supplementary

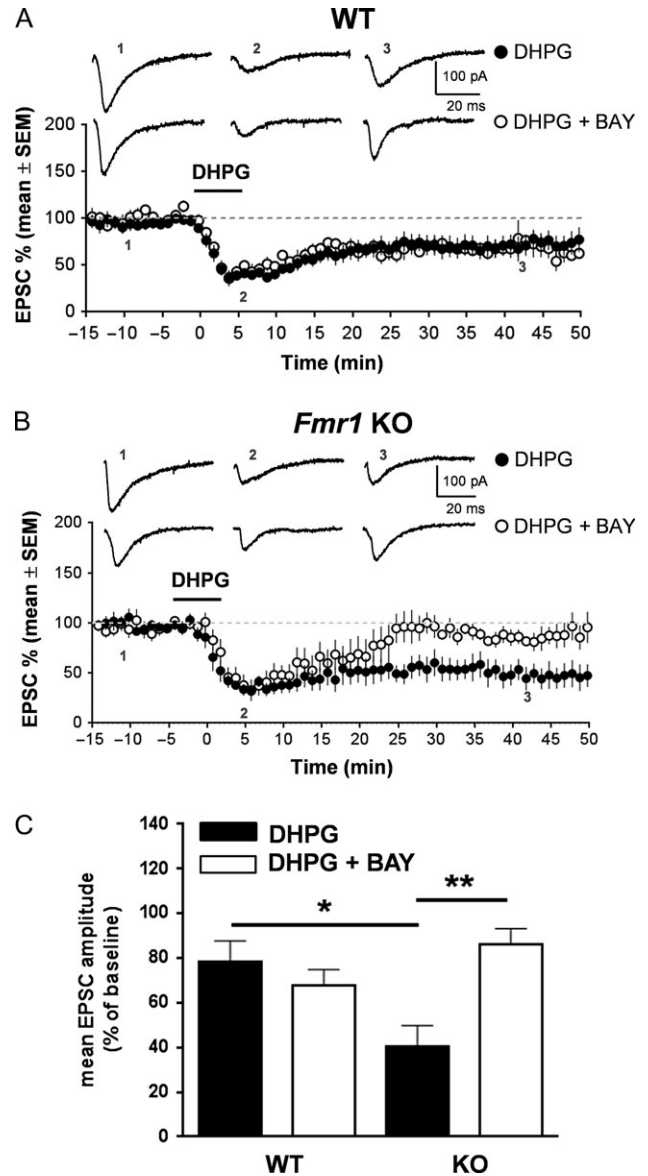


Figure 2. Blockade of PDE2A rescues the exaggerated hippocampal mGluR-dependent LTD in the *Fmr1*-KO brain. (A) DHPG (100 μ M, 5 min) induces a mGluR-LTD of EPSCs recorded from CA1 pyramidal neurons obtained from WT mouse slices ($n = 6$). BAY607550 (50 nM, added intracellularly in the recording pipette) did not modify the amount of mGluR-LTD of EPSCs recorded from CA1 pyramidal neurons in WT slices ($n = 6$). (B) In mouse *Fmr1*-KO slices ($n = 9$), mGluR-LTD was reversed in the presence of intracellular BAY607550 (50 nM). (C) Bar graphs show % EPSC amplitude (mean \pm SEM from groups of neurons) 40 min after application of DHPG in control conditions or in the presence of intracellular BAY607550 (50 nM). Bar graphs show the mean \pm SEM values of EPSC % after the indicated pharmacological treatments. Two-way ANOVA were computed ($F_{\text{genotype}(1,22)} = 1.159, P = 0.2933$; $F_{\text{treatment}(1,22)} = 3.919, P = 0.2933$; $F_{\text{genotype} \times \text{treatment}(1,22)} = 10.24, P = 0.0041$) with Bonferroni's post-tests for multiple comparisons of data sets, using genotype (*Fmr1*-KO or WT) and treatment (BAY607550 or vehicle) as between-subjects factor (adjusted P value: * $P = 0.0276$; ** $P = 0.0037$).

Fig. S2B). Conversely, the specific blockade of PDE2A activity by BAY607550 promoted a significant increase in cAMP levels in *Fmr1*-KO neurons without affecting its abundance in WT neurons (Supplementary Fig. S2C). This finding suggests a PDE2A-dependent regulation of cAMP levels in *Fmr1*-KO neurons.

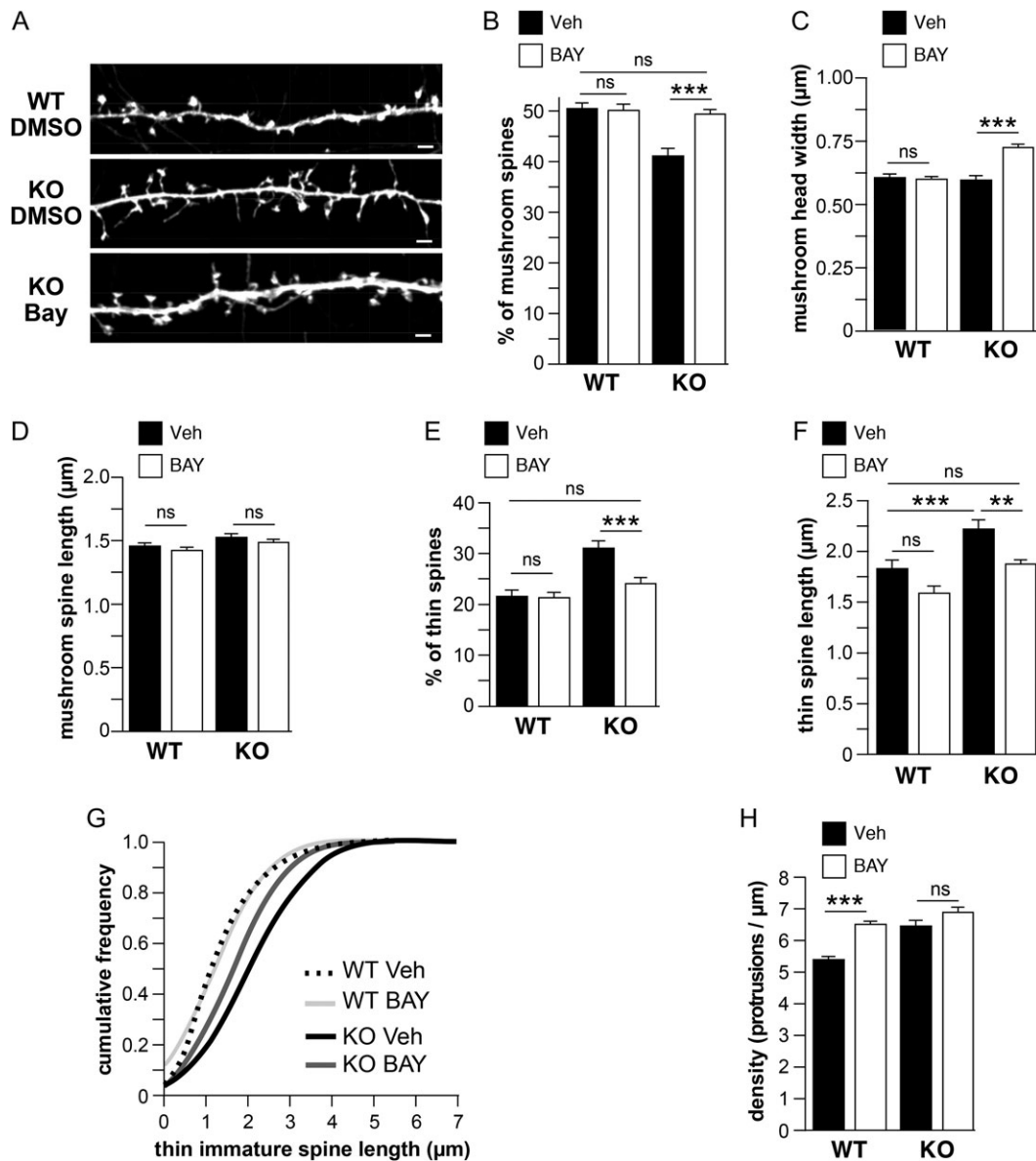


Figure 3. Inhibition of PDE2A activity improves *Fmr1*-KO dendritic spine morphology in cultured cortical neurons. (A) Representative high-resolution confocal images showing GFP-expressing WT and *Fmr1*-KO mouse secondary dendrites treated or not for 24 h with 0.2 μM BAY607550 to block PDE2A activity. Spine morphology was assessed using NeuronStudio software 19 h post-transduction and compared with the measurement obtained from control DMSO-treated neurons. Scale bars: 2 μm. All summary histograms present mean ± SEM values, statistical significance was assessed with 2-way ANOVA. The percentage of mature mushroom spines ($F_{\text{genotype}}(1,110) = 10.98, P = 0.0012; F_{\text{treatment}}(1,110) = 7.042, P = 0.0091; F_{\text{genotype} \times \text{treatment}}(1,110) = 8.984; P = 0.0034$), (B) mushroom head width ($F_{\text{genotype}}(1,1678) = 18.15, P < 0.0001; F_{\text{treatment}}(1,1678) = 22.06, P < 0.0001; F_{\text{genotype} \times \text{treatment}}(1,1678) = 28.41; P < 0.0001$), (C) and mushroom spine length ($F_{\text{genotype}}(1,1599) = 7.217, P = 0.0073; F_{\text{treatment}}(1,1599) = 3.665, P = 0.0558; F_{\text{genotype} \times \text{treatment}}(1,1599) = 0.002329; P = 0.9615$) (D) measured in secondary dendrites of control and BAY607550-treated neurons. The percentage of immature thin spines ($F_{\text{genotype}}(1,111) = 30.25, P < 0.0001; F_{\text{treatment}}(1,111) = 12.09, P = 0.0007; F_{\text{genotype} \times \text{treatment}}(1,111) = 8.911; P = 0.0035$) (E) and thin spine length ($F_{\text{genotype}}(1,878) = 23.16, P < 0.0001; F_{\text{treatment}}(1,878) = 17.37, P < 0.0001; F_{\text{genotype} \times \text{treatment}}(1,878) = 0.6166; P = 0.4325$) (F) is presented. The consequence of the BAY607550 treatment on the distribution of the thin spine length is depicted as cumulative frequency curves in (G). (H) Histograms showing the mean ± SEM values of protrusion frequency after the indicated pharmacological treatments. Two-way ANOVA were computed with Bonferroni post hoc test to assess the treatment effect in neurons from each genotype. (Adjusted P value: ** $P < 0.01$; *** $P < 0.001$. $N = \sim 1000$.) Protrusions per condition (3 independent mouse cortical neuron cultures; 24–30 neurons per condition). ns, not significant.

In cultured *Fmr1*-KO neurons (Fig. 3A), the specific inhibition of PDE2A by BAY607550 strongly promoted spine maturation by increasing the number of mushroom spines (Fig. 3B) and reduced the number of immature filopodia (Fig. 3E) to normal WT levels. BAY607550 also had a positive impact on the maturity of *Fmr1*-KO neurons by increasing the head size of mushroom spines (Fig. 3C) and concomitantly reducing the length of thin immature spines to WT levels (Fig. 3F–G). Finally, the

BAY607550 treatment affected neither the length of mature spines (Fig. 3D) nor the density of dendritic protrusions (Fig. 3H) in *Fmr1*-KO neurons.

Abnormal axonal growth has been observed in the fly model of FXS (Morales et al. 2002). Since both cAMP and cGMP fulfill critical roles in axonal growth (Shelly et al. 2010; Shen and Cowan 2010; Averaimo and Nicol 2014; Akiyama et al. 2016), we assessed whether PDE2A activity regulates the length of axons.

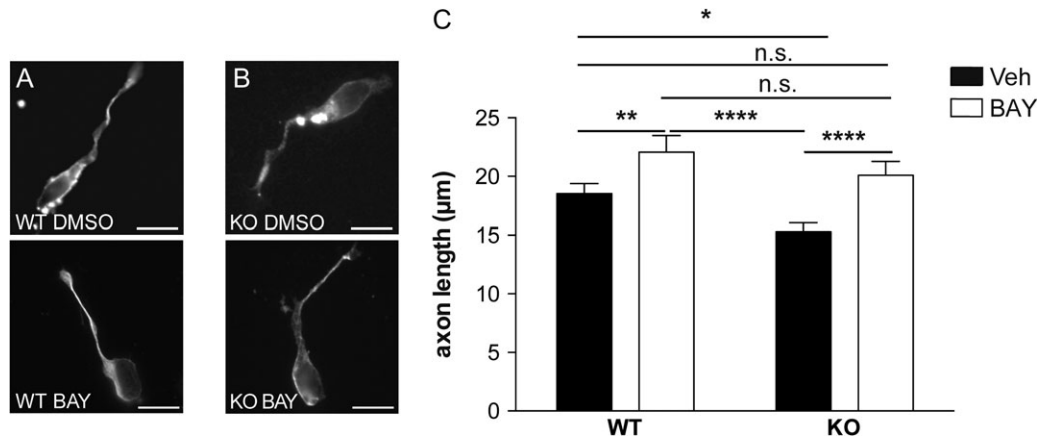


Figure 4. PDE2A activity is associated to axon growth regulation. (A, B) Representative pictures of 2 days in vitro cultured WT (A) and *Fmr1*-KO (B) primary cortical neurons treated with vehicle or 1 μ M BAY607550 as indicated (scale bar: 10 μ m). (C) Histogram of axon length of WT and *Fmr1*-KO neurons treated with vehicle or with 1 μ M BAY607550 for 24 h. Results show the mean axon length \pm SEM from 3 independent cultures on 73 randomly selected cells for each condition. Two-way ANOVA with Tukey post hoc test: DMSO:KO versus DMSO:WT. *Adjusted P value = 0.0256; BAY:WT versus DMSO:WT. **Adjusted P value = 0.0081; BAY:KO versus DMSO:WT. ns: Adjusted P value = 0.4114; BAY:WT versus DMSO:KO. ****Adjusted P value < 0.0001; BAY:KO versus DMSO:KO. ****Adjusted P value < 0.0001; BAY:KO versus BAY:WT. ns: Adjusted P value = 0.3547; ns, not significant.

Using an immunocytochemistry-based approach, we measured axon length of 2 days in vitro neurons and showed that *Fmr1*-KO neurons had significantly shorter axons than WT cells (Fig. 4A–C). The blockade of PDE2A for 24 h with BAY607550 was sufficient to fully rescue the axonal growth defect of FXS neurons (Fig. 4).

Critical Role of PDE2A Activity in Defining Social Deficits Displayed by 2 Rodent Models of FXS

The *Fmr1*-KO mouse model of FXS recapitulates the main behavioral traits initially described in FXS patients, such as cognitive deficit and social interaction impairments (Mientjes et al. 2006; Maurin et al. 2014). Since we identified *Pde2a* mRNA as a target of FMRP during the early postnatal life in the mouse brain and since we showed that PDE2A expression was increased in *Fmr1*-KO brains (Maurin et al. 2018), we investigated whether an acute PDE2A blockade in vivo rescued the altered phenotype of *Fmr1*-KO infant (PND 10–14) and adolescent (PND 30) mice in FXS-relevant behaviors (Fig. 5). At infancy, *Fmr1*-KO pups displayed early communicative deficits, since they vocalized significantly less compared with WT pups when separated from the dam and siblings at PND 10 (Fig. 5A,B). Furthermore, *Fmr1*-KO animals showed early deficits in social discrimination, since they were unable to use olfactory cues to discriminate between a neutral odor and their own cage odor in the homing behavior test (Fig. 5C,D). BAY607550 has been shown to efficiently cross the blood-brain barrier when administered i.p., promoting comparable PDE2A inhibition levels as the intracranial injection route (Wang et al. 2017). Our results showed that inhibition of PDE2A activity through i.p. administration of BAY607550 normalized the altered USV profile displayed by PND 10 *Fmr1*-KO mice (Fig. 5B). Remarkably, we validated this result by inhibiting PDE2A with Lu AF64280, another highly specific PDE2A inhibitor (Redrobe et al. 2014). Similar to BAY607550, Lu AF64280 was able to revert the altered USV frequency displayed by *Fmr1*-null pups (Supplementary Fig. S3). This confirms that PDE2A blockade is able to rescue the communicative deficit displayed by *Fmr1*-KO mice in the USV test. Furthermore, we found that treatment with BAY607550 improved the performance of *Fmr1*-KO pups in the homing behavior test (Fig. 5C–E) without

altering the performance of WT pups. Our results pointed out that altered social behavior is a core phenotypic characteristic of the FXS mouse model. Accordingly, compared with WT animals, adolescent *Fmr1*-KO mice showed reduced social interaction, a phenotype that was rescued by PDE2A inhibition (Fig. 5F).

PDE2A is a Therapeutic Target for FXS

The elevated activity of PDE2A may underlie the deficits in communicative and social domains displayed by *Fmr1*-KO mice throughout development. To confirm this possibility, we chronically treated *Fmr1*-KO mice with BAY607550 from PND 5 to PND21, and tested their social abilities after a washout interval of 9 days. Strikingly, early treatment with BAY607550 reversed the social deficits displayed by *Fmr1*-KO mice at PND 30, showing that the beneficial effects of early PDE2A pharmacological blockade are long-lasting (Fig. 5G). Importantly, the administration of BAY607550 had no effect on the behavior of WT mice (Fig. 5B,D–G), further indicating the specificity of this treatment for the FXS phenotype. Finally, chronically administered BAY607550 rescued the abnormal dendritic spine length in the CA1 region of the hippocampus of *Fmr1*-KO mice (Supplementary Fig. S4). To validate PDE2A as a therapeutic target for FXS, we extended the behavioral analysis to *Fmr1*-KO infant rats. Similar to *Fmr1*-KO mice, *Fmr1*-KO rats vocalized less than WT controls when separated from their mother and siblings at PND 5 and PND 9 (Fig. 6A,B). Remarkably, acute administration of BAY607550 also normalized their altered USV pattern (Fig. 6A,B) and the ability of these infant rats to communicate, without affecting the behavior of WT control animals (Fig. 6A,B).

Discussion

Role of PDE2A in Hippocampus and Cortex Development

We have shown that an elevated amount of the PDE2A protein is present in *Fmr1*-null cortex and hippocampus (Maurin et al. 2018). Due to the heterogeneous pattern of the expression level of PDE2A in these brain regions (Stephenson et al. 2009, 2012), we measured here the PDE2A activity at the single cell level demonstrating that the activity of PDE2A is also significantly increased

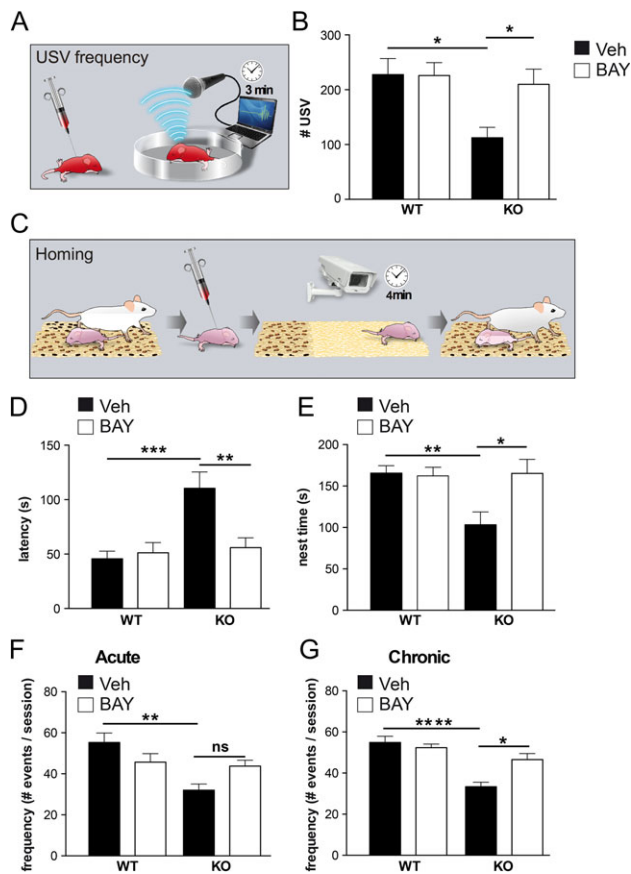


Figure 5. Inhibition of PDE2A activity rescues abnormal behaviors in infant and adolescent *Fmr1*-null mice. (A) Scheme of the USV test performed at PND 10. The 30 min after treatment with BAY607550 or vehicle, pups were separated from the dam and ultrasonic vocalizations (USV) were recorded for 3 min. (B) *Fmr1*-KO mice emit less USVs when removed from the nest at PND 10, and this communicative deficit is reversed upon BAY607550 injection ($F_{\text{genotype}(1,63)} = 7.07$, $P = 0.01$; $F_{\text{treatment}(1,63)} = 3.80$, $P = 0.05$; $F_{\text{genotype} \times \text{treatment}(1,63)} = 4.09$; $P = 0.04$); n : WT-VEH = 17; WT-BAY = 17; KO-VEH = 16; KO-BAY = 17). (C) presentation of the homing test performed at PND 14; *Fmr1*-KO mice show (D) longer latency to reach the home-cage bedding ($F_{\text{genotype}(1,45)} = 11.79$, $P = 0.001$; $F_{\text{treatment}(1,45)} = 5.86$, $P = 0.02$; $F_{\text{genotype} \times \text{treatment}(1,45)} = 8.81$; $P = 0.005$) and (E) spend less time in the nest area ($F_{\text{genotype}(1,45)} = 5.51$, $P = 0.02$; $F_{\text{treatment}(1,45)} = 5.37$, $P = 0.02$; $F_{\text{genotype} \times \text{treatment}(1,45)} = 6.63$; $P = 0.013$) in the homing behavior test at PND 14 (n : WT-VEH = 14; WT-BAY = 16; KO-VEH = 9; KO-BAY = 10); both these parameters are normalized when *Fmr1*-KO mice are treated with BAY 607 550. (F, G) Social interaction was evaluated at PND 30, results are reported for acute (F) (n : WT-VEH = 18; WT-BAY = 22; KO-VEH = 12; KO-BAY = 9) ($F_{\text{genotype}(1,57)} = 7.53$, $P = 0.008$; $F_{\text{treatment}(1,57)} = 0.05$, $P = 0.82$; $F_{\text{genotype} \times \text{treatment}(1,57)} = 5.43$; $P = 0.02$), and chronic treatment (G) (n : WT-VEH = 11; WT-BAY = 14; KO-VEH = 8; KO-BAY = 7) ($F_{\text{genotype}(1,36)} = 28.71$ $P < 0.0001$; $F_{\text{treatment}(1,36)} = 4.358$ $P = 0.0440$; $F_{\text{genotype} \times \text{treatment}(1,36)} = 9.539$ $P = 0.0039$). Data represent mean \pm SEM (adjusted P value: * $P < 0.05$, ** $P < 0.01$, *** $P < 0.001$). Two-way ANOVA was used to assess the effects of BAY607550 in *Fmr1*-KO and WT mice, using genotype (*Fmr1*-KO or WT) and treatment (BAY607550 or vehicle) as between-subjects factor, followed by Tukey multiple comparison post hoc test where appropriate.

in the absence of FMRP. Since an important fraction of PDE2A is localized at the synapse (Russwurm et al. 2009; Maurin et al. 2018), we reasoned that its elevated activity in FXS neurons could impact local cAMP and cGMP homeostasis. It has been reported that the levels of both cAMP and cGMP have critical roles in axon elongation and guidance (Shelly et al. 2010; Akiyama et al. 2016) and in regulating the morphology and growth of dendritic spines

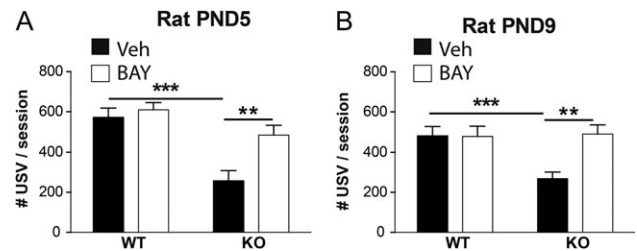


Figure 6. Inhibition of PDE2A activity rescues communication deficit in infant *Fmr1*-KO rats. *Fmr1*-KO rats emit less USVs when removed from the nest at PND 5 and 9, and this communicative deficit is reversed upon BAY607550 injection at (A) PND 5 (n : WT-Veh = 8; WT-Bay = 8; KO-Veh = 9; KO-Bay = 9) ($F_{\text{genotype}(1,32)} = 5.67$, $P = 0.023$; $F_{\text{treatment}(1,32)} = 6.76$, $P = 0.014$; $F_{\text{genotype} \times \text{treatment}(1,32)} = 7.12$; $P = 0.012$) and (B) at PND 9 (n : WT-Veh = 8; WT-Bay = 8; KO-Veh = 10; KO-Bay = 10) ($F_{\text{genotype}(1,30)} = 22.72$, $P < 0.001$; $F_{\text{treatment}(1,30)} = 8.27$, $P = 0.007$; $F_{\text{genotype} \times \text{treatment}(1,30)} = 4.28$; $P = 0.047$). Data represent the mean number of emitted USV (\pm SEM) per 3 min-recording session. (Adjusted P value ** $P < 0.01$, *** $P < 0.001$.) Two-way ANOVA was used to assess the effects of BAY607550 in *Fmr1*-KO and WT rats, using genotype (*Fmr1*-KO or WT) and treatment (BAY607550 or vehicle) as between-subjects factors, followed by Tukey multiple comparison post hoc test where appropriate.

(Dityatev and El-Husseini 2011). Indeed, *Fmr1*-KO neurons show an increased PDE2A activity as well as an increased density of spines compared with WT neurons. Blocking the excess of PDE2A activity in *Fmr1*-KO cells leads to spine maturation without decreasing the protrusion density. In WT cells, there is no effect of the BAY607550 on spine maturation but there is an increase in the density of protrusion suggesting separated roles of PDE2A activity in spine formation and maturation but not in spine elimination. This latter result is consistent with our recent findings showing that the density of spines is restored in *Fmr1*-KO olfactory neurons by depleting CYFIP1, a protein connecting FMRP with actin remodeling via Rac1 (Abekhoukh et al. 2017). Moreover, the reduced length of growing axons that we found in 2 DIV *Fmr1*-KO neurons may result from the elevated levels of PDE2A that lead, in turn, to a reduced concentration of axonal cAMP and cGMP. Indeed, the normal length of growing axons is restored after treatment with the specific PDE2A inhibitor BAY607550. Furthermore, it is known that cGMP stimulates synthesis of glutamate via phosphoglycerate kinase (PGK) (Neitz et al. 2011). Consistent with a reduction of cGMP, glutamate levels are reduced in the *Fmr1*-KO cortex (Davidovic et al. 2011) and hippocampus (Hebert et al. 2014). PDE2A is the only PDE identified so far at the presynaptic active zone, associated with docked vesicles and illustrating the importance of such a compartmentalized action (Maurin et al. 2018). Indeed, cAMP abundance coupled to PKA signaling is critical to modulate assembly/disassembly/priming/recycling of neurotransmitter vesicles and, consequently, for synaptic transmission and plasticity events (Crawford and Mennerick 2012) and basal synaptic transmission (Gomez and Breitenbucher 2013). Here we show that the pharmacological inhibition of PDE2A activity rescues the exaggerated mGluR-dependent LTD in *Fmr1*-KO hippocampal slices, a well-characterized hallmark of *Fmr1*-KO brain (Huber et al. 2002).

As we already explained, cGMP and cAMP are involved in axonal growth, spine maturation and synaptic plasticity. Since PDE2A modulates the level of both cAMP and cGMP, we can suggest that its elevated activity in the absence of FMRP contributes to the definition of a neuronal FXS phenotype characterized by altered dendritic morphology, altered axonal length and exaggerated mGluR-LTD.

PDE2A has a Crucial and Evolutionarily Conserved Role in the Physiopathology of FXS

We show here that *Fmr1*-KO pups have profound deficits in both social communication and social discrimination from the first days of life, as revealed by their altered USV profile and impaired homing behavior, respectively. This, in turn, may alter the proper development of social behavior and social recognition (Terry and Johanson 1996; Melo et al. 2006). In line with this hypothesis, *Fmr1*-KO mice show deficits in social interaction at the adolescent age (Liu and Smith 2009; Dahlhaus and El-Husseini 2010; Kazdoba et al. 2014) that mirror the phenotype observed in FXS patients. Considering the impact of the pharmacological inhibition of PDE2A on the in vitro and ex vivo FXS phenotypes, we assessed whether the PDE2A inhibitor BAY607550 could revert the altered phenotype displayed by *Fmr1*-KO animals in social communication, social discrimination, and social interaction. Administration of BAY607550 normalizes the USV profile displayed by *Fmr1*-KO mice and rats. In addition, this treatment rescues the altered performance of *Fmr1*-KO pups in the homing behavior test, and increases the frequency of social interactions observed in *Fmr1*-KO mice to similar levels as WT animals. While PDE2A was previously linked to cognitive processes (Gomez and Breitenbucher 2013; Redrobe et al. 2014; Lueptow et al. 2016), here, for the first time, we associate its increased activity with altered social deficits. It is interesting to notice that PDE2A is coexpressed with FMRP in a specific class of neurons in the olfactory bulb (Korsak et al. 2017). These neurons have been shown to play a role in thermosensing and detecting stress in congeners as well as in pheromone sensing behavior (Juilfs et al. 1997). This can lead to the speculation that modulating PDE2A activity in these neurons may influence the social behavior. In conclusion, PDE2A may be an attractive target to simultaneously treat the social and communicative dysfunctions characterizing FXS patients. Importantly, mice chronically treated with BAY607550 during the early postnatal development period clearly benefit of the positive effect of this therapy when tested at adolescence. This result strongly suggests that inhibition of PDE2A during infancy has long-term positive effects and provides a strong preclinical rationale for a new therapeutic strategy for FXS patients. Remarkably, we used very low doses of BAY607550 that do not affect the behavior of WT animals. This is important not only because our approach targets a pediatric population but also because low doses should reduce possible toxic side effects of the drug. Interestingly, several trials have been performed in the past with various formulations and dosages of PF-05180999 to treat migraine. We note that the trial in which the highest dosage (360 mg) was tested was discontinued for safety issues, nevertheless former trials using lower doses (30 or 120 mg) were completed but results are yet to be published (<https://clinicaltrials.gov>; #NCT01429740 and #NCT01981499). These studies are however encouraging for future therapeutic intervention for central nervous system (CNS) disorders. Indeed, a phase 1 study has been conducted to investigate the pharmacological properties of TAK915 (another PDE2A inhibitor from Takeda pharmaceuticals (Nakashima et al. 2018)) in order to guide dosage in future clinical studies in schizophrenia (<https://clinicaltrials.gov/ct2/show/results/NCT02584569>). We would suggest that TAK915 may also be used to investigate other CNS disorders in the future.

Our data clearly highlight that PDE2A abundance has a pivotal role in the physiopathology of FXS (Maurin et al. 2018). While cGMP metabolism had never been studied in FXS, it has

already been proposed that the convergence of altered pathways in FXS neurons is responsible for an altered abundance of cAMP in this syndrome. All these pathways are mostly postsynaptic signaling cascades and their relevance for FXS up to date was only studied in adult *Fmr1*-KO mice (Choi et al. 2016; Sethna et al. 2017). Inhibition of *Pde4D* was recently shown to have positive effects on LTD, learning and memory in adult *Fmr1*-KO mice (Gurney et al. 2017). These results provide evidence for the crucial role of cAMP abundance in synaptic plasticity in *Fmr1*-KO mice. However, the PDE4 enzyme family modulates cAMP but not cGMP levels and does not appear to be directly involved in the pathophysiology of FXS since its expression is not deregulated in the synaptosomal preparations obtained from both young and adult *Fmr1*-KO mice (Tang et al. 2015). Furthermore, *Pde4D* mRNA is not a prominent FMRP target in all the CLIP assays that have been performed so far (Darnell et al. 2011; Ascano et al. 2012; Tabet et al. 2016; Maurin et al. 2018).

Also, up to now, most of the treatments proposed for FXS have been tested in adult mice and, even when successful, their translation to the clinic failed (Budimirovic et al. 2017; Castagnola et al. 2017; Erickson et al. 2017). Considering these unsuccessful results, an increasing amount of data suggests the need to treat patients affected by neurodevelopmental disorders at the earliest possible age (Khalfallah et al. 2017 for review, and this study) and for a long period of time (Erickson et al. 2017). Remarkably, BAY607550 treatment rescues the communication deficits in both *Fmr1*-KO mice and rats. This strongly argues in favor of a conserved contribution of PDE2A activity in the regulation of processes and/or communication circuits underpinning social behaviors. In the same direction, our findings showing the rescue of social interaction after 9 days of washout suggest that the chronic treatment performed in infancy of these mice was sufficient to modify circuits for an extended time-period. Even if these processes should be investigated in depth in the near future, overall these findings further reinforce the translation potential of this targeted therapeutic approach for FXS.

Conclusions

PDE2A is an overlooked phosphodiesterase previously linked to cognitive processes (Boess et al. 2004; Redrobe et al. 2014; Mikami et al. 2017; Nakashima et al. 2018). Here, for the first time, we establish a relationship between its altered expression and defects in axonal growth, maturation of dendritic spines, mGluR-dependent hippocampal LTD and altered social communication, social discrimination and social interaction behaviors at early developmental ages in *Fmr1*-KO animals. FXS is the leading inherited cause of ID and ASD and the *Fmr1*-KO mouse and rat models are not only widely recognized animal models of FXS but also genetic models of ASD. Since we highlight here that PDE2A abundance has a pivotal role in the pathophysiology of FXS, an implication of PDE2A in other forms of autism can be hypothesized and therefore, targeting PDE2A could be considered a generalized pharmacological target to treat social deficits common to both ASD and FXS.

Supplementary Material

Supplementary material is available at *Cerebral Cortex* online.

Funding

Institut National de la Santé et de la Recherche Médicale (INSERM); Centre National de la Recherche Scientifique (CNRS); Université Côte d'Azur (UCA); Agence Nationale de la Recherche: ANR-12-BSV4-0020 to B.B. and ANR-15-CE16-0015 to B.B. and S.M. Fondation Recherche Médicale (FRM) DEQ20140329490 to BB and FRM-ING20140129004 to B.B. and T.M.; Fondation Jérôme Lejeune to B.B. and S.M. FRAXA Foundation to T.M. PV was supported (in part) by the Investissements d'Avenir program managed by the ANR under reference ANR-11-IDEX-0004-02 (LabEx Bio-Psy). VT was in part supported by Grant to Department of Science, Roma Tre University (MIUR-Italy Dipartimenti di eccellenza, ARTICOLO 1, COMMI 314-337 LEGGE 232/2016). S.C. and M.D. are recipient of international PhD fellowships "LabEx Signallife Program" by ANR-11-LABX-0028-01 (to B.B. and SM.).

Author's Contribution

Li.C. and E.M. performed biosensor cAMP experiments under the guidance of P.V. T.M. performed cAMP and cGMP measures in cultured neurons as described in M&M. La.C. and L.S. performed LTD studies under the supervision of Lu.C. S.C. and M.D. performed cortical neuronal cultures under the guidance of T.M. and B.B. S.C. and M.J. performed RT-qPCR studies under the guidance of B.B. A.K. and G.P. performed dendritic spines analysis under the guidance of S.M. M.J. performed axonal studies under the guidance of T.M. and B.B. M.J., S.D., F.M., M.S., and S.S. performed behavioral studies under the supervision of V.T. M.J., S.D., and T.M. performed Golgi staining under the supervision of B.B. A.D.G. synthesized Lu AF64280 under the guidance of S.A. T.M. and B.B. designed the study, T.M., V.T., L.C., P.V., S.M., and B.B. analyzed the data and wrote the article.

Notes

The authors are indebted with E. Lalli and M. Capovilla for critical reading of the article, M. Grossi, M. Beal and C. Gandin for technical help, F. Aguila for graphical artwork and I. Caillé for discussion and gift of some materials. *Conflict of interest:* The authors declare no competing financial interests.

References

Abekhouk S, Sahin HB, Grossi M, Zongaro S, Maurin T, Madrigal I, Kazue-Sugioka D, Raas-Rothschild A, Doulazmi M, Carrera P, et al. 2017. New insights into the regulatory function of CYFIP1 in the context of WAVE- and FMRP-containing complexes. *Dis Model Mech.* 10:463–474.

Akiyama H, Fukuda T, Tojima T, Nikolaev VO, Kamiguchi H. 2016. Cyclic nucleotide control of microtubule dynamics for axon guidance. *J Neurosci.* 36:5636–5649.

Antar LN, Dichtenberg JB, Plociniak M, Afroz R, Bassell GJ. 2005. Localization of FMRP-associated mRNA granules and requirement of microtubules for activity-dependent trafficking in hippocampal neurons. *Genes Brain Behav.* 4:350–359.

Antar LN, Li C, Zhang H, Carroll RC, Bassell GJ. 2006. Local functions for FMRP in axon growth cone motility and activity-dependent regulation of filopodia and spine synapses. *Mol Cell Neurosci.* 32:37–48.

Ascano M Jr., Mukherjee N, Bandaru P, Miller JB, Nusbaum JD, Corcoran DL, Langlois C, Munschauer M, Dewell S, Hafner M, et al. 2012. FMRP targets distinct mRNA sequence elements to regulate protein expression. *Nature.* 492:382–386.

Averaimo S, Nicol X. 2014. Intermingled cAMP, cGMP and calcium spatiotemporal dynamics in developing neuronal circuits. *Front Cell Neurosci.* 8:376.

Bassell GJ, Warren ST. 2008. Fragile X syndrome: loss of local mRNA regulation alters synaptic development and function. *Neuron.* 60:201–214.

Boess FG, Hendrix M, van der Staay FJ, Erb C, Schreiber R, van Staveren W, de Vente J, Prickaerts J, Blokland A, Koenig G. 2004. Inhibition of phosphodiesterase 2 increases neuronal cGMP, synaptic plasticity and memory performance. *Neuropharmacology.* 47:1081–1092.

Budimirovic DB, Berry-Kravis E, Erickson CA, Hall SS, Hessler D, Reiss AL, King MK, Abbeduto L, Kaufmann WE. 2017. Updated report on tools to measure outcomes of clinical trials in fragile X syndrome. *J Neurodev Dis.* 9:14.

Castagnola S, Bardoni B, Maurin T. 2017. The search for an effective therapy to treat fragile X syndrome: dream or reality? *Front Syn Neurosci.* 9:15.

Choi CH, Schoenfeld BP, Bell AJ, Hinchey J, Rosenfelt C, Gertner MJ, Campbell SR, Emerson D, Hinchey P, Kollaros M, et al. 2016. Multiple drug treatments that increase cAMP signaling restore long-term memory and aberrant signaling in fragile X syndrome models. *Front Behav Neurosci.* 10:136.

Comery TA, Harris JB, Willems PJ, Oostra BA, Irwin SA, Weiler JJ, Greenough WT. 1997. Abnormal dendritic spines in fragile X knockout mice: maturation and pruning deficits. *Proc Natl Acad Sci USA.* 94:5401–5404.

Costa L, Spatuzza M, D'Antoni S, Bonaccorso CM, Trovato C, Musumeci SA, Leopoldo M, Lacivita E, Catania MV, Ciranna L. 2012. Activation of 5-HT7 serotonin receptors reverses metabotropic glutamate receptor-mediated synaptic plasticity in wild-type and Fmr1 knockout mice, a model of Fragile X syndrome. *Biol Psychiatry.* 72:924–933.

Crawford DC, Mennerick S. 2012. Presynaptically silent synapses: dormancy and awakening of presynaptic vesicle release. *Neuroscientist.* 18:216–223.

Dahlhaus R, El-Husseini A. 2010. Altered neuroligin expression is involved in social deficits in a mouse model of the fragile X syndrome. *Behav Brain Res.* 208:96–105.

Darnell JC, Van Driesche SJ, Zhang C, Hung KY, Mele A, Fraser CE, Stone EF, Chen C, Fak JJ, Chi SW, et al. 2011. FMRP stalls ribosomal translocation on mRNAs linked to synaptic function and autism. *Cell.* 146:247–261.

Davidovic L, Navratil V, Bonaccorso CM, Catania MV, Bardoni B, Dumas ME. 2011. A metabolomic and systems biology perspective on the brain of the fragile X syndrome mouse model. *Genome Res.* 21:2190–2202.

Devader C, Khayachi A, Veyssière J, Moha Ou Maati H, Roulot M, Moreno S, Borsotto M, Martin S, Heurteaux C, Mazella J. 2015. In vitro and in vivo regulation of synaptogenesis by the novel antidepressant spadin. *Br J Pharmacol.* 172:2604–2617.

Ding L, Zhang C, Masood A, Li J, Sun J, Nadeem A, Zhang HT, O'Donnell JM, Xu Y. 2014. Protective effects of phosphodiesterase 2 inhibitor on depression- and anxiety-like behaviors: involvement of antioxidant and anti-apoptotic mechanisms. *Behav Brain Res.* 268:150–158.

Dityatev A, El-Husseini A. 2011. *Molecular mechanisms of synaptogenesis.* New York; London: Springer.

Erickson CA, Davenport MH, Schaefer TL, Wink LK, Pedapati EV, Sweeney JA, Fitzpatrick SE, Brown WT, Budimirovic D, Hagerman RJ, et al. 2017. Fragile X targeted pharmacotherapy: lessons learned and future directions. *J Neurodev Disord.* 9:7.

- Gomez L, Breitenbucher JG. 2013. PDE2 inhibition: potential for the treatment of cognitive disorders. *Bioorg Med Chem Lett*. 23:6522–6527.
- Gothelf D, Furfaro JA, Hoeft F, Hoeft F, Eckert MA, Hall SS, O'Hara R, Erba HW, Ringel J, Hayashi KM, et al. 2008. Neuroanatomy of Fragile X syndrome is associated with aberrant behavior and the FragileX mental retardation protein (FMRP). *Ann Neurol*. 63:40–51.
- Gurney ME, Cogram P, Deacon RM, Rex C, Tranfaglia M. 2017. Multiple behavior phenotypes of the fragile-X syndrome mouse model respond to chronic inhibition of phosphodiesterase-4D (PDE4D). *Sci Rep*. 7:14653.
- Hebert B, Pietropaolo S, Meme S, Laudier B, Laugeray A, Doisne N, Quartier A, Lefeuvre S, Got L, Cahard D, et al. 2014. Rescue of fragile X syndrome phenotypes in Fmr1 KO mice by a BKCa channel opener molecule. *Orphanet J Rare Dis*. 9:124.
- Hoeft F, Carter JC, Lightbody AA, Cody Hazlett H, Piven J, Reiss AL. 2010. Region-specific alterations in brain development in one- to three-year-old boys with fragile X syndrome. *Proc Natl Acad Sci USA*. 107:9335–9339.
- Huber KM, Gallagher SM, Warren ST, Bear MF. 2002. Altered synaptic plasticity in a mouse model of fragile X mental retardation. *Proc Natl Acad Sci USA*. 99:7746–7750.
- Irwin SA, Galvez R, Greenough WT. 2000. Dendritic spine structural anomalies in fragile-X mental retardation syndrome. *Cereb Cortex*. 10:1038–1044.
- Jamain S, Radyushkin K, Hammerschmidt K, Granon S, Boretius S, Varoqueaux F, Ramanantsoa N, Gallego J, Ronnenberg A, Winter D, et al. 2008. Reduced social interaction and ultrasonic communication in a mouse model of monogenic heritable autism. *Proc Natl Acad Sci USA*. 105:1710–1715.
- Juilfs DM, Fülle HJ, Zhao AZ, Houslay MD, Garbers DL, Beavo JA. 1997. A subset of olfactory neurons that selectively express cGMP-stimulated phosphodiesterase (PDE2) and guanylyl cyclase-D define a unique olfactory signal transduction pathway. *Proc Natl Acad Sci USA*. 94:3388–3395.
- Kazdoba TM, Leach PT, Silverman JL, Crawley JN. 2014. Modeling fragile X syndrome in the Fmr1 knockout mouse. *Intractable Rare Dis Res*. 3:118–133.
- Khalfallah O, Jarjat M, Davidovic L, Nottet N, Cestele S, Mangegazza M, Bardoni B. 2017. Depletion of the fragile X mental retardation protein in embryonic stem cells alters the kinetics of neurogenesis. *Stem Cells*. 35:374–385.
- Khayachi A, Gwizdek C, Poupon G, Alcor D, Chafai M, Cassé F, Maurin T, Prieto M, Folci A, De Graeve F, et al. 2018. Sumoylation regulates FMRP-mediated dendritic spine elimination and maturation. *Nat Commun*. 9:757.
- Kilkenny C, Browne WJ, Cuthill IC, Emerson M, Altman DG. 2010. Improving bioscience research reporting: the ARRIVE guidelines for reporting animal research. *PLoS Biol*. 8:e1000412.
- Korsak LIT, Shepard KA, Akins MR. 2017. Cell type-dependent axonal localization of translational regulators and mRNA in mouse peripheral olfactory neurons. *J Comp Neurol*. 525:2201–2215.
- Lai JK, Lerch JP, Doering LC, Foster JA, Ellegood J. 2016. Regional brain volumes changes in adult male FMR1-KO mouse on the FVB strain. *Neurosci*. 318:12–21.
- Liu ZH, Smith CB. 2009. Dissociation of social and nonsocial anxiety in a mouse model of fragile X syndrome. *Neurosci Lett*. 454:62–66.
- Lueptow LM, Zhan CG, O'Donnell JM. 2016. Cyclic GMP-mediated memory enhancement in the object recognition test by inhibitors of phosphodiesterase-2 in mice. *Psychopharmacology (Berl)*. 233:447–456.
- Masood A, Huang Y, Hajjhussein H, Xiao L, Li H, Sun J, Nadeem A, Zhang HT, O'Donnell JM, Xu Y. 2009. Anxiolytic effects of phosphodiesterase-2 inhibitors associated with increased cGMP signaling. *J Pharmacol Exp Ther*. 331:690–699.
- Masood A, Nadeem A, Mustafa SJ, O'Donnell JM. 2008. Reversal of oxidative stress-induced anxiety by inhibition of phosphodiesterase-2 in mice. *J Pharmacol Exp Ther*. 326:369–379.
- Maurice DH, Ke H, Ahmad F, Wang Y, Chung J, Manganiello VC. 2014. Advances in targeting cyclic nucleotide phosphodiesterases. *Nat Rev Drug Discov*. 13:290–314.
- Maurin T, Lebrigand L, Castagnola S, Paquet A, Jarjat M, Grossi M, Popa A, Rage F, Bardoni B. 2018. HITS-CLIP in various brain areas reveals new targets and new modalities of RNA binding by fragile X mental retardation protein. *Nucleic Acids Res*. 46:6344–6355.
- Maurin T, Zongaro S, Bardoni B. 2014. Fragile X syndrome: from molecular pathology to therapy. *Neurosci Biobehav Rev*. 2:242–255.
- Melo AI, Lovic V, Gonzalez A, Madden M, Sinopoli K, Fleming AS. 2006. Maternal and littermate deprivation disrupts maternal behavior and social-learning of food preference in adulthood: tactile stimulation, nest odor, and social rearing prevent these effects. *Dev Psychobiol*. 48:209–219.
- Mientjes EJ, Nieuwenhuizen I, Kirkpatrick L, Zu T, Hoogeveen-Westerveld M, Severijnen L, Rifé M, Willemsen R, Nelson DL, Oostra BA. 2006. The generation of a conditional Fmr1 knockout mouse model to study Fmrp function in vivo. *Neurobiol Dis*. 21:549–555.
- Mikami S, Sasaki S, Asano Y, Ujikawa O, Fukumoto S, Nakashima K, Oki H, Kamiguchi N, Imada H, Iwashita H, et al. 2017. Discovery of an orally bioavailable, brain-penetrating, in vivo active phosphodiesterase 2A inhibitor lead series for the treatment of cognitive disorders. *J Med Chem*. 60:7658–7676.
- Morales J, Hiesinger PR, Schroeder AJ, Kume K, Verstreken P, Jackson FR, Nelson DL, Hassan BA. 2002. Drosophila fragile X protein, DFXR, regulates neuronal morphology and function in the brain. *Neuron*. 34:961–972.
- Nakashima M, Imada H, Shiraishi E, Ito Y, Suzuki N, Miyamoto M, Taniguchi T, Iwashita H. 2018. Phosphodiesterase 2A inhibitor TAK-915 ameliorates cognitive impairments and social withdrawal in N-methyl-D-aspartate receptor antagonist-induced rat models of schizophrenia. *J Pharmacol Exp Ther*. 365:179–188.
- Neitz A, Mergia E, Eysel UT, Koesling D, Mittmann T. 2011. Presynaptic nitric oxide/cGMP facilitates glutamate release via hyperpolarization-activated cyclic nucleotide-gated channels in the hippocampus. *Eur J Neurosci*. 33:1611–1621.
- Nimchinsky EA, Oberlander AM, Svoboda K. 2001. Abnormal development of dendritic spines in FMR1 knock-out mice. *J Neurosci*. 21:5139–5146.
- Park AJ, Havekes R, Choi JH, Luczak V, Nie T, Huang T, Abel T. 2014. A presynaptic role for PKA in synaptic tagging and memory. *Neurobiol Learn Mem*. 114:101–112.
- Polito M, Klarenbeek J, Jalink K, Paupardin-Tritsch D, Vincent P, Castro LR. 2013. The NO/cGMP pathway inhibits transient cAMP signals through the activation of PDE2 in striatal neurons. *Front Cell Neurosci*. 7:211.
- Redrobe JP, Jorgensen M, Christoffersen CT, Montezinho LP, Bastlund JF, Carnerup M, Bundgaard C, Lerdrup L, Plath N. 2014. In vitro and in vivo characterisation of Lu AF64280, a novel, brain penetrant phosphodiesterase (PDE) 2A inhibitor: potential relevance to cognitive deficits in schizophrenia. *Psychopharmacology (Berl)*. 231:3151–3167.

- Rodriguez A, Ehlenberger DB, Dickstein DL, Hof PR, Wearne SL. 2008. Automated three-dimensional detection and shape classification of dendritic spines from fluorescence microscopy images. *PLoS One*. 3:e1997.
- Russwurm C, Zoidl G, Koesling D, Russwurm M. 2009. Dual acylation of PDE2A splice variant 3: targeting to synaptic membranes. *J Biol Chem*. 284:25782–25790.
- Servadio M, Melancia F, Manduca A, di Masi A, Schiavi S, Cartocci V, Pallottini V, Campolongo P, Ascenzi P, Trezza V. 2016. Targeting anandamide metabolism rescues core and associated autistic-like symptoms in rats prenatally exposed to valproic acid. *Transl Psychiatry*. 6:e902.
- Sethna F, Feng W, Ding Q, Robison AJ, Feng Y, Wang H. 2017. Enhanced expression of ADCY1 underlies aberrant neuronal signalling and behaviour in a syndromic autism model. *Nat Commun*. 8:14359.
- Shelly M, Lim BK, Cancedda L, Heilshorn SC, Gao H, Poo MM. 2010. Local and long-range reciprocal regulation of cAMP and cGMP in axon/dendrite formation. *Science*. 327:547–552.
- Shen K, Cowan CW. 2010. Guidance molecules in synapse formation and plasticity. *Cold Spring Harb Perspect Biol*. 2:a001842.
- Stephenson DT, Coskran TM, Kelly MP, Kleiman RJ, Morton D, O'Neill SM, Schmidt CJ, Weinberg RJ, Menniti FS. 2012. The distribution of phosphodiesterase 2A in the rat brain. *Neurosci*. 226:145–155.
- Stephenson DT, Coskran TM, Wilhelms MB, Adamowicz WO, O'Donnell MM, Muravnick KB, Menniti FS, Kleiman RJ, Morton D. 2009. Immunohistochemical localization of phosphodiesterase 2A in multiple mammalian species. *J Histochem Cytochem*. 57:933–949.
- Tabet R, Moutin E, Becker JA, Heintz D, Fouillen L, Flatter E, Krężel W, Alunni V, Koebel P, Dembélé D, et al. 2016. Fragile X mental retardation protein (FMRP) controls diacylglycerol kinase activity in neurons. *Proc Natl Acad Sci USA*. 113:E3619–E3628.
- Tang B, Wang T, Wan H, Han L, Qin X, Zhang Y, Wang J, Yu C, Berton F, Francesconi W, et al. 2015. *Fmr1* deficiency promotes age-dependent alterations in the cortical synaptic proteome. *Proc Natl Acad Sci USA*. 112:E4697–E4706.
- Terranova ML, Laviola G. 2005. Scoring of social interactions and play in mice during adolescence. *Curr Protoc Toxicol*. Chapter. 13: 13.10.1–13.10.11.
- Terry LM, Johanson IB. 1996. Effects of altered olfactory experiences on the development of infant rats' responses to odors. *Dev Psychobiol*. 29:353–377.
- Wang L, Xiaokaiti Y, Wang G, Xu X, Chen L, Huang X, Liu L, Pan J, Hu S, Chen Z, et al. 2017. Inhibition of PDE2 reverses beta amyloid induced memory impairment through regulation of PKA/PKG-dependent neuro-inflammatory and apoptotic pathways. *Sci Rep*. 7:12044.

Article 4: PDE10A - Fragile X syndrome - striatum

Reduced striatal PDE10A activity in a mouse model of Fragile X syndrome.

Mota É, Stoufflet J, Castro LRV, Vincent P.

in preparation.

Considering the hyperactivity phenotype of *Fmr1*-KO mice, we decided to evaluate the activity of PDEs in the striatum of these mice.

Our observations:

- Unaltered PDE2A activity in the striatum, compared to WT mice. Normal cGMP levels; Normal regulation of forskolin-induced cAMP signal by PDE2A in both D1 and D2 MSNs.
- No change in the amplitude of the cAMP response to transient dopamine signals.
- Profound alterations in the amplitude of the cAMP response to transient dopamine signals when PDE2A and PDE4 are inhibited, suggesting a reduced of other striatal PDE, possibly PDE10A.

Reduced striatal PDE10A activity in a mouse model of Fragile X syndrome

Authors

Élia Mota, Julie Stoufflet, Yohan Legueux-Cajgfinger, Manon Dobrigna, Ilyes Nedjar, Liliana R.V. Castro and Pierre Vincent.

Author affiliation

Sorbonne Université, CNRS, Biological Adaptation and Ageing, F-75005 Paris, France.

Corresponding Author

Pierre Vincent: pierre.vincent@upmc.fr; mailbox #256; UMR8256; 7 quai Saint-Bernard; 75005 Paris, France

ORCID numbers

Élia Mota: 0000-0003-4393-5781

Liliana Castro: 0000-0001-8902-089X

Pierre Vincent: 0000-0002-8479-1908

Keywords

Dopamine, striatum, cAMP/PKA signaling pathway, phosphodiesterases, fragile X mental retardation protein

Introduction

The Fragile X syndrome, a leading cause of autism, results from the lack of "fragile X mental retardation protein" (*Fmrp*). The *Fmrp* protein binds to a variety of mRNA, regulating their translation and vectoring mRNA to specific subcellular domains. For example, it is a translational modulator of synaptic proteins and a regulator of mRNA transport at the synapse. Using tagged *Fmrp* as bait, the team of Barbara Bardoni (CNRS, Nice) fished a series of mRNA in the cortex and striatum which included PDE2A mRNA {Maurin et al., 2018, Nucleic Acids Res, 46, 6344-6355}. *Fmrp* negatively regulates the translation of PDE2A mRNA, such that PDE2A protein is expressed to a higher level in hippocampus and cortex of *Fmr1*-null mice. Biochemical data and biosensor imaging (including our experiments) showed that PDE2A activity was more efficient in the hippocampus of *Fmr1*-null and PDE2A inhibition in newborn period rescued altered social behaviour in adolescent *Fmr1*-null animals {Maurin et al., 2018, Cereb Cortex, In press.}.

As a follow-up of this project, we wanted to see whether the lack of *Fmrp* might also affect functional PDE activity pattern in the striatum. First, we did not observe in the striatum the alterations in PDE2A action that were measured in the hippocampus. No major changes in the cAMP responses to transient dopamine. However, when PDE2A and PDE4 were inhibited, we observed profound defects in the regulation of basal cAMP, as well as much larger and longer lasting cAMP responses to the transient stimulation of D1 dopamine receptors. This suggests that *Fmr1*-null mice exhibit a reduced PDE10A activity which is compensated by other PDEs, mainly PDE2 and PDE4. D2 MSNs displayed more complex alterations which remain to be analyzed.

These results are presented here in a preliminary form.

Results

Normal cGMP response and PDE2A function in MSNs of Fmr1-null mice.

PDE2A degrades both cAMP and cGMP, and to test its action on cGMP, we used the cGMP sensor cygNAL {Betolngar et al., 2019, Cereb Cortex}. First, the nitric oxide (NO) donor, DEANO (10 μ M) was used to increase cGMP levels in MSNs (Figure 1). The PDE2 inhibitor BAY607550 was applied at time 0, to reveal the functional contribution of PDE2A action on the regulation of steady-state cGMP. The maximal ratio change was measured at the end of the experiment by applying the non selective PDE2 inhibitor IBMX (200 μ M). DEANO increased the emission ratio of the sensor to approximately half the maximal response; the addition of the PDE2 inhibitor further increase cGMP level to approximately $\frac{3}{4}$ of the maximum, confirming that PDE2 regulates NO/cGMP signaling in MSNs. The same protocol was tested in *Fmr1*-null mice and no difference was observed in amplitude of the cGMP response to DEANO alone or in the presence of BAY607550.

These results indicate that cGMP response to NO and its regulation by PDE2A in MSNs is not altered in the striatum of *Fmr1*-null mice.

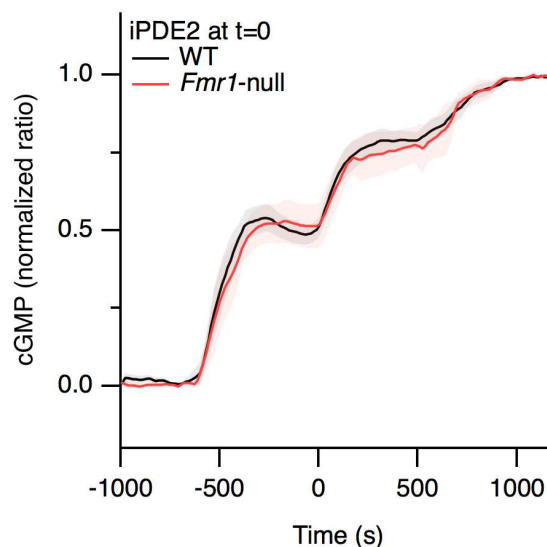


Figure 1 - PDE2A regulates cGMP response in MSNs in both *Fmr1*-null and WT mice. cGMP levels in MSNs were measured with the cGMP biosensor cygNAL and the responses were normalised to the maximal ratio obtained with DEANO (10 μ M) and the non selective inhibitor IBMX (200 μ M). The PDE2A inhibitor, BAY607550 (200 nM) was applied at t=0. No differences in the amplitude of the responses to DEANO and DEANO+BAY607550 were observed between WT (N=7, n=49) and *Fmr1*-null (N=5, n=41) mice. Trace shading indicates SEM calculated per experiment.

Normal regulation of forskolin-induced cAMP signal by PDE2A in both D1 and D2 MSNs of Fmr1-null mice.

Previous studies have shown that PDE2 activity is increased in the presence of cGMP {Polito et al., 2013, Front Cell Neurosci, 7, 211}. Here we wanted to compare the functional contribution of PDE2A in the regulation of steady-state cAMP level between WT and *Fmr1*-null in the striatum (Figure 2). Therefore, we acutely increased PDE2A activity by applying the cGMP-elevating agent DEANO (10 μ M), while measuring cAMP level with the Epac-S^{H150} sensor {Polito et al., 2013, Front Cell Neurosci, 7, 211; Yapo et al., 2017, J Physiol, 595, 7451-7475}. For unknown reasons, forskolin increases cAMP more efficiently in D2 MSNs than in D1 MSNs, and to obtain a steady-state cAMP level in a suitable concentration range for optimal measurement with Epac-SH150, we used 200 nM fsk for D1 MSNs and 63 nM for D2 MSNs. This protocol increased the emission ratio to ??? and ??? in D1 and D2 MSNs respectively, corresponding to an approximative cAMP concentration of 4 μ M. On this steady-state level, activation of PDE2A by DEANO (at t=0 seconds) led to a decrease in the emission ratio to half of the steady-state level, ie ??? and ??? in D1 and D2 MSNs, respectively, corresponding to approximately ?? μ M cAMP. The effect of the DEANO was reversible after its wash out.

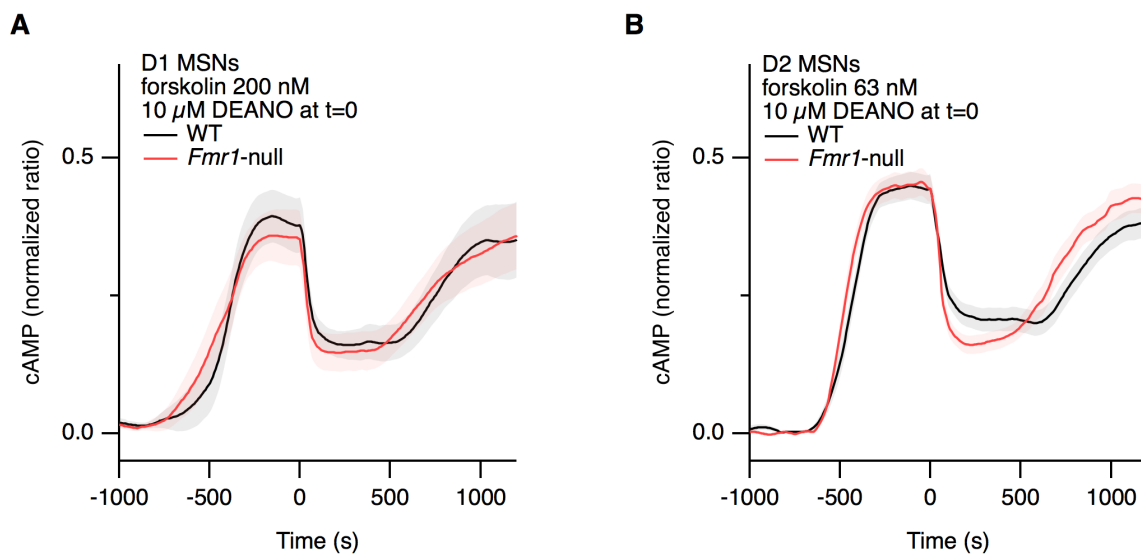


Figure 2 - PDE2A activation down-regulates cAMP levels induced by forskolin in both D1 and D2 MSNs in *Fmr1*-null and WT mice. cAMP responses to forskolin (200 nM in D1 MSNs, A; 63 nM in D2 MSNs, B) were measured with the cAMP biosensor Epac-SH150. Application of the NO donor DEANO (10 μ M) at t=0 seconds decreased cAMP level in both D1 (A) and D2 MSNs (B). No difference was observed between WT (D1: N=10, n=64; D2: N=8, n=38) and *Fmr1*-null (D1: N=10, n=49; D2: N=5, n=23). Trace shading indicates SEM calculated per experiment.

Lack of alteration in the transient response to dopamine in D1 MSNs

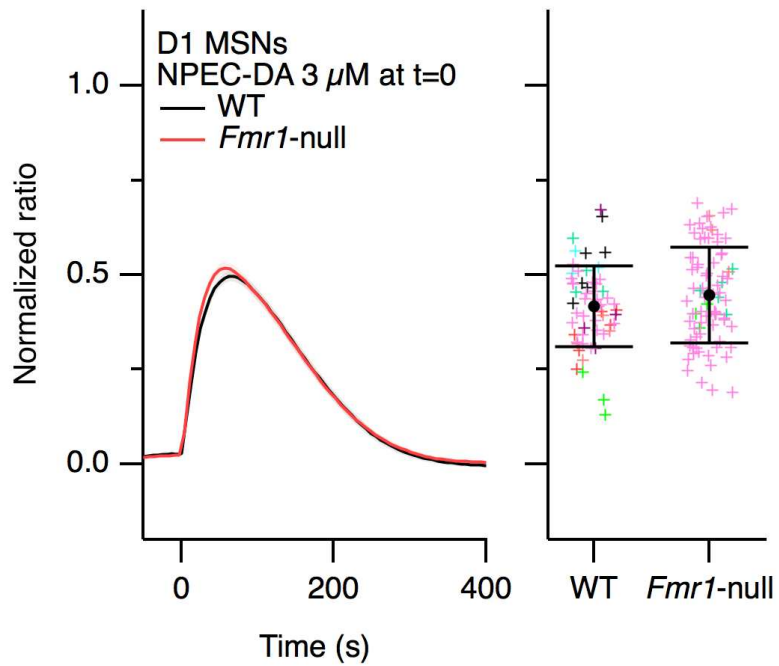


Figure 3 - The suppression of *Fmr1* gene doesn't change the amplitude of the cAMP response to transient dopamine in the striatum. cAMP imaging with Epac-SH150. NPEC-DA (3 μ M) uncaging. WT: N=13, n=57; *Fmr1*-null: N=18, n=80. Data points obtained from the same experiment are plotted with the same color.

Fmr1-null show profound alterations when PDE2A and PDE4 are inhibited

We then tested whether the relative contribution of the different phosphodiesterases in the regulation of the cAMP response to dopamine might be different in the *Fmr1*-null condition (Figure 3). To this end, a first dopamine uncaging was performed, to record a reference response to dopamine, and again, these responses were not significantly different between WT and *Fmr1*-null. Then, PDE2A and PDE4 were both inhibited using BAY607550 and rolipram. While bath application of this combination of inhibitors had little or no effect in WT mice, it induced a clear increase in baseline ratio in *Fmr1*-null mice. When uncaging dopamine in the presence of BAY and rolipram, the response was increased in WT mice, as already described, but this increase was much larger in *Fmr1*-null. Moreover, the response to dopamine displayed a prolonged elevated cAMP level, indicating a plateau of very high cAMP level for several minutes.

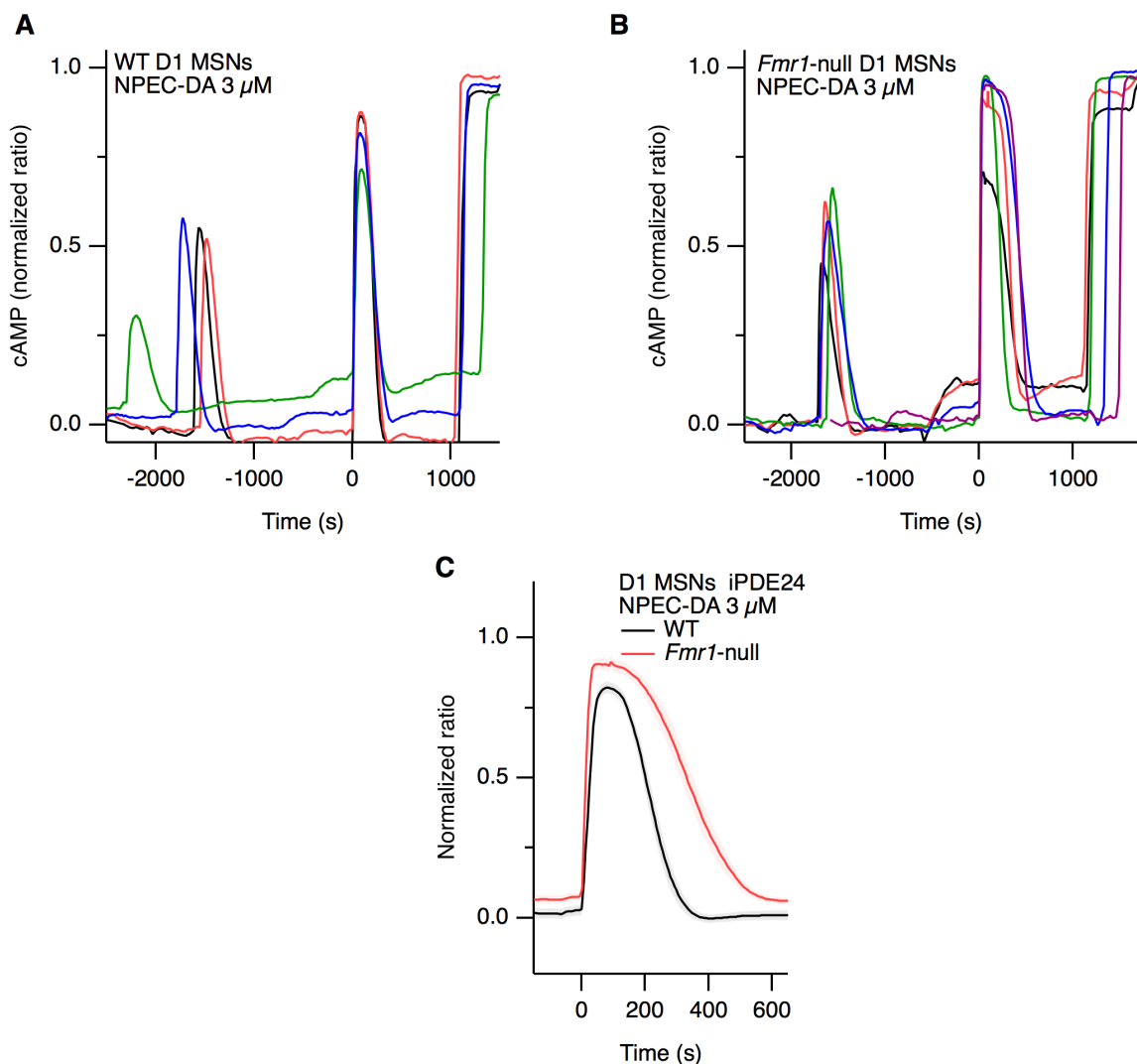


Figure 4 - Inhibition of PDE2A and PDE4 leave insufficient cAMP control in *Fmr1*-null MSNs. Brain slices from wild type (A) and *Fmr1*-null (B) neonate mice were imaged with the cAMP biosensor Epac-SH150. NPEC-DA (3 μM) was uncaged twice in each experiment: the first time to produce a control response, the second time in the presence of BAY607550 (200 nM) and rolipram (100 nM). Experiments are synchronized at the time of the 2d uncaging, indicated by time 0. C: Overlay of the 2d response (in the presence of rolipram and BAY). Shading indicates SEM calculated per experiment.

Discussion

These experiments show reveal several important points.

1/ Although PDE2A activity was clearly increased in *Fmr1*-null in the hippocampus, an effect that was shown to be a cause of some aspects of the fragile-X syndrome pathology {Maurin et al., 2018, Cereb Cortex, In press.}, no change in PDE2A function was observed in the striatum of the same mouse line. This indicates that molecular mechanisms in action in one brain region may not be engaged in another part of the brain.

2/ When PDE2 and PDE4 are inhibited, D1 MSNs have a hard time maintaining their cAMP level. This suggests that the remaining PDE, PDE10A, might be deficient in the *Fmr1*-KO.

3/ It is interesting to note that, in the context of this hypothesis, homeostatic adaptations occur to compensate for the lack of PDE10A action with an increased activity of PDE2A and/or PDE4, leading to a normal cAMP response to dopamine.

More experiments are required to determine whether this imbalance in PDE job sharing has a biochemical counterpart. This will be tested by performing western blots, to quantify the amount of each PDE subtype in the striatum.

Unpublished data: non-canonical signaling

Mental illnesses such as schizophrenia, bipolar disorders and depression are major public health concerns worldwide. In the search for better treatments, it appears that the fundamental basis of psychiatric diseases are highly complex and the mechanisms of action of drugs remain largely ignored. In this part of my thesis work, I wanted to explore whether dopamine signal was integrated through two alternative signaling nodes, Akt/GSK3 β and Erk. This approach will allow us to understand how drugs of clinical interest affect intracellular signal with the hope that a better understanding of the mechanism of action of such drugs might shed light on the pathophysiology, and eventually indicate novel therapeutic strategies.

Imaging the Akt/GSK3 β signaling cascade

In this project, our aim was to determine how lithium and antipsychotic drugs affects the dynamics of Akt/GSK3 β pathway and the cAMP/PKA pathway during the response to dopamine. Specific biosensors for Akt-dependent phosphorylation were selected from the literature. We prepared the Sindbis virus encoding the AktAR2 (Zhou *et al.*, 2015) biosensor sequence. This biosensor was tested in culture cells and in brain slices but without success: in brain slice preparations as well as in NIH3T3 cells, no response was obtained (Figure 21). Then we decided to prepare the Eevee-iAkt biosensor for Akt (Miura *et al.*, 2014) but we just have some preliminary data that we still need to confirm.

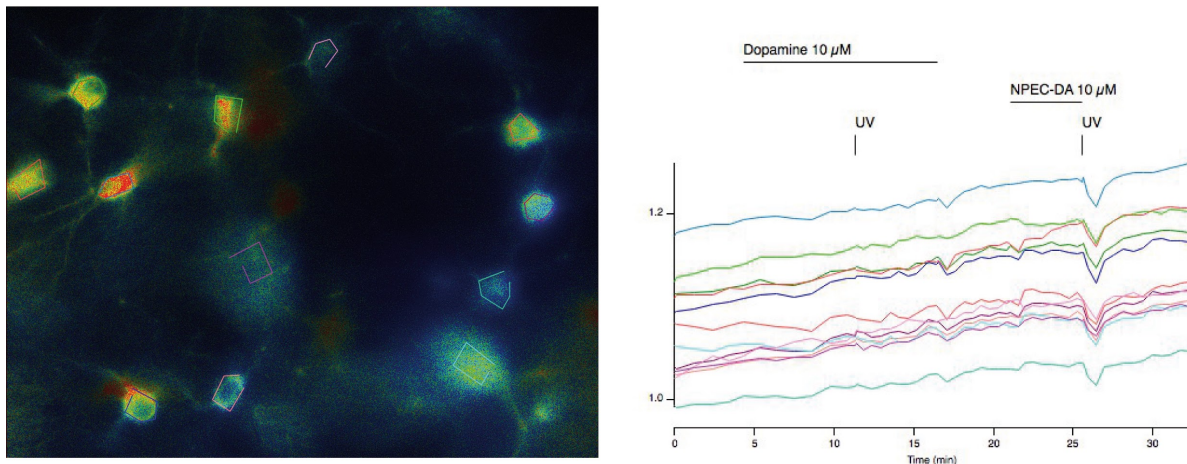


Figure 21 - Akt ratio levels showed no change in MSNs during transient dopamine receptors activation.

Observations:

- Response to NPEC-DA 10 μ M ($n = 2$);
- No response to Dopamine 10 μ M in the bath ($n = 1$).

Imaging the ERK signaling cascade

For this project, we want to acknowledge Dr. Nicolas GERVASI for providing us with the EKAREV biosensor and Dr. Franck RIQUET for developing and providing us with the EKAR-EV GW4.0 biosensor.

In this project, our aim was to determine how the dynamics of ERK pathway is affected during the response to dopamine (Table 5).

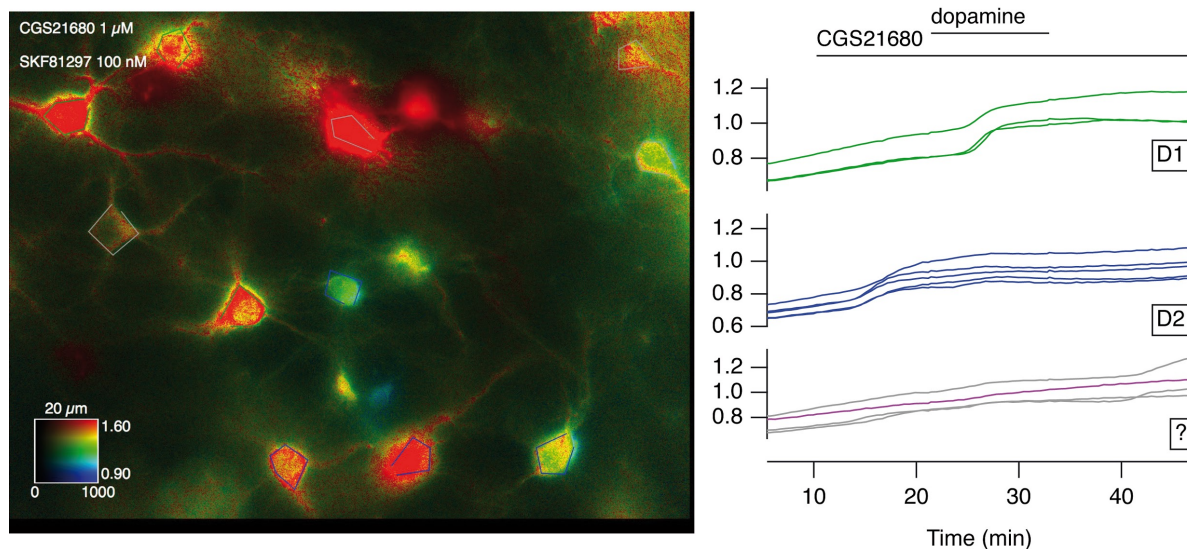


Figure 22 - A_{2A} and D₁ receptors activation (with dopamine 10 μM and CGS21680 1 μM, respectively) increases ERK levels.

Table 5 - ERK responses in the striatum.

Positive responses	Negative response	No response
Dopamine 1 and 3 μM	NMDA 50 μM	NMDA 5 μM
SKF81297 100 nM		U0126 10 μM
CGS21680 1 μM		UNC 9994 1 μM
Fsk 12.5 μM + IBMX 200 μM		Aripiprazole 100 nM and 1 μM
		LiCl 2 mM
		Quinpirole

In addition, we also observed a tendency of baseline ratio to slowly drift up with time (Figure 22). We suspected that this slow upward drift resulted from tonic Erk kinase activity together with insufficient phosphatase activity, thereby slowly shifting the biosensor equilibrium toward the phosphorylated state. In other words, the Ekar biosensor, which reports the kinase / phosphatase equilibrium, accumulates phosphorylation with too little

dephosphorylation. Therefore, we tested a biosensor with faster dephosphorylation rate, which is EKAR-EV GW4.0 biosensor developed and provided by Franck Riquet. This other biosensor showed no clear difference with the previous EKAR-EV, in our conditions (Figure 23).

In conclusion, we observed that all pharmacological stimulations that lead to an activation of the cAMP/PKA signaling pathway also led, with a longer delay, to an increase in Ekar ratio. Agonists of dopamine D₂ receptors had no effect in MSNs. Responses were small compared to a large time-dependent drift. Therefore, we conclude that these experimental conditions are not suitable to explore the coupling between D₂ receptors and Erk activity.

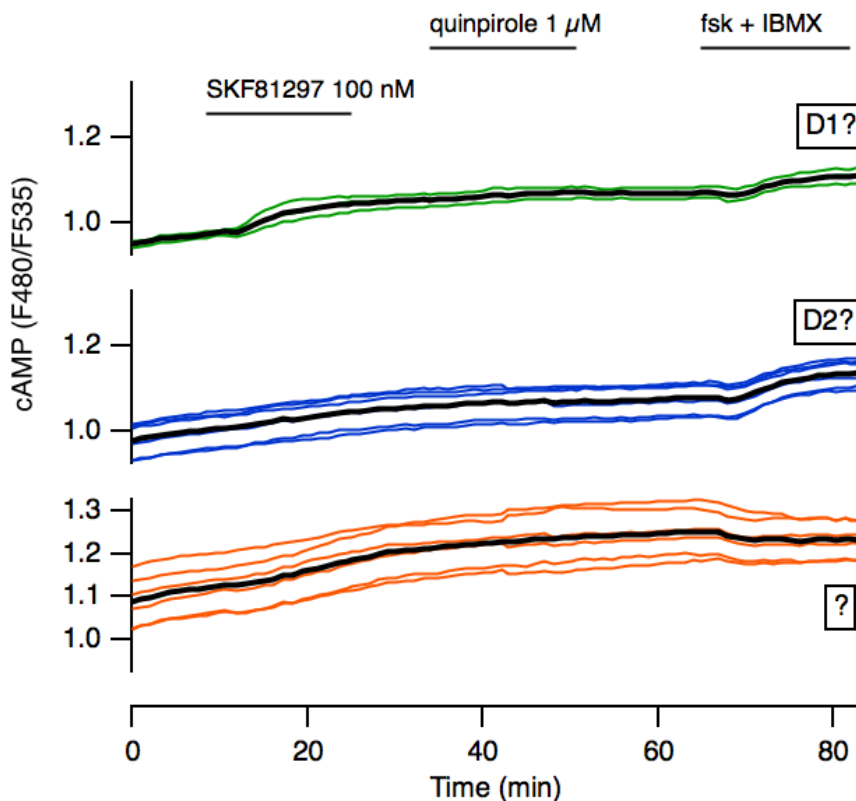


Figure 23 - Positive response to SKF81297, similar to what was obtained with EKAR-EV GW4.0.

Why some neurons respond negatively to fsk + IBMX is hard to explain and needs further investigations.

Side project: β -adrenergic receptors in the striatum

Besides dopamine receptors, many other monoamines receptors are expressed in the striatum, like serotonin receptors (5-HT_{2A}, 5-HT₄, 5-HT₆ and 5-HT₇) and β -adrenergic receptors. While dopamine action through the canonical cAMP/PKA pathway in the striatum is well known, the role of serotonin and noradrenaline neuromodulators is less understood.

I participated in the characterisation of how these receptors affect the dynamics of the cAMP/PKA signaling cascade in D1 and D2 MSNs.

Observations:

- MSNs expressing Epac-S^{H150} biosensor showed a cAMP increase in response to isoproterenol and a desensitization;
- These neurons exhibit a response to isoproterenol, indicating the functional presence of β -adrenergic receptors;
- The serotonin responses were small and complex.

Conclusions: MSNs express functional beta-adrenergic receptors.

IV - Discussion

During my thesis I wanted to understand how the phasic dopamine release in the striatum is integrated at cellular level by MSNs. Using biosensors for cAMP and PKA, it was possible to better understand the integration of phasic dopamine at the level of cAMP and PKA phosphorylation in the canonical signaling. I was interested in understanding the dynamics of the individual D1 and D2 MSNs integrating this phasic dopamine, analysing 1) the role of the principal striatal expressed PDEs, PDE1B, PDE2A, PDE4 and PDE10A; 2) then comparing these normal responses with a pathological situation, in the context of fragile X syndrome; 3) because I worked in collaboration with a team that found an elevated expression of PDE2A in hippocampal *Fmr1*-KO neurons, I assessed whether the increased abundance of the PDE2A protein in *Fmr1*-KO mouse was affecting the cAMP levels in CA1 area of the hippocampus. I also tried to analyze non-canonical signaling cascades activated by dopamine receptors.

1. PDE10A is a critical regulator of cAMP in D1 and D2 MSNs

The phasic release of dopamine in the striatum associated with rewarding events regulates direct and indirect pathway MSNs in opposite ways:

- Phasic activation of D₁ receptors in direct-pathway MSNs induces a peak of cAMP concentration followed by a fast decrease of cAMP due to the extinction of dopamine action together with an efficient degradation of cAMP by PDEs. The transient increase in cAMP is sufficient to activate PKA.
- Symmetrically, phasic activation of D₂ receptors in indirect-pathway MSNs induce a decrease in cAMP and PDE activity is crucial to obtain this reduction of cAMP. This decrease in cAMP down to the lowest level allows for the de-activation of PKA.

Of all PDEs functionally present in the striatum, PDE10A appears as the main route of cAMP degradation. In a previous work, the team has shown that PDE10A is responsible for degrading the low cAMP levels tonically produced in basal condition (Polito *et al.*, 2015). My thesis work largely extended this observation by showing the critical role also played by PDE10A in the integration of transient dopamine signals: we found that PDE10A is required for degrading cAMP down to a low level that permits the rapid neuronal integration of dopamine signals in both D1 and D2 MSNs. In the context of the negative cAMP response in D2 MSNs, PDE10A appears indispensable for the degradation of cAMP levels down to the lowest level, sufficiently low to de-activate PKA and allow for the dephosphorylation of PKA targets. Indeed, the affinity of the regulatory subunit of PKA for cAMP is in the sub-micromolar range, while PDE10A has a K_m of 0.25 μ M for cAMP. PDE10A being the only high-affinity PDE in the striatum, its action is required to transduce a negative dopamine D2 signal into a suppression of PKA activity. Functionally, PDE10A inhibition thus plays a similar role as the inhibition of D₂ dopamine receptors, which was the initial mechanistic explanation for PDE10 inhibitors exhibiting some antipsychotic features.

At high levels of cAMP, ie, in the context of D1 MSN responses, after the fast cAMP

increase, we observed that PDE10A inhibition considerably slowed-down cAMP degradation. PDE10A inhibition thus profoundly impaired dopamine signal integration in D1 MSNs, with transient dopamine signals translating into long-lasting phosphorylation of PKA targets in D1 MSNs. Again, this situation prevents the detection of phasic dopamine: a single dopamine signal turned-on PKA-dependent phosphorylation for a long time in brain slices (Figure 5 in article #2). D1 MSNs remained at an elevated PKA phosphorylation state for the duration of our recordings in brain slice preparations (how the phosphorylation state eventually returns to baseline level remains to be studied). In any case, such long-lasting high phosphorylation state was observed *in vivo*, where PDE10A inhibition led to histone phosphorylation in D1 MSNs in the dorsolateral striatum (Polito *et al.*, 2015). It is likely that, even though PDE10A inhibition alone was not sufficient to turn on PKA-dependent phosphorylation *ex vivo*, when a PDE10A inhibitor was administered *in vivo*, it led to the phosphorylation of a PKA target in both D1 MSNs and D2 MSNs.

In summary, PDE10A inhibition blunts the integration of transient dopamine signal and tends to switch both D1 and D2 MSNs to the PKA phosphorylated up-state.

2. PDE1B, PDE2A and PDE4 degrade high levels of cAMP

While PDE10A operates on both low and high cAMP concentrations, PDE1B, PDE2A and PDE4, with K_m ranging from micromolar to 100 μM , should work primarily on relatively high cAMP concentration levels. As previously published by our team, PDEs 2 and 4 have shown no activity on basal cAMP levels in D1 or D2 MSNs (Polito *et al.*, 2013; Castro *et al.*, 2013), which is consistent with their low affinity for cAMP. In this work, we explored how can these PDEs regulate higher cAMP levels.

Our experiments show that indeed, PDE 1, 2, 4 degrade cAMP at micromolar levels and above. This was observed with PDE1 in Article #1, where PDE1 was shown to regulate elevated steady-state cAMP or cGMP levels. PDE1 was also shown to regulate the peak cAMP response to transient dopamine stimulation. The effect of PDE2A was also seen on cAMP peaks produced by forskolin, or on the PKA response to dopamine (Polito *et al.*, 2013). This observation was clearly confirmed on the response to transient dopamine in D1 MSNs as well as on the steady-state cAMP level produced by adenosine receptors in D2 MSNs (Article #2). Similarly, PDE4 also showed a contribution in the regulation of the cAMP peak resulting from transient dopamine stimulation, and in the regulation of the steady-state response to adenosine receptor stimulation (Article #2).

These observations point at a role of these PDEs during the integration of dopamine signals as well as in the regulation of steady-state (high) cAMP levels.

3. Phosphodiesterases as coincidence detectors

However, we believe that the importance of these PDEs lies in their ability to integrate other neuromodulatory inputs on the cAMP response to dopamine.

The coincidence of glutamatergic and dopaminergic inputs is of critical importance in the induction of synaptic plasticity and constitutes one cornerstone of theories of striatal function in reward-mediated learning. Being activated by calcium, PDE1 is thus positioned at a key place to detect the simultaneous release of glutamate and dopamine.

In our protocols, to clearly observe the cAMP or cGMP degradation by PDE1, it was necessary to previously artificially increase these nucleotides concentration to observe a transient decrease of these cyclic nucleotides levels during transient NMDA (glutamate) release in both MSNs, an effect that was blocked by the selective PDE1 inhibitor.

PDE1 activity was only observed in the presence of calcium in striatum, prefrontal cortex and hippocampus (regions CA1, CA3 and dentate gyrus) of mice brain slices. Although PDE1 is highly expressed in MSNs, this enzyme is overall inactive in our conditions because our experiments are always performed in hyperpolarized conditions and in the presence of TTX to block electrical activity. Thus, PDE1 is active only during biological events that promote calcium increases, like glutamate release, in our experiments. It is likely that other events triggering an increase in intracellular calcium such as the activation of voltage-activated calcium channels, or the release of intracellular calcium stores may also activate PDE1, but this remains to be verified experimentally in neurons.

Some forms of long-term potentiation (LTP), which plays a critical role in reward-mediated learning in the striatum require the simultaneous activation of D₁ receptors by dopamine and NMDA receptors. As indicated above, in D1 MSNs, a phasic dopamine signal is down-regulated by PDEs 2, 4 and 10, but if there is a coincidence of dopamine and glutamate in D1 MSNs the signal is also down-regulated by PDE1. Consistent with PDE1 opposing the cAMP signals which are required for LTP induction, LTP was more powerful when PDE1 was inhibited (in rat ventral striatum), which potentially have important functional consequences in the regulation of synaptic plasticity and transmission. This is consistent with PDE1 opposing the cAMP signals which are required for LTP induction. The increase of cAMP response elicited by D₁ receptors is reduced by the co-activation of DA and NMDA receptors, due to the PDE1 activation.

PDE2A can also play an interesting role in the detection of dopamine and NO coincidence. Although PDE2A is tonically active, its activity can be largely potentiated by cGMP, which is produced upon NO release by neighboring neurons. Thus, the biological coincidence of NO and dopamine will increase PDE2A activity degrading cAMP.

4. PDE2A is critical for normal hippocampal neurons maturation

cAMP levels were compared in *Fmr1*-KO and WT mice using cAMP biosensor imaging in single neurons of the CA1 region of the hippocampus. cAMP levels elicited by PDE2A activation, via NO donor DEANO, on the steady-state of forskolin stimulation were significantly lower in the absence of *FMR1* expression, consistent with an elevated PDE2A activity in the *Fmr1*-KO hippocampus. Moreover, the cAMP decreasing kinetics upon PDE2A stimulation with DEANO was significantly faster in *Fmr1*-KO neurons than in WT, proving again an elevated activity or expression of PDE2A in hippocampal *Fmr1*-KO neurons.

Elevated PDE2A activity dysregulation is involved in the pathophysiology of FXS, due to the absence of FMRP, which is resulting in decreased cAMP levels in mice CA1 region of the hippocampus from *Fmr1*-KO mice brain slices.

An overexpression of PDE2A is deleterious and critical for proper neuronal maturation. In fact, the decreased cAMP levels due to the excessive PDE2A activity results in an exaggerated long-term depression (LTD) induced by mGluR activation (AMPA receptor-mediated excitatory postsynaptic currents (EPSCs)) in the *Fmr1*-KO CA1 pyramidal neurons synapses. Blockade of PDE2A reverted (rescued) the exaggerated mGluR-LTD in the *Fmr1*-KO mice CA1 pyramidal neurons from hippocampus. This shows the implication of PDE2A-mediated regulation of cAMP and cGMP in the exaggerated mGluR-dependent LTD in *Fmr1*-KO mice. Thus, inhibition of PDE2A can prevent the exaggerated synaptic plasticity.

Both cAMP and cGMP have been reported to play critical roles in axonal growth and dendritic spine maturation. Another hallmark of the functional absence of FMRP is the presence of abnormal immature dendritic spines and axonal length in the brain of FXS patients and models. Inhibition of PDE2A activity restores/rescues the maturation of axonal length and dendritic spine morphology in *Fmr1*-KO cultured cortical neurons. Importantly, PDE2A inhibitor treatment affected neither the length of mature spines nor the density of dendritic protrusions in FXS neurons.

All these observations proves clearly that PDE2A overexpression is critical for a healthy brain maturation/development.

Although PDE2A activity was clearly increased in *Fmr1*-KO in the hippocampus, resulting in the FXS pathology, no change in PDE2A activity was observed in the striatum during AC responses. This indicates that PDE alterations in one brain region may not be engaged in another part of the brain. Thus a treatment with a PDE2A inhibitor to restore the cAMP in CA1 region of hippocampus can affect the normal activity of PDE2A in the striatum, in other brain regions or even in others peripheral organs.

5. Is striatal PDE10A activity decreased in a genetic model of mental retardation ?

An optimal PDE10A activity in MSNs is essential for a balanced integration of phasic dopamine signals through both D₁ and D₂ receptors. This led us to analyze striatal PDEs contribution in an animal model of fragile X syndrome. cAMP levels of *Fmr1*-KO and WT mice were compared during DA responses by MSNs and no differences were observed. However, when PDE2A and PDE4 were inhibited, D1 and D2 MSNs could no longer maintain their basal cAMP levels, suggesting that the remaining PDE, most likely PDE10A, might be deficient in the *Fmr1*-KO. This reduced PDE10A is essentially critical for the cAMP/PKA signaling in D2 MSNs, considering the important role of PDE10A for the negative cAMP responses in D2 MSNs, as referred above.

Considering that this PDE alteration was only observed when PDEs were individually analysed, our hypothesis is that the dopamine responses are apparently normal due to

homeostatic adaptations, which are occurring to compensate for the lack of PDE10A action. This reduced PDE10A activity may be compensated with an increased activity of other PDEs, leading to a normal cAMP response to dopamine. More experiments are required to determine whether this imbalance in PDE job sharing has a biochemical counterpart (extrusion through multi-drug-resistant protein, reduction of adenylyl cyclase activity, ...). This will be tested by performing western blots, to quantify the amount of each PDE subtype in the dorsomedial striatum.

If this reduction in PDE10A expression level is confirmed biochemically, this may lead to a novel understanding of FXS, a complex syndrome which includes some features indicative of striatal dysfunctions like hyperactivity.

This critical role played by PDE10A thus seems to result from the high affinity for cAMP so that the enzyme works on very low cAMP concentration, together with a very high expression level, which provides a high total activity affecting high cAMP levels as well. An optimal PDE10A activity in MSNs is thus essential for a balanced integration of phasic DA signals.

6. Advantages and limitations of biosensor imaging

In order to understand what happens intracellularly at the biochemical level, we used several biosensors to monitor cyclic nucleotide signaling at different levels: we used very efficient biosensors to measure cAMP concentration, PKA/phosphatase activity, cGMP concentration and calcium concentration. This biosensor approach had several key advantages over more classical biochemical or immunohistochemical approaches. First, cellular imaging provided simultaneous recording of D1 and D2 MSNs: while dopamine activates D₁ and D₂ receptors simultaneously, imaging at the single cell level allowed the simultaneous recording of the opposite cAMP responses, something that would be impossible with classical biochemistry techniques.

The temporal dimension is critical in the integration of transient dopamine signals, with phasic dopamine release occurring over time-scales covering a range from sub-second to several seconds to minutes. While biosensor recordings can easily monitor events at the sub-second time-scale, we couldn't benefit from this since we were unable to produce dopamine transients that were short enough to mimic real phasic dopamine release, since diffusion of dopamine out of the imaging field requires ~100 s (Yapo *et al.*, 2017). Nevertheless, dopamine stimulation in the 100 s time-range was still a large improvement over resolution obtained with former approaches and nicely matched the dynamics of cAMP signals.

Biosensor imaging allows to measure the concentration of a molecule within the detection limit (sensitivity) specific of the biosensor. For example, it is possible to follow the gradual change in cAMP concentration over time within a concentration range that allowed us to monitor D1 and D2 responses. This approach also allows to do an internal control with two successive stimulations in the same neurons, because the biosensor recording of two successive stimulations is reproducible.

Biosensor imaging allows the measurement at two levels of the signaling cascade, in order to better understand the signal integration: it is possible to measure intracellular cAMP levels and PKA activity. Although we did not measure both signals at the same time, the signals are reproducible and homogeneous enough to repeat several times each measure with either cAMP or PKA biosensor, to analyze how changes in cAMP concentration affects the phosphorylation at PKA level. In the same way, biosensor imaging also allows the measurement of parallel signaling cascades such as cAMP and cGMP.

Another example is the use of calcium biosensor to confirm that it was effectively the calcium level increase in presence of NMDA that activated PDE1. In this way, we know that the PDE1 activity can be properly followed using cAMP or cGMP biosensors with this protocol previously validated with calcium biosensor in exactly the same conditions. This kind of measurements helps to better understand the relationship between different molecular signals.

Still, biosensor imaging presents some limitations, like the difficulty to measure two signals simultaneously. However, in our type of protocol, this limitation can be circumvented easily with the repetition of the same protocol using different biosensors. Alternatively, simultaneous recording with a second biosensor with a different pair of fluorescent proteins is also a possibility, as illustrated recently (Demeautis *et al.*, 2017).

Our experiments were all performed in wide field microscopy, which limits the detection of the signal to the cellular body of the neurons; to observe the signal from the dendrites it would be necessary to image with two-photon excitation microscopy; however the phasic liberation of dopamine performed with the uncaging of a caged-dopamine molecule and the kinetics of the responses to this stimulation are faster than the full-frame acquisition rate with the 2-photon microscope.

We also tested Akt and ERK biosensors (AktAR2, Eevee-iAkt, EKAR-EV and EKAR-EV GW4.0) in order to explore the non-canonical signaling downstream of dopamine D₂ receptor. However, in our experimental conditions, the activation of D₂ receptors produced no signal with these biosensors. As a control, we verified that the different variants of Erk biosensors responded positively to the activation of the cAMP/PKA signaling pathway, as well as to NMDA stimulation in the striatum and in the hippocampus. Akt biosensors also responded positively to a chemical activator of Akt. We hypothesized that can be due to the fact that our basal conditions are already inducing a maximal phosphorylation of AktAR2, Eevee-iAkt, EKAR-EV and EKAR-EV GW4.0 biosensors. However, phasic NMDA stimulation in striatum and hippocampus induced slow but significant ERK responses. In this way, maybe it is necessary to adapt and optimise our experimental conditions in order to be able to read this kind of biosensors. Still, it can be also necessary to improve the quality of this kind of biosensors.

V - Conclusions and perspectives

In conclusion, my thesis work contributes to a better understanding of the integration of phasic dopamine signals by MSNs in the striatum. FRET biosensors for cAMP and PKA were revealed as powerful approach to observe fast events, at cellular level, the integration of phasic dopamine signals at the level of cAMP and PKA phosphorylation in the canonical signaling.

My thesis work revealed the crucial role played by PDE10A in the integration of transient dopamine signals in the striatum, in both D1 and D2 MSNs. Inhibiting PDE10A can seem an excellent therapeutic target due to its high and selective expression in MSNs, but considering the crucial physiological role played by PDE10A, which can not be replaced by any other PDE, it is not surprising that some undesirable side effects have been reported. Even if PDE10A inhibition suppresses the negative action of dopamine on PKA-dependent targets in D2 MSNs, working like an antipsychotic, PDE10A inhibition also affects D1 MSNs, which can then switch to a state of high PKA-dependent phosphorylation level. This may explain why phase II clinical trials (ClinicalTrials.gov: NCT01175135) with PDE10A inhibitors reported unwanted effects.

In the fragile X syndrome, PDE2A was revealed to be expressed at a higher than normal level in the hippocampus, and PDE2A could therefore be considered as a therapeutic target. However, in striatal MSNs, we observed that PDE2A activity was not altered. Moreover, PDE2A is broadly expressed not only in CNS but also in peripheral organs. Thus we must consider that PDE2A inhibition as a pharmaceutical strategy to regulate cyclic nucleotides in hippocampus can dysregulate cyclic nucleotides in other brain regions or peripheral organs. One of the PDE2A inhibitors was tested in two phase I clinical trials for the treatment of migraine: one test terminated prematurely due to safety concerns and the other was withdrawn prior to participant enrollment (ClinicalTrials.gov: NCT01981499 and NCT01981486). There are no published details about these safety concerns. Moreover, PDE2A knockout mouse phenotype is lethal at embryonic day 17. Despite these drawbacks, there are still clinical trials in development.

Still in the pathology of FXS, our work shows that PDE10A activity is possibly reduced in the striatum. However, the cAMP levels apparently are not altered, which means that are a cellular mechanism that compensate for the lower activity of PDE10A. Western Blot analyses are already being performed to check which striatal PDEs are altered in the context of FXS.

I believe that with my thesis work I contributed to the understanding of the dynamics of the individual D1 and D2 MSNs integrating the phasic dopamine signal and the role of the principal striatal expressed PDEs. At physiological level, PDE1B, PDE2A, PDE4 and PDE10A moderate high cAMP levels in MSNs. PDE1B and PDE2A detect the coincidence of dopamine with glutamate or NO, respectively.

In general, this thesis proves how important are PDEs in the spatio-temporal regulation of cAMP during the integration of transient dopamine signals. The role of PDE1B, PDE2A and PDE4 in D1 MSNs and the role of PDE10A in both D1 and D2 MSNs in the

integration of transient dopamine signals can be useful to better understand how these PDEs can be targeted in diseases related with dopamine signaling alterations. These findings can be useful to understand and develop better therapeutic strategies related to alterations in dopamine release. In fact, PDE1 inhibition has been indicated as a potential therapeutic for Parkinson's disease, PDE2A inhibition for cognition and learning, PDE4 inhibition for depression, anxiety, cognition enhancement, Alzheimer's disease and Parkinson's disease, and PDE10A inhibition for Schizophrenia, Huntington's disease and cognition enhancement (Maurice *et al.*, 2014).

Finally, my thesis work is essentially about the canonical cAMP/PKA signaling in response to dopamine. But, I also tried to analyze non-canonical signaling cascades activated by dopamine receptors. Several studies suggest that the D₂ receptor is coupled to others signaling cascade, such as the Akt/GSK3-beta and MAPK. Moreover, it seems that the therapeutic activity of antipsychotics activates these cascades. Antipsychotics, like haloperidol and aripiprazole, work as D₂ receptor inhibitors. Thus, we wanted to understand how dopamine and antipsychotics modulate signaling cascades like Akt/GSK3-beta and the Erk signaling cascades. Akt biosensor was functional but did not respond to dopamine or antipsychotics drugs. Erk biosensor responded via cAMP/PKA to dopamine and adenosine, but not to D₂ receptor drugs. Thus, the coupling of dopamine receptors with alternative signaling cascades remains unclear in our experimental conditions.

It is amazing how dopamine signaling is vital. It is essential for our mental health an equilibrated balance of dopamine signaling, that is highly associated with reward and learning, and has an impact in our life in all aspects, economic and political power, knowledge, relationships, ... everything in our life that give us reward and motivation; an imbalance in dopamine signaling in MSNs is translated in diseases that affect our life quality, health, and even our social life. The dopamine system internal signals to behavior is not simple, and we also must consider the other neuromodulatory systems: norepinephrine, serotonin, acetylcholine. There is still a lot of functions to unravel not only at physiological level, but also in brain disorders or lesions. The investigation of dopamine function and the underlying networks is still a big challenge but it is of public interest. An equilibrated dopamine signaling cascade in our brain is what gives us reasons to live!

VI - Bibliography

- Abudukeyoumu N, Hernandez-Flores T, Garcia-Munoz M & Arbuthnott GW (2019). Cholinergic modulation of striatal microcircuits. *Eur J Neurosci* **49**, 604–622.
- Adams SR, Harootunian AT, Buechler YJ, Taylor SS & Tsien RY (1991). Fluorescence ratio imaging of cyclic AMP in single cells. *Nature* **349**, 694–697.
- Ahmad R, Bourgeois S, Postnov A, Schmidt ME, Bormans G, Van Laere K & Vandenberghe W (2014). PET imaging shows loss of striatal PDE10A in patients with Huntington disease. *Neurology* **82**, 279–281.
- Ai M, Mills H, Kanai M, Lai J, Deng J, Schreiter E, Looger L, Neubert T & Suh G (2015). Green-to-Red Photoconversion of GCaMP. *PLoS One* **10**, e0138127.
- Akerboom J, Rivera JD, Guilbe MM, Malavé EC, Hernandez HH, Tian L, Hires SA, Marvin JS, Looger LL & Schreiter ER (2009). Crystal structures of the GCaMP calcium sensor reveal the mechanism of fluorescence signal change and aid rational design. *J Biol Chem* **284**, 6455–6464.
- Albin RL, Young AB & Penney JB (1989). The functional anatomy of basal ganglia disorders. *Trends Neurosci* **12**, 366–375.
- Allen MD & Zhang J (2006). Subcellular dynamics of protein kinase A activity visualized by FRET-based reporters. *Biochem Biophys Res Commun* **348**, 716–721.
- Altar CA, Hunt RA, Jurata LW, Webster MJ, Derby E, Gallagher P, Lemire A, Brockman J & Laeng P (2008). Insulin, IGF-1, and muscarinic agonists modulate schizophrenia-associated genes in human neuroblastoma cells. *Biol Psychiatry* **64**, 1077–1087.
- Archer SL & Michelakis ED (2009). Phosphodiesterase type 5 inhibitors for pulmonary arterial hypertension. *N Engl J Med* **361**, 1864–1871.
- Ariano MA, Lewicki JA, Brandwein HJ & Murad F (1982). Immunohistochemical localization of guanylate cyclase within neurons of rat brain. *Proc Natl Acad Sci U S A* **79**, 1316–1320.
- Bacskai BJ, Hochner B, Mahaut-Smith M, Adams SR, Kaang BK, Kandel ER & Tsien RY (1993). Spatially resolved dynamics of cAMP and protein kinase A subunits in *Aplysia* sensory neurons. *Science* **260**, 222–226.
- Bagni C & Oostra BA (2013). Fragile X syndrome: From protein function to therapy. *Am J Med Genet A* **161A**, 2809–2821.
- Baillie GS, MacKenzie SJ, McPhee I & Houslay MD (2000). Sub-family selective actions in the ability of Erk2 MAP kinase to phosphorylate and regulate the activity of PDE4 cyclic AMP-specific phosphodiesterases. *Br J Pharmacol* **131**, 811–819.
- Baillie GS, Tejeda GS & Kelly MP (2019). Therapeutic targeting of 3',5'-cyclic nucleotide phosphodiesterases: inhibition and beyond. *Nat Rev Drug Discov* **18**, 770–796.
- Baird GS, Zacharias DA & Tsien RY (1999). Circular permutation and receptor insertion within green fluorescent proteins. *Proc Natl Acad Sci U S A* **96**, 11241–11246.
- Balleine BW, Delgado MR & Hikosaka O (2007). The role of the dorsal striatum in reward and decision-making. *J Neurosci* **27**, 8161–8165.
- Ballion B, Mallet N, Bézard E, Lanciego JL & Gonon F (2008). Intratelencephalic corticostriatal neurons equally excite striatonigral and striatopallidal neurons and their discharge activity is selectively reduced in experimental parkinsonism. *Eur J Neurosci* **27**, 2313–2321.

- Bamford NS, Zhang H, Schmitz Y, Wu NP, Cepeda C, Levine MS, Schmauss C, Zakharenko SS, Zablow L & Sulzer D (2004). Heterosynaptic dopamine neurotransmission selects sets of corticostriatal terminals. *Neuron* **42**, 653–663.
- Barnes PJ (2013). Corticosteroid resistance in patients with asthma and chronic obstructive pulmonary disease. *J Allergy Clin Immunol* **131**, 636–645.
- Bateup HS, Santini E, Shen W, Birnbaum S, Valjent E, Surmeier DJ, Fisone G, Nestler EJ & Greengard P (2010). Distinct subclasses of medium spiny neurons differentially regulate striatal motor behaviors. *Proc Natl Acad Sci U S A* **107**, 14845–14850.
- Bateup HS, Svenningsson P, Kuroiwa M, Gong S, Nishi A, Heintz N & Greengard P (2008). Cell type-specific regulation of DARPP-32 phosphorylation by psychostimulant and antipsychotic drugs. *Nat Neurosci* **11**, 932–939.
- Beard MB, Olsen AE, Jones RE, Erdogan S, Houslay MD & Bolger GB (2000). UCR1 and UCR2 domains unique to the cAMP-specific phosphodiesterase family form a discrete module via electrostatic interactions. *J Biol Chem* **275**, 10349–10358.
- Beaulieu JM & Caron MG (2008). Looking at lithium: molecular moods and complex behaviour. *Mol Interv* **8**, 230–241.
- Beaulieu JM, Espinoza S & Gainetdinov RR (2015). Dopamine receptors - IUPHAR Review 13. *Br J Pharmacol* **172**, 1–23.
- Beaulieu JM, Marion S, Rodriguiz RM, Medvedev IO, Sotnikova TD, Ghisi V, Wetsel WC, Lefkowitz RJ, Gainetdinov RR & Caron MG (2008). A beta-arrestin 2 signaling complex mediates lithium action on behavior. *Cell* **132**, 125–136.
- Beaulieu JM, Sotnikova TD, Marion S, Lefkowitz RJ, Gainetdinov RR & Caron MG (2005). An Akt/beta-arrestin 2/PP2A signaling complex mediates dopaminergic neurotransmission and behavior. *Cell* **122**, 261–273.
- Beaulieu JM, Sotnikova TD, Yao WD, Kockeritz L, Woodgett JR, Gainetdinov RR & Caron MG (2004). Lithium antagonizes dopamine-dependent behaviors mediated by an AKT/glycogen synthase kinase 3 signaling cascade. *Proc Natl Acad Sci U S A* **101**, 5099–5104.
- Beckstead RM (1988). Association of dopamine D1 and D2 receptors with specific cellular elements in the basal ganglia of the cat: the uneven topography of dopamine receptors in the striatum is determined by intrinsic striatal cells, not nigrostriatal axons. *Neuroscience* **27**, 851–863.
- Beckstead RM & Kersey KS (1985). Immunohistochemical demonstration of differential substance P-, met-enkephalin-, and glutamic-acid-decarboxylase-containing cell body and axon distributions in the corpus striatum of the cat. *J Comp Neurol* **232**, 481–498.
- Belal AS, Sell BR, Hoi H, Davidson MW & Campbell RE (2014). Optimization of a genetically encoded biosensor for cyclin B1-cyclin dependent kinase 1. *Mol Biosyst* **10**, 191–195.
- Bender AT & Beavo JA (2006). Cyclic nucleotide phosphodiesterases: molecular regulation to clinical use. *Pharmacol Rev* **58**, 488–520.
- Bertolin G, Sizaire F, Déméautis C, Chapuis C, Mérola F, Erard M & Tramier M (2019). Optimized FRET Pairs and Quantification Approaches To Detect the Activation of Aurora Kinase A at Mitosis. *ACS Sens* **4**, 2018–2027.
- Bertran-Gonzalez J, Bosch C, Maroteaux M, Matamales M, Hervé D, Valjent E & Girault JA (2008). Opposing patterns of signaling activation in dopamine D1 and D2 receptor-

- expressing striatal neurons in response to cocaine and haloperidol. *J Neurosci* **28**, 5671–5685.
- Bertran-Gonzalez J, Håkansson K, Borgkvist A, Irinopoulou T, Brami-Cherrier K, Usiello A, Greengard P, Hervé D, Girault JA, Valjent E & Fisone G (2009). Histone H3 phosphorylation is under the opposite tonic control of dopamine D2 and adenosine A2A receptors in striatopallidal neurons. *Neuropsychopharmacology* **34**, 1710–1720.
- Betolngar DB, Mota É, Fabritius A, Nielsen J, Hougaard C, Christoffersen CT, Yang J, Kehler J, Griesbeck O, Castro LRV & Vincent P (2019). Phosphodiesterase 1 Bridges Glutamate Inputs with NO- and Dopamine-Induced Cyclic Nucleotide Signals in the Striatum. *Cereb Cortex* **29**, 5022–5036.
- Bevan MD, Magill PJ, Terman D, Bolam JP & Wilson CJ (2002). Move to the rhythm: oscillations in the subthalamic nucleus-external globus pallidus network. *Trends Neurosci* **25**, 525–531.
- Bhat S, Acharya UR, Adeli H, Bairy GM & Adeli A (2014). Autism: cause factors, early diagnosis and therapies. *Rev Neurosci* **25**, 841–850.
- Björklund A & Dunnett SB (2007). Dopamine neuron systems in the brain: an update. *Trends Neurosci* **30**, 194–202.
- Blokland A, Schreiber R & Prickaerts J (2006). Improving memory: a role for phosphodiesterases. *Curr Pharm Des* **12**, 2511–2523.
- Bockaert J, Perroy J, Bécamel C, Marin P & Fagni L (2010). GPCR interacting proteins (GIPs) in the nervous system: Roles in physiology and pathologies. *Annu Rev Pharmacol Toxicol* **50**, 89–109.
- Boess FG, Hendrix M, van der Staay FJ, Erb C, Schreiber R, van Staveren W, de Vente J, Prickaerts J, Blokland A & Koenig G (2004). Inhibition of phosphodiesterase 2 increases neuronal cGMP, synaptic plasticity and memory performance. *Neuropharmacology* **47**, 1081–1092.
- Bolam JP, Hanley JJ, Booth PA & Bevan MD (2000). Synaptic organisation of the basal ganglia. *J Anat* **196**, 527–542.
- Bolger G, Michaeli T, Martins T, St John T, Steiner B, Rodgers L, Riggs M, Wigler M & Ferguson K (1993). A family of human phosphodiesterases homologous to the dunce learning and memory gene product of *Drosophila melanogaster* are potential targets for antidepressant drugs. *Mol Cell Biol* **13**, 6558–6571.
- Bolger GB, Baillie GS, Li X, Lynch MJ, Herzyk P, Mohamed A, Mitchell LH, McCahill A, Hundsrucker C, Klusmann E, Adams DR & Houslay MD (2006). Scanning peptide array analyses identify overlapping binding sites for the signalling scaffold proteins, beta-arrestin and RACK1, in cAMP-specific phosphodiesterase PDE4D5. *Biochem J* **398**, 23–36.
- Bonaccorso CM, Spatuzza M, Di Marco B, Gloria A, Barrancotto G, Cupo A, Musumeci SA, D'Antoni S, Bardoni B & Catania MV (2015). Fragile X mental retardation protein (FMRP) interacting proteins exhibit different expression patterns during development. *Int J Dev Neurosci* **42**, 15–23.
- Börner S, Schwede F, Schlipp A, Berisha F, Calebiro D, Lohse MJ & Nikolaev VO (2011). FRET measurements of intracellular cAMP concentrations and cAMP analog permeability in intact cells. *Nat Protoc* **6**, 427–438.
- Boscutti G, A Rabiner E & Plisson C (2019). PET Radioligands for imaging of the PDE10A in human: current status. *Neurosci Lett* **691**, 11–17.

- Brackett DM, Qing F, Amieux PS, Sellers DL, Horner PJ & Morris DR (2013). FMR1 transcript isoforms: association with polyribosomes; regional and developmental expression in mouse brain. *PLoS One* **8**, e58296.
- Breakefield XO, Blood AJ, Li Y, Hallett M, Hanson PI & Standaert DG (2008). The pathophysiological basis of dystonias. *Nat Rev Neurosci* **9**, 222–234.
- Brown MT, Henny P, Bolam JP & Magill PJ (2009). Activity of neurochemically heterogeneous dopaminergic neurons in the substantia nigra during spontaneous and driven changes in brain state. *J Neurosci* **29**, 2915–2925.
- Brown P (2007). Abnormal oscillatory synchronisation in the motor system leads to impaired movement. *Curr Opin Neurobiol* **17**, 656–664.
- Cahill E, Pascoli V, Trifilieff P, Savoldi D, Kappès V, Lüscher C, Caboche J & Vanhoutte P (2014a). D1R/GluN1 complexes in the striatum integrate dopamine and glutamate signalling to control synaptic plasticity and cocaine-induced responses. *Mol Psychiatry* **19**, 1295–1304.
- Cahill E, Salery M, Vanhoutte P & Caboche J (2014b). Convergence of dopamine and glutamate signaling onto striatal ERK activation in response to drugs of abuse. *Front Pharmacol* **4**, 172.
- Calabresi P, Centonze D, Gubellini P, Marfia GA, Pisani A, Sancesario G & Bernardi G (2000). Synaptic transmission in the striatum: from plasticity to neurodegeneration. *Prog Neurobiol* **61**, 231–265.
- Calabresi P, Gubellini P, Centonze D, Sancesario G, Morello M, Giorgi M, Pisani A & Bernardi G (1999). A critical role of the nitric oxide/cGMP pathway in corticostriatal long-term depression. *J Neurosci* **19**, 2489–2499.
- Calebiro D, Nikolaev VO, Gagliani MC, de Filippis T, Dees C, Tacchetti C, Persani L & Lohse MJ (2009). Persistent cAMP-signals triggered by internalized G-protein-coupled receptors. *PLoS Biol* **7**, e1000172.
- Card GL, England BP, Suzuki Y, Fong D, Powell B, Lee B, Luu C, Tabrizizad M, Gillette S, Ibrahim PN, Artis DR, Bollag G, Milburn MV, Kim SH, Schlessinger J & Zhang KY (2004). Structural basis for the activity of drugs that inhibit phosphodiesterases. *Structure* **12**, 2233–2247.
- Castro LR, Brito M, Guiot E, Polito M, Korn CW, Hervé D, Girault JA, Paupardin-Tritsch D & Vincent P (2013). Striatal neurones have a specific ability to respond to phasic dopamine release. *J Physiol* **591**, 3197–3214.
- Castro LR, Gervasi N, Guiot E, Cavellini L, Nikolaev VO, Paupardin-Tritsch D & Vincent P (2010). Type 4 phosphodiesterase plays different integrating roles in different cellular domains in pyramidal cortical neurons. *J Neurosci* **30**, 6143–6151.
- Castro LR, Verde I, Cooper DM & Fischmeister R (2006). Cyclic guanosine monophosphate compartmentation in rat cardiac myocytes. *Circulation* **113**, 2221–2228.
- Cepeda C, Buchwald NA & Levine MS (1993). Neuromodulatory actions of dopamine in the neostriatum are dependent upon the excitatory amino acid receptor subtypes activated. *Proc Natl Acad Sci U S A* **90**, 9576–9580.
- Chan CS, Surmeier DJ & Yung WH (2005). Striatal information signaling and integration in globus pallidus: timing matters. *Neurosignals* **14**, 281–289.
- Chappie T, Humphrey J, Menniti F & Schmidt C (2009). PDE10A inhibitors: an assessment of the current CNS drug discovery landscape. *Curr Opin Drug Discov Devel* **12**, 458–467.

- Chappie TA, Helal CJ & Hou X (2012). Current landscape of phosphodiesterase 10A (PDE10A) inhibition. *J Med Chem* **55**, 7299–7331.
- Charych EI & Brandon NJ (2014). Molecular and cellular understanding of PDE10A: a dual-substrate phosphodiesterase with therapeutic potential to modulate basal ganglia function. *Cyclic-nucleotide phosphodiesterases in the central nervous system New York: Wiley* p. 247–68.
- Charych EI, Jiang LX, Lo F, Sullivan K & Brandon NJ (2010). Interplay of palmitoylation and phosphorylation in the trafficking and localization of phosphodiesterase 10A: implications for the treatment of schizophrenia. *J Neurosci* **30**, 9027–9037.
- Chen TW, Wardill TJ, Sun Y, Pulver SR, Renninger SL, Baohan A, Schreiter ER, Kerr RA, Orger MB, Jayaraman V, Looger LL, Svoboda K & Kim DS (2013). Ultrasensitive fluorescent proteins for imaging neuronal activity. *Nature* **499**, 295–300.
- Chesselet MF & Graybiel AM (1983). Met-enkephalin-like and dynorphin-like immunoreactivities of the basal ganglia of the cat. *Life Sci* **33 Suppl 1**, 37–40.
- Chevalier G, Vacher S, Deniau JM & Desban M (1985). Disinhibition as a basic process in the expression of striatal functions. I. The striato-nigral influence on tecto-spinal/tecto-diencephalic neurons. *Brain Res* **334**, 215–226.
- Cisek P & Kalaska JF (2010). Neural mechanisms for interacting with a world full of action choices. *Annu Rev Neurosci* **33**, 269–298.
- Conti M & Beavo J (2007). Biochemistry and physiology of cyclic nucleotide phosphodiesterases: essential components in cyclic nucleotide signaling. *Annu Rev Biochem* **76**, 481–511.
- Coskran TM, Morton D, Menniti FS, Adamowicz WO, Kleiman RJ, Ryan AM, Strick CA, Schmidt CJ & Stephenson DT (2006). Immunohistochemical localization of phosphodiesterase 10A in multiple mammalian species. *J Histochem Cytochem* **54**, 1205–1213.
- Costa RM (2007). Plastic corticostriatal circuits for action learning: what's dopamine got to do with it. *Ann N Y Acad Sci* **1104**, 172–191.
- Cui G, Jun SB, Jin X, Pham MD, Vogel SS, Lovinger DM & Costa RM (2013). Concurrent activation of striatal direct and indirect pathways during action initiation. *Nature* **494**, 238–242.
- Dahlhaus R (2018). Of Men and Mice: Modeling the Fragile X Syndrome. *Front Mol Neurosci* **11**, 41.
- Day M, Wokosin D, Plotkin JL, Tian X & Surmeier DJ (2008). Differential excitability and modulation of striatal medium spiny neuron dendrites. *J Neurosci* **28**, 11603–11614.
- de Rooij J, Zwartkruis FJ, Verheijen MH, Cool RH, Nijman SM, Wittinghofer A & Bos JL (1998). Epac is a Rap1 guanine-nucleotide-exchange factor directly activated by cyclic AMP. *Nature* **396**, 474–477.
- de Vente J, Asan E, Gambaryan S, Markerink-van Ittersum M, Axer H, Gallatz K, Lohmann SM & Palkovits M (2001). Localization of cGMP-dependent protein kinase type II in rat brain. *Neuroscience* **108**, 27–49.
- (2011). Deal watch: Intra-Cellular Therapies and Takeda to develop PDE1 inhibitors for schizophrenia. *Nat Rev Drug Discov* **10**, 329.
- DeLong MR (1983). The neurophysiologic basis of abnormal movements in basal ganglia disorders. *Neurobehav Toxicol Teratol* **5**, 611–616.

- DeLong MR (1990). Primate models of movement disorders of basal ganglia origin. *Trends Neurosci* **13**, 281–285.
- DeLong MR & Wichmann T (2007). Circuits and circuit disorders of the basal ganglia. *Arch Neurol* **64**, 20–24.
- Demeautis C, Sipieter F, Roul J, Chapuis C, Padilla-Parra S, Riquet FB & Tramier M (2017). Multiplexing PKA and ERK1&2 kinases FRET biosensors in living cells using single excitation wavelength dual colour FLIM. *Sci Rep* **7**, 41026.
- Deniau JM & Chevalier G (1985). Disinhibition as a basic process in the expression of striatal functions. II. The striato-nigral influence on thalamocortical cells of the ventromedial thalamic nucleus. *Brain Res* **334**, 227–233.
- Depry C, Allen MD & Zhang J (2011). Visualization of PKA activity in plasma membrane microdomains. *Mol Biosyst* **7**, 52–58.
- Deuschle K, Okumoto S, Fehr M, Looger LL, Kozhukh L & Frommer WB (2005). Construction and optimization of a family of genetically encoded metabolite sensors by semirational protein engineering. *Protein Sci* **14**, 2304–2314.
- Di Benedetto G, Zoccarato A, Lissandron V, Terrin A, Li X, Houslay MD, Baillie GS & Zaccolo M (2008). Protein kinase A type I and type II define distinct intracellular signaling compartments. *Circ Res* **103**, 836–844.
- Di Martino A, Kelly C, Grzadzinski R, Zuo XN, Mennes M, Mairena MA, Lord C, Castellanos FX & Milham MP (2011). Aberrant striatal functional connectivity in children with autism. *Biol Psychiatry* **69**, 847–856.
- Ding JD, Burette A, Nedvetsky PI, Schmidt HH & Weinberg RJ (2004). Distribution of soluble guanylyl cyclase in the rat brain. *J Comp Neurol* **472**, 437–448.
- DiPilato LM, Cheng X & Zhang J (2004). Fluorescent indicators of cAMP and Epac activation reveal differential dynamics of cAMP signaling within discrete subcellular compartments. *Proc Natl Acad Sci U S A* **101**, 16513–16518.
- Dodge KL, Khouangsathiene S, Kapiloff MS, Mouton R, Hill EV, Houslay MD, Langeberg LK & Scott JD (2001). mAKAP assembles a protein kinase A/PDE4 phosphodiesterase cAMP signaling module. *EMBO J* **20**, 1921–1930.
- Doly S, Bertran-Gonzalez J, Callebert J, Bruneau A, Banas SM, Belmer A, Boutourlinsky K, Hervé D, Launay JM & Maroteaux L (2009). Role of serotonin via 5-HT2B receptors in the reinforcing effects of MDMA in mice. *PLoS One* **4**, e7952.
- Doyle TB, Muntean BS, Ejendal KF, Hayes MP, Soto-Velasquez M, Martemyanov KA, Dessauer CW, Hu CD & Watts VJ (2019). Identification of Novel Adenylyl Cyclase 5 (AC5) Signaling Networks in D₁ and D₂ Medium Spiny Neurons using Bimolecular Fluorescence Complementation Screening. *Cells* **8**,
- Drago J, Padungchaichot P, Wong JY, Lawrence AJ, McManus JF, Sumarsono SH, Natoli AL, Lakso M, Wreford N, Westphal H, Kola I & Finkelstein DI (1998). Targeted expression of a toxin gene to D1 dopamine receptor neurons by cre-mediated site-specific recombination. *J Neurosci* **18**, 9845–9857.
- Drobac E, Tricoire L, Chaffotte AF, Guiot E & Lambolez B (2010). Calcium imaging in single neurons from brain slices using bioluminescent reporters. *J Neurosci Res* **88**, 695–711.
- Durieux PF, Bearzatto B, Guiducci S, Buch T, Waisman A, Zoli M, Schiffmann SN & de Kerchove d'Exaerde A (2009). D2R striatopallidal neurons inhibit both locomotor and drug reward processes. *Nat Neurosci* **12**, 393–395.

- Durieux PF, Schiffmann SN & de Kerchove d'Exaerde A (2012). Differential regulation of motor control and response to dopaminergic drugs by D1R and D2R neurons in distinct dorsal striatum subregions. *EMBO J* **31**, 640–653.
- Ehrengruber MU, Lundstrom K, Schweitzer C, Heuss C, Schlesinger S & Gähwiler BH (1999). Recombinant Semliki Forest virus and Sindbis virus efficiently infect neurons in hippocampal slice cultures. *Proc Natl Acad Sci U S A* **96**, 7041–7046.
- Ehrman LA, Williams MT, Schaefer TL, Gudelsky GA, Reed TM, Fienberg AA, Greengard P & Vorhees CV (2006). Phosphodiesterase 1B differentially modulates the effects of methamphetamine on locomotor activity and spatial learning through DARPP32-dependent pathways: evidence from PDE1B-DARPP32 double-knockout mice. *Genes Brain Behav* **5**, 540–551.
- el-Husseini AE, Bladen C & Vincent SR (1995). Molecular characterization of a type II cyclic GMP-dependent protein kinase expressed in the rat brain. *J Neurochem* **64**, 2814–2817.
- El-Husseini AE, Williams J, Reiner PB, Pelech S & Vincent SR (1999). Localization of the cGMP-dependent protein kinases in relation to nitric oxide synthase in the brain. *J Chem Neuroanat* **17**, 45–55.
- Eliez S, Blasey CM, Freund LS, Hastie T & Reiss AL (2001). Brain anatomy, gender and IQ in children and adolescents with fragile X syndrome. *Brain* **124**, 1610–1618.
- Erard M, Fredj A, Pasquier H, Beltolngar DB, Bousmah Y, Derrien V, Vincent P & Merola F (2013). Minimum set of mutations needed to optimize cyan fluorescent proteins for live cell imaging. *Mol Biosyst* **9**, 258–267.
- Erneux C, Couchie D, Dumont JE, Baraniak J, Stec WJ, Abbad EG, Petridis G & Jastorff B (1981). Specificity of cyclic GMP activation of a multi-substrate cyclic nucleotide phosphodiesterase from rat liver. *Eur J Biochem* **115**, 503–510.
- Escande MV, Taravini IR, Zold CL, Belforte JE & Murer MG (2016). Loss of Homeostasis in the Direct Pathway in a Mouse Model of Asymptomatic Parkinson's Disease. *J Neurosci* **36**, 5686–5698.
- Fakhoury M (2015). Autistic spectrum disorders: A review of clinical features, theories and diagnosis. *Int J Dev Neurosci* **43**, 70–77.
- Fidock M, Miller M & Lanfear J (2002). Isolation and differential tissue distribution of two human cDNAs encoding PDE1 splice variants. *Cell Signal* **14**, 53–60.
- Fink JS, Weaver DR, Rivkees SA, Peterfreund RA, Pollack AE, Adler EM & Reppert SM (1992). Molecular cloning of the rat A2 adenosine receptor: selective co-expression with D2 dopamine receptors in rat striatum. *Brain Res Mol Brain Res* **14**, 186–195.
- Francis SH, Blount MA & Corbin JD (2011). Mammalian cyclic nucleotide phosphodiesterases: molecular mechanisms and physiological functions. *Physiol Rev* **91**, 651–690.
- Francis SH & Corbin JD (2011). PDE5 inhibitors: targeting erectile dysfunction in diabetics. *Curr Opin Pharmacol* **11**, 683–688.
- Fu Y, Yuan Y, Halliday G, Rusznák Z, Watson C & Paxinos G (2012). A cytoarchitectonic and chemoarchitectonic analysis of the dopamine cell groups in the substantia nigra, ventral tegmental area, and retrorubral field in the mouse. *Brain Struct Funct* **217**, 591–612.
- Fu YH, Kuhl DP, Pizzuti A, Pieretti M, Sutcliffe JS, Richards S, Verkerk AJ, Holden JJ, Fenwick RG & Warren ST (1991). Variation of the CGG repeat at the fragile X site results in genetic instability: resolution of the Sherman paradox. *Cell* **67**, 1047–1058.

- Fuccillo MV (2016). Striatal Circuits as a Common Node for Autism Pathophysiology. *Front Neurosci* **10**, 27.
- Fujishige K, Kotera J & Omori K (1999). Striatum- and testis-specific phosphodiesterase PDE10A isolation and characterization of a rat PDE10A. *Eur J Biochem* **266**, 1118–1127.
- Fujishige K, Kotera J, Yuasa K & Omori K (2000). The human phosphodiesterase PDE10A gene genomic organization and evolutionary relatedness with other PDEs containing GAF domains. *Eur J Biochem* **267**, 5943–5951.
- Gagnon D, Petryszyn S, Sanchez MG, Bories C, Beaulieu JM, De Koninck Y, Parent A & Parent M (2017). Striatal Neurons Expressing D1 and D2 Receptors are Morphologically Distinct and Differently Affected by Dopamine Denervation in Mice. *Sci Rep* **7**, 41432.
- Galarraga E, Hernández-López S, Reyes A, Barral J & Bargas J (1997). Dopamine facilitates striatal EPSPs through an L-type Ca²⁺ conductance. *Neuroreport* **8**, 2183–2186.
- Gandal MJ, Haney JR, Parikshak NN, Leppa V, Ramaswami G, Hartl C, Schork AJ, Appadurai V, Buil A, Werge TM, Liu C, White KP, CommonMind C, PsychENCODE C, iPSYCH-BROAD WG, Horvath S & Geschwind DH (2018). Shared molecular neuropathology across major psychiatric disorders parallels polygenic overlap. *Science* **359**, 693–697.
- Gangarossa G, Castell L, Castro L, Tarot P, Veyrunes F, Vincent P, Bertaso F & Valjent E (2019). Contrasting patterns of ERK activation in the tail of the striatum in response to aversive and rewarding signals. *J Neurochem*
- Gao T, Yatani A, Dell'Acqua ML, Sako H, Green SA, Dascal N, Scott JD & Hosey MM (1997). cAMP-dependent regulation of cardiac L-type Ca²⁺ channels requires membrane targeting of PKA and phosphorylation of channel subunits. *Neuron* **19**, 185–196.
- Gao X & Zhang J (2008). Spatiotemporal analysis of differential Akt regulation in plasma membrane microdomains. *Mol Biol Cell* **19**, 4366–4373.
- Garthwaite J (2008). Concepts of neural nitric oxide-mediated transmission. *Eur J Neurosci* **27**, 2783–2802.
- Geoffroy V, Fouque F, Nivet V, Clot JP, Lugnier C, Desbuquois B & Benelli C (1999). Activation of a cGMP-stimulated cAMP phosphodiesterase by protein kinase C in a liver Golgi-endosomal fraction. *Eur J Biochem* **259**, 892–900.
- Gerfen CR (1992a). The neostriatal mosaic: multiple levels of compartmental organization in the basal ganglia. *Annu Rev Neurosci* **15**, 285–320.
- Gerfen CR (1992b). The neostriatal mosaic: multiple levels of compartmental organization. *Trends Neurosci* **15**, 133–139.
- Gerfen CR, Baimbridge KG & Thibault J (1987). The neostriatal mosaic: III. Biochemical and developmental dissociation of patch-matrix mesostriatal systems. *J Neurosci* **7**, 3935–3944.
- Gerfen CR, Engber TM, Mahan LC, Susel Z, Chase TN, Monsma FJ & Sibley DR (1990). D1 and D2 dopamine receptor-regulated gene expression of striatonigral and striatopallidal neurons. *Science* **250**, 1429–1432.
- Gerfen CR, Paletzki R & Worley P (2008). Differences between dorsal and ventral striatum in Drd1a dopamine receptor coupling of dopamine- and cAMP-regulated

- phosphoprotein-32 to activation of extracellular signal-regulated kinase. *J Neurosci* **28**, 7113–7120.
- Gerfen CR & Surmeier DJ (2011). Modulation of striatal projection systems by dopamine. *Annu Rev Neurosci* **34**, 441–466.
- Gershman SJ & Uchida N (2019). Believing in dopamine. *Nat Rev Neurosci* **20**, 703–714.
- Gertler TS, Chan CS & Surmeier DJ (2008). Dichotomous anatomical properties of adult striatal medium spiny neurons. *J Neurosci* **28**, 10814–10824.
- Gervasi N, Hepp R, Tricoire L, Zhang J, Lambolez B, Paupardin-Tritsch D & Vincent P (2007). Dynamics of protein kinase A signaling at the membrane, in the cytosol, and in the nucleus of neurons in mouse brain slices. *J Neurosci* **27**, 2744–2750.
- Ghofrani HA, Osterloh IH & Grimminger F (2006). Sildenafil: from angina to erectile dysfunction to pulmonary hypertension and beyond. *Nat Rev Drug Discov* **5**, 689–702.
- Giampà C, Laurenti D, Anzilotti S, Bernardi G, Menniti FS & Fusco FR (2010). Inhibition of the striatal specific phosphodiesterase PDE10A ameliorates striatal and cortical pathology in R6/2 mouse model of Huntington’s disease. *PLoS One* **5**, e13417.
- Ginovart N & Kapur S (2012). Role of dopamine D(2) receptors for antipsychotic activity. *Handb Exp Pharmacol* 27–52.
- Giorgi M, Melchiorri G, Nuccetelli V, D’Angelo V, Martorana A, Sorge R, Castelli V, Bernardi G & Sancesario G (2011). PDE10A and PDE10A-dependent cAMP catabolism are dysregulated oppositely in striatum and nucleus accumbens after lesion of midbrain dopamine neurons in rat: a key step in parkinsonism physiopathology. *Neurobiol Dis* **43**, 293–303.
- Goaillard JM & Vincent P (2002). Serotonin suppresses the slow afterhyperpolarization in rat intralaminar and midline thalamic neurones by activating 5-HT(7) receptors. *J Physiol* **541**, 453–465.
- Goldberg JH & Fee MS (2012). A cortical motor nucleus drives the basal ganglia-recipient thalamus in singing birds. *Nat Neurosci* **15**, 620–627.
- Golden CE, Buxbaum JD & De Rubeis S (2018). Disrupted circuits in mouse models of autism spectrum disorder and intellectual disability. *Curr Opin Neurobiol* **48**, 106–112.
- Gonon F, Burie JB, Jaber M, Benoit-Marand M, Dumartin B & Bloch B (2000). Geometry and kinetics of dopaminergic transmission in the rat striatum and in mice lacking the dopamine transporter. *Prog Brain Res* **125**, 291–302.
- Gorbunova YV & Spitzer NC (2002). Dynamic interactions of cyclic AMP transients and spontaneous Ca(2+) spikes. *Nature* **418**, 93–96.
- Grashoff C, Hoffman BD, Brenner MD, Zhou R, Parsons M, Yang MT, McLean MA, Sligar SG, Chen CS, Ha T & Schwartz MA (2010). Measuring mechanical tension across vinculin reveals regulation of focal adhesion dynamics. *Nature* **466**, 263–266.
- Grauer SM, Pulito VL, Navarra RL, Kelly MP, Kelley C, Graf R, Langen B, Logue S, Brennan J, Jiang L, Charych E, Egerland U, Liu F, Marquis KL, Malamas M, Hage T, Comery TA & Brandon NJ (2009). Phosphodiesterase 10A inhibitor activity in preclinical models of the positive, cognitive, and negative symptoms of schizophrenia. *J Pharmacol Exp Ther* **331**, 574–590.
- Graveland GA, Williams RS & DiFiglia M (1985). A Golgi study of the human neostriatum: neurons and afferent fibers. *J Comp Neurol* **234**, 317–333.
- Graybiel AM (2000). The basal ganglia. *Curr Biol* **10**, R509–11.

- Graybiel AM (2008). Habits, rituals, and the evaluative brain. *Annu Rev Neurosci* **31**, 359–387.
- Greif GJ, Lin YJ, Liu JC & Freedman JE (1995). Dopamine-modulated potassium channels on rat striatal neurons: specific activation and cellular expression. *J Neurosci* **15**, 4533–4544.
- Grynkiewicz G, Poenie M & Tsien RY (1985). A new generation of Ca²⁺ indicators with greatly improved fluorescence properties. *J Biol Chem* **260**, 3440–3450.
- Håkansson K, Galdi S, Hendrick J, Snyder G, Greengard P & Fisone G (2006). Regulation of phosphorylation of the GluR1 AMPA receptor by dopamine D2 receptors. *J Neurochem* **96**, 482–488.
- Hallett PJ, Spoelgen R, Hyman BT, Standaert DG & Dunah AW (2006). Dopamine D1 activation potentiates striatal NMDA receptors by tyrosine phosphorylation-dependent subunit trafficking. *J Neurosci* **26**, 4690–4700.
- Harada A, Suzuki K, Kamiguchi N, Miyamoto M, Tohyama K, Nakashima K, Taniguchi T & Kimura H (2015). Characterization of binding and inhibitory properties of TAK-063, a novel phosphodiesterase 10A inhibitor. *PLoS One* **10**, e0122197.
- Harrison MB, Tissot M & Wiley RG (1996). Expression of m1 and m4 muscarinic receptor mRNA in the striatum following a selective lesion of striatonigral neurons. *Brain Res* **734**, 323–326.
- Harvey CD, Ehrhardt AG, Cellurale C, Zhong H, Yasuda R, Davis RJ & Svoboda K (2008). A genetically encoded fluorescent sensor of ERK activity. *Proc Natl Acad Sci U S A* **105**, 19264–19269.
- Hasbi A, Fan T, Alijaniam M, Nguyen T, Perreault ML, O’Dowd BF & George SR (2009). Calcium signaling cascade links dopamine D1-D2 receptor heteromer to striatal BDNF production and neuronal growth. *Proc Natl Acad Sci U S A* **106**, 21377–21382.
- Hatzelmann A, Morcillo EJ, Lungarella G, Adnot S, Sanjar S, Beume R, Schudt C & Tenor H (2010). The preclinical pharmacology of roflumilast--a selective, oral phosphodiesterase 4 inhibitor in development for chronic obstructive pulmonary disease. *Pulm Pharmacol Ther* **23**, 235–256.
- Haznedar MM, Buchsbaum MS, Hazlett EA, LiCalzi EM, Cartwright C & Hollander E (2006). Volumetric analysis and three-dimensional glucose metabolic mapping of the striatum and thalamus in patients with autism spectrum disorders. *Am J Psychiatry* **163**, 1252–1263.
- Hebb AL, Robertson HA & Denovan-Wright EM (2004). Striatal phosphodiesterase mRNA and protein levels are reduced in Huntington’s disease transgenic mice prior to the onset of motor symptoms. *Neuroscience* **123**, 967–981.
- Heiman M, Schaefer A, Gong S, Peterson JD, Day M, Ramsey KE, Suárez-Fariñas M, Schwarz C, Stephan DA, Surmeier DJ, Greengard P & Heintz N (2008). A translational profiling approach for the molecular characterization of CNS cell types. *Cell* **135**, 738–748.
- Hempel CM, Vincent P, Adams SR, Tsien RY & Saverston AI (1996). Spatio-temporal dynamics of cyclic AMP signals in an intact neural circuitm. *Nature* **384**, 166–169.
- Hepp R, Tricoire L, Hu E, Gervasi N, Paupardin-Tritsch D, Lambolez B & Vincent P (2007). Phosphodiesterase type 2 and the homeostasis of cyclic GMP in living thalamic neurons. *J Neurochem* **102**, 1875–1886.

- Herman JP, Dolgas CM, Rucker D & Langub MC (1996). Localization of natriuretic peptide-activated guanylate cyclase mRNAs in the rat brain. *J Comp Neurol* **369**, 165–187.
- Hernández-Echeagaray E, Starling AJ, Cepeda C & Levine MS (2004). Modulation of AMPA currents by D2 dopamine receptors in striatal medium-sized spiny neurons: are dendrites necessary. *Eur J Neurosci* **19**, 2455–2463.
- Hernandez-Lopez S, Tkatch T, Perez-Garci E, Galarraga E, Bargas J, Hamm H & Surmeier DJ (2000). D2 dopamine receptors in striatal medium spiny neurons reduce L-type Ca²⁺ currents and excitability via a novel PLC[β]₁-IP₃-calcineurin-signaling cascade. *J Neurosci* **20**, 8987–8995.
- Hersch SM, Ciliax BJ, Gutekunst CA, Rees HD, Heilman CJ, Yung KK, Bolam JP, Ince E, Yi H & Levey AI (1995). Electron microscopic analysis of D1 and D2 dopamine receptor proteins in the dorsal striatum and their synaptic relationships with motor corticostriatal afferents. *J Neurosci* **15**, 5222–5237.
- Higley MJ & Sabatini BL (2010). Competitive regulation of synaptic Ca²⁺ influx by D2 dopamine and A2A adenosine receptors. *Nat Neurosci* **13**, 958–966.
- Hikida T, Kimura K, Wada N, Funabiki K & Nakanishi S (2010). Distinct roles of synaptic transmission in direct and indirect striatal pathways to reward and aversive behavior. *Neuron* **66**, 896–907.
- Hikosaka O, Sesack SR, Lecourtier L & Shepard PD (2008). Habenula: crossroad between the basal ganglia and the limbic system. *J Neurosci* **28**, 11825–11829.
- Hikosaka O, Takikawa Y & Kawagoe R (2000). Role of the basal ganglia in the control of purposive saccadic eye movements. *Physiol Rev* **80**, 953–978.
- Hikosaka O & Wurtz RH (1983). Visual and oculomotor functions of monkey substantia nigra pars reticulata. III. Memory-contingent visual and saccade responses. *J Neurophysiol* **49**, 1268–1284.
- Hoffman RM & Yang M (2006). Whole-body imaging with fluorescent proteins. *Nat Protoc* **1**, 1429–1438.
- Hollander E, Anagnostou E, Chaplin W, Esposito K, Haznedar MM, Licalzi E, Wasserman S, Soorya L & Buchsbaum M (2005). Striatal volume on magnetic resonance imaging and repetitive behaviors in autism. *Biol Psychiatry* **58**, 226–232.
- Hollerman JR & Schultz W (1998). Dopamine neurons report an error in the temporal prediction of reward during learning. *Nat Neurosci* **1**, 304–309.
- Honda A, Adams SR, Sawyer CL, Lev-Ram V, Tsien RY & Dostmann WR (2001). Spatiotemporal dynamics of guanosine 3',5'-cyclic monophosphate revealed by a genetically encoded, fluorescent indicator. *Proc Natl Acad Sci U S A* **98**, 2437–2442.
- Hong KP, Spitzer NC & Nicol X (2011). Improved molecular toolkit for cAMP studies in live cells. *BMC Res Notes* **4**, 241.
- Hopkins AL (2008). Network pharmacology: the next paradigm in drug discovery. *Nat Chem Biol* **4**, 682–690.
- Houslay MD & Adams DR (2003). PDE4 cAMP phosphodiesterases: modular enzymes that orchestrate signalling cross-talk, desensitization and compartmentalization. *Biochem J* **370**, 1–18.
- Houslay MD, Baillie GS & Maurice DH (2007). cAMP-Specific phosphodiesterase-4 enzymes in the cardiovascular system: a molecular toolbox for generating compartmentalized cAMP signaling. *Circ Res* **100**, 950–966.

- Hyman SE, Malenka RC & Nestler EJ (2006). Neural mechanisms of addiction: the role of reward-related learning and memory. *Annu Rev Neurosci* **29**, 565–598.
- Ince E, Ciliax BJ & Levey AI (1997). Differential expression of D1 and D2 dopamine and m4 muscarinic acetylcholine receptor proteins in identified striatonigral neurons. *Synapse* **27**, 357–366.
- Jäger R, Russwurm C, Schwede F, Genieser HG, Koesling D & Russwurm M (2012). Activation of PDE10 and PDE11 phosphodiesterases. *J Biol Chem* **287**, 1210–1219.
- Jäger R, Schwede F, Genieser HG, Koesling D & Russwurm M (2010). Activation of PDE2 and PDE5 by specific GAF ligands: delayed activation of PDE5. *Br J Pharmacol* **161**, 1645–1660.
- Jares-Erijman EA & Jovin TM (2003). FRET imaging. *Nat Biotechnol* **21**, 1387–1395.
- Johnston LA, Erdogan S, Cheung YF, Sullivan M, Barber R, Lynch MJ, Baillie GS, Van Heeke G, Adams DR, Huston E & Houslay MD (2004). Expression, intracellular distribution and basis for lack of catalytic activity of the PDE4A7 isoform encoded by the human PDE4A cAMP-specific phosphodiesterase gene. *Biochem J* **380**, 371–384.
- Jurevicius J & Fischmeister R (1996). cAMP compartmentation is responsible for a local activation of cardiac Ca²⁺ channels by beta-adrenergic agonists. *Proc Natl Acad Sci U S A* **93**, 295–299.
- Kaidanovich-Beilin O & Woodgett JR (2011). GSK-3: Functional Insights from Cell Biology and Animal Models. *Front Mol Neurosci* **4**, 40.
- Kaufmann WE, Cohen S, Sun HT & Ho G (2002). Molecular phenotype of Fragile X syndrome: FMRP, FXRPs, and protein targets. *Microsc Res Tech* **57**, 135–144.
- Kawaguchi Y (1993). Physiological, morphological, and histochemical characterization of three classes of interneurons in rat neostriatum. *J Neurosci* **13**, 4908–4923.
- Kawaguchi Y (1997). Neostriatal cell subtypes and their functional roles. *Neurosci Res* **27**, 1–8.
- Kawaguchi Y, Wilson CJ, Augood SJ & Emson PC (1995). Striatal interneurons: chemical, physiological and morphological characterization. *Trends Neurosci* **18**, 527–535.
- Kawasaki H, Springett GM, Mochizuki N, Toki S, Nakaya M, Matsuda M, Housman DE & Graybiel AM (1998). A family of cAMP-binding proteins that directly activate Rap1. *Science* **282**, 2275–2279.
- Ke H & Wang H (2007). Crystal structures of phosphodiesterases and implications on substrate specificity and inhibitor selectivity. *Curr Top Med Chem* **7**, 391–403.
- Ke H, Wang H & Ye M (2011). Structural insight into the substrate specificity of phosphodiesterases. *Handb Exp Pharmacol* 121–134.
- Kehler J & Nielsen J (2011). PDE10A inhibitors: novel therapeutic drugs for schizophrenia. *Curr Pharm Des* **17**, 137–150.
- Kelly MP, Adamowicz W, Bove S, Hartman AJ, Mariga A, Pathak G, Reinhart V, Romegialli A & Kleiman RJ (2014). Select 3',5'-cyclic nucleotide phosphodiesterases exhibit altered expression in the aged rodent brain. *Cell Signal* **26**, 383–397.
- Kemp JM & Powell TP (1971a). The structure of the caudate nucleus of the cat: light and electron microscopy. *Philos Trans R Soc Lond B Biol Sci* **262**, 383–401.
- Kemp JM & Powell TP (1971b). The termination of fibres from the cerebral cortex and thalamus upon dendritic spines in the caudate nucleus: a study with the Golgi method. *Philos Trans R Soc Lond B Biol Sci* **262**, 429–439.

- Keravis T & Lugnier C (2012). Cyclic nucleotide phosphodiesterase (PDE) isozymes as targets of the intracellular signalling network: benefits of PDE inhibitors in various diseases and perspectives for future therapeutic developments. *Br J Pharmacol* **165**, 1288–1305.
- Khammy MM, Dalsgaard T, Larsen PH, Christoffersen CT, Clausen D, Rasmussen LK, Folkersen L, Grunnet M, Kehler J, Aalkjaer C & Nielsen J (2017). PDE1A inhibition elicits cGMP-dependent relaxation of rat mesenteric arteries. *Br J Pharmacol* **174**, 4186–4198.
- Kitai ST & Surmeier DJ (1993). Cholinergic and dopaminergic modulation of potassium conductances in neostriatal neurons. *Adv Neurol* **60**, 40–52.
- Klarenbeek J, Goedhart J, van Batenburg A, Groenewald D & Jalink K (2015). Fourth-generation epac-based FRET sensors for cAMP feature exceptional brightness, photostability and dynamic range: characterization of dedicated sensors for FLIM, for ratiometry and with high affinity. *PLoS One* **10**, e0122513.
- Klarenbeek JB, Goedhart J, Hink MA, Gadella TW & Jalink K (2011). A mTurquoise-based cAMP sensor for both FLIM and ratiometric read-out has improved dynamic range. *PLoS One* **6**, e19170.
- Klaus A, Alves da Silva J & Costa RM (2019). What, If, and When to Move: Basal Ganglia Circuits and Self-Paced Action Initiation. *Annu Rev Neurosci* **42**, 459–483.
- Kleiman RJ, Kimmel LH, Bove SE, Lanz TA, Harms JF, Romegialli A, Miller KS, Willis A, des Etages S, Kuhn M & Schmidt CJ (2011). Chronic suppression of phosphodiesterase 10A alters striatal expression of genes responsible for neurotransmitter synthesis, neurotransmission, and signaling pathways implicated in Huntington's disease. *J Pharmacol Exp Ther* **336**, 64–76.
- Komatsu H, Fukuchi M & Habata Y (2019). Potential Utility of Biased GPCR Signaling for Treatment of Psychiatric Disorders. *Int J Mol Sci* **20**,
- Komatsu N, Aoki K, Yamada M, Yukinaga H, Fujita Y, Kamioka Y & Matsuda M (2011). Development of an optimized backbone of FRET biosensors for kinases and GTPases. *Mol Biol Cell* **22**, 4647–4656.
- Kotera J, Fujishige K, Yuasa K & Omori K (1999). Characterization and phosphorylation of PDE10A2, a novel alternative splice variant of human phosphodiesterase that hydrolyzes cAMP and cGMP. *Biochem Biophys Res Commun* **261**, 551–557.
- Kotera J, Sasaki T, Kobayashi T, Fujishige K, Yamashita Y & Omori K (2004). Subcellular localization of cyclic nucleotide phosphodiesterase type 10A variants, and alteration of the localization by cAMP-dependent protein kinase-dependent phosphorylation. *J Biol Chem* **279**, 4366–4375.
- Kravitz AV, Freeze BS, Parker PR, Kay K, Thwin MT, Deisseroth K & Kreitzer AC (2010). Regulation of parkinsonian motor behaviours by optogenetic control of basal ganglia circuitry. *Nature* **466**, 622–626.
- Kreitzer AC (2009). Physiology and pharmacology of striatal neurons. *Annu Rev Neurosci* **32**, 127–147.
- Kritzer MD, Li J, Dodge-Kafka K & Kapiloff MS (2012). AKAPs: the architectural underpinnings of local cAMP signaling. *J Mol Cell Cardiol* **52**, 351–358.
- Kukreja RC, Salloum FN, Das A, Koka S, Ockaili RA & Xi L (2011). Emerging new uses of phosphodiesterase-5 inhibitors in cardiovascular diseases. *Exp Clin Cardiol* **16**, e30–5.

- Kunitomo J, Yoshikawa M, Fushimi M, Kawada A, Quinn JF, Oki H, Kokubo H, Kondo M, Nakashima K, Kamiguchi N, Suzuki K, Kimura H & Taniguchi T (2014). Discovery of 1-[2-fluoro-4-(1H-pyrazol-1-yl)phenyl]-5-methoxy-3-(1-phenyl-1H-pyrazol-5-yl)pyridazin-4(1H)-one (TAK-063), a highly potent, selective, and orally active phosphodiesterase 10A (PDE10A) inhibitor. *J Med Chem* **57**, 9627–9643.
- Kunkel MT, Ni Q, Tsien RY, Zhang J & Newton AC (2005). Spatio-temporal dynamics of protein kinase B/Akt signaling revealed by a genetically encoded fluorescent reporter. *J Biol Chem* **280**, 5581–5587.
- Kuo HY & Liu FC (2019). Synaptic Wiring of Corticostriatal Circuits in Basal Ganglia: Insights into the Pathogenesis of Neuropsychiatric Disorders. *eNeuro* **6**,
- Lakics V, Karran EH & Boess FG (2010). Quantitative comparison of phosphodiesterase mRNA distribution in human brain and peripheral tissues. *Neuropharmacology* **59**, 367–374.
- Lanciego JL, Luquin N & Obeso JA (2012). Functional neuroanatomy of the basal ganglia. *Cold Spring Harb Perspect Med* **2**, a009621.
- Lange H, Thörner G, Hopf A & Schröder KF (1976). Morphometric studies of the neuropathological changes in choreatic diseases. *J Neurol Sci* **28**, 401–425.
- Langen M, Durston S, Staal WG, Palmén SJ & van Engeland H (2007). Caudate nucleus is enlarged in high-functioning medication-naïve subjects with autism. *Biol Psychiatry* **62**, 262–266.
- Langen M, Leemans A, Johnston P, Ecker C, Daly E, Murphy CM, Dell’acqua F, Durston S, AIMS C & Murphy DG (2012). Fronto-striatal circuitry and inhibitory control in autism: findings from diffusion tensor imaging tractography. *Cortex* **48**, 183–193.
- Le Moine C & Bloch B (1995). D1 and D2 dopamine receptor gene expression in the rat striatum: sensitive cRNA probes demonstrate prominent segregation of D1 and D2 mRNAs in distinct neuronal populations of the dorsal and ventral striatum. *J Comp Neurol* **355**, 418–426.
- Lee KW, Hong JH, Choi IY, Che Y, Lee JK, Yang SD, Song CW, Kang HS, Lee JH, Noh JS, Shin HS & Han PL (2002). Impaired D2 dopamine receptor function in mice lacking type 5 adenylyl cyclase. *J Neurosci* **22**, 7931–7940.
- Lee LC, Maurice DH & Baillie GS (2013). Targeting protein-protein interactions within the cyclic AMP signaling system as a therapeutic strategy for cardiovascular disease. *Future Med Chem* **5**, 451–464.
- Lee Y, Kim H, Kim JE, Park JY, Choi J, Lee JE, Lee EH & Han PL (2018). Excessive D1 Dopamine Receptor Activation in the Dorsal Striatum Promotes Autistic-Like Behaviors. *Mol Neurobiol* **55**, 5658–5671.
- Lei W, Jiao Y, Del Mar N & Reiner A (2004). Evidence for differential cortical input to direct pathway versus indirect pathway striatal projection neurons in rats. *J Neurosci* **24**, 8289–8299.
- Levitt JG, O’Neill J, Blanton RE, Smalley S, Fadale D, McCracken JT, Guthrie D, Toga AW & Alger JR (2003). Proton magnetic resonance spectroscopic imaging of the brain in childhood autism. *Biol Psychiatry* **54**, 1355–1366.
- Li W & Pozzo-Miller L (2019). Dysfunction of the corticostriatal pathway in autism spectrum disorders. *J Neurosci Res*

- Lim J, Pahlke G & Conti M (1999). Activation of the cAMP-specific phosphodiesterase PDE4D3 by phosphorylation. Identification and function of an inhibitory domain. *J Biol Chem* **274**, 19677–19685.
- Lin DT, Fretier P, Jiang C & Vincent SR (2010). Nitric oxide signaling via cGMP-stimulated phosphodiesterase in striatal neurons. *Synapse* **64**, 460–466.
- Lissandron V, Terrin A, Collini M, D'alfonso L, Chirico G, Pantano S & Zaccolo M (2005). Improvement of a FRET-based indicator for cAMP by linker design and stabilization of donor-acceptor interaction. *J Mol Biol* **354**, 546–555.
- Lugnier C (2006). Cyclic nucleotide phosphodiesterase (PDE) superfamily: a new target for the development of specific therapeutic agents. *Pharmacol Ther* **109**, 366–398.
- Lugnier C, Keravis T, Le Bec A, Pauvert O, Proteau S & Rousseau E (1999). Characterization of cyclic nucleotide phosphodiesterase isoforms associated to isolated cardiac nuclei. *Biochim Biophys Acta* **1472**, 431–446.
- Lugnier C, Muller B, Le Bec A, Beaudry C & Rousseau E (1993). Characterization of indolidan- and rolipram-sensitive cyclic nucleotide phosphodiesterases in canine and human cardiac microsomal fractions. *J Pharmacol Exp Ther* **265**, 1142–1151.
- Lugnier C, Schoeffter P, Le Bec A, Strouthou E & Stoclet JC (1986). Selective inhibition of cyclic nucleotide phosphodiesterases of human, bovine and rat aorta. *Biochem Pharmacol* **35**, 1743–1751.
- Luo Y, Kokkonen GC, Wang X, Neve KA & Roth GS (1998). D2 dopamine receptors stimulate mitogenesis through pertussis toxin-sensitive G proteins and Ras-involved ERK and SAP/JNK pathways in rat C6-D2L glioma cells. *J Neurochem* **71**, 980–990.
- MacMullen CM, Vick K, Pacifico R, Fallahi-Sichani M & Davis RL (2016). Novel, primate-specific PDE10A isoform highlights gene expression complexity in human striatum with implications on the molecular pathology of bipolar disorder. *Transl Psychiatry* **6**, e742.
- Manallack DT, Hughes RA & Thompson PE (2005). The next generation of phosphodiesterase inhibitors: structural clues to ligand and substrate selectivity of phosphodiesterases. *J Med Chem* **48**, 3449–3462.
- Mank M & Griesbeck O (2008). Genetically encoded calcium indicators. *Chem Rev* **108**, 1550–1564.
- Mank M, Santos AF, Drenberger S, Mrcic-Flogel TD, Hofer SB, Stein V, Hendel T, Reiff DF, Levelt C, Borst A, Bonhoeffer T, Hübener M & Griesbeck O (2008). A genetically encoded calcium indicator for chronic in vivo two-photon imaging. *Nat Methods* **5**, 805–811.
- Martinez SE, Wu AY, Glavas NA, Tang XB, Turley S, Hol WG & Beavo JA (2002). The two GAF domains in phosphodiesterase 2A have distinct roles in dimerization and in cGMP binding. *Proc Natl Acad Sci U S A* **99**, 13260–13265.
- Martins TJ, Mumby MC & Beavo JA (1982). Purification and characterization of a cyclic GMP-stimulated cyclic nucleotide phosphodiesterase from bovine tissues. *J Biol Chem* **257**, 1973–1979.
- Matamales M, Bertran-Gonzalez J, Salomon L, Degos B, Deniau JM, Valjent E, Hervé D & Girault JA (2009). Striatal medium-sized spiny neurons: identification by nuclear staining and study of neuronal subpopulations in BAC transgenic mice. *PLoS One* **4**, e4770.

- Matsuoka I, Giuli G, Poyard M, Stengel D, Parma J, Guellaen G & Hanoune J (1992). Localization of adenylyl and guanylyl cyclase in rat brain by in situ hybridization: comparison with calmodulin mRNA distribution. *J Neurosci* **12**, 3350–3360.
- Matthiesen K & Nielsen J (2009). Binding of cyclic nucleotides to phosphodiesterase 10A and 11A GAF domains does not stimulate catalytic activity. *Biochem J* **423**, 401–409.
- Maurice DH (2005). Cyclic nucleotide phosphodiesterase-mediated integration of cGMP and cAMP signaling in cells of the cardiovascular system. *Front Biosci* **10**, 1221–1228.
- Maurice DH (2011). Subcellular signaling in the endothelium: cyclic nucleotides take their place. *Curr Opin Pharmacol* **11**, 656–664.
- Maurice DH, Ke H, Ahmad F, Wang Y, Chung J & Manganiello VC (2014). Advances in targeting cyclic nucleotide phosphodiesterases. *Nat Rev Drug Discov* **13**, 290–314.
- Maurin T, Lebrigand K, Castagnola S, Paquet A, Jarjat M, Popa A, Grossi M, Rage F & Bardoni B (2018a). HITS-CLIP in various brain areas reveals new targets and new modalities of RNA binding by fragile X mental retardation protein. *Nucleic Acids Res* **46**, 6344–6355.
- Maurin T, Melancia F, Jarjat M, Castro L, Costa L, Delhaye S, Khayachi A, Castagnola S, Mota E, Di Giorgio A, Servadio M, Drozd M, Poupon G, Schiavi S, Sardone L, Azoulay S, Ciranna L, Martin S, Vincent P, Trezza V & Bardoni B (2018b). Involvement of Phosphodiesterase 2A Activity in the Pathophysiology of Fragile X Syndrome. *Cereb Cortex* **29**, 3241–3252.
- Medina AE (2011). Therapeutic utility of phosphodiesterase type I inhibitors in neurological conditions. *Front Neurosci* **5**, 21.
- Menniti FS, Chappie TA, Humphrey JM & Schmidt CJ (2007). Phosphodiesterase 10A inhibitors: a novel approach to the treatment of the symptoms of schizophrenia. *Curr Opin Investig Drugs* **8**, 54–59.
- Mika D & Conti M (2016). PDE4D phosphorylation: A coincidence detector integrating multiple signaling pathways. *Cell Signal* **28**, 719–724.
- Mink JW (2003). The Basal Ganglia and involuntary movements: impaired inhibition of competing motor patterns. *Arch Neurol* **60**, 1365–1368.
- Mironov SL, Skorova E, Taschenberger G, Hartelt N, Nikolaev VO, Lohse MJ & Kügler S (2009). Imaging cytoplasmic cAMP in mouse brainstem neurons. *BMC Neurosci* **10**, 29.
- Missale C, Nash SR, Robinson SW, Jaber M & Caron MG (1998). Dopamine receptors: from structure to function. *Physiol Rev* **78**, 189–225.
- Miura H, Matsuda M & Aoki K (2014). Development of a FRET biosensor with high specificity for Akt. *Cell Struct Funct* **39**, 9–20.
- Miyawaki A (2003). Visualization of the spatial and temporal dynamics of intracellular signaling. *Dev Cell* **4**, 295–305.
- Miyawaki A, Llopis J, Heim R, McCaffery JM, Adams JA, Ikura M & Tsien RY (1997). Fluorescent indicators for Ca²⁺ based on green fluorescent proteins and calmodulin. *Nature* **388**, 882–887.
- Mongillo M, Tocchetti CG, Terrin A, Lissandron V, Cheung YF, Dostmann WR, Pozzan T, Kass DA, Paolucci N, Houslay MD & Zaccolo M (2006). Compartmentalized phosphodiesterase-2 activity blunts beta-adrenergic cardiac inotropy via an NO/cGMP-dependent pathway. *Circ Res* **98**, 226–234.
- Movsesian MA & Kukreja RC (2011). Phosphodiesterase inhibition in heart failure. *Handb Exp Pharmacol* 237–249.

- Nagai T, Yamada S, Tominaga T, Ichikawa M & Miyawaki A (2004). Expanded dynamic range of fluorescent indicators for Ca(2+) by circularly permuted yellow fluorescent proteins. *Proc Natl Acad Sci U S A* **101**, 10554–10559.
- Nair AG, Castro LRV, El Khoury M, Gorgievski V, Giros B, Tzavara ET, Hellgren-Kotaleski J & Vincent P (2019). The high efficacy of muscarinic M4 receptor in D1 medium spiny neurons reverses striatal hyperdopaminergia. *Neuropharmacology* **146**, 74–83.
- Nair AG, Gutierrez-Arenas O, Eriksson O, Vincent P & Hellgren Kotaleski J (2015). Sensing Positive versus Negative Reward Signals through Adenylyl Cyclase-Coupled GPCRs in Direct and Indirect Pathway Striatal Medium Spiny Neurons. *J Neurosci* **35**, 14017–14030.
- Nakai J, Ohkura M & Imoto K (2001). A high signal-to-noise Ca(2+) probe composed of a single green fluorescent protein. *Nat Biotechnol* **19**, 137–141.
- Nakanishi M, Anderson MP & Takumi T (2019). Recent genetic and functional insights in autism spectrum disorder. *Curr Opin Neurol* **32**, 627–634.
- Nakashima M, Imada H, Shiraishi E, Ito Y, Suzuki N, Miyamoto M, Taniguchi T & Iwashita H (2018). Phosphodiesterase 2A Inhibitor TAK-915 Ameliorates Cognitive Impairments and Social Withdrawal in. *J Pharmacol Exp Ther* **365**, 179–188.
- Nambu A (2008). Seven problems on the basal ganglia. *Curr Opin Neurobiol* **18**, 595–604.
- Nelson AB & Kreitzer AC (2014). Reassessing models of basal ganglia function and dysfunction. *Annu Rev Neurosci* **37**, 117–135.
- Neve KA, Seamans JK & Trantham-Davidson H (2004). Dopamine receptor signaling. *J Recept Signal Transduct Res* **24**, 165–205.
- Neves-Zaph SR (2017). Phosphodiesterase Diversity and Signal Processing Within cAMP Signaling Networks. *Adv Neurobiol* **17**, 3–14.
- Nicolini F, Foltynie T, Reis Marques T, Muhlert N, Tziortzi AC, Searle GE, Natesan S, Kapur S, Rabiner EA, Gunn RN, Piccini P & Politis M (2015). Loss of phosphodiesterase 10A expression is associated with progression and severity in Parkinson's disease. *Brain* **138**, 3003–3015.
- Nicola SM (2007). The nucleus accumbens as part of a basal ganglia action selection circuit. *Psychopharmacology (Berl)* **191**, 521–550.
- Nikolaev VO, Bünemann M, Hein L, Hannawacker A & Lohse MJ (2004). Novel single chain cAMP sensors for receptor-induced signal propagation. *J Biol Chem* **279**, 37215–37218.
- Nikolaev VO, Bünemann M, Schmitteckert E, Lohse MJ & Engelhardt S (2006). Cyclic AMP imaging in adult cardiac myocytes reveals far-reaching beta1-adrenergic but locally confined beta2-adrenergic receptor-mediated signaling. *Circ Res* **99**, 1084–1091.
- Nikolaev VO, Gambaryan S, Engelhardt S, Walter U & Lohse MJ (2005). Real-time monitoring of the PDE2 activity of live cells: hormone-stimulated cAMP hydrolysis is faster than hormone-stimulated cAMP synthesis. *J Biol Chem* **280**, 1716–1719.
- Nishi A, Kuroiwa M, Miller DB, O'Callaghan JP, Bateup HS, Shuto T, Sotogaku N, Fukuda T, Heintz N, Greengard P & Snyder GL (2008). Distinct roles of PDE4 and PDE10A in the regulation of cAMP/PKA signaling in the striatum. *J Neurosci* **28**, 10460–10471.
- Nishi A, Snyder GL & Greengard P (1997). Bidirectional regulation of DARPP-32 phosphorylation by dopamine. *J Neurosci* **17**, 8147–8155.
- Norris RP, Ratzan WJ, Freudzon M, Mehlmann LM, Krall J, Movsesian MA, Wang H, Ke H, Nikolaev VO & Jaffe LA (2009). Cyclic GMP from the surrounding somatic cells regulates cyclic AMP and meiosis in the mouse oocyte. *Development* **136**, 1869–1878.

- Oak JN, Lavine N & Van Tol HH (2001). Dopamine D(4) and D(2L) Receptor Stimulation of the Mitogen-Activated Protein Kinase Pathway Is Dependent on trans-Activation of the Platelet-Derived Growth Factor Receptor. *Mol Pharmacol* **60**, 92–103.
- Oberlé I, Rousseau F, Heitz D, Kretz C, Devys D, Hanauer A, Boué J, Bertheas MF & Mandel JL (1991). Instability of a 550-base pair DNA segment and abnormal methylation in fragile X syndrome. *Science* **252**, 1097–1102.
- Ohkura M, Matsuzaki M, Kasai H, Imoto K & Nakai J (2005). Genetically encoded bright Ca²⁺ probe applicable for dynamic Ca²⁺ imaging of dendritic spines. *Anal Chem* **77**, 5861–5869.
- Olson PA, Tkatch T, Hernandez-Lopez S, Ulrich S, Ilijic E, Mugnaini E, Zhang H, Bezprozvanny I & Surmeier DJ (2005). G-protein-coupled receptor modulation of striatal CaV1.3 L-type Ca²⁺ channels is dependent on a Shank-binding domain. *J Neurosci* **25**, 1050–1062.
- Omori K & Kotera J (2007). Overview of PDEs and their regulation. *Circ Res* **100**, 309–327.
- Oorschot DE (1996). Total number of neurons in the neostriatal, pallidal, subthalamic, and substantia nigral nuclei of the rat basal ganglia: a stereological study using the cavalieri and optical disector methods. *J Comp Neurol* **366**, 580–599.
- Padilla-Parra S & Tramier M (2012). FRET microscopy in the living cell: different approaches, strengths and weaknesses. *Bioessays* **34**, 369–376.
- Palmer AE, Giacomello M, Kortemme T, Hires SA, Lev-Ram V, Baker D & Tsien RY (2006). Ca²⁺ indicators based on computationally redesigned calmodulin-peptide pairs. *Chem Biol* **13**, 521–530.
- Pandit J, Forman MD, Fennell KF, Dillman KS & Menniti FS (2009). Mechanism for the allosteric regulation of phosphodiesterase 2A deduced from the X-ray structure of a near full-length construct. *Proc Natl Acad Sci U S A* **106**, 18225–18230.
- Parthasarathy HB & Graybiel AM (1997). Cortically driven immediate-early gene expression reflects modular influence of sensorimotor cortex on identified striatal neurons in the squirrel monkey. *J Neurosci* **17**, 2477–2491.
- Pascoli V, Cahill E, Bellivier F, Caboche J & Vanhoutte P (2014). Extracellular signal-regulated protein kinases 1 and 2 activation by addictive drugs: a signal toward pathological adaptation. *Biol Psychiatry* **76**, 917–926.
- Pekcec A, Schülert N, Stierstorfer B, Deiana S, Dorner-Ciossek C & Rosenbrock H (2018). Targeting the dopamine D. *Br J Pharmacol* **175**, 3021–3033.
- Penney JB & Young AB (1983). Speculations on the functional anatomy of basal ganglia disorders. *Annu Rev Neurosci* **6**, 73–94.
- Pérez-Torres S, Miró X, Palacios JM, Cortés R, Puigdoménech P & Mengod G (2000). Phosphodiesterase type 4 isozymes expression in human brain examined by in situ hybridization histochemistry and [³H]rolipram binding autoradiography. Comparison with monkey and rat brain. *J Chem Neuroanat* **20**, 349–374.
- Pieretti M, Zhang FP, Fu YH, Warren ST, Oostra BA, Caskey CT & Nelson DL (1991). Absence of expression of the FMR-1 gene in fragile X syndrome. *Cell* **66**, 817–822.
- Plattner F, Hayashi K, Hernández A, Benavides DR, Tassin TC, Tan C, Day J, Fina MW, Yuen EY, Yan Z, Goldberg MS, Nairn AC, Greengard P, Nestler EJ, Taussig R, Nishi A, Houslay MD & Bibb JA (2015). The role of ventral striatal cAMP signaling in stress-induced behaviors. *Nat Neurosci* **18**, 1094–1100.

- Podda MV & Grassi C (2014). New perspectives in cyclic nucleotide-mediated functions in the CNS: the emerging role of cyclic nucleotide-gated (CNG) channels. *Pflugers Arch* **466**, 1241–1257.
- Polito M, Guiot E, Gangarossa G, Longueville S, Doulazmi M, Valjent E, Hervé D, Girault JA, Paupardin-Tritsch D, Castro LR & Vincent P (2015). Selective Effects of PDE10A Inhibitors on Striatopallidal Neurons Require Phosphatase Inhibition by DARPP-32. *eNeuro* **2**,
- Polito M, Klarenbeek J, Jalink K, Paupardin-Tritsch D, Vincent P & Castro LR (2013). The NO/cGMP pathway inhibits transient cAMP signals through the activation of PDE2 in striatal neurons. *Front Cell Neurosci* **7**, 211.
- Polito M, Vincent P & Guiot E (2014). Biosensor imaging in brain slice preparations. *Methods Mol Biol* **1071**, 175–194.
- Polli JW & Kincaid RL (1994). Expression of a calmodulin-dependent phosphodiesterase isoform (PDE1B1) correlates with brain regions having extensive dopaminergic innervation. *J Neurosci* **14**, 1251–1261.
- Ponsioen B, Zhao J, Riedl J, Zwartkruis F, van der Krogt G, Zaccolo M, Moolenaar WH, Bos JL & Jalink K (2004). Detecting cAMP-induced Epac activation by fluorescence resonance energy transfer: Epac as a novel cAMP indicator. *EMBO Rep* **5**, 1176–1180.
- Poppe H, Rybalkin SD, Rehmann H, Hinds TR, Tang XB, Christensen AE, Schwede F, Genieser HG, Bos JL, Doskeland SO, Beavo JA & Butt E (2008). Cyclic nucleotide analogs as probes of signaling pathways. *Nat Methods* **5**, 277–278.
- Poulin JF, Caronia G, Hofer C, Cui Q, Helm B, Ramakrishnan C, Chan CS, Dombeck DA, Deisseroth K & Awatramani R (2018). Mapping projections of molecularly defined dopamine neuron subtypes using intersectional genetic approaches. *Nat Neurosci* **21**, 1260–1271.
- Poulin JF, Zou J, Drouin-Ouellet J, Kim KY, Cicchetti F & Awatramani RB (2014). Defining midbrain dopaminergic neuron diversity by single-cell gene expression profiling. *Cell Rep* **9**, 930–943.
- Prensa L & Parent A (2001). The nigrostriatal pathway in the rat: A single-axon study of the relationship between dorsal and ventral tier nigral neurons and the striosome/matrix striatal compartments. *J Neurosci* **21**, 7247–7260.
- Rampersad SN, Ovens JD, Huston E, Umana MB, Wilson LS, Netherton SJ, Lynch MJ, Baillie GS, Houslay MD & Maurice DH (2010). Cyclic AMP phosphodiesterase 4D (PDE4D) Tethers EPAC1 in a vascular endothelial cadherin (VE-Cad)-based signaling complex and controls cAMP-mediated vascular permeability. *J Biol Chem* **285**, 33614–33622.
- Redgrave P, Rodriguez M, Smith Y, Rodriguez-Oroz MC, Lehericy S, Bergman H, Agid Y, DeLong MR & Obeso JA (2010). Goal-directed and habitual control in the basal ganglia: implications for Parkinson's disease. *Nat Rev Neurosci* **11**, 760–772.
- Redrobe JP, Jørgensen M, Christoffersen CT, Montezinho LP, Bastlund JF, Carnerup M, Bundgaard C, Lerdrup L & Plath N (2014). In vitro and in vivo characterisation of Lu AF64280, a novel, brain penetrant phosphodiesterase (PDE) 2A inhibitor: potential relevance to cognitive deficits in schizophrenia. *Psychopharmacology (Berl)* **231**, 3151–3167.

- Redrobe JP, Rasmussen LK, Christoffersen CT, Bundgaard C & Jørgensen M (2015). Characterisation of Lu AF33241: A novel, brain-penetrant, dual inhibitor of phosphodiesterase (PDE) 2A and PDE10A. *Eur J Pharmacol* **761**, 79–85.
- Reed TM, Repaske DR, Snyder GL, Greengard P & Vorhees CV (2002). Phosphodiesterase 1B knock-out mice exhibit exaggerated locomotor hyperactivity and DARPP-32 phosphorylation in response to dopamine agonists and display impaired spatial learning. *J Neurosci* **22**, 5188–5197.
- Reneerkens OA, Rutten K, Steinbusch HW, Blokland A & Prickaerts J (2009). Selective phosphodiesterase inhibitors: a promising target for cognition enhancement. *Psychopharmacology (Berl)* **202**, 419–443.
- Repaske DR, Corbin JG, Conti M & Goy MF (1993). A cyclic GMP-stimulated cyclic nucleotide phosphodiesterase gene is highly expressed in the limbic system of the rat brain. *Neuroscience* **56**, 673–686.
- Reyes-Irisarri E, Markerink-Van Ittersum M, Mengod G & de Vente J (2007). Expression of the cGMP-specific phosphodiesterases 2 and 9 in normal and Alzheimer's disease human brains. *Eur J Neurosci* **25**, 3332–3338.
- Richter W & Conti M (2004). The oligomerization state determines regulatory properties and inhibitor sensitivity of type 4 cAMP-specific phosphodiesterases. *J Biol Chem* **279**, 30338–30348.
- Rothwell PE (2016). Autism Spectrum Disorders and Drug Addiction: Common Pathways, Common Molecules, Distinct Disorders. *Front Neurosci* **10**, 20.
- Rushlow W, Flumerfelt BA & Naus CC (1995). Colocalization of somatostatin, neuropeptide Y, and NADPH-diaphorase in the caudate-putamen of the rat. *J Comp Neurol* **351**, 499–508.
- Russell DS, Barret O, Jennings DL, Friedman JH, Tamagnan GD, Thomae D, Alagille D, Morley TJ, Papin C, Papapetropoulos S, Waterhouse RN, Seibyl JP & Marek KL (2014). The phosphodiesterase 10 positron emission tomography tracer, [18F]MNI-659, as a novel biomarker for early Huntington disease. *JAMA Neurol* **71**, 1520–1528.
- Russell DS, Jennings DL, Barret O, Tamagnan GD, Carroll VM, Caillé F, Alagille D, Morley TJ, Papin C, Seibyl JP & Marek KL (2016). Change in PDE10 across early Huntington disease assessed by [18F]MNI-659 and PET imaging. *Neurology* **86**, 748–754.
- Russwurm C, Koesling D & Russwurm M (2015). Phosphodiesterase 10A Is Tethered to a Synaptic Signaling Complex in Striatum. *J Biol Chem* **290**, 11936–11947.
- Russwurm M, Mullershausen F, Friebe A, Jäger R, Russwurm C & Koesling D (2007). Design of fluorescence resonance energy transfer (FRET)-based cGMP indicators: a systematic approach. *Biochem J* **407**, 69–77.
- Rymar VV, Sasseville R, Luk KC & Sadikot AF (2004). Neurogenesis and stereological morphometry of calretinin-immunoreactive GABAergic interneurons of the neostriatum. *J Comp Neurol* **469**, 325–339.
- Sadhu K, Hensley K, Florio VA & Wolda SL (1999). Differential expression of the cyclic GMP-stimulated phosphodiesterase PDE2A in human venous and capillary endothelial cells. *J Histochem Cytochem* **47**, 895–906.
- Sano H, Yasoshima Y, Matsushita N, Kaneko T, Kohno K, Pastan I & Kobayashi K (2003). Conditional ablation of striatal neuronal types containing dopamine D2 receptor disturbs coordination of basal ganglia function. *J Neurosci* **23**, 9078–9088.

- Sasaki K, Sato M & Umezawa Y (2003). Fluorescent indicators for Akt/protein kinase B and dynamics of Akt activity visualized in living cells. *J Biol Chem* **278**, 30945–30951.
- Savchenko A, Barnes S & Kramer RH (1997). Cyclic-nucleotide-gated channels mediate synaptic feedback by nitric oxide. *Nature* **390**, 694–698.
- Schiffmann SN, Desdouits F, Menu R, Greengard P, Vincent JD, Vanderhaeghen JJ & Girault JA (1998). Modulation of the voltage-gated sodium current in rat striatal neurons by DARPP-32, an inhibitor of protein phosphatase. *Eur J Neurosci* **10**, 1312–1320.
- Schiffmann SN, Jacobs O & Vanderhaeghen JJ (1991). Striatal restricted adenosine A2 receptor (RDC8) is expressed by enkephalin but not by substance P neurons: an in situ hybridization histochemistry study. *J Neurochem* **57**, 1062–1067.
- Schiffmann SN & Vanderhaeghen JJ (1993). Adenosine A2 receptors regulate the gene expression of striatopallidal and striatonigral neurons. *J Neurosci* **13**, 1080–1087.
- Schmidt CJ, Chapin DS, Cianfrogna J, Corman ML, Hajos M, Harms JF, Hoffman WE, Lebel LA, McCarthy SA, Nelson FR, Proulx-LaFrance C, Majchrzak MJ, Ramirez AD, Schmidt K, Seymour PA, Siuciak JA, Tingley FD, Williams RD, Verhoest PR & Menniti FS (2008). Preclinical characterization of selective phosphodiesterase 10A inhibitors: a new therapeutic approach to the treatment of schizophrenia. *J Pharmacol Exp Ther* **325**, 681–690.
- Schröder S, Wenzel B, Deuther-Conrad W, Scheunemann M & Brust P (2016). Novel Radioligands for Cyclic Nucleotide Phosphodiesterase Imaging with Positron Emission Tomography: An Update on Developments Since 2012. *Molecules* **21**,
- Schudt C, Hatzelmann A, Beume R & Tenor H (2011). Phosphodiesterase inhibitors: history of pharmacology. *Handb Exp Pharmacol* 1–46.
- Schülke JP & Brandon NJ (2017). Current Understanding of PDE10A in the Modulation of Basal Ganglia Circuitry. *Adv Neurobiol* **17**, 15–43.
- Schülke JP, McAllister LA, Geoghegan KF, Parikh V, Chappie TA, Verhoest PR, Schmidt CJ, Johnson DS & Brandon NJ (2014). Chemoproteomics demonstrates target engagement and exquisite selectivity of the clinical phosphodiesterase 10A inhibitor MP-10 in its native environment. *ACS Chem Biol* **9**, 2823–2832.
- Schultz W (1998). Predictive reward signal of dopamine neurons. *J Neurophysiol* **80**, 1–27.
- Schultz W (2007). Multiple dopamine functions at different time courses. *Annu Rev Neurosci* **30**, 259–288.
- Schultz W (2019). Recent advances in understanding the role of phasic dopamine activity. *F1000Res* **8**,
- Schwabe U, Miyake M, Ohga Y & Daly JW (1976). 4-(3-Cyclopentyloxy-4-methoxyphenyl)-2-pyrrolidone (ZK 62711): a potent inhibitor of adenosine cyclic 3',5'-monophosphate phosphodiesterases in homogenates and tissue slices from rat brain. *Mol Pharmacol* **12**, 900–910.
- Sears LL, Vest C, Mohamed S, Bailey J, Ranson BJ & Piven J (1999). An MRI study of the basal ganglia in autism. *Prog Neuropsychopharmacol Biol Psychiatry* **23**, 613–624.
- Seeger TF, Bartlett B, Coskran TM, Culp JS, James LC, Krull DL, Lanfear J, Ryan AM, Schmidt CJ, Strick CA, Varghese AH, Williams RD, Wylie PG & Menniti FS (2003). Immunohistochemical localization of PDE10A in the rat brain. *Brain Res* **985**, 113–126.
- Shepherd GM (2013). Corticostriatal connectivity and its role in disease. *Nat Rev Neurosci* **14**, 278–291.

- Shioda N, Yabuki Y, Wang Y, Uchigashima M, Hikida T, Sasaoka T, Mori H, Watanabe M, Sasahara M & Fukunaga K (2017). Endocytosis following dopamine D₂ receptor activation is critical for neuronal activity and dendritic spine formation via Rabex-5/PDGFR β signaling in striatopallidal medium spiny neurons. *Mol Psychiatry* **22**, 1205–1222.
- Silk TJ, Rinehart N, Bradshaw JL, Tonge B, Egan G, O’Boyle MW & Cunnington R (2006). Visuospatial processing and the function of prefrontal-parietal networks in autism spectrum disorders: a functional MRI study. *Am J Psychiatry* **163**, 1440–1443.
- Simpson EH, Kellendonk C & Kandel E (2010). A possible role for the striatum in the pathogenesis of the cognitive symptoms of schizophrenia. *Neuron* **65**, 585–596.
- Sitges M & Nekrassov V (1999). Vinpocetine selectively inhibits neurotransmitter release triggered by sodium channel activation. *Neurochem Res* **24**, 1585–1591.
- Siuciak JA, Chapin DS, Harms JF, Lebel LA, McCarthy SA, Chambers L, Shrikhande A, Wong S, Menniti FS & Schmidt CJ (2006). Inhibition of the striatum-enriched phosphodiesterase PDE10A: a novel approach to the treatment of psychosis. *Neuropharmacology* **51**, 386–396.
- Skroblin P, Grossmann S, Schäfer G, Rosenthal W & Klusmann E (2010). Mechanisms of protein kinase A anchoring. *Int Rev Cell Mol Biol* **283**, 235–330.
- Smith Y, Bennett BD, Bolam JP, Parent A & Sadikot AF (1994). Synaptic relationships between dopaminergic afferents and cortical or thalamic input in the sensorimotor territory of the striatum in monkey. *J Comp Neurol* **344**, 1–19.
- Smith Y, Bevan MD, Shink E & Bolam JP (1998). Microcircuitry of the direct and indirect pathways of the basal ganglia. *Neuroscience* **86**, 353–387.
- Snyder GL, Allen PB, Fienberg AA, Valle CG, Haganir RL, Nairn AC & Greengard P (2000). Regulation of phosphorylation of the GluR1 AMPA receptor in the neostriatum by dopamine and psychostimulants in vivo. *J Neurosci* **20**, 4480–4488.
- Snyder GL, Prickaerts J, Wadenberg ML, Zhang L, Zheng H, Yao W, Akkerman S, Zhu H, Hendrick JP, Vanover KE, Davis R, Li P, Mates S & Wennogle LP (2016). Preclinical profile of ITI-214, an inhibitor of phosphodiesterase 1, for enhancement of memory performance in rats. *Psychopharmacology (Berl)* **233**, 3113–3124.
- Soderling SH & Beavo JA (2000). Regulation of cAMP and cGMP signaling: new phosphodiesterases and new functions. *Curr Opin Cell Biol* **12**, 174–179.
- Sparta B, Pargett M, Minguet M, Distor K, Bell G & Albeck JG (2015). Receptor Level Mechanisms Are Required for Epidermal Growth Factor (EGF)-stimulated Extracellular Signal-regulated Kinase (ERK) Activity Pulses. *J Biol Chem* **290**, 24784–24792.
- Stangherlin A, Gesellchen F, Zoccarato A, Terrin A, Fields LA, Berrera M, Surdo NC, Craig MA, Smith G, Hamilton G & Zaccolo M (2011). cGMP signals modulate cAMP levels in a compartment-specific manner to regulate catecholamine-dependent signaling in cardiac myocytes. *Circ Res* **108**, 929–939.
- Stangherlin A & Zaccolo M (2012). cGMP-cAMP interplay in cardiac myocytes: a local affair with far-reaching consequences for heart function. *Biochem Soc Trans* **40**, 11–14.
- Stephenson DT, Coskran TM, Kelly MP, Kleiman RJ, Morton D, O’Neill SM, Schmidt CJ, Weinberg RJ & Menniti FS (2012). The distribution of phosphodiesterase 2A in the rat brain. *Neuroscience* **226**, 145–155.
- Stephenson DT, Coskran TM, Wilhelms MB, Adamowicz WO, O’Donnell MM, Muravnick KB, Menniti FS, Kleiman RJ & Morton D (2009). Immunohistochemical localization of

- phosphodiesterase 2A in multiple mammalian species. *J Histochem Cytochem* **57**, 933–949.
- Stoof JC & Kebabian JW (1984). Two dopamine receptors: biochemistry, physiology and pharmacology. *Life Sci* **35**, 2281–2296.
- Strick CA, James LC, Fox CB, Seeger TF, Menniti FS & Schmidt CJ (2010). Alterations in gene regulation following inhibition of the striatum-enriched phosphodiesterase, PDE10A. *Neuropharmacology* **58**, 444–451.
- Strick CA, Schmidt CJ & Menniti FS (2006). PDE10A: a striatum-enriched, dual-substrate phosphodiesterase. *Cyclic nucleotide phosphodiesterases in health and disease Boca Raton: CRC Press* p. 237–54.
- Sun X, Zhao Y & Wolf ME (2005). Dopamine receptor stimulation modulates AMPA receptor synaptic insertion in prefrontal cortex neurons. *J Neurosci* **25**, 7342–7351.
- Surmeier DJ, Bargas J, Hemmings HC, Nairn AC & Greengard P (1995). Modulation of calcium currents by a D1 dopaminergic protein kinase/phosphatase cascade in rat neostriatal neurons. *Neuron* **14**, 385–397.
- Surmeier DJ, Ding J, Day M, Wang Z & Shen W (2007). D1 and D2 dopamine-receptor modulation of striatal glutamatergic signaling in striatal medium spiny neurons. *Trends Neurosci* **30**, 228–235.
- Surmeier DJ, Eberwine J, Wilson CJ, Cao Y, Stefani A & Kitai ST (1992). Dopamine receptor subtypes colocalize in rat striatonigral neurons. *Proc Natl Acad Sci U S A* **89**, 10178–10182.
- Sutcliffe JS, Nelson DL, Zhang F, Pieretti M, Caskey CT, Saxe D & Warren ST (1992). DNA methylation represses FMR-1 transcription in fragile X syndrome. *Hum Mol Genet* **1**, 397–400.
- Tabolacci E, Palumbo F, Nobile V & Neri G (2016). Transcriptional Reactivation of the FMR1 Gene. A Possible Approach to the Treatment of the Fragile X Syndrome. *Genes (Basel)* **7**,
- Tai LH, Lee AM, Benavidez N, Bonci A & Wilbrecht L (2012). Transient stimulation of distinct subpopulations of striatal neurons mimics changes in action value. *Nat Neurosci* **15**, 1281–1289.
- Takarae Y, Minshew NJ, Luna B & Sweeney JA (2007). Atypical involvement of frontostriatal systems during sensorimotor control in autism. *Psychiatry Res* **156**, 117–127.
- Tallini YN, Ohkura M, Choi BR, Ji G, Imoto K, Doran R, Lee J, Plan P, Wilson J, Xin HB, Sanbe A, Gulick J, Mathai J, Robbins J, Salama G, Nakai J & Kotlikoff MI (2006). Imaging cellular signals in the heart in vivo: Cardiac expression of the high-signal Ca²⁺ indicator GCaMP2. *Proc Natl Acad Sci U S A* **103**, 4753–4758.
- Tenor H, Hatzelmann A, Beume R, Lahu G, Zech K & Bethke TD (2011). Pharmacology, clinical efficacy, and tolerability of phosphodiesterase-4 inhibitors: impact of human pharmacokinetics. *Handb Exp Pharmacol* 85–119.
- Tepper JM & Bolam JP (2004). Functional diversity and specificity of neostriatal interneurons. *Curr Opin Neurobiol* **14**, 685–692.
- Tepper JM, Koós T, Ibanez-Sandoval O, Tecuapetla F, Faust TW & Assous M (2018). Heterogeneity and Diversity of Striatal GABAergic Interneurons: Update 2018. *Front Neuroanat* **12**, 91.
- Tepper JM, Koós T & Wilson CJ (2004). GABAergic microcircuits in the neostriatum. *Trends Neurosci* **27**, 662–669.

- Tepper JM, Wilson CJ & Koós T (2008). Feedforward and feedback inhibition in neostriatal GABAergic spiny neurons. *Brain Res Rev* **58**, 272–281.
- Teroganova N, Girshkin L, Suter CM & Green MJ (2016). DNA methylation in peripheral tissue of schizophrenia and bipolar disorder: a systematic review. *BMC Genet* **17**, 27.
- Terrin A, Monterisi S, Stangherlin A, Zoccarato A, Koschinski A, Surdo NC, Mongillo M, Sawa A, Jordanides NE, Mountford JC & Zaccolo M (2012). PKA and PDE4D3 anchoring to AKAP9 provides distinct regulation of cAMP signals at the centrosome. *J Cell Biol* **198**, 607–621.
- Thestrup T, Litzlbauer J, Bartholomäus I, Mues M, Russo L, Dana H, Kovalchuk Y, Liang Y, Kalamakis G, Laukat Y, Becker S, Witte G, Geiger A, Allen T, Rome LC, Chen TW, Kim DS, Garaschuk O, Griesinger C & Griesbeck O (2014). Optimized ratiometric calcium sensors for functional in vivo imaging of neurons and T lymphocytes. *Nat Methods* **11**, 175–182.
- Thibault D, Loustalot F, Fortin GM, Bourque MJ & Trudeau LÉ (2013). Evaluation of D1 and D2 dopamine receptor segregation in the developing striatum using BAC transgenic mice. *PLoS One* **8**, e67219.
- Tian L, Hires SA, Mao T, Huber D, Chiappe ME, Chalasani SH, Petreanu L, Akerboom J, McKinney SA, Schreiter ER, Bargmann CI, Jayaraman V, Svoboda K & Looger LL (2009). Imaging neural activity in worms, flies and mice with improved GCaMP calcium indicators. *Nat Methods* **6**, 875–881.
- Turner KC, Frost L, Linsenhardt D, McIlroy JR & Müller RA (2006). Atypically diffuse functional connectivity between caudate nuclei and cerebral cortex in autism. *Behav Brain Funct* **2**, 34.
- Turner RS & Anderson ME (1997). Pallidal discharge related to the kinematics of reaching movements in two dimensions. *J Neurophysiol* **77**, 1051–1074.
- Turner RS & Anderson ME (2005). Context-dependent modulation of movement-related discharge in the primate globus pallidus. *J Neurosci* **25**, 2965–2976.
- Umezawa Y (2005). Genetically encoded optical probes for imaging cellular signaling pathways. *Biosens Bioelectron* **20**, 2504–2511.
- Urs NM, Peterson SM & Caron MG (2017). New Concepts in Dopamine D. *Biol Psychiatry* **81**, 78–85.
- Urs NM, Snyder JC, Jacobsen JP, Peterson SM & Caron MG (2012). Deletion of GSK3 β in D2R-expressing neurons reveals distinct roles for β -arrestin signaling in antipsychotic and lithium action. *Proc Natl Acad Sci U S A* **109**, 20732–20737.
- Valjent E, Bertran-Gonzalez J, Aubier B, Greengard P, Hervé D & Girault JA (2010). Mechanisms of locomotor sensitization to drugs of abuse in a two-injection protocol. *Neuropsychopharmacology* **35**, 401–415.
- Valjent E, Bertran-Gonzalez J, Hervé D, Fisone G & Girault JA (2009). Looking BAC at striatal signaling: cell-specific analysis in new transgenic mice. *Trends Neurosci* **32**, 538–547.
- Valjent E, Caboche J & Vanhoutte P (2001). Mitogen-activated protein kinase/extracellular signal-regulated kinase induced gene regulation in brain: a molecular substrate for learning and memory. *Mol Neurobiol* **23**, 83–99.
- Valjent E, Pascoli V, Svenningsson P, Paul S, Enslen H, Corvol JC, Stipanovich A, Caboche J, Lombroso PJ, Nairn AC, Greengard P, Hervé D & Girault JA (2005). Regulation of a

- protein phosphatase cascade allows convergent dopamine and glutamate signals to activate ERK in the striatum. *Proc Natl Acad Sci U S A* **102**, 491–496.
- Vallin B, Legueux-Cajgfinger Y, Clément N, Glorian M, Duca L, Vincent P, Limon I & Blaise R (2018). Novel short isoforms of adenylyl cyclase as negative regulators of cAMP production. *Biochim Biophys Acta* **1865**, 1326–1340.
- van der Krogt GN, Ogink J, Ponsioen B & Jalink K (2008). A comparison of donor-acceptor pairs for genetically encoded FRET sensors: application to the Epac cAMP sensor as an example. *PLoS One* **3**, e1916.
- van der Wal J, Habets R, Várnai P, Balla T & Jalink K (2001). Monitoring agonist-induced phospholipase C activation in live cells by fluorescence resonance energy transfer. *J Biol Chem* **276**, 15337–15344.
- Van Staveren WC, Steinbusch HW, Markerink-Van Ittersum M, Repaske DR, Goy MF, Kotera J, Omori K, Beavo JA & De Vente J (2003). mRNA expression patterns of the cGMP-hydrolyzing phosphodiesterases types 2, 5, and 9 during development of the rat brain. *J Comp Neurol* **467**, 566–580.
- Verheij C, Bakker CE, de Graaff E, Keulemans J, Willemsen R, Verkerk AJ, Galjaard H, Reuser AJ, Hoogeveen AT & Oostra BA (1993). Characterization and localization of the FMR-1 gene product associated with fragile X syndrome. *Nature* **363**, 722–724.
- Verhoest PR, Chapin DS, Corman M, Fonseca K, Harms JF, Hou X, Marr ES, Menniti FS, Nelson F, O'Connor R, Pandit J, Proulx-Lafrance C, Schmidt AW, Schmidt CJ, Suiciak JA & Liras S (2009). Discovery of a novel class of phosphodiesterase 10A inhibitors and identification of clinical candidate 2-[4-(1-methyl-4-pyridin-4-yl-1H-pyrazol-3-yl)-phenoxy-methyl]-quinoline (PF-2545920) for the treatment of schizophrenia. *J Med Chem* **52**, 5188–5196.
- Verkerk AJ, de Graaff E, De Boule K, Eichler EE, Konecki DS, Reyniers E, Manca A, Poustka A, Willems PJ & Nelson DL (1993). Alternative splicing in the fragile X gene FMR1. *Hum Mol Genet* **2**, 399–404.
- Verkerk AJ, Pieretti M, Sutcliffe JS, Fu YH, Kuhl DP, Pizzuti A, Reiner O, Richards S, Victoria MF & Zhang FP (1991). Identification of a gene (FMR-1) containing a CGG repeat coincident with a breakpoint cluster region exhibiting length variation in fragile X syndrome. *Cell* **65**, 905–914.
- Verma V, Paul A, Amrapali Vishwanath A, Vaidya B & Clement JP (2019). Understanding intellectual disability and autism spectrum disorders from common mouse models: synapses to behaviour. *Open Biol* **9**, 180265.
- Vicente AM, Galvão-Ferreira P, Tecuapetla F & Costa RM (2016). Direct and indirect dorsolateral striatum pathways reinforce different action strategies. *Curr Biol* **26**, R267–9.
- Vilchis C, Bargas J, Ayala GX, Galván E & Galarraga E (2000). Ca²⁺ channels that activate Ca²⁺-dependent K⁺ currents in neostriatal neurons. *Neuroscience* **95**, 745–752.
- Vincent P & Bruscianno D (2001). Cyclic AMP imaging in neurones in brain slice preparations. *J Neurosci Methods* **108**, 189–198.
- Vincent SR & Kimura H (1992). Histochemical mapping of nitric oxide synthase in the rat brain. *Neuroscience* **46**, 755–784.
- Violin JD, DiPilato LM, Yildirim N, Elston TC, Zhang J & Lefkowitz RJ (2008). beta2-adrenergic receptor signaling and desensitization elucidated by quantitative modeling of real time cAMP dynamics. *J Biol Chem* **283**, 2949–2961.

- Voelbel GT, Bates ME, Buckman JF, Pandina G & Hendren RL (2006). Caudate nucleus volume and cognitive performance: Are they related in childhood psychopathology. *Biol Psychiatry* **60**, 942–950.
- Wachtel H & Schneider HH (1986). Rolipram, a novel antidepressant drug, reverses the hypothermia and hypokinesia of monoamine-depleted mice by an action beyond postsynaptic monoamine receptors. *Neuropharmacology* **25**, 1119–1126.
- Wang H, Peng MS, Chen Y, Geng J, Robinson H, Houslay MD, Cai J & Ke H (2007). Structures of the four subfamilies of phosphodiesterase-4 provide insight into the selectivity of their inhibitors. *Biochem J* **408**, 193–201.
- Wang H, Robinson H & Ke H (2010). Conformation changes, N-terminal involvement, and cGMP signal relay in the phosphodiesterase-5 GAF domain. *J Biol Chem* **285**, 38149–38156.
- Watabe-Uchida M & Uchida N (2018). Multiple Dopamine Systems: Weal and Woe of Dopamine. *Cold Spring Harb Symp Quant Biol* **83**, 83–95.
- Wei JY, Roy DS, Leconte L & Barnstable CJ (1998). Molecular and pharmacological analysis of cyclic nucleotide-gated channel function in the central nervous system. *Prog Neurobiol* **56**, 37–64.
- Welch EJ, Jones BW & Scott JD (2010). Networking with AKAPs: context-dependent regulation of anchored enzymes. *Mol Interv* **10**, 86–97.
- West AR, Galloway MP & Grace AA (2002). Regulation of striatal dopamine neurotransmission by nitric oxide: effector pathways and signaling mechanisms. *Synapse* **44**, 227–245.
- West AR & Grace AA (2004). The nitric oxide-guanylyl cyclase signaling pathway modulates membrane activity States and electrophysiological properties of striatal medium spiny neurons recorded in vivo. *J Neurosci* **24**, 1924–1935.
- West AR & Tseng KY (2011). Nitric Oxide-Soluble Guanylyl Cyclase-Cyclic GMP Signaling in the Striatum: New Targets for the Treatment of Parkinson’s Disease. *Front Syst Neurosci* **5**, 55.
- Wickens J & Arbutnott GW (2005). Dopamine. pp. 199–236.
- Wilson CJ (1993). The generation of natural firing patterns in neostriatal neurons. *Prog Brain Res* **99**, 277–297.
- Wilson CJ, Chang HT & Kitai ST (1990). Firing patterns and synaptic potentials of identified giant aspiny interneurons in the rat neostriatum. *J Neurosci* **10**, 508–519.
- Wilson CJ & Groves PM (1980). Fine structure and synaptic connections of the common spiny neuron of the rat neostriatum: a study employing intracellular inject of horseradish peroxidase. *J Comp Neurol* **194**, 599–615.
- Wilson H, Niccolini F, Haider S, Marques TR, Pagano G, Coello C, Natesan S, Kapur S, Rabiner EA, Gunn RN, Tabrizi SJ & Politis M (2016). Loss of extra-striatal phosphodiesterase 10A expression in early premanifest Huntington’s disease gene carriers. *J Neurol Sci* **368**, 243–248.
- Wilson LS, Baillie GS, Pritchard LM, Umana B, Terrin A, Zaccolo M, Houslay MD & Maurice DH (2011). A phosphodiesterase 3B-based signaling complex integrates exchange protein activated by cAMP 1 and phosphatidylinositol 3-kinase signals in human arterial endothelial cells. *J Biol Chem* **286**, 16285–16296.
- Wilson LS & Brandon NJ (2015). Emerging biology of PDE10A. *Curr Pharm Des* **21**, 378–388.

- Woolfrey KM, Srivastava DP, Photowala H, Yamashita M, Barbolina MV, Cahill ME, Xie Z, Jones KA, Quilliam LA, Prakriya M & Penzes P (2009). Epac2 induces synapse remodeling and depression and its disease-associated forms alter spines. *Nat Neurosci* **12**, 1275–1284.
- Wouters FS, Verveer PJ & Bastiaens PI (2001). Imaging biochemistry inside cells. *Trends Cell Biol* **11**, 203–211.
- Wykes V, Bellamy TC & Garthwaite J (2002). Kinetics of nitric oxide-cyclic GMP signalling in CNS cells and its possible regulation by cyclic GMP. *J Neurochem* **83**, 37–47.
- Xie W, Dolzhanskaya N, LaFauci G, Dobkin C & Denman RB (2009). Tissue and developmental regulation of fragile X mental retardation 1 exon 12 and 15 isoforms. *Neurobiol Dis* **35**, 52–62.
- Xie Z, Adamowicz WO, Eldred WD, Jakowski AB, Kleiman RJ, Morton DG, Stephenson DT, Strick CA, Williams RD & Menniti FS (2006). Cellular and subcellular localization of PDE10A, a striatum-enriched phosphodiesterase. *Neuroscience* **139**, 597–607.
- Xu Y, Zhang HT & O'Donnell JM (2011). Phosphodiesterases in the central nervous system: implications in mood and cognitive disorders. *Handb Exp Pharmacol* 447–485.
- Yan C, Bentley JK, Sonnenburg WK & Beavo JA (1994). Differential expression of the 61 kDa and 63 kDa calmodulin-dependent phosphodiesterases in the mouse brain. *J Neurosci* **14**, 973–984.
- Yapo C, Nair AG, Clement L, Castro LR, Hellgren Kotaleski J & Vincent P (2017). Detection of phasic dopamine by D1 and D2 striatal medium spiny neurons. *J Physiol*
- Yin HH, Mulcare SP, Hilário MR, Clouse E, Holloway T, Davis MI, Hansson AC, Lovinger DM & Costa RM (2009). Dynamic reorganization of striatal circuits during the acquisition and consolidation of a skill. *Nat Neurosci* **12**, 333–341.
- Yoshikawa M, Kamisaki H, Kunitomo J, Oki H, Kokubo H, Suzuki A, Ikemoto T, Nakashima K, Kamiguchi N, Harada A, Kimura H & Taniguchi T (2015). Design and synthesis of a novel 2-oxindole scaffold as a highly potent and brain-penetrant phosphodiesterase 10A inhibitor. *Bioorg Med Chem* **23**, 7138–7149.
- Yoshizaki H, Mochizuki N, Gotoh Y & Matsuda M (2007). Akt-PDK1 complex mediates epidermal growth factor-induced membrane protrusion through Ral activation. *Mol Biol Cell* **18**, 119–128.
- Zaccolo M, De Giorgi F, Cho CY, Feng L, Knapp T, Negulescu PA, Taylor SS, Tsien RY & Pozzan T (2000). A genetically encoded, fluorescent indicator for cyclic AMP in living cells. *Nat Cell Biol* **2**, 25–29.
- Zaccolo M, Di Benedetto G, Lissandron V, Mancuso L, Terrin A & Zamparo I (2006). Restricted diffusion of a freely diffusible second messenger: mechanisms underlying compartmentalized cAMP signalling. *Biochem Soc Trans* **34**, 495–497.
- Zafarullah M & Tassone F (2019). Molecular Biomarkers in Fragile X Syndrome. *Brain Sci* **9**,
- Zhang J, Campbell RE, Ting AY & Tsien RY (2002). Creating new fluorescent probes for cell biology. *Nat Rev Mol Cell Biol* **3**, 906–918.
- Zhang J, Hupfeld CJ, Taylor SS, Olefsky JM & Tsien RY (2005). Insulin disrupts beta-adrenergic signalling to protein kinase A in adipocytes. *Nature* **437**, 569–573.
- Zhang J, Ma Y, Taylor SS & Tsien RY (2001). Genetically encoded reporters of protein kinase A activity reveal impact of substrate tethering. *Proc Natl Acad Sci U S A* **98**, 14997–15002.

Zhou X, Clister TL, Lowry PR, Seldin MM, Wong GW & Zhang J (2015). Dynamic Visualization of mTORC1 Activity in Living Cells. *Cell Rep*

Zhuang X, Belluscio L & Hen R (2000). G(olf)alpha mediates dopamine D1 receptor signaling. *J Neurosci* **20**, RC91.

Dopamine and non-canonical signaling

Abstract

Striatal medium-sized spiny neurons (MSNs) integrate dopamine signals mainly through the cAMP signaling pathway. Dopamine D₁ or D₂ receptors trigger an increase or a decrease in cAMP levels, respectively. My thesis focuses on how phosphodiesterases (PDEs), which degrade cAMP, are involved in the integration of dopamine signals in the striatum. I used genetically-encoded FRET biosensors to monitor cAMP level in real time in individual living neurons in striatal brain slice preparations. I used selective inhibitors to determine the function of each PDE.

PDE1B, which is activated by calcium-calmodulin, appears as a detector of the coincidence of dopamine and glutamate signals, which is critical in the regulation of synaptic plasticity involved in reward-based learning. PDE10A shows the most prominent activity, efficiently degrading both high and low cAMP levels. PDE10A activity is required to allow for PKA de-activation, and therefore needed to transduce a dopamine signal through D₂ receptors into a decrease in PKA-dependent phosphorylation. PDE2A and PDE4 appeared to degrade only high levels of cAMP, preventing large increases in cAMP. PDE2A, which activity can be increased by cGMP, also appears as a detector of dopamine and NO coincidence.

Understanding PDE functions can highlight their potential as therapeutic targets in CNS pathologies. As an example, we showed an increased PDE2A function in the hippocampus of a mouse model of Fragile X syndrome.

Besides the cAMP/PKA pathway, dopamine D₂ receptors is reported to activate non-canonical pathways. Attempts to use biosensors for Akt and ERK pathways did not provide conclusive data.

Keywords

Dopamine, striatum, cAMP/PKA signaling pathway, phosphodiesterases, genetically-encoded FRET biosensor imaging, cyclic GMP.

Dopamine et signalisation non canonique

Résumé

Les neurones épineux striataux de taille moyenne (MSN) intègrent les signaux médiés par la dopamine principalement par la voie de signalisation de l'AMPC. Les récepteurs dopaminergiques D₁ ou D₂ déclenchent respectivement une augmentation ou une diminution du taux d'AMPC. Ma thèse porte sur la manière dont les phosphodiesterases (PDE), qui dégradent l'AMPC, sont impliquées dans l'intégration des signaux de dopamine dans le striatum. J'ai utilisé des biosenseurs FRET génétiquement codés pour surveiller le niveau d'AMPC en temps réel dans des neurones individuels vivants dans des préparations de tranches de cerveau striatal. J'ai utilisé des inhibiteurs sélectifs pour déterminer la fonction de chaque PDE.

La PDE1B, qui est activée par la calcium-calmoduline, apparaît comme un détecteur de la coïncidence des signaux de dopamine et de glutamate, ce qui est essentiel dans la régulation de la plasticité synaptique impliquée dans l'apprentissage par récompense. La PDE10A montre l'activité la plus importante, dégradant efficacement les taux d'AMPC élevés et faibles. L'activité PDE10A est nécessaire pour permettre la désactivation de la PKA, et donc nécessaire pour transduire un signal de dopamine à travers les récepteurs D₂ en une diminution de la phosphorylation dépendante de la PKA. PDE2A et PDE4 ont semblé ne dégrader que des niveaux élevés d'AMPC, empêchant de fortes augmentations d'AMPC. La PDE2A, dont l'activité peut être augmentée par le GMPc, apparaît également comme un détecteur de coïncidence dopamine et NO.

Comprendre les fonctions des PDE peut mettre en évidence leur potentiel en tant que cibles thérapeutiques dans les pathologies du SNC. A titre d'exemple, nous avons montré une fonction accrue de PDE2A dans un modèle de souris du syndrome du X fragile.

En plus de la voie AMPC/PKA, les récepteurs de la dopamine D₂ pourraient également activer des voies non canoniques. Les tentatives d'utilisation de biosenseurs pour les voies Akt et ERK n'ont pas fourni de données concluantes.

Mots clés

Dopamine, striatum, voie de signalisation AMPC/PKA, phosphodiesterases, imagerie par biosenseur FRET génétiquement codée, GMP cyclique.